THE ROLE OF EXTRACELLULAR PROTEASES, MATRIX-METALLOPROTEINASE-2 AND -9 IN REGULATING THE MAMMALIAN CIRCADIAN CLOCK

A Dissertation Presented for the
Doctor of Philosophy
Degree
The University of Tennessee, Knoxville

Kathryn Abrahamsson Halter
May 2020

Copyright © 2019 by Kathryn Abrahamsson Halter.
All rights reserved.

DEDICATION

I would like to dedicate this dissertation to all of the strong women that have influenced me. To my kindergarten teacher, Mrs. Lowenstein, for recognizing my intellectual gift and giving my parents extra books for me to read as a child. To my high school volleyball coach, Kerri Morrison, who took me to my first Women in Leadership conference and taught me the value of coaching and mentorship. To my high school physics teacher, Mrs. Jennifer Gottlieb, who showed me the excitement that comes from a mathematical understanding of the rollercoasters. To my high school counselor, Michelle Kosi, who helped me find scholarships to pay for my undergraduate education. To Dr. Kate Teeter, who taught me to critically evaluate scientific literature and be inspired by evolution. To Paula Genovese, an inspirational laboratory instructor and mentor in the importance of volunteering. To Mary Martin, my determined genetics instructor dedicated to her students and getting to the bottom of each of their questions. To Marsha Lucas, my biochemistry laboratory instructor who challenged her students and imparted the necessity of keeping a good laboratory notebook. To the late Dr. Elizabeth Howell, an advocate of scientific ethics, visual communication methods and effective mentorship techniques. To Dean Theresa Lee and Dr. Rebecca Prosser, for forging the way for young women leaders in the fields of circadian rhythms and neuroscience. To Dean Cynthia Peterson, for creating a program for women and minorities to pursue scientific research and for being an example of “the Volunteer spirit”. To Ana Bernal Gomez, who taught me that professionalism can be incorporated to every life aspect. To Abby Trotter, who helped facilitate my introduction to advocating for science and for supporting comradery between academics and entrepreneurs alike. To Sheila Headrick Halter, for her advice and mentorship in navigating male-dominated professions. To Erika Halter, who taught me that successful women offer thoughtful and creative solutions. To my sister, Meagan Abrahamsson, who continues to be a reminder that education can be your passport to the world and that listening to others is the best way to lead. To my godmother, Donna Giannola, who lifts up women with her kindness and laughter. To my aunt, Rosemary Kadrich, who taught me the importance of our actions on the young people that look up to us and for supporting my independence. To my aunt, Loretta Abrahamsson, who has shown me that education is priceless, and persistence can get you anywhere. To my late

grandmother, Eleanor Giannola, who taught me that a homecooked meal brings people together and heals all wounds. To the next generation of women scientists, including Alyssa Briggs, I hope that your curiosity continues to bring up exciting questions about the world we live in that still need to be answered. Importantly, I dedicate this dissertation to the strongest woman I knew, my mother, the late Tina Abrahamsson. She was the first one to notice that I was observant and curious. She facilitated my siblings and my learning throughout each summer by giving us extra workbooks to complete that were above our grade level. She spent hours in the library with us helping pick out books and late nights making sure we finished school projects. She taught me the importance of independence and gave me the freedom to follow my dreams. Most of all, she taught me that the strength of women lies within their capacity to love, and I am thankful that hers was unlimited.

ACKNOWLEDGEMENTS

Throughout the writing of this dissertation I have received a great deal of support and assistance. I would first like to thank my advisor, Dr. Rebecca Prosser, whose expertise was invaluable in formulating the research topic, methodology, and composition of dissertation in particular. Thank you for pushing my intellectual boundaries and for supporting my project.

I would like to thank members of the Program for Excellence and Equity in Research (PEER). The mentoring and financial support I received early on in my graduate education was essential to make it through the first tough years. I also would like to acknowledge the PEER community, including Dr. Seekenia Haynes, for their encouragement and allowing me to mentor younger students as well.

I would like to thank Dean Cynthia B. Peterson for introducing me to Dr. Prosser, and to the research opportunities at the University of Tennessee, Knoxville (and its football program). Thank you for seeing something in a young scientist and inspiring me to join the PEER family and the Department of Biochemistry & Cell and Molecular Biology (BCMB).

I would like to thank Dean Theresa Lee of the College of Arts and Sciences, Dr. Jim Hall of the BCMB Department and Dr. Matthew Cooper of the Psychology Department for their mentorship, guidance and constructive critiques of my research projects and dissertation.

I would like to thank my BCMB colleagues. First my lab members, Dr. Yukihiro Yamada, Dr. Jonathan Lindsay, and Dr. Joanna Cooper; thanks to each of you for your guidance, willingness to help, and to help make sense of my research findings. Thank you to Dr. Andrew Stafford for being our adopted lab member and a great source of support. Thank you to Ana Bernal Gomez for volunteering her time to help keep the BCMB Graduate Student Organization running and for her valuable friendship. Thank you to Debalina Acharyya for bringing a ray of sunshine to work every day. I would like to acknowledge the hard-working undergraduate students that assisted in the completion of many of the

experiments included in this dissertation, including Jessica Grenvik, Sarah Grace Lebovitz, Randy Carpenter, Jessica Bertram, Cynthia Ellis and Catherine Bagby.

I would like to acknowledge Dr. Karen Gamble and Dr. Lauren Hablitz, trusted collaborators of our laboratory in the circadian rhythms field.

I would like to thank the BCMB and UTK faculty for imparting on me a diversity of knowledge, especially to Dr. Tessa Burch-Smith and Dr. Brad Binder for giving their time and lab space during my laboratory rotations. Many thanks are due to Dr. Maitreyi Das and Dr. Mariano Labrador for allowing me to use their microscopes and for their technical support. I would also like to thank Dr. Keerthi Krishnan and Dr. Billy Lau for teaching me immunohistochemical techniques. I would like to thank Dr. James Fordyce for facilitating many stimulating discussions about statistics, likelihood, and for his extensive knowledge of binomial nomenclature. The BCMB staff (LaShel Brown, Cheryl Hodge and Lori Daniels) for helping support me and resolve a myriad of matters.

I would like to thank my undergraduate mentor, Dr. Erich Ottem, for his inspiring lectures on neuroendocrinology, for taking the time to train me in performing “real” research, and for recognizing that I could successfully get through graduate school.

I would like to thank my family, especially my brother Cameron Abrahamsson and sister Meagan Abrahamsson, for their heartfelt support and keeping our family foundation a solid part of all of our successes. To my late mother, Tina Abrahamsson and father, Robert Abrahamsson, for supporting my growth as a young woman. Thank you to Sara Briggs, for your support and kindness. Thank you also to the Halter family, as each of you have for lent sympathetic ear and provided priceless advice. Many thanks are deserved by my (mostly) loyal companion, Cubby B. Dog, for collecting the mail for me and spending many late nights curled by my feet while I wrote this dissertation.

Most importantly, I would like to thank my husband, Mathew Halter, for his unconditional commitment. As my confidant and champion, thank you for helping me rise to the occasion and for reminding me of the greater goal.

ABSTRACT

Molecules existing in the extracellular space (ECS) make up a complicated network of structural proteins, signaling molecules, cellular adhesion molecules and transmembrane receptors. Many ECS molecules are implicated as active regulators of structural and functional brain plasticity. When molecules in the ECS are improperly expressed or degraded, cellular communication becomes disrupted and can lead to a variety of disease pathologies. Thus, there are myriad overlapping regulatory mechanisms that determine and maintain the composition of the ECS. Research investigating extracellular molecule expression in the brain identified that some exhibit cyclic, near 24-hour rhythms and may be under circadian control. Further, extracellular molecules are hypothesized to help perpetuate the oscillations of the mammalian master clock located in the suprachiasmatic nucleus (SCN). Our goal was to expand upon past findings in our laboratory that implicate a pivotal role of extracellular proteases, namely those in the plasminogen activation cascade, in gating glutamate-induced phase shifts. Two proteases activated by this cascade are matrix metalloproteinase-2 and -9 (MMP-2/9). Across the brain, MMP-2/9 catalytically cleave extracellular scaffolding molecules like β-dystroglycan in response to increased neuronal activity. MMP-2/9-mediated degradation of extracellular molecules is also known to facilitate changes in neuronal and astrocytic morphology and alter N-methyl-D-aspartate receptor (NMDAR) activity. Interestingly, a previous study of MMP-2/9 in the hamster SCN found that MMP-9 activity exhibits a diurnal rhythm in activity, while MMP-2 does not. For this project, we aimed to elucidate the role of MMP-2/9 by further characterizing their expression and activity in mouse SCN tissue. We found that MMP-2/9 activity is highest during the day and that inhibiting their activity phase shifts neuronal activity rhythms in a time dependent manner. Further, we sought to better understand physiologic consequences of MMP-2/9 mediated cleavage of β-dystroglycan in regulating astrocytic diurnal morphologic rhythms. We confirmed that astrocyte morphology exhibits a day to night transition toward a highly ramified state. Although β-dystroglycan expression is constitutive across the day and potentially interacts with SCN astrocytes, their degradation does not appear to be regulated by MMP-2/9 activity.

TABLE OF CONTENTS

Chapter I: Introduction 1
The mammalian master clock regulates circadian rhythms 2
The molecular master clock is a transcriptional-translational feedback loop 3
Signaling molecules and peptides in the SCN 5
Light-induced glutamate release synchronizes the clock 7
Rhythmic properties of SCN astrocytes 9
The extracellular environment's role in circadian rhythm regulation 11
Changes in extracellular matrix affect cellular communication 12
Extracellular adhesion molecules and their links to the clock 13
Matrix Metalloproteinases 14
MMP's are pivotal regulators of structural brain plasticity 15
MMP-2/9 dependent cleavage of β-dystroglycan regulates cellular activity and morphology 18
Linking MMP's to the mammalian circadian clock 19
Appendix: Figures for Chapter 1 20
Chapter II: Time of day determines level and outcome of matrix metalloproteinase-2 and -9 Activity in the mammalian circadian clock. 23
Abstract 24
Introduction 25
Materials and Methods 27
Brain slice preparation 27
Western blotting 28
Gelatin zymography 29
In situ gelatin zymography 29
In vitro extracellular electrophysiology 30
Chemical treatments 31
Statistical analysis 31
Results 32
MMP-9 enzymatic activity, but not expression, is lowest during the late night 32
In situ zymography confirms enhanced MMP activity of in SCN tissue 34
Blocking MMP-2/9 activity alters SCN neuronal activity rhythms 35
BiPS-induced phase shifts require NMDAR activity 35
Daytime but not early night phase shifts induced by BiPS require plasmin and TrkB activation 36
BiPS treatment does not affect CAMKII phosphorylation 37
Discussion 38
Appendix: Figures for Chapter 2 43
Chapter III: Linking time dependent state changes in astrocytic ramification to the extracellular environment 58
Abstract 59
Introduction 60
Materials and Methods 64
Immunohistochemistry 64
Sholl analysis 65

Colocalization analysis using Coloc-2 ImageJ Program 66
Brain slice preparation 66
Chemical treatment 67
Western blotting 67
Statistical Analysis 68
Results 68
Staining patterns revealed by two β-dystroglycan antibodies 68
β-dystroglycan and GFAP colocalization is highest during the late night 71
Sholl analysis of GFAP positive cells in the SCN suggests astrocytes at ZT 23 are more ramified 71
Beta-dystroglycan protein expression in SCN tissue slices is not rhythmic and is not affected by inhibiting MMP-2/9 activity 74
Discussion 75
Appendix: Figures for Chapter 3 81
Chapter IV: Conclusions and Future Directions 94
Summary 95
Regulating MMP-9 diurnal activity 98
Reciprocal relationship between MMP-2/9 and NMDAR activity 100
How does BiPS affect NMDARs? 103
MMP-2/9 and β-dystroglycan involvement in astrocytic morphological changes 108
Circadian matrisome and proteomic profiling of the SCN 109
Linking the ECM to the intracellular circadian clock 112
Appendix: Figures for Chapter 4 117
References 126
Appendix 173
Supplementary Protocols 176
Western Blotting for Protein Expression 176
Gelatin Zymography Protocol 179
In Situ Zymography Protocol 182
Immunohistochemistry of Thin Sections on Slides Protocol 184
Colocalization Using Coloc 2 ImageJ Analysis Protocol 186
Simple Neurite Tracer and Sholl Analysis Protocol 188
Astrocyte Soma Cell Body Fill Volume Protocol 192
Vita 193

LIST OF TABLES

Table 1. Primary Antibody information 174
Table 2: Secondary Antibody Information 175

LIST OF FIGURES

Figure 1.1: Potential pathways linking MMP-2/9 activity to circadian processes in the SCN. 21
Figure 2.1: Protein expression of MMP-2 and MMP-9 in SCN tissue does not change between ZT 6, ZT 16 and ZT 23..... 44
Figure 2.2: MMP-9, but not MMP-2, activity varies across the circadian cycle. 45
Figure 2.3: Increasing protein content does not increase detection of MMP-2 in SCN tissue extract. 47
Figure 2.4: In situ zymography confirms activity of MMP-2/9 in the SCN. 48
Figure 2.5: Inhibiting MMP-2/9 activity during the day and early night phase-shifts the clock. 51
Figure 2.6: Inhibition of MMP-2/9 at ZT 23 acutely affects firing rates but does not phase-shift the SCN circadian clock..... 54
Figure 2.7: Inhibition of MMP's does not affect phosphorylation of α- and β-CAMKII.... 56
Figure 3.1: β-dystroglycan is expressed in the SCN. 82
Figure 3.2: Expression of β-dystroglycan and GFAP does not change over time. 83
Figure 3.3: β-dystroglycan and GFAP fluorescence overlaps at multiple time-points and is highest at ZT 23..... 86
Figure 3.4: Examination of astrocyte morphology over time using Sholl analysis. 89
Figure 3.5: β-dystroglycan expression in SCN tissue homogenate does not change over time and is unaffected by MMP-2/9 inhibition. 92
Figure 4.1: Acute recording of *in vitro* SCN firing rate surrounding BiPS treatment at ZT 16. 118
Figure 4.2: Preliminary data showing α-dystroglycan antibody application to SCN slices does not phase shift the clock. 119
Figure 4.3: Hypothesized reciprocal feedback between MMP-2/9 and NMDAR activity in the SCN. 120
Figure 4.4: MMP-9 participation in SCN circadian clock regulation. 122
Figure 4.5: The effects of MMP-2/9 inhibition on NMDAR are time dependent. 124

LIST OF ABBREVIATIONS

1-Na-PP1	1-Naphthyl-PP1 (tyrosine kinase inhibitor)
aaMMP-9	auto-activating matrixmetalloproteinase-9
AAV	Adeno-associated virus
AH	Anterior hypothalamus
AMAPAR	α-amino-3-hydroxy-5-methyl-4-isoxazolepropionic acid receptor
AP5	(2R)-amino-5-phosphonovaleric acid
ATP	Adenosine triphosphate
AVP	Arginine vasopressin
BDNF	Brain derived neurotrophic factor
BiPS	(2R)-[(4-Biphenylylsulfonyl)amino]-N-hydroxy-3-phenylpropionamide
BMAL1	Brain and muscle ARNT-like protein
CA1	Region CA1 of the hippocampus
CAM	Cell adhesion molecule
CAMK	Calcium/calmodulin-dependent kinase
cAMP	3',5' cyclic adenosine monophosphate
CLOCK or *clock*	Circadian locomotor output cycles kaput
CRE	cAMP response element
CREB	cAMP response element binding protein
CRY or *cry*	Cryptochrome
DAPI	4′,6-diamidino-2-phenylindole (DNA stain)
ECS	Extracellular space
ECM	Extracellular matrix
EAAT1	Excitatory amino acid transporter-1
ERK	Extracellular signal-related kinase
f-iNMDARs	Flux-independent NMDAR signaling
FLIM	Fluorescence lifetime imaging
FRET	Forster resonance energy transfer
GABA/GABAR	γ-aminobutyric acid/ GABA receptor

GCaMP	Genetically encoded calcium indicator
GFAP	Glial fibrillary acidic protein
Little SASS	Pepitide fragment of proSAAS (a granin-like neuroendocrine peptide precursor)
LUC or *luc*	Luciferase
LTD	Long-term depression
LTP	Long-term potentiation
MAPK	Mitogen-activated protein kinase
MEC	Mammary epithelial cell
mEPSC	Miniature excitatory post-synaptic current
mGluR	Metabotropic glutamate receptor
MMP	Matrix metalloproteinase
MS	Mass spectrometry
NCAM	Neural cell adhesion molecule
NLGN	Neuroligin
NMDAR	N-methyl-D-aspartate receptor
NRXN	Neurexin
PACAP	Pituitary adenylate cyclase-activating polypeptide
PAI-1	Plasminogen activator inhibitor-1
PER or *per*	Period
PSA-NCAM	Polysialyated-neural cell adhesion molecule
PSD-95	Post-synaptic density protein 95
REV-ERBα	An orphan nuclear receptor transcribed on the reverse (REV) strand of the thyroid recptor α (c-erbAα) gene
r-MMP-2/9	Recombinant MMP-2/9
ROI	Region of interest
RORα	Retinoic acid receptor-related orphan receptor α
RHT	Retinohypothalamic tract
SCN	Suprachiasmatic nucleus
shRNAi	Short hairpin RNA inhibitor
siRNA	Small interfering ribonucleic acid

TIMP	Tissue inhibitor of metalloproteinase
tPA	Tissue-type plasminogen activator
TTFL	Transcriptional-translational feedback loop
uPA	Urokinase-type plasminogen activator
VIP	Vasoactive intestinal peptide
ZT	Zeitgeber time

CHAPTER I: INTRODUCTION

The mammalian master clock regulates circadian rhythms

Nearly every organism on earth exhibits daily cycles in behavior, physiology and metabolism. These iterative, near 24-hr patterns are called circadian (Latin; *circa*=approximate, *diem*=day) rhythms. Examples of these rhythms in mammals include melatonin secretion, blood pressure, body temperature and sleep-wake cycles (Refinetti & Menaker, 1992; Schulz & Steimer, 2009; Albrecht, 2012; Bollinger & Schibler, 2014). In mammals, the master clock is located in a brain region called the suprachiasmatic nucleus (SCN). The SCN is a bilateral nucleus in the ventral hypothalamus that consists of about 20,000 neurons (Van den Pol, 1980; Reiter, 1991; Moore, 1995; 2007). Not only does this region generate endogenous circadian rhythms, but it also integrates "time of day" information and communicates these signals to the rest of the brain to synchronize peripheral clocks with the daily light cycle (Moore & Eichler, 1972; Stephan & Zucker, 1972).

Proper maintenance and synchronization of circadian rhythms is important for maintaining a healthy lifestyle. However, our modern society sometimes exposes individuals to artificial light at night or demands travel across time zones. In these cases, our circadian rhythms experience a disruption, or phase shift, in their oscillatory patterns (Rajaratnam & Arendt, 2001; Touitou *et al.*, 2017). Acute phase shifting can result in health consequences such as fatigue, jet-lag and/or increased inflammation as our bodies entrain to the new light cycle (Scheer *et al.*, 2009; Castanon-Cervantes *et al.*, 2010). On the other hand, chronic circadian rhythm disruption leads to detrimental conditions such as depression (Lall *et al.*, 2012; LeGates *et al.*, 2012; Obayashi *et al.*, 2018), shift-work disorder (resulting from working on-call, rotating, or extended overnight shifts) (Sack *et al.*, 2007), metabolic disorder (Scheer *et al.*, 2009), increased risk for neurodegenerative diseases like Alzheimer's Disease (Reisberg *et al.*, 1987; Witting *et al.*, 1990; Wulff *et al.*, 2010; Hastings & Goedert, 2013) or for certain cancers (Filipski *et al.*, 2005; Costa, 2010). In practice, clinicians can perform circadian rhythm evaluations (also called "chronotyping") and prescribe circadian alignment practices, like appropriate sleep scheduling or medication to help "reset" their patient's clocks and improve health outcomes. (Arendt *et al.*, 1997; Morgenthaler *et al.*, 2007; Sack *et al.*, 2007; Sánchez-Barceló *et al.*, 2010; Bubenik & Konturek, 2011; Adan *et al.*, 2012). Thus, understanding

the underlying mechanisms of the mammalian circadian clock and how it adapts to changes in the light cycle is imperative for maximizing human health.

Studies investigating the mechanisms that underlie circadian rhythm generation show that lesions of SCN or retinohypothalamic tract (RHT) neurons disrupt an organism's behavioral and physiologic rhythms (Moore & Eichler, 1972; Moore & Klein, 1974; Morin & Cummings, 1981; Moore, 1995). Remarkably, transplantation of embryonic SCN tissue into the third ventricle, dorsal to the ablated region, restores behavioral rhythms in SCN lesioned mammals (Drucker-Colín *et al.*, 1984; Sawaki *et al.*, 1984; DeCoursey & Buggy, 1989; Aguilar-Roblero *et al.*, 1994; Tousson & Meissl, 2004). Certain hormonal cycles (i.e. rhythmic secretion of cortisol, adrenal hormone, and melatonin), however, are not restored by embryonic SCN implantation (Meyer-Bernstein *et al.*, 1999). Although donor SCN tissue continues to produce rhythms in metabolic and electrical activity (Aguilar-Roblero *et al.*, 1992), transplanted embryonic tissue encapsulated in permeable acrylic polymer tubes only restores behavioral rhythms (Lehman *et al.*, 1995). These studies indicate that the SCN sends efferent entrainment signals via two distinct methods: by secretion of diffusible factors (Egli *et al.*, 2004) and electrically by axonal projections to regions specific for neuroendocrine function, such as the anterior hypothalamus and the anteroventral periventricular nucleus (Watts *et al.*, 1987; Watson *et al.*, 1995). Collectively, these data support that the SCN uses both electrical and chemical outputs to synchronize behavioral and physiologic circadian rhythms.

The molecular master clock is a transcriptional-translational feedback loop

The core molecular clock mechanism in the SCN and in peripheral oscillators is a transcriptional-translational feedback loop (TTFL). Study of mutant mouse and drosophila strains exhibiting longer, shorter or arrhythmic free-running periods helped identify the core clock genes: *period (per), cryptochrome (cry,* or *timeless* in Drosophila*), clock* (circadian locomotor output cycles kaput) and *Bmal1* (brain and muscle ARNT-like protein 1) (Vitaterna *et al.*, 1994; Allada *et al.*, 1998; Emery *et al.*, 1998; Vitaterna *et al.*, 1999; Reppert & Weaver, 2002; Ko & Takahashi, 2006). These genes encode for a group of

proteins that together form the TTFL, and their proper expression and function drives circadian rhythm generation (Antoch *et al.*, 1997; Dunlap, 1999; Yamazaki *et al.*, 2000).

At the cellular level, the TTFL proteins CLOCK and BMAL1 first form a heterodimer in the cytoplasm. After entering the nucleus, the heterodimer binds to DNA sequences (called E-Boxes) upstream of a variety of genes, including *per* and *cry,* and acts as a transcriptional activator (Gekakis *et al.*, 1998). Increased transcription and subsequent translation lead to PER and CRY accumulation in the cytoplasm. PER and CRY proteins also form heterodimers and are transported back into the nucleus where they repress CLOCK/BMAL1 activity (Curtin *et al.*, 1995; Shafer *et al.*, 2002), which inhibits their own transcription. Over time, the remaining PER and CRY are ubiquinated and degraded. The decrease in PER and CRY levels reduces CLOCK/BMAL1 inhibition and the entire TTFL starts again (Price *et al.*, 1995; Darlington *et al.*, 1998; Sangoram *et al.*, 1998). CLOCK/BMAL1 binding to DNA also drives expression of the nuclear receptors REV-ERBα and RORα, which form a secondary negative feedback loop to cyclically suppress expression of *Bmal1* (Preitner *et al.*, 2002; Cho *et al.*, 2012). Transcriptomic studies estimate that endogenous oscillation of the TTFL loop in SCN and somatic tissues (i.e., liver, lung, kidney, etc.) results in cyclic expression of 10%-20% of the genome (Akhtar *et al.*, 2002; Panda *et al.*, 2002; Reddy *et al.*, 2006; Pizarro *et al.*, 2013). The largest proportion of these genes encode for transcription factors, cell-cycle and proliferation-promoting proteins (Kondratov & Antoch, 2007). Evidence in rats indicates that light pulses administered at night phase-shift TTFL gene expression in the SCN more rapidly than locomotor or peripheral rhythms (Field *et al.*, 2000; Yamazaki *et al.*, 2000; Maywood *et al.*, 2013), demonstrating that the TTFL in the master clock responds to environmental stimuli first and then drives synchronization of peripheral clocks (Takahashi *et al.*, 2008).

As mentioned above, the SCN communicates time of day signals to the rest of the brain electrically. Neurons in the SCN exhibit endogenous, spontaneous action potentials that peaks in rate during the middle of the day as opposed to during the night. This rhythm can be detected using both *in vivo* and *in vitro* electrophysiological techniques (Inouye & Kawamura, 1979; Green & Gillette, 1982; Groos & Hendriks, 1982; Gillette & Prosser, 1988; Prosser & Gillette, 1989; Gillette, 1991; Yamazaki *et al.*, 1998; Schaap & Meijer, 2001; Lundkvist *et al.*, 2002; van Oosterhout *et al.*, 2012). When the SCN is removed

from wild-type mammals and maintained *in vitro*, its neurons continue to exhibit persistent, robust rhythms in molecular and neuronal activity (Gillette & Prosser, 1988; Jiang *et al.*, 1997). In fact, Yamazaki and Takahashi found that cultured organotypic slices expressing *Per2:luc* (a genetic knock-in of the luciferase protein fused to the C-terminus of the *Per2* gene) can produce luminescence rhythms for up to 478 days (Yamazaki & Takahashi, 2005). Combined *in vivo* and *in vitro* studies demonstrate that proper expression of TTFL elements is necessary to generate and maintain SCN circadian neuronal activity rhythms (Inouye & Kawamura, 1979; Rusak & Zucker, 1979; Watanabe *et al.*, 1995; Lundkvist *et al.*, 2002; Kudo *et al.*, 2015). For example, the *clock* gene mutation lengthens the period of behavioral wheel running in mice and desynchronizes SCN neuronal electrical rhythms (Herzog *et al.*, 1998).

Physiologically, the TTFL drives rhythmic expression of ion channels, which help maintain SCN neuronal activity oscillations (Ko *et al.*, 2009; Allen *et al.*, 2017). For example, evidence in rat SCN shows that the neuronal Na^+/K^+-ATPase ion-pump, which regulates the resting membrane potential, exhibits a daytime peak in protein expression and activity as compared to the night (Wang & Huang, 2004). The gene *Kcnma1,* which encodes for a Ca^{2+} activated K^+ channel (also called large conductance potassium channels) subunit, is highly transcribed during the night (Panda *et al.*, 2002). Genes encoding for L-Type and T-type Ca^{2+} channels are also expressed rhythmically (Panda *et al.*, 2002; Nahm *et al.*, 2005). As a result, electrophysiologic properties like membrane potential, input resistance and holding current are under the influence of clock genes and ultimately lead to an SCN that is more depolarized during the day than during the night (Jiang *et al.*, 1997; de Jeu *et al.*, 1998; Colwell, 2011). From this, we can infer that alterations in the electrophysiologic rhythms in SCN tissue slices and cultures may signal that the underlying TTFL is disrupted.

Signaling molecules and peptides in the SCN

The heterogeneous population of SCN neurons contains a variety of neurotransmitters (Pennartz *et al.*, 1998) and produces both inhibitory and excitatory signals (Jiang *et al.*, 1997). The majority of SCN neurons express the neurotransmitter γ-aminobutyric acid (GABA) (Moore & Speh, 1993), which peaks in abundance during the

night. Animals in constant darkness continue to exhibit a rhythm in GABA expression, which indicates GABA expression in the SCN is controlled by the circadian clock (Aguilar-Roblero *et al.*, 1993; van den Pol, 1993). Interestingly, the effect of GABA can be either inhibitory or excitatory. In rat and mouse SCN tissue, GABA application predominantly leads to neuronal inhibition at night and excitation during the day (Wagner *et al.*, 1997; Liu & Reppert, 2000). An experiment by Lundkvist *et. al* (2000) investigated GABA signaling using whole-cell patch clamp recordings in rat SCN slices *in vitro* and found that spontaneous inhibitory postsynaptic activity was not rhythmic, but appeared to be regulated by glutamate-mediated activation of α-amino-3-hydroxy-5-methyl-4-isoxazolepropionic acid receptors (AMPARs) (Lundkvist *et al.*, 2002). Studies focusing on downstream GABA-ergic molecular signaling mechanisms are currently ongoing (Moldavan *et al.*, 2017; Walton *et al.*, 2017; McNeill *et al.*, 2018; van der Vinne *et al.*, 2018; Ono *et al.*, 2019) and excellent reviews (Albers *et al.*, 2017; Ono *et al.*, 2018) highlight the recent work in understanding GABA's role in the SCN.

Two additional major neurotransmitters expressed by the SCN are arginine vasopressin (AVP) and vasoactive intestinal peptide (VIP). Expression of these two peptides helps define subdivisions within the SCN: neurons in the ventral "core" region express VIP, while neurons in the dorsal "shell" region express AVP. Functionally, the core receives retinal input from the RHT and intergeniculate leaflet and sends efferent projections to the shell. The shell receives inputs from the limbic system, hypothalamus and brainstem and sends projections to brain areas like the forebrain, thalamus and hypothalamus (Moore, 1995; Moga & Moore, 1996; 1997; Abrahamson & Moore, 2001). While mice and rats deficient in AVP display decreased amplitudes in activity or sleep rhythms, genetic knockout mice lacking VIP or it's complimentary receptor are completely arrhythmic, implicating VIP as more responsible than AVP in maintaining circadian rhythms (Brown & Nunez, 1989; Harmar *et al.*, 2002; Colwell *et al.*, 2003; Aton & Herzog, 2005; Maywood *et al.*, 2006; Brown *et al.*, 2007; Dragich *et al.*, 2010; Mieda, 2019). Consistent with this, optogenetic studies recently demonstrated that specific stimulation of VIP expressing neurons entrains behavioral activity rhythms in mice (Mazuski *et al.*, 2018). Readers interested in a more extensive discussion of the intertwined role of AVP

and VIP molecular signaling in the SCN are directed to the following reviews: (Welsh *et al.*, 2010; Colwell, 2011; Hastings *et al.*, 2014).

The heterogeneity of SCN signaling molecules is even more complex, as a variety of amino acids, neurotransmitters, and small peptides exhibit rhythmic expression as well. For example, a microdialysis experiment measuring hamster SCN neuron exudate across the day saw that the amino acids glutamate, glutamine, and aspartate display peak abundance during the night (Rea *et al.*, 1993b). GABA and serotonin also exhibit peak expression during the night in SCN tissue (Aguilar-Roblero *et al.*, 1993; Rea *et al.*, 1993b). Recently, a study that combined microdissection of the SCN and liquid chromatography/tandem mass spectrometry detected 18 amino acids and identified ten (including proline, histidine and lysine) that exhibit peak expression during the day (Fustin *et al.*, 2017). Utilization of mass spectrometry also led to identification of known and novel small peptides (i.e., gastrin releasing peptide, little SAAS, and VIP) that are diurnally expressed in SCN tissue (Hatcher *et al.*, 2008; Lee *et al.*, 2010; Southey *et al.*, 2014; Atkins *et al.*, 2018). Characterizing the circadian profile and localization pattern of SCN signaling molecules helps us understand which signals may be important for the maintenance of endogenous and peripheral circadian rhythms. This information is also necessary to understand which signals drive synchronization of the SCN to the environment.

Light-induced glutamate release synchronizes the clock

Daily entrainment cues to the circadian clock are called Zeitgebers (which is German for “time giver”, first coined by Jürgen Aschoff). Non-photic signals to the central clock, like restricted locomotor activity or feeding time, are sufficient to entrain an organism to a particular time schedule (Mistlberger, 1994; Mrosovsky, 1996), but daily photic cues are by far the most powerful entrainment signal to the circadian clock (Rea, 1998; Meijer & Schwartz, 2003; Novak *et al.*, 2008; Colwell, 2011; Fonken & Nelson, 2014). Mechanistically, light stimulates melanopsin-expressing retinal ganglion cells in the eye, which send axonal projections through the RHT that terminate in the SCN (Moore & Lenn, 1972; Pickard, 1985; Johnson *et al.*, 1988; Morin *et al.*, 1992; Morin *et al.*, 1994; Moore, 1995; Morin *et al.*, 2003; Hattar *et al.*, 2006). Electrical or light stimulation of the

RHT results in pre-synaptic release of both glutamate and pituitary adenylate cyclase-activating polypeptide (PACAP) into the ventrolateral core of the SCN (van den Pol, 1991; Castel *et al.*, 1993; de Vries *et al.*, 1993; Shirakawa & Moore, 1994; Berson *et al.*, 2002; Hannibal, 2002; Warren *et al.*, 2003; Tu *et al.*, 2005). This increases the spontaneous action potential rates of neurons up to 20 Hz (Meijer *et al.*, 1998; Aggelopoulos & Meissl, 2000; Drouyer *et al.*, 2007; Golombek & Rosenstein, 2010) and ultimately synchronizes spontaneous neuronal activity rhythms to the light cycle.

In vitro, early- or late-night glutamate application to SCN tissue slices produces an approximate 3 hour phase-delay or -advance, respectively (Ding *et al.*, 1994; Shirakawa & Moore, 1994; Gillette & Mitchell, 2002). Similarly, PACAP application to hamster SCN slices or direct injection to the SCN results in photic-like phase shifts (Harrington *et al.*, 1999). Moreover, PACAP application during the day phase-advances the SCN clock, a time when glutamate and light have no effect (Hannibal *et al.*, 1998; Chen *et al.*, 1999; Gillette & Mitchell, 2002; Beaule *et al.*, 2009). This suggests that the circadian clock's response to light is both time of day dependent and reliant on crosstalk between glutamate and PACAP signaling pathways. Work continues to investigate downstream PACAP signaling mechanisms (Dragich *et al.*, 2010; Webb *et al.*, 2013; Hannibal *et al.*, 2017), but we are more interested in further understanding glutamatergic signaling mechanisms in the SCN.

The SCN expresses a variety of glutamate receptors, including AMPARs, metabotropic glutamate receptors (mGluRs) and N-methyl-D-aspartate receptors (NMDARs). Although AMPARs and mGluRs are involved in the balance of inhibitory and excitatory intracellular communication in the SCN, NMDAR signaling is most responsible for regulating light- and glutamate-induced phase shifts. Application of NMDA induces glutamate-like phase shifts (Hamada *et al.*, 1998; Mintz *et al.*, 1999). Additionally, both *in vivo* light pulses at night (Colwell *et al.*, 1991; Vindlacheruvu *et al.*, 1992; Mintz & Albers, 1997) and *in vitro* glutamate application to SCN slices induce phase shifts that are blocked by NMDAR antagonist co-application (Colwell & Menaker, 1992; Ding *et al.*, 1994; Shibata *et al.*, 1994). This suggests that the phase shifting effects of light at night rely on NMDAR activation. Together, these studies highlight the importance of studying downstream mechanisms occurring after NMDAR activation in the SCN.

NMDARs are ionotropic, hetero-tetrameric transmembrane receptors that are permeable to Na^+, K^+, and Ca^{2+}. NMDAR-dependent intracellular signaling pathways in the SCN are thought to relay time-of-day information to the TTFL via transient influx of extracellular Ca^{2+} (van den Pol *et al.*, 1992; Brancaccio *et al.*, 2013). Molecularly, increases in intracellular Ca^{2+} activate a protein kinase cascade that converges to initiate gene transcription. Briefly, Ca^{2+} binds to and activates calmodulin, which in turn activates calcium/calmodulin-dependent kinase CAMKII via phosphorylation of the Thr286 residue (Agostino *et al.*, 2004). CAMKII then activates the mitogen-activated protein kinase (MAPK) cascade (Akashi & Nishida, 2000) and leads to activation of cAMP response element binding protein (CREB) via phosphorylation of Ser133 and Ser 142 (Ginty *et al.*, 1993; Ding *et al.*, 1997; von Gall *et al.*, 1998; Yokota *et al.*, 2001; Gau *et al.*, 2002). CREB is a transcriptional regulator that binds to DNA sequences (called CRE-elements) to stimulate immediate-early gene (Hastings *et al.*, 1995) and clock gene transcription (Yokota *et al.*, 2001; Tischkau *et al.*, 2003). Thus, application of NMDA to SCN cells results in MAPK and CAMKII activation, phosphorylation of CREB, and induction of the immediate early gene c-fos (Vindlacheruvu *et al.*, 1992), which ultimately phase-shifts SCN circadian clock gene expression (Tamaru *et al.*, 2000).

Rhythmic properties of SCN astrocytes

Contributing to the complexity of cellular communication in the SCN, astrocytic signaling is as vital to the SCN circadian clock as neuronal signaling. Extracellular electrophysiology recordings of SCN slices treated with a glial metabolism inhibitor (fluorocitrate) produced ultradian rhythms in neuronal activity the day after drug treatment, demonstrating a role for astrocytes in generating circadian rhythms in the SCN (Prosser *et al.*, 1994). In the SCN, astrocytes display multiple rhythms that persist in slice culture and are required for circadian rhythm synchronization. For example, expression of the astrocyte-specific transporter excitatory amino acid transporter-1 (EAAT1) is rhythmic and peaks the early morning. The EAAT1 expression rhythm is lost in *Per2* mutant mice, which suggests that astrocytic uptake of extracellular glutamate is under circadian control (Spanagel *et al.*, 2005). Other astrocyte-specific rhythms include cycles in metabolism, cytoplasmic Ca^{2+} concentration, glutamate release and adenosine triphosphate (ATP)

release (van den Pol *et al.*, 1992; Womac *et al.*, 2009; Burkeen *et al.*, 2011; Marpegan *et al.*, 2011; Brancaccio *et al.*, 2013).

Recent work shows that both astrocytic intracellular Ca^{2+} concentration and glutamate release oscillate with ~ 24-hour periods that peak during the night and are out of phase with neuronal activity rhythms (Brancaccio *et al.*, 2013; Brancaccio *et al.*, 2017). Later studies found that SCN astrocyte-specific *Bmal1* deletion or removal of *CK1ε tau* (a genetic mutation that shortens the period of behavioral locomotor rhythms) lengthens the period of wheel running behavior in mice (Barca-Mayo *et al.*, 2017). Further, Brancaccio *et. al* (2019) found that transfection of SCN slices obtained from CRY1/2-null mice with an adeno-associated virus (AAV) that initiates astrocyte-specific expression of CRY1 restores rhythms in astrocytic glutamate release and behavioral activity. Thus, endogenous rhythms generated by astrocytes are necessary to maintain SCN and organismal circadian rhythms.

An important characteristic of astrocytes is that the extent and efficiency of their communication depends on their proximity to each other and to neuronal synapses. Therefore, changes in astrocytic morphology (for example, in response to increased neuronal activation, injury, or as a result of neurological disease) can disrupt intercellular communication (Theodosis *et al.*, 2004; Theodosis *et al.*, 2008; Cheng *et al.*, 2019; Zhou *et al.*, 2019). In the hamster SCN, cells containing glial fibrillary acidic protein (GFAP), an astrocyte-specific cytoskeletal protein, are more ramified (a more complex morphological phenotype as compared to cells with an amoeboid shape) during the night than during the day (Lavialle & Serviere, 1993). Subsequent ultrastructural analysis of astrocytes in the SCN determined that astrocytic filopodial insertion into the synaptic space is rhythmic (Becquet *et al.*, 2008). This rhythmic synaptic insertion is cell-type specific, as dendrites of VIP neurons interface with glial appositions more at night [Zeitgeber time (ZT) 18], while the highest coverage of AVP dendrites occurs during the day (ZT 2) (Girardet *et al.*, 2010). Diurnal variation in glial coverage of VIP neurons is eliminated when mice are treated with a tyrosine receptor kinase-B (TrkB) inhibitor, 1NaPP1, suggesting the involvement of brain derived neurotrophic factor [(BDNF); a synaptic plasticity protein that is the ligand for TrkB)], in regulating astrocyte morphology in the SCN (Girardet *et al.*, 2013). Astrocyte-specific *Bmal1* deletion increases gene transcription of markers

associated with “activated” astrocytes (including *Gfap, Aquaporin 4,* and *Serpina3n*), a phenotype that normally describes astrocytic responses after neuronal stimulation or injury (Zamanian *et al.*, 2012; Lananna *et al.*, 2018). Additionally, the complexity of astrocytic filopodial extensions increases, suggesting that cyclic changes in astrocytic morphology are regulated by the TTFL (Lananna *et al.*, 2018).

The extracellular environment’s role in circadian rhythm regulation

The mechanisms that underlie phase-shifting in the SCN circadian clock not only depend on the intracellular processes described above, but also on a variety of extracellular processes that regulate the composition of the extracellular space (ECS). Summarized in a recent review, many ECS components and related proteins [i.e., membrane receptors, cellular adhesion molecules, extracellular proteases, extracellular matrix (ECM) molecules] are implicated in circadian rhythm regulation (Cooper *et al.*, 2018). Here, we will introduce a few that are relevant to the research presented in the upcoming chapters.

BDNF is involved in myriad neuronal processes (Kowiański *et al.*, 2018), including the promotion of long-term potentiation (LTP) (Li *et al.*, 1998; Ying *et al.*, 2002) and suppression of NMDAR-mediated glutamatergic excitotoxicity (Mattson *et al.*, 1995; Almeida *et al.*, 2005; Lau *et al.*, 2015). In other brain regions, increased neuronal activity increases *bndf* transcription and translation of pro-BDNF. In order for pro-BDNF to be fully active, it must have its pro-domain removed by proteases, either intra- or extracellulary (Tongiorgi *et al.*, 1997; Hetman *et al.*, 1999; Balkowiec & Katz, 2002; Pang & Lu, 2004; Ethell & Ethell, 2007).

Extracellular proteolysis of pro-BDNF to its mature form (mBDNF) is part of a web of interconnected extracellular catabolic pathways. Of importance to our research in the SCN, and to synaptic plasticity across the brain, is mBDNF activation by the serine protease plasmin (Pang *et al.*, 2004). To become proteolytically active, the precursor of plasmin, plasminogen, must have a pro-domain catalytically removed by either tissue-type plasminogen activator (tPA) or its homolog urokinase-type plasminogen activator (uPA) (Tomimatsu *et al.*, 2002; Pang *et al.*, 2004; Hoirisch-Clapauch & Nardi, 2013; Wiera & Mozrzymas, 2015). Once activated by plasmin, mBDNF can bind to and initiate TrkB

kinase activity, which leads to phosphorylation and activation of NMDARs (Black, 1999; Lu, 2003; Yamada & Nabeshima, 2004).

In the hamster SCN, *bdnf* transcription peaks during the day, which precedes the nighttime protein expression peak (Liang *et al.*, 1998). Heterozygous *bdnf* ($BDNF^{+/-}$) knockout mice display dampened amplitudes in behavioral rhythms and take longer to phase shift to light pulses (Liang *et al.*, 2000). It is suggested that TrkB modulates SCN circadian rhythms because TrkB inhibition (using K-252A) blocks both light- and glutamate-induced phase shifts *in vivo* and *in vitro*, respectively (Liang *et al.*, 2000; Allen *et al.*, 2005; Michel *et al.*, 2006). Further, either tPA or uPA activity is required for glutamate-induced phase shifts *in vitro* (Mou *et al.*, 2009; Cooper *et al.*, 2017). Co-application of glutamate with an upstream regulator of tPA/uPA, plasminogen activator inhibitor-1 (PAI-1)(Rockway *et al.*, 2002; Aso, 2007), blocks glutamate-induced phase shifts (Mou *et al.*, 2009; Cooper *et al.*, 2017). Additionally, Cooper et al. (2017) found that uPA mediates glutamate-induced phase shifting in tPA knockout mice, and that uPA support of glutamate-induced phase shifts involves mBDNF-independent mechanisms. Together, these studies highlight the importance of extracellular activation of extracellular proteases and mBDNF in regulating circadian rhythms. However, the precise downstream mechanisms through which these proteolytic cascades affect NMDAR signaling in the SCN are still unknown.

Changes in extracellular matrix affect cellular communication

The ECS contains a complex network of interacting molecules that help regulate cellular communication. ECS components include the extracellular domains of membrane receptors, cell adhesion molecules, neurotransmitters, extracellular proteases, and extracellular matrix (ECM) molecules. Once thought to play a passive role, research within the last 10-15 years collectively agrees that the specific composition of the ECS actively determines the efficacy of a variety of signaling processes (Ruoslahti, 1996; Frischknecht *et al.*, 2009; Frischknecht *et al.*, 2014; Tsilibary *et al.*, 2014). Therefore, correct development and maintenance of the ECS is a requirement for maintaining intercellular signaling events in the brain.

One signaling process affected by changes in the ECM and associated molecules is neurotransmitter diffusion. For example, high densities of intersecting molecules in the synaptic space can impede neurotransmitter diffusion through the ECS (Dityatev & Schachner, 2003; Syková, 2004; Dityatev *et al.*, 2006; Syková & Vargová, 2008). Thus, the composition of the ECS determines the diffusion rate of molecules within the space and thereby affects synaptic signaling efficiency (Rusakov & Kullmann, 1998; Binder *et al.*, 2004; Syková & Vargová, 2008; Vargová & Syková, 2008). When ECM associated molecules are deformed or are deteriorated improperly, it can lead to disrupted neurotransmitter diffusion and can contribute to the development of conditions like schizophrenia, bipolar disease, autism spectrum disorders, and other memory and learning disorders (Bajor & Kaczmarek, 2013; Frischknecht *et al.*, 2014; Tsilibary *et al.*, 2014; Song & Dityatev, 2018).

Extracellular adhesion molecules and their links to the clock

There is wide interest in cell-attached proteins and receptors that interact with the ECM or act trans-synaptically as mediators of intercellular communication in the brain (Dityatev & Schachner, 2003; Cauwe *et al.*, 2007; Frischknecht & Gundelfinger, 2012; Frischknecht *et al.*, 2014; Lassek *et al.*, 2015; Marcoli *et al.*, 2015; O'Callaghan *et al.*, 2017; Ferrer-Ferrer & Dityatev, 2018; Hillen *et al.*, 2018; Song & Dityatev, 2018; Fawcett *et al.*, 2019). These molecules include pre- and post-synaptic cellular adhesion molecules (CAMs), neural cellular adhesion molecules (NCAMs), synaptic CAMs, neuroligins, neurexins, dystroglycans, Ephrins and their receptors, and integrins. These molecules bind to ECM molecules such as collagen, laminin, elastin, fibronectin, and chondroitin sulfate proteoglycans, as well as to their trans-synaptic adhesion molecule partners and ligands. These interactions stabilize the ECM and cellular morphology, thereby affecting synaptic communication (De Luca & Papa, 2017; Song & Dityatev, 2018). Many of these molecules participate in strengthening and/or weakening of neuronal synaptic communication (synaptic plasticity) that occurs during neurodevelopment, fear learning, memory formation, addiction, etc. (Bajor & Kaczmarek, 2013). Because the SCN exhibits multiple forms of iterative plasticity in regards to intercellular communication (Iyer *et al.*,

2014), full understanding of clock regulation requires the study of ECM-associated mechanisms.

Certain CAMs that facilitate the connection between pre- and post-synaptic neurons are emerging as extracellular circadian clock regulators. For example, neuroligins, neurexins, and polysialyated neural cell adhesion molecule (PSA-NCAM) have all been linked to the mammalian master clock (Glass *et al.*, 1994; Shen *et al.*, 1997; Shen *et al.*, 1999; Glass *et al.*, 2000; Shen *et al.*, 2001; Fedorkova *et al.*, 2002; Glass *et al.*, 2003; Prosser *et al.*, 2003; Kiessling *et al.*, 2017). Neuroligin-1 (NLG-1), a CAM known to interact with NMDARs (Barrow *et al.*, 2009), exhibits diurnal differences mRNA transcription and protein expression that are lowest in the mouse forebrain during the night and that are eliminated in *Clock* mutant mice (Hannou *et al.*, 2018a). Neurexins, the trans-synaptic binding partners of neuroligins, exhibit cyclic mRNA and protein expression in the mouse SCN (Shapiro-Reznik *et al.*, 2012). PSA-NCAM is highly expressed, particularly on neuronal somas, in the central region of the Syrian hamster SCN during the early morning (Glass *et al.*, 1994; Shen *et al.*, 1999; Glass *et al.*, 2003). The rhythm in PSA-NCAM is also expressed in rat SCN slices, and exogenous application of endoneuraminidase-N (which cleaves PSA from NCAM) *in vitro* eliminates glutamate-induced phase shifts in neuronal activity rhythms (Prosser *et al.*, 2003). As intercellular communication relies on the interactions of CAMs with themselves and other extracellular molecules, their cleavage by extracellular proteases can be disruptive. Two of these proteases, matrix metalloproteinase 2 and 9 (MMP-2 and -9), are associated with CAM degradation and are implicated in circadian rhythm regulation.

Matrix Metalloproteinases

The MMP's are a large family of extracellular proteases that contain at least 25 different members. MMP's are translated and secreted into the ECS as zymogens, inactive proteins containing a short pro-domain that blocks their active site. Collectively, activated MMP's degrade a large proportion of ECM proteins and can be subdivided into groups based on their structural homology. For example, "membrane-type" MMP's (MT1-MMP, MT2-MMP, MT3-MMP, and MT5-MMP) contain a unique transmembrane domain followed by a cytoplasmic tail. Some MMP's are glycosylphosphatidylinisotol-linked, like

MT4-MMP and MT6-MMP. Other subgroups, like the collagenases (MMP-1, MMP-8, MMP-13, and MMP-14) and the gelatinases (MMP-2 and MMP-9), are categorized by their preferred substrate (Ethell & Ethell, 2007; Cieplak & Strongin, 2017). A comprehensive discussion of each member of the MMP family reaches beyond the scope of this introduction, but are the focus of excellent reviews (Visse & Nagase, 2003; Nagase *et al.*, 2006; Ethell & Ethell, 2007; Rodriguez *et al.*, 2010; Cieplak & Strongin, 2017). For our investigation, we chose to focus on two prominent MMP's in the brain that are expressed in the SCN, MMP-2 and MMP-9 (Agostino *et al.*, 2002).

MMP-2 and MMP-9 are the sole members the gelatinase MMP sub-family. Both MMP-2 and MMP-9 are Zn^{2+}-dependent endopeptidases that contain a short N-terminal pro-domain, a conserved Zn^{2+} binding (HExxHxxGxxH) catalytic domain, three cytosine-rich fibronectin-type II inserts, a short hinge domain and a C-terminal hemopexin domain. Activation of MMP-2/9 occurs after secretion into ECS, where a short pro-domain is removed by extracellular proteases. For MMP-2, this is accomplished by either stromelysin (also called MMP-3) or by plasmin. MMP-2 and plasmin both can activate MMP-9. In the ECS, tissue inhibitors of metalloproteinase-1 and -2 (TIMP-1 and TIMP-2) can bind and inhibit MMP-9 and MMP-2, respectively. Mechanistically, the TIMP-1/MMP-9 heterodimer binds to MT1-MMP and forms a large cell membrane complex that is internalized and marked for proteolytic degradation. After seizure induction in the prefrontal cortex, TIMP-1 is initially secreted into the ECS by astrocytes and then by neurons (Rivera *et al.*, 1997), suggesting MMP-9 inhibition could be time-dependent and cell-type specific.

MMP's are pivotal regulators of structural brain plasticity

Most MMPs can degrade ECM scaffolding molecules like collagen, laminin and fibronectin (Mott & Werb, 2004), but MMP-2 and MMP-9 are best known for their ability to cleave cellular adhesion molecules (i.e. β- dystroglycan, neuroligins, and NCAMs) (Michaluk *et al.*, 2007; Shichi *et al.*, 2011; Peixoto *et al.*, 2012), cell surface receptors (EphB2 and β1-integrin) (Ogier *et al.*, 2006; Atapattu *et al.*, 2014) and extracellular growth factors [pro-BDNF, transforming growth factor-β (TGFβ), and vascular endothelial growth factor (VEGF)] (Bruno & Cuello, 2006; Mizoguchi *et al.*, 2011). Due to their wide range

of substrates and their ubiquitous expression throughout the brain, it is not surprising that MMP-2/9 participate in many neuronal plasticity processes (Van den Steen *et al.*, 2002; Rodriguez *et al.*, 2010).

Structural plasticity is a hallmark of many brain functions and dysfunctions. Growth and development, healthy and cancerous cell migration (Demuth & Berens, 2004; Björklund & Koivunen, 2005), synaptic plasticity, (Nagy *et al.*, 2006), cell death (Gu *et al.*, 2002) and neurodegeneration all involve extracellular structural rearrangements and generally require MMP-2 and/or MMP-9 activity (Malemud, 2006). As MMP-2/9 are expressed by neurons (Backstrom *et al.*, 1996), astrocytes and microglia (Maeda & Sobel, 1996), and cleave myriad extracellular molecules (Cauwe *et al.*, 2007), they are pivotal regulators of cellular morphology in development and throughout adulthood. For example, during developmental granular cell migration in the cerebellum, MMP-2, MMP-9, TIMP-1, and TIMP-2 expression is upregulated (Rivera *et al.*, 1997; Vaillant *et al.*, 1999; Jaworski, 2000). Further, MMP-2/9 mRNA transcript expression increases during cerebellar cortex development and levels off around post-natal day 6, but MMP-2/9 proteolytic activity remains high until post-natal day 21 (Ayoub *et al.*, 2005). This activity is important for neuronal stem cell migration in mice, because either MMP-2/9 inhibition or genetic deletion of MMP-9 disrupts this developmental process (Vaillant *et al.*, 2003; Ayoub *et al.*, 2005).

Throughout the adult brain, the roles of MMP-2/9 are multifaceted (De Luca & Papa, 2017). MMP-2/9 knock-out mice show deficiencies in learning, memory, addiction formation and fear acquisition, poor stroke outcome, increased risk of seizures, etc., which suggests that the effects of MMP-2 and MMP-9 catalytic activity are stimulus dependent. In cultured hippocampal neurons, glutamate application increases MMP-9 protein expression in dendrites and increases MMP-9 activation; as measured by increased cleavage of its substrate, β-dystroglycan (Dziembowska *et al.*, 2012). Hippocampal LTP, a form of synaptic plasticity necessary for learning and memory formation that is initiated by increased excitatory post-synaptic current, is eliminated by chemical inhibition of MMP-9 or by exogenous TIMP-1 application (Nagy *et al.*, 2006; Bozdagi *et al.*, 2007; Meighan *et al.*, 2007; Okulski *et al.*, 2007). Additionally, acquisition of fear memories in the amygdala is dependent on MMP-9 activity (Ganguly *et al.*, 2013;

Knapska *et al.*, 2013). MMP-2 and MMP-9 are also activated by more traumatic stimuli. Excitotoxic events like kainate-induced seizures or focal cerebral ischemia increase both MMP-2 and MMP-9 mRNA expression in neuronal dendrites and astrocytic filopodia (Heo *et al.*, 1999; Konopacki *et al.*, 2007). Together these studies illustrate that increased MMP-2/9 activity is a common response to a variety of stimuli in the adult brain.

Alterations in cellular morphology are also regulated by MMP-2/9 activity. For example, dendritic spine formation and retraction that occur during LTP both require MMP-2/9 enzymatic activity (Wang *et al.*, 2008a; Bilousova *et al.*, 2009; Ould-yahoui *et al.*, 2009; Michaluk *et al.*, 2011). Studies in the supraoptic nucleus, a brain region known to undergo morphological plasticity associated with AVP and oxytocin secretion (Oliet *et al.*, 2004; Theodosis *et al.*, 2004), show that MMP-2/9 activity is necessary for neuronal structural rearrangements of magnocellular neurons (Maolood *et al.*, 2008). MMP-2 and -9 have also been shown to modulate astrocyte morphology, which in turn affects astrocyte function (Abbott, 2002). In primary astrocytic cultures, MMP-2 expression is pericellular and localizes to astrocytic filopodial-like processes (called endfeet). Further, MMP-2 activity is required for astrocytic migration through an agarose drop (Ogier *et al.*, 2006). In a similar study that used interleukin-1β to induce astrocytic migration, both MMP-2/9 chemical inhibition and siRNA (specifically targeting MMP-9 transcription) treatment reduced the number of migratory astrocytic cells cultured from the rat cerebrum (Yang *et al.*, 2015). These studies show proteolytic regulation of the extracellular environment, by both MMP-2 and MMP-9, is necessary for the structural changes that facilitate synaptic plasticity and cellular morphology (Romanic *et al.*, 1998).

Although the actions of MMP-2 and -9 are often studied together, there is evidence for divergent functions of the two proteases. For example, specific inhibition of MMP-9, but not MMP-2, reduces excitotoxic cell death in rats (Jourquin *et al.*, 2003). Only MMP-2 activity, on the other hand, is necessary for increased migration of cultured astrocytes (Ogier *et al.*, 2006). Along the same line, NMDA treatment only increases MMP-2 activity in a glioma cell model (U251MG cells) (Ramaswamy *et al.*, 2014). Thus, it is important to differentiate between the activities of these proteases when possible.

MMP-2/9 dependent cleavage of β-dystroglycan regulates cellular activity and morphology

Ultimately, the consequence of MMP-2 and/or MMP-9 activity depends on substrate availability. One well-characterized substrate of MMP-2/9 implicated in cellular and synaptic plasticity regulation is the dystroglycan complex (Michaluk *et al.*, 2007; Bozzi *et al.*, 2009; Sbardella *et al.*, 2012). This protein complex contains two subunits, the transmembrane β-dystroglycan and extracellular α-dystroglycan. β-dystroglycan binds intracellularly to dystrophin (Jung *et al.*, 1995), while α-dystroglycan interacts with extracellular molecules like laminin, neurexin, agrin, aggrecan and perlecan via carbohydrates on its glycosylated sidechains (Sugita *et al.*, 2001; Michele *et al.*, 2002; Barresi & Campbell, 2006). Together they act as a bridge to stabilize intracellular actin cytoskeleton interactions with ECM molecules (Ibraghimov-Beskrovnaya *et al.*, 1992). In the brain, the interaction of α-dystroglycan with β-dystroglycan is disrupted by MMP-2/9-mediated cleavage of β-dystroglycan. Functionally, this event is necessary for establishment and maintenance of LTP (Michaluk *et al.*, 2007; Huntley, 2012). Addition of an auto-activating form of MMP-9 (aaMMP-9) to neuronal cell cultures increases β-dystroglycan cleavage and decreases dendritic branching complexity (Bijata *et al.*, 2015). Overexpression of a defective form of β-dystroglycan, which eliminates both α-dystroglycan binding and MMP-9 catalysis, restores dendritic branch complexity (Bijata *et al.*, 2015). Together, these studies provide evidence that dystroglycan subunits facilitate synaptic plasticity.

The function of α- and β-dystroglycan is also tied to astrocytic morphologic regulation. Ultrastructural studies examining α-dystroglycan expression revealed that it localizes to both neuronal post-synaptic membranes and to perivascular astrocytic endfeet, which indirectly places β-dystroglycan expression near astrocytic extensions (Zaccaria *et al.*, 2001). In dystroglycan knockout mice, astrocytic endfeet association with the vasculature decreases and is disorganized, leading to leakage of the blood-brain barrier (Noell *et al.*, 2011). Further studies show that astrocytic morphological changes are initiated by acute cerebral ischemia and mediated by MMP-2/9 cleavage of β-dystroglycan (Gondo *et al.*, 2014; Yan *et al.*, 2016). To our knowledge, β-dystroglycan has not been studied in the SCN or within the context of circadian rhythms. Given the

close mechanistic ties to MMP-2/9-dependent cleavage, synaptic plasticity and astrocytic morphology regulation, it is worth investigating the role of β-dystroglycan in the mammalian master clock.

Linking MMP's to the mammalian circadian clock

Currently, only one study examining MMP-2/9 activity in the SCN exists (Agostino *et al.*, 2002). Based on the aforementioned evidence that tPA and uPA activity is necessary for glutamate-induced phase shifts in the SCN (Mou *et al.*, 2009; Cooper *et al.*, 2017) and that tPA/uPA activity leads to plasmin-mediated MMP activation (Wang 2003), we hypothesized that MMP activity gates glutamate-induced phase shifting in the SCN. Therefore, we began investigating the role of MMP-2 and MMP-9 enzymatic activity in the SCN.

Figure 1.1 contains a diagram outlining potential actions through which MMP-2/9 could be acting within the SCN. We hypothesize that proteolytic activation of MMP-2/9 by plasmin increases mBDNF-mediated TrkB activation and therefore modulates NMDAR activity. If true, this would suggest that MMP-2/9 activity gates glutamate-induced phase-shifts in SCN neuronal activity rhythms. Secondly, we hypothesize that MMP-2/9 extracellular activity in the SCN regulates the diurnal rhythm in astrocytic morphology via CAM cleavage. Because MMP-2/9 cleavage of β-dystroglycan alters astrocytic morphology in other brain regions, we also hypothesize day vs. night differences in astrocytic morphology are mediated by β-dystroglycan degradation.

In Chapter 2, we focus on experiments characterizing MMP-2/9 expression, activity and related signaling mechanisms in the SCN. The data suggest a functional role of MMP-2/9 in maintaining SCN circadian rhythms phase regulation via NMDAR activation. In Chapter 3, we use quantitative measurements to characterize SCN astrocytic morphology across time and examine a potential link between MMP-2/9-mediated β-dystroglycan degradation as an underlying mechanism regulating diurnal changes in astrocytic morphology.

Appendix: Figures for Chapter 1

Figure 1.1: Potential pathways linking MMP-2/9 activity to circadian processes in the SCN.

We hypothesize that in the suprachiasmatic nucleus (SCN) plasmin proteolytically activates matrix metalloproteinase (MMP)-2 and MMP-9. In the extracellular space (ECS), activation of plasmin occurs through tissue/urokinase-type plasminogen activator (tPA/uPA)-mediated proteolysis of plasminogen. Activated plasmin cleaves pro-brain derived neurotrophic factor (pro-BDNF) to its mature form (mBDNF), which then binds to and activates tyrosine kinase B (TrkB) receptors. TrkB phosphorylates and primes N-methyl-D-aspartate receptors (NMDARs); which is known to gate glutamate-induced, Ca^{2+} dependent phase shifts of the SCN circadian clock. In other areas of the brain, intracellular Ca^{2+} also leads increased pro-MMP secretion into the ECS. Because pro-BDNF is a substrate for MMP-2/9 as well, we predict that MMP-2/9 activity mediates glutamate-induced phase shifts. However, due to the variety of potential MMP-2/9 substrates, MMP-2/9 may play multiple roles in the SCN. For example, MMP-2/9 could cleave extracellular matrix (ECM) molecules (i.e., collagen and laminin) and/or pre- and post- synaptic adhesion molecules. MMP-2/9 dependent cleavage of the dystroglycan complex could also mediate diurnal changes in astrocytic morphology, a phenomenon under circadian regulation in the SCN.

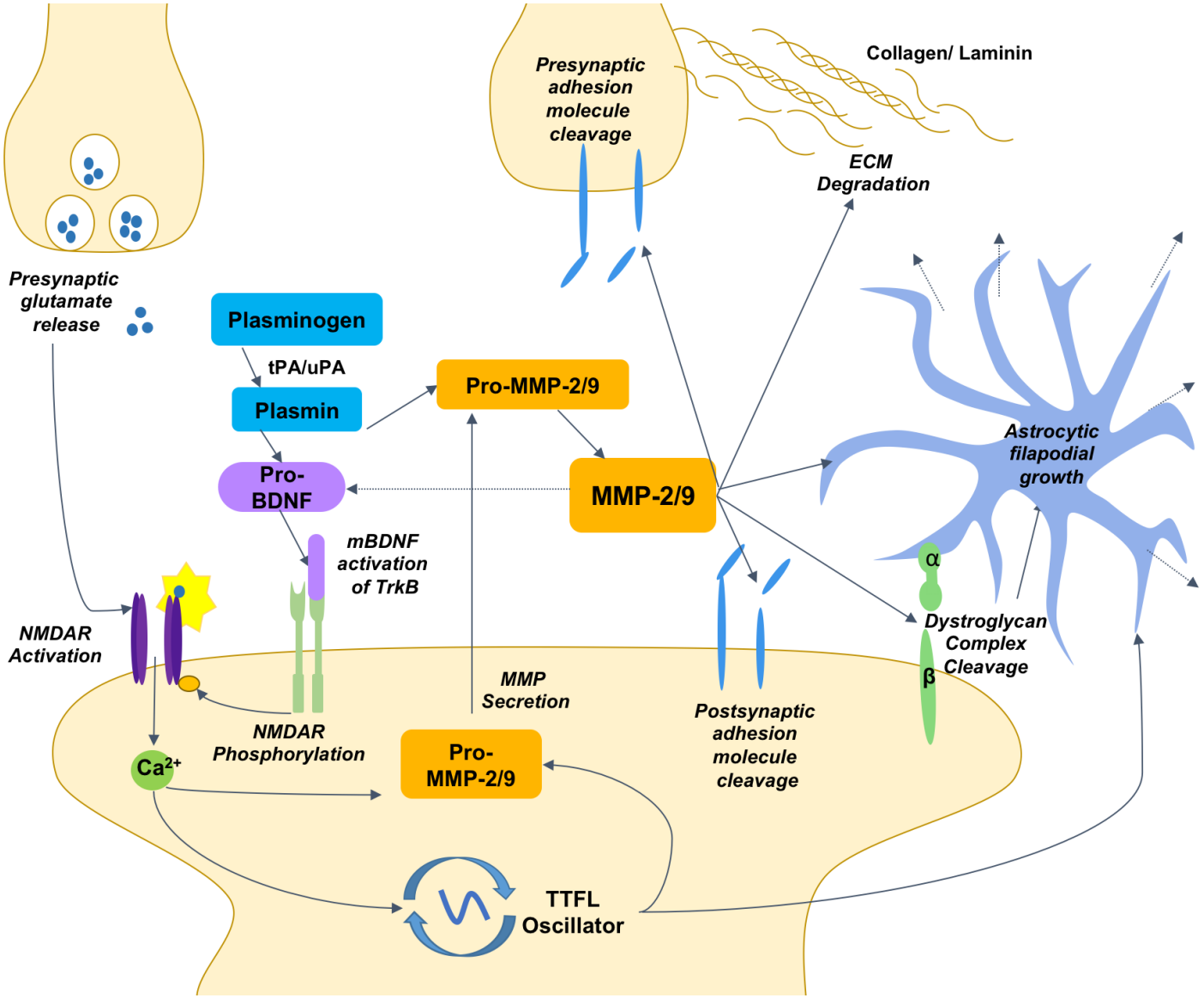
Presynaptic adhesion molecule cleavage
Collagen/ Laminin
ECM Degradation
Presynaptic glutamate release
Plasminogen
tPA/uPA
Plasmin
Pro-MMP-2/9
Pro-BDNF
MMP-2/9
Astrocytic filapodial growth
mBDNF activation of TrkB
NMDAR Activation
α
Dystroglycan Complex Cleavage
β
MMP Secretion
NMDAR Phosphorylation
Postsynaptic adhesion molecule cleavage
Ca2+
Pro-MMP-2/9
TTFL Oscillator

CHAPTER II: TIME OF DAY DETERMINES LEVEL AND OUTCOME OF MATRIX METALLOPROTEINASE-2 AND -9 ACTIVITY IN THE MAMMALIAN CIRCADIAN CLOCK.

A version of this chapter is currently being prepared for submission by Kathryn A. Halter and Rebecca A. Prosser.

The manuscript written below contains original work designed, executed and analyzed by Kathryn Halter. Rebecca Prosser contributed to the experimental design, data analysis, and revisions of the manuscript.

Abstract

Coordinating endogenous physiological and behavioral rhythms with the external environment is an important function of the mammalian master clock, located in the suprachiasmatic nucleus (SCN). Proper entrainment depends on a complex network of intracellular mechanisms. However, the extent to which the extracellular matrix (ECM) and associated molecules participate in this process is only beginning to be appreciated. This study aims to elucidate the role of two ECM proteases, matrix metalloproteinase (MMP) 2 and 9, in the SCN. Our results demonstrate that both MMP-2 and MMP-9 proteins are expressed and active in mouse SCN tissue. Utilizing *in situ* zymography, we confirmed MMP-2/9 activity is greater in the SCN than in the surrounding hypothalamus. Although total expression of neither protein exhibits day-night differences, analysis of their enzymatic activity using gelatin zymography revealed that MMP-9 activity is highest during the day. Investigation of MMP-2/9 functional relevance using *in vitro* extracellular electrophysiological recordings demonstrates that blocking MMP-2/9 activity using the selective inhibitor 2-(benzenesulfonylamino)-N-hydroxy-3-phenylpropionamide (BiPS) shifts SCN circadian clock phase in a time dependent manner. Application of BiPS during the mid-day and early night induces phase advances and delays, respectively. Conversely, BiPS application during the late night, when MMP-9 activity is lowest, has no effect on clock phase. We further determined that all phase shifts induced by BiPS depend on NMDA receptor activity, but only daytime phase advances require catalytic activity of plasmin and TrkB receptor activation. Together, these findings suggest clock regulation of MMP-9 activity and highlight metalloprotease involvement in SCN circadian clock phase regulation.

Introduction

The mammalian circadian clock in the suprachiasmatic nucleus (SCN) generates endogenous daily rhythms and synchronizes mammalian physiology and behavior to the external environment. Generation and maintenance of these rhythms depends on multiple levels of neuronal plasticity. Oscillations in gene transcription, protein expression, metabolism and neuronal activity in the SCN, which are fundamental elements of the circadian oscillator, adjust their phase in response to entraining signals to maintain proper phase with the environment (Golombek & Rosenstein, 2010; Muraro *et al.*, 2013). Desynchronization of circadian rhythms contributes to poor health outcomes. For example, chronic phase misalignment of circadian rhythms to the environment contributes to disorders in metabolism, sleep, mood, and endocrine function (Scheer *et al.*, 2009; Golombek & Rosenstein, 2010; Lall *et al.*, 2012; LeGates *et al.*, 2012; Lucassen *et al.*, 2016). Therefore, a full understanding of the underlying mechanisms that regulate phase-shifting is warranted.

Many factors can serve as “time of day” signals (or Zeitgebers; German for “time-giver”) but the circadian clock is primarily entrained by light. In animals kept in constant darkness, light signals during the early or late night can delay or advance, respectively, the phase of the SCN circadian clock. This effect is mimicked *in vitro* by glutamate application to SCN-containing brain slices during the early and late night, where a change in clock phase is detected as a shift in the peak of neuronal activity rhythms (Prosser *et al.*, 1993; Ding *et al.*, 1994; Gillette & Mitchell, 2002). It is established that photic/glutamate entrainment of behavioral and neuronal activity rhythms requires activation of N-methyl D-aspartate receptors (NMDARs) (Rea *et al.*, 1993a; Mintz *et al.*, 1999; Bendova *et al.*, 2012). The mechanisms contributing to NMDAR-mediated phase shifts are complex. Growth factors, protein kinases, intracellular scaffold proteins and a variety of extracellular molecules are all implicated in modulating NMDAR-dependent signaling in the SCN (Blanke & VanDongen, 2009; Cooper *et al.*, 2017; Cooper *et al.*, 2018)

Intracellular mechanisms of NMDAR-mediated regulation of the circadian clock have been investigated extensively in the SCN, but the exact extracellular proteolytic mechanisms governing NMDAR-dependent phase shifts are unknown. Previous work in

our laboratory determined that glutamate-induced phase shifts in SCN brain slices require activity of the extracellular protease tissue-type plasminogen activator (tPA) (Mou *et al.*, 2009). Additionally, cleavage of pro-brain derived neurotrophic factor (pro-BDNF) to its mature form (mBDNF) by tPA mediated activation of the serine protease plasmin is necessary for glutamate-induced phase shifts. More recently, Cooper et al. (2017) found that urokinase-type plasminogen activator (uPA) mediates glutamate-induced phase shifts in tPA knockout mice, although uPA appears to act through mBDNF-independent mechanisms (Cooper *et al.*, 2017). Thus, extracellular proteolytic activity tightly regulates entrainment of the SCN circadian clock and we hypothesize that other substrates of plasmin known to affect NMDAR signaling could likewise be involved in glutamate-induced phase shifts.

Two candidate molecules activated by plasmin are the extracellular matrix (ECM) proteases matrix metalloproteinase 2 and 9 (MMP-2 and MMP-9) (Ethell & Ethell, 2007; Rodriguez *et al.*, 2010; Li *et al.*, 2016). These two metalloproteases are initially secreted into the extracellular space as inactive zymogens and activated after the catalytic site of the protein is exposed by removal of a small, pro-domain peptide (Visse & Nagase, 2003; Verslegers *et al.*, 2013). MMP-2 and MMP-9 are often studied together, due to their structural homology and their shared ability to cleave similar extracellular matrix (ECM)-associated substrates (Ethell & Ethell, 2007). These proteases are ubiquitously expressed in the brain and their activity is necessary for regulating cellular growth, development, synaptic plasticity and injury response in a variety of brain regions (Malemud, 2006; Ogier *et al.*, 2006; Bozdagi *et al.*, 2007; Michaluk *et al.*, 2011; Szepesi *et al.*, 2013; Stawarski *et al.*, 2014; De Stefano & Herrero, 2016; Abdelnaseer *et al.*, 2017). MMP-2/9 also play a role in neuronal activity regulation, as MMP-2/9 mediated cleavage of ECM and cellular adhesion molecules (CAMs) increases NMDAR activation and trafficking to the post-synaptic membrane (Bozdagi *et al.*, 2007; Gorkiewicz *et al.*, 2010; Kupai *et al.*, 2010; Ning *et al.*, 2015; Niculescu *et al.*, 2018).

MMP expression and/or activity has been linked to circadian clocks in both vertebrates and invertebrates. Expression of two *Drosophila melanogaster* homologs of mammalian MMPs*, Dm1-MMP* and *Dm2-MMP*, is required for motorneuron development and axonal growth (Miller *et al.*, 2008). Moreover, *Dm1-MMP* exhibits increased

expression in response to Clock-induced DNA transcription (Kadener *et al.*, 2007). In *Drosophila*, it is known that the axonal projections of circadian clock neurons exhibit greater complexity during the day than the night. Interestingly, this rhythm is eliminated by genetic overexpression of *Dm1-MMP* and *Dm2-MMP* (Depetris-Chauvin et al., 2014). Further, wildtype *Drosophila* given an shRNAi to knockdown *Dm1-MMP* transcription exhibit arrhythmic locomotor behavior (Depetris-Chauvin *et al.*, 2014). In hamsters, both MMP-2 and MMP-9 are enzymatically active in SCN tissue homogenates, but only MMP-9 shows increased activity during the night (Agostino *et al.*, 2002).

In addition to the MMP-2/9 studies performed in the hamster SCN (Agostino *et al.*, 2002) and the clock neurons in drosophila (Kadener *et al.*, 2007; Nagoshi *et al.*, 2010), other researchers have explored circadian regulation of MMP-2/9 in other locations. One study examined MMP-2/9 activity in the hippocampus and did not observe a diurnal variation in enzymatic activity of either protease (Nishijima *et al.*, 2015). Using isolated trabecular meshwork cells of the eye, Li et al. found that 24-hr temperature oscillations drive rhythmic MMP-2/9 activity (Li *et al.*, 2015). In a cardiac tissue-specific *Bmal1* knockout mouse, MMP-9 and its endogenous inhibitor TIMP-1 exhibit increased expression in the heart relative to wildtype mice (Ingle *et al.*, 2015), suggesting that MMP-9 expression could be under circadian clock control.

While intriguing, these studies provide little insight into the functional role of MMP-2 and MMP-9 in modulating mammalian circadian rhythms. Given the importance of NMDAR activity in modulating SCN circadian clock phase and evidence that MMP-2/9 affects NMDAR activity, we sought to determine MMP2/9 expression and activity in the mouse SCN and test whether they modulate SCN circadian clock phase.

Materials and Methods

Brain slice preparation

All mice handling and dissection followed University of Tennessee, Knoxville Institutional Animal Care and Use Committee approved protocols. Brains were harvested during the lights-on period from adult male, C57BL/6 mice (Envigo, Indianapolis, IN) housed in a 12:12 light:dark cycle, with food available *ad libitum*. Brain slices containing the SCN were maintained in a perfusion dish containing Earle's Balanced Salt Solution

(EBSS; MP Biomedicals, Solon, OH), supplemented with gentamicin, dextrose, and sodium bicarbonate, saturated with 95% O_2/5% CO_2, and kept at 37°C (Prosser & Gillette, 1989; Prosser *et al.*, 1994; Mou *et al.*, 2009; Yamada & Prosser, 2014; Cooper *et al.*, 2017).

Western blotting

SCN brain slices prepared as described above were maintained in constant conditions until collection at Zeitgeber time (ZT; where ZT 0 corresponds to lights-on and ZT 12 corresponds to lights-off in the animal colony) 6, ZT 16 or ZT 23 on the day of brain slice preparation (Day One *in vitro)*. SCN tissue was rapidly frozen at -80°C at the time of collection. Protein extraction occurred under reducing conditions and protein concentration was measured using the Bradford assay. SCN protein samples (10 µg), recombinant human MMP-2, and recombinant mouse MMP-9 (Calbiochem, San Diego, CA; 100 ng each), were loaded into 4-12% Bis-Tris BOLT gels (Invitrogen, Carlsbad, CA) and separated by electrophoresis in 1X MOPS [(3-(N-morpholino)propanesulfonic acid] buffer (Invitrogen). Proteins were transferred to Immobilon-PVDF membranes using a Trans-Blot Turbo transfer system (BioRad, Hercules, CA). The IR-Western blot protocol provided by Li-COR ["Near-Infrared (NIR) Western Blot Detection Protocol", available online] was used to fluorescently label pCAMKII (p1005-286, 1:1000; PhosphoSolutions, Aurora, CO), MMP-2 (MAB13406, 1:1,000 dilution; EMD Millipore, Billerica, MA) or MMP-9 (AB19016, 1:1,000 dilution, EMD Millipore). Actin (sc-1616, Santa Cruz Biotechnologies, Dallas, TX) served as a loading control. Blots were then incubated with fluorescent secondary antibodies conjugated to LI-COR IR-Dye® and signal intensities for protein samples were collected with an Odyssey®-CLx system (LI-COR Biosciences, Lincoln, NE). Band intensity analysis was performed using the Image Studio Lite™ v 5.0 software (LI-COR Biosciences). Fluorescent signal for each protein was measured as pixel density minus background pixel density and reported as total signal. The total signal of bands corresponding to each protein was normalized to the total signal of the actin band.

Gelatin zymography

SCN-containing brain slices were prepared and maintained as described above. Tissue was collected at ZT 6, ZT 16 and ZT 23 and frozen at -80°C. Proteins for gelatin zymography were extracted following an adapted zymography protocol (Toth & Fridman, 2001; Kupai *et al.*, 2010). Briefly, samples were lysed in buffer containing 0.5% Triton-X-100 and 50 mM Tris (BioRad). Samples were centrifuged at 13,000 g for 10 min at 4°C. Protein concentration was measured using a Bradford assay. Protein samples were diluted with Gelatin Zymography Sample Buffer (BioRAD) and then loaded into a 0.1% gelatin zymogram (Invitrogen). After separation by electrophoresis, zymograms were washed in a renaturing solution of 2.5% Triton-X100 and subsequently incubated in a solution of 50 mM Tris, 0.15 M NaCl, and 10 mM $CaCl_2$ at 37°C for five days. Gels were stained with Coomassie blue for one hour and destained with 4.0/8.0% methanol/ethanol solution until clear, gelatinolytic bands were visible. Gels were imaged using the Odyssey-Clx and inverted images were used for measurement of gelatinolytic bands. Bands were compared to 100 ng of recombinant human MMP-2 and mouse MMP-9 protein for identification. Gelatinolytic activity was measured as pixel density minus background pixel density using Image J Fiji and reported as the mean grey value. For statistical analysis, the mean grey value of all gelatinolytic bands was set relative to the mean grey value of the r-MMP-2 gelatinolytic band.

In situ gelatin zymography

SCN brain slices were prepared and maintained as described above. Control slices were collected 20 minutes before ZT 6, 16 or 23 and slices remaining in the perfusion dish received bath application of 100 nM MMP-2/9 Inhibitor II [2-(benzenesulfonylamino)-N-hydroxy-3-phenylpropionamide, (BiPS; Calbiochem)] (see drug treatment protocol, below) for the 40 minutes surrounding each time point. At collection time, slices were placed in a 1X phosphate buffered saline (PBS, pH 7.4) solution containing 30% sucrose and maintained at 4°C overnight. Slices were then placed in OCT and stored at -80°C until sectioning. Tissue was cut into 10 µM sections with a Leica cryostat. Serial sections were collected and divided onto two VWR Vista Vision™ Histobond® adhesive slides. Slides were stored at -80°C.

In situ zymography was performed according to established protocols (Oh *et al.*, 1999; Gawlak *et al.*, 2009; Aguayo *et al.*, 2018). Slides (thawed to room temperature) were rinsed once with 1X PBS and incubated with a 20 µg/µL stock solution of DQ-Gelatin from Pig Skin, Fluoroscein Conjugate (catalog # D12054, Thermofisher Scientific, Waltham, MA) in zymography reaction buffer (100 mM NaCl, 10 mM $CaCl_2$, 100 mM Tris-HCl, 0.05% Brij-35, pH=7.5) for 18 hours. Negative control slides were incubated with 4% paraformaldehyde (PFA) or 100 nM BiPS to inhibit MMP activity during DQ-Gelatin incubation. Slides were rinsed 3 X 5 minutes in 1X PBS and cover-slipped using Vectashield Antifade mounting medium containing DAPI (Vector Laboratories, Cambridgeshire, UK). Brain regions containing the SCN were identified using neuroanatomical landmarks (the third ventricle and optic chiasm) and the DAPI nuclear stain. Images of sections containing the SCN were taken using a Leica CTR600 Florescence Microscope at 20X magnification for integrated pixel density measurements of the SCN region. DQ-Gelatin, a substrate for MMP-2/9, contains a conjugated fluorophore that becomes unquenched after cleavage by MMP-2/9 and is excited by the 488 nm wavelength. For fluorescent signal analysis, collected images were split into blue (DAPI stain) and green (DQ-Gelatin) channels and a circular region of interest (ROI) was drawn around the SCN region in the blue channel using Image J, Fiji (NCBI) (Schindelin *et al.*, 2012). ROIs were transferred to the green channel and the mean grey value (average pixel density/area) of DQ-gelatin signal in the SCN was measured. This ROI was also duplicated and shifted to a nearby portion of the anterior hypothalamus (AH) to collect the mean grey value. If both bilateral SCN nuclei were present in the tissue sample, the process was repeated for the contralateral nuclei and the two mean grey values were averaged.

In vitro extracellular electrophysiology

Extracellular electrophysiology experiments were performed as outlined previously (Prosser & Gillette, 1989; Prosser *et al.*, 1994; Mou *et al.*, 2009; Yamada & Prosser, 2014; Cooper *et al.*, 2017). Briefly, brain slices were prepared and maintained in a perfusion dish as described earlier, and drug treatments were applied as described below. On the morning of Day 2 or Day 3 *in vitro*, single unit recordings were collected using a glass

electrode containing 3 M NaCl. Neuronal activity was recorded and analyzed from 6-8 neurons each hour, for five minutes each, for a total of 8-10 hours. The data were collected and analyzed using DataWave SciWorks software (DataWave Technologies, Loveland, CO). The average firing rate from each cell recording was calculated and these were then grouped into two-hour running averages for the entirety of the recording. As in prior experiments (Prosser & Gillette, 1989; Prosser *et al.*, 1994; Yamada & Prosser, 2014; Cooper *et al.*, 2017), the mean firing rates ± SEM for each experiment were calculated and plotted using SigmaPlot v 12.0. The time of peak neuronal activity was assessed visually to the nearest quarter hour, and the change in the time of peak firing was expressed in hours deviating from ZT 6 (the time of peak activity in untreated SCN tissue).

Chemical treatments

Drugs were administered to SCN slices via bath application for 40 minutes surrounding ZT 6, ZT 16 or ZT 23 (Day One *in vitro)*. Experimental treatments included: 100 nM BiPS (Calbiochem) to block MMP-2/9 activity (Tamura *et al.*, 1998; Lauzier *et al.*, 2008); 50 µM D-(–)-2-Amino-5-phosphonopentanoic acid, (AP5; Calbiochem), an NMDAR antagonist; 1.0 µM K252a, *Nocardiopsis* sp. (EMD Millipore) to inhibit TrkB receptor activity; and 50 µM α_2-antiplasmin, (α_2-AP; Calbiochem) to inhibit plasmin. Concentrations of the drugs were chosen based on previous findings by our laboratory (Mou *et al.*, 2009) or by the IC_{50} determined by the manufacturer's specifications.

Statistical analysis

Graphpad Prism software v 8.0.1 was used to generate histogram graphs and run statistical analyses. For western blotting (n=5-6) and gelatin zymography experiments (n=5) a significant difference between Zeitgeber times was determined using a One Way ANOVA. Where significant differences were found, a post-hoc Tukey test was performed to assess all pairwise comparisons (Holm-Sidak method). *In situ* zymography results (n=3-6) were analyzed using a Two Way ANOVA with a post-hoc Tukey's multiple comparisons test to assess the effect of time and/or drug treatment between the SCN and the anterior hypothalamus. For electrophysiology experiments where experimental groups were compared to a no-treatment control group (n=3), the differences between

means were determined using a One Way ANOVA analysis with a post-hoc Dunnett's test.

Results

MMP-9 enzymatic activity, but not expression, is lowest during the late night

To begin investigating MMP-2/9 in the SCN, we evaluated both the protein expression level and enzymatic activity of these metalloproteases during the day (ZT 6), early night (ZT 16) and late night (ZT 23). The expression of both MMP-2 and MMP-9 proteins in the SCN was confirmed at each of the time points using western blotting (Fig 2.1 A and B). To assess differences in protein expression across circadian time, fluorescent signal intensity for bands corresponding to MMP-2 and MMP-9 were divided by actin signal (as a loading control). One-way ANOVA of MMP-2 and MMP-9 expression [relative to actin (Fig 2.1 C and D)] revealed no significant time-dependent differences between groups ($p=0.372$, $n=6$; $p=0.064$, $n=5$, respectively).

Next, we investigated the enzymatic activity of MMP-2 and MMP-9 using gelatin zymography (Fig 2.2 A). Similar to western blotting, protein extracts were separated via gel electrophoresis, but gels used for gelatin zymography contain gelatin, a substrate for both MMP-2 and MMP-9. The incubation buffer used contains a mild detergent that exposes the active sites of the proteins, which means that both pro- and active forms of MMP-2 and MMP-9 enzymes can be detected. It also removes any endogenous inhibitors. After staining with Coomassie blue, clear bands corresponding to the molecular weights of the proteins are reported as "gelatinolytic activity" bands. Thus, gelatin zymography does not measure endogenous activity; rather, it is a measure of potential enzymatic activity away from the normal environment and any endogenous regulators (Toth & Fridman, 2001; Vandooren *et al.*, 2013a; Ren *et al.*, 2017). Traditionally, the incubation period of a gelatin zymography gel is 72 hours. However, after 72 h we were unable to visualize any gelatinolytic activity (data not shown). Extension of the incubation period increases the sensitivity of the assay (Kleiner & Stetler-Stevenson, 1994; Ren *et al.*, 2017); therefore, we incubated the gels for five days and detected gelatinolytic activity of our recombinant proteins and in our SCN tissue extracts (Fig 3A). In our SCN extract lanes, we detected MMP-9 at ~98 kD. We also saw a much fainter band at ~72 kD, the

molecular weight of active MMP-2, which can be seen more clearly when the image exposure is increased (Fig 2.2 B). The slight size differences between the recombinant proteins (r-MMP-2 and r-MMP-9) and those in the SCN protein extracts may be due to *in vivo* post translational modifications of MMP-2 and -9 and/or species differences between the human derived r-MMP-2 and our murine samples (Vandooren *et al.*, 2013b).

For comparative analysis, the total signal of gelatinolytic activity of both MMP-2 and MMP-9 on each gel was set relative to the amount of signal produced by the r-MMP-2 band on the same gel (Figure 2.2 C). This was done to control for potential inter-gel variability due to differences occurring during the staining and de-staining procedures. SCN tissue extracts collected at ZT 6, ZT 16 and ZT 23 showed robust differences between MMP-9 gelatinolytic activity than MMP-2 at ZT 6 ($p=0.0023$), ZT 16 ($p=0.009$), and ZT 23 ($p=0.008$). Comparing activity across time, MMP-2 gelatinolytic activity was not different between ZT 6 and ZT 16 (Two Way ANOVA followed by post-hoc Tukey test $n=5$; $p=0.993$) nor ZT 6 and ZT 23 ($p=0.995$). However, the relative level of MMP-9 gelatinolytic activity showed a statistically significant difference. Post-hoc analysis indicated that MMP-9 gelatinolytic activity was significantly higher at ZT 6 than at ZT 23 ($p=0.008$) but not different at ZT 16 ($p=0.337$).

To assess if changing the amount of protein loaded in the zymogram would improve detection of MMP-2 protein in our extracts, we performed an additional experiment in which we loaded increasing amounts of SCN extract into a zymography gel along with SCN samples that had been incubated with BiPS (Fig 2.3). Increasing the total amount of SCN extract did not substantially change the amount of detected MMP-2 or MMP-9 gelatinolytic activity. Further, incubation with BiPS before separation on a gelatin zymogram did not alter the activity of the MMP-9 in the zymogram. We believe that this is due to treating the zymogram with the detergent Triton-X100 after electrophoretic separation. Just as this incubation step removes the pro- domain of the protein from the active site and removes endogenous inhibitors from the MMPs, the detergent likely removed BiPS from the active site of the protein, allowing proteolytic activity.

In situ zymography confirms enhanced MMP activity of in SCN tissue

Next, we assessed MMP-2/9 activity in SCN tissue slices using *in situ* zymography. *In situ* zymography aids in visualizing and localizing MMP-2/9 gelatinolytic activity in brain and other tissues (Gross & Lapiere, 1962; Oh *et al.*, 1999; Yan & Blomme, 2003; Gawlak *et al.*, 2009; Vandooren *et al.*, 2013a; Chhabra & Rani, 2017; Aguayo *et al.*, 2018). Hypothalamic slices containing the SCN were prepared and maintained in a perfusion dish as described above. Control and BiPS-treated slices were collected and prepared as described in the Methods section. Slides containing SCN tissue sections were incubated overnight in zymography buffer containing gelatin molecules fused to quenched fluorescent FITC molecules (DQ-gelatin). The overnight incubation allows active MMP-2/9 to cleave the gelatin and unquench the fluorescent molecules (Mook *et al.*, 2003; Guo *et al.*, 2007). Thus, fluorescence indicates areas containing MMP-2/9 activity. Unlike with gelatin zymography, the activity of MMP-2 vs. MMP-9 cannot be distinguished with *in situ* zymography. After sectioning and staining with DQ-gelatin and DAPI (to confirm the location of SCN nuclei), 20X magnification images of the brain regions containing the SCN and the AH were taken with a fluorescent microscope.

In both our no-treatment and BiPS-treated SCN tissue slices, we observed DQ-gelatin fluorescent signal that overlapped the SCN region (Fig 2.4 A & B). To confirm that the fluorescence was an effect of MMP-2/9 activity, we co-incubated negative control sections with either 4% PFA or 100 nM BiPS in the DQ-Gelatin solution to inhibit MMP-2/9 catalysis. In both cases we observed markedly dampened fluorescent signal (Fig 2.4 C and D). We then quantified the mean grey value corresponding to the fluorescent signal for both the SCN and adjacent AH in the control and BiPS treated slices. This analysis revealed that pre-treatment with 100 nM BiPS *in vitro* did not reduce gelatinolytic activity at any time point, as compared to untreated tissue (Fig 2.4 E, n=3-6, Two-way ANOVA comparison of means ± SEM; $\alpha=0.05$, $p=0.8670$). However, there were regional differences within both control and BiPS treated slices. In ZT 6 control and BiPS slices, the SCN displayed higher gelatinolytic activity than the AH ($p=0.0246$ and $p=0.0225$, respectively). The SCN also displayed higher activity than the AH at ZT 23 ($p=0.0125$), but only in the BiPS treated slices. At ZT 16 no significant differences between gelatinolytic activity between the SCN and AH were observed, although the data in both

cases trended towards significance (control slices, p= 0.0821 and BiPS slices, p=0.0670). To examine this further, we combined the mean grey values of control and BiPS treated SCN tissue samples of all SCN or AH regions at each ZT. One-way ANOVA analysis indicates that the gelatinolytic activity of MMP-2/9 is significantly higher in the SCN at each time point examined (ZT6, p=0.0008; ZT 16, p=0.0004; ZT 23, p=0.0074) as compared to the surrounding AH.

Blocking MMP-2/9 activity alters SCN neuronal activity rhythms

Based on our data showing MMP-2/9 expression and activity in the SCN, next we tested the hypothesis that MMP-2/9 are involved in circadian clock phase regulation. For this we bath-applied the MMP-2/9 inhibitor, BiPS (100 nM) to SCN-containing brain slices and assessed circadian phase of the neuronal activity rhythm the following day. Compared to control slices, which exhibit a peak of activity on the second day *in vitro* at ZT 6 (Fig 2.5 A), we found that BiPS applied at ZT 6 resulted in a significant phase advance of 3.0 ± 0.58 h (n=3; One-way ANOVA, post-hoc Dunnett's Test result p=0.015; Fig 2.5 B, D). Next, we found that bath application of 100 nM BiPS at ZT 16 resulted in a phase delay (-2.7 ± 0.34 h, n=3, Fig 2.5 C, D). In a third set of experiments, we evaluated the effect of BiPS applied at ZT 23. Neuronal activity during the second day *in vitro*, immediately following the ZT 23 treatment, did not exhibit a clear peak in neuronal activity (Fig 2.6 A & B), likely because of acute effects of BiPS on neuronal firing rates. Therefore, we conducted additional experiments where we assessed the phase of the neuronal activity rhythm during the second day after drug treatment at ZT 23 (Day 3 *in vitro*) (Fig 2.6 C, D). Previous studies demonstrate that the phase of the neuronal activity rhythm is consistent across the first 3 days *in vitro* (Gillette & Prosser, 1988), which we confirmed (Fig 2.6 C). Further, BiPS treatment did not significantly shift peak neuronal activity on Day 3 *in vitro* [mean phase shift= 1.0 ± 0.33 h, n=3, Student's t-test with a Mann-Whitney ranked sum test, p=0.333; Fig 2.6 D).

BiPS-induced phase shifts require NMDAR activity

Because BiPS treatment at ZT 16 induced glutamate-like phase delays (Ding *et al.*, 1994), we investigated whether NMDAR activity was required for BiPS-induced phase shifts. The selective NMDAR selective antagonist, AP5, was previously shown to not

affect clock phase when applied alone, but can block glutamate-induced phase shifts and NMDAR dependent excitatory post synaptic potentials in the SCN (Biello *et al.*, 1997; Mintz *et al.*, 1999; Yamada & Prosser, 2014). We followed up these previous studies by assessing the effect of AP5 on SCN neuronal activity rhythms when applied alone at ZT 16 and found no effect on SCN circadian phase (data not shown). Co-application of BiPS with AP5 at ZT 16 induced a mean phase shift of -0.333 ± 0.333 h (n=3) (Fig 2.5 D). One-way ANOVA with a post-hoc Dunnett's test revealed this treatment was significantly different from BiPS application alone, indicating that the ZT 16 phase delay was blocked (p=0.00197). Interestingly, even though glutamate does not induce phase advances when applied alone to the SCN at ZT 6 (Ding *et al.*, 1994; Biello *et al.*, 1997; Mou *et al.*, 2009), co-application of AP5 with BiPS at ZT 6 significantly inhibited the BiPS-induced phase advance (mean phase shift = -0.330 ± 0.333 h, p= <0.001, n=3; Fig 2.5 D).

Daytime but not early night phase shifts induced by BiPS require plasmin and TrkB activation

In other brain regions MMP-2 and MMP-9 are activated by plasmin, and in turn can facilitate activation of pro-BDNF to mBDNF (Ethell & Ethell, 2007; Cao *et al.*, 2014). Given that previous work supports SCN circadian clock phase regulation by mBDNF/TrkB (Liang *et al.*, 1998; Prosser *et al.*, 2008; Mou *et al.*, 2009; Girardet *et al.*, 2013; Yamada & Prosser, 2014), we assessed plasmin and TrkB involvement in BiPS-induced phase shifts. Mou *et al.*, (2009) showed that inhibition of **a)** TrkB activation using K252a and **b)** plasmin activity using α_2-antiplasmin by themselves have no effect on *in vitro* SCN circadian neuronal activity rhythms. When we applied α_2-antiplasmin with BiPS at ZT 16 this treatment resulted in a phase delay of -3.3 ± 0.33 h, (Fig 2.5 D), which was not significantly different from that of BiPS treatment alone (p=0.382, n=3; one-way ANOVA with a post-hoc Dunnett's test). Likewise, when we co-applied K252a with BiPS at ZT 16 this resulted in a phase delay of -2.0 ± 0.30 h (Fig 2.5 D, which again was not statistically different from the effect of BiPS-only treatment (p=0.382, n=3; Fig 2.5 D). Interestingly, when we co-applied α_2-antiplasmin with BiPS at ZT 6, the results showed a significantly decreased phase shift vs. BiPS alone (mean phase shift= 1.3 ± 0.33 h, p=0.0448, n=3; Fig 2.5 D). Similarly, K252A co-application with BiPS at ZT 6 resulted in a significant

inhibition of the phase shift induced by BiPS alone (mean phase shift= 0.50 ± 0.30, p=0.00556, n=3; Fig 2.5 D). Together, these data suggest that early night phase delays induced by disrupting MMP-2/9 activity require activity of NMDARs but appear to be independent of both plasmin activity and TrkB signaling. Conversely, we observed that application of BiPS during the mid-day induced phase advances that depend on the activity of plasmin, NMDARs, and mBDNF activation of TrkB receptors.

BiPS treatment does not affect CAMKII phosphorylation

To better understand the mechanisms involved in BiPS-induced phase shifts, we investigated whether BiPS treatment activates calcium/calmodulin-dependent protein kinase II (CAMKII) in the SCN. Phosphorylation of CAMKII by calmodulin increases after Ca^{2+} influx through active NMDAR or AMPA channels. In addition to serving as a marker of increased neuronal activity, CAMKII phosphorylation is also necessary for long-term potentiation in multiple brain regions (Miller & Kennedy, 1986; Giese *et al.*, 1998; Wang & Peng, 2016). There are four isoforms of CAMKII, of which the α- and β-isoforms are expressed specifically in brain tissue. Phosphorylation of α- and/or β-CAMKII on the Thr-286 residue occurs 1-2 minutes after LTP induction in hippocampal slices and serves as a marker for increased intracellular Ca^{2+} levels and synaptic plasticity (Cho *et al.*, 2007; Senga *et al.*, 2015; Chang *et al.*, 2017). In the hamster SCN, CAMKII phosphorylation, and subsequent kinase activity, peak during the day and are required for light-induced phase shifts, clock gene induction, and circadian rhythms of locomotor activity (Yokota *et al.*, 2001; Nomura *et al.*, 2003; Agostino *et al.*, 2004; Kon *et al.*, 2014). We hypothesized that if BiPS-induced phase shifts at ZT 6 and ZT 16 require NMDAR activation, then these phase shifts would be accompanied by increased phosphorylation of either or both isoforms of CAMKII. Thus, we measured CAMKII phosphorylation of the Thr-286 residue in control SCN tissue and after BiPS treatment using western blotting.

As seen in Figure 2.7, two-way ANOVA revealed no statistically significant differences in either CAMKII isoform across time (p=0.8667) or in response to BiPS treatment (p=0.3436). We further analyzed our data by examining the ratio of phosphorylated α-CAMKII to β-CAMKII (α:β-CAMKII). Previous research shows that higher α:β-CAMKII ratios lead to increased translocation of heteromeric CAMKII to the

post-synaptic density, where its kinase activity is important for elongation of dendritic spines (Shen *et al.*, 1998). Specifically, increased β-CAMKII can "dock" α-CAMKII to the actin cytoskeleton and promote synaptic plasticity. Comparison of the α:β ratio of CAMKII using a two-way ANOVA also revealed no significant differences across ZT ($p=0.3898$) or between BiPS treatment groups ($p=0.2202$). This indicates that although NMDAR receptor activity is required for BiPS-induced phase shifts at ZT 6 and ZT 16, the level of CAMKII phosphorylation on Thr-286 remains unaffected.

Discussion

The results of these experiments reveal that the extracellular proteases MMP-2 and MMP-9 are expressed and active in the SCN, and that one or both play a role in phase regulation of the SCN circadian clock. Specifically, we show that MMP-2/9 are highly expressed in the SCN compared to surrounding areas, and that MMP-9 exhibits a circadian rhythm in gelatinolytic activity. We further demonstrate that inhibition of MMP-2/9 activity with BiPS at ZT 6 and ZT 16, but not ZT 23, phase-shifts the SCN circadian clock. These are the first data that implicate a functional role for MMP-2/9 in the SCN.

Our data confirm previous work showing that MMP-2/9 are expressed in the SCN and that MMP-9, but not MMP-2, exhibits a circadian rhythm in gelatinolytic activity. While our observation indicates higher MMP-9 activity at ZT 6 vs. ZT 23, Agostino et al. (2002) found that MMP-9 gelatinolytic activity is higher at night (ZT 16) than it is during the day (ZT 4). A few differences exist between these two studies, including the light schedule of housed animals (14:10 LD vs 12:12 LD) and the times of enzymatic assessment. The Agostino *et. al* daytime samples were collected 4 h after lights-on and 10 h before lights-off, while our mid-day collection time was 6 h after lights-on. Additionally, their nighttime collection time was 2 h after lights off, while ours was 4 h. Differences may also be due to our SCN slices being maintained *in vitro* prior to tissue collection rather than the tissue being collected immediately after brain extraction. Importantly, our experimental design allowed us to assess MMP-2/9 expression/activity at the same circadian time points when we assessed their ability to modulate clock phase. Still, we must interpret the results of both studies cautiously because the zymography assay assesses proteolytic activity after removing MMP-2/9 from the endogenous extracellular milieu and electrophoretically

separating them from their endogenous inhibitors, TIMP-1 and TIMP-2. Combined, the results indicate that further research on diurnal and/or circadian differences in MMP-2/9 activation is necessary.

Using *in situ* zymography to assess MMP-2/9 gelatinolytic activity in intact brain slices, we confirmed that MMP-2/9 enzymatic activity is higher in the SCN than in the surrounding AH. However, we did not observe a significant diurnal variation in MMP-2/9 gelatinolytic activity using this assay. Because both MMP-2 and MMP-9 cleave the DQ-Gelatin molecule, it is possible that non-rhythmic endogenous MMP-2 activity obscures a diurnal variation in MMP-9 gelatinolytic activity *in situ*. Further, bound endogenous inhibitors of either MMP, such as TIMP-1 and TIMP-2, could block the detectable level of MMP gelatinolytic activity and account for the differences observed between the level of MMP-9 activity in our assays. Together, our results suggest that BiPS-induced phase shifts coincide with times of higher endogenous MMP-9 enzymatic activity, as indicated by gelatin zymography. These data add to literature supporting circadian regulation of MMP-9 activity, and importantly, are the first to evaluate functional effects of metalloprotease activity in the SCN.

Our MMP-2/9 gelatinolytic activity data also highlight the importance of concurrently investigating protease expression and proteolytic activity. In other brain regions, expression of both MMP-2 and MMP-9 is constitutive, and they only become activated under specific circumstances such as during increased neuronal activity, injury or inflammation (Bozdagi *et al.*, 2007; Ethell & Ethell, 2007; Michaluk *et al.*, 2007; Konnecke & Bechmann, 2013; Ramaswamy *et al.*, 2013; Verslegers *et al.*, 2013). Our results align with this, given that total expression of both MMP-2 and MMP-9 is constant in the SCN, while the gelatinolytic activity of MMP-9 changes across time, and is higher in the daytime when neuronal activity peaks in the SCN. However, we attribute this difference to the higher sensitivity (lower limit protein concentration= 10 pg) of the gelatin zymography assay, as opposed to western blotting (detection range= 50 pg - 100ng) (Ren *et al.*, 2017).

Additional investigations are needed to clarify the regulatory mechanisms controlling the diurnal difference in MMP-9 endogenous activity in the SCN. One candidate protein for this is stromelysin 1 (also known as MMP-3), which also can cleave

pro-MMP-9 (Ogata *et al.*, 1992). Inactivation of MMP-9 can involve TIMP-1 or can occur through MMP-9 binding to membrane bound receptors RECK (reversion-inducing-cysteine-rich protein with kazal motifs) or LRP-1 (low-density lipoprotein receptor-related protein-1), leading to its internalization (Bernardo & Fridman, 2003; Fridman *et al.*, 2003; Toth *et al.*, 2003; De Stefano & Herrero, 2016). It is thus noteworthy that LRP-1 is expressed in the SCN, and that LRP-1 inhibition also phase-shifts the SCN circadian clock *in vitro* (Cooper & Prosser, 2014).

Previous research suggests that MMP-9 in particular can act as a positive or negative regulator of NMDAR activity. MMP-2 and -9 can cleave a variety of substrates, including cellular adhesion molecules (CAMs) like neuroligin 1 (NLG1), EphB, and β1-integrin, which in turn can regulate NMDAR activity (Dalva *et al.*, 2000; Tian *et al.*, 2007; Michaluk *et al.*, 2009; Peixoto *et al.*, 2012; Sloniowski & Ethell, 2012). These proteins function in part to maintain the structural integrity of pre- to post-synaptic adhesion, which is thought to affect the strength of synaptic signaling.

Mechanistically, cleavage of CAMs by MMP-2/9 can increase the trafficking and/or lateral mobility of membrane-bound NMDARs on the post-synaptic membrane. For example, MMP-2 and -9 cleavage of NLG1 can increase the recruitment of NMDARs to the post-synaptic membrane (Barrow *et al.*, 2009; Peixoto *et al.*, 2012). Integrins, another MMP-2/9 substrate, recruit NMDARs to the post-synaptic membrane via interaction with PSD-95 (Barrow *et al.*, 2009) and their cleavage increases lateral movement (surface diffusion) of NMDAR in the post-synaptic membrane (Michaluk *et al.*, 2009). More evidence implicating MMP-9 in NMDAR activity regulation includes a study by Tian *et al*. showing that MMP-9 cleavage of intercellular adhesion molecule-5 enhances activation of NMDARs (Tian *et al.*, 2007). Another study showed that adult MMP-9 knockout mice exhibit increased excitability, indicated by increased mEPSC frequency in CA1 pyramidal neurons and enhanced severity and duration of kainate induced seizures (Murase *et al.*, 2016). Also, application of auto-activating MMP-9 to hippocampal slices accelerates the deactivation kinetics of NMDARs (Gorkiewicz *et al.*, 2010). Taken together, these studies suggest that MMP-2/9 cleavage of CAMs can negatively affect NMDAR activity either through downstream signaling pathways, altering channel kinetics, or by modulating NMDAR localization within the synaptic membrane.

Our data showing that daytime phase advances induced by BiPS application at ZT 6 are blocked by the NMDAR antagonist AP5 were unexpected. It has been shown previously that glutamate or glutamate agonist application to SCN slices *in vitro* at ZT 6 does not phase-shift the SCN circadian clock (Ding *et al.*, 1994; Prosser, 2001; Yamada & Prosser, 2014). On the other hand, co-application of mBDNF with glutamate to SCN brain slices at ZT 6 induces phase advances much like those seen here (Mou *et al.*, 2009). Similarly, we found that K252a is able to block these phase advances, illustrating that NMDAR-dependent phase advances during the day require co-activation of TrkB. Previous studies have shown that mBDNF levels are low in the SCN during the daytime (Liang *et al.*, 1998). Thus, one possible scenario is that MMP-2/9 inhibition increases the probability of NMDAR activation by extracellular glutamate via mBDNF binding to TrkB.

Because BiPS-induced phase shifts at both ZT 6 and ZT 16 are blocked by the NMDAR antagonist AP5, we were surprised to see that phosphorylation of α- or β-CAMKII did not change in response to BiPS treatment. In the SCN, activation of NMDAR leads to increased intracellular Ca^{2+} and subsequent CAMKII phosphorylation. This pathway is commonly observed as a downstream signaling mechanism that phase-shifts the clock (Vindlacheruvu *et al.*, 1992; Colwell *et al.*, 1994). However, in cultures of cortical neurons, CAMKIV, but not CAMKII, activity regulates activity-dependent BDNF long-term potentiation mechanisms (Shieh *et al.*, 1998). Thus, the presence of different isoforms of CAMK and their overlapping calcium-dependent mechanisms may contribute to why we did not see increased phosphorylation of either α- or β-CAMKII.

There is evidence that the master clock regulates cyclic expression of CAMs, and MMP-2/9 cleavage of CAMs could provide feedback to the clock. Candidate MMP-2/9 substrates include the neuroligins, neurexins, and polysialyated neural cell adhesion molecule (PSA-NCAM), (Glass *et al.*, 1994; Shen *et al.*, 1997; Shen *et al.*, 1999; Glass *et al.*, 2000; Shen *et al.*, 2001; Fedorkova *et al.*, 2002; Glass *et al.*, 2003; Prosser *et al.*, 2003; Kiessling *et al.*, 2017). For example, NLG-1 exhibits a diurnal oscillation in mRNA transcription and protein expression in the mouse forebrain that decreases during the night and is absent in *Clock* mutant mice (Hannou *et al.*, 2018a). The transynaptic binding partners of neuroligins, neurexins, are also linked to the circadian clock, as they exhibit cyclic mRNA expression in the mouse SCN that peaks at approximately mid-day, followed

by peak protein expression shortly after lights off (Shapiro-Reznik *et al.*, 2012). PSA-NCAM is another MMP-2/9 substrate that is highly expressed in the Syrian hamster SCN during the early morning with lower expression at night (Glass *et al.*, 1994; Shen *et al.*, 1999; Glass *et al.*, 2003). Application of endoneuramidase (which cleaves PSA from NCAM, similar to the action of MMP-2/9) to *in vitro* SCN slices prevents glutamate-induced phase shifts (Prosser *et al.*, 2003). Thus, BiPS application may affect SCN circadian clock phase by altering the expression of various CAMs, but this possibility has yet to be studied.

Given that the network of interacting partners of MMP-2/9 is extensive, future work is necessary to parse out the mechanisms underlying the phase shifts we observed. Nevertheless, our results add to a growing body of evidence (Cooper *et al.*, 2018) that the differential expression and enzymatic activities of extracellular proteases in the SCN across circadian time may help constrain the abilities of particular stimuli to phase-shift the clock to specific circadian times. The field of neuroscience is showing a robust appreciation of the ECM and its interacting proteins as active participants in neuronal communication. Our research on the role of MMP-2/9 in the SCN is consistent with this viewpoint. The results suggest that endogenous MMP-2/9 activity participates in SCN circadian clock phase regulation. Moreover, they demonstrate that MMP-9, but not MMP-2, activity could be under circadian regulation by the master clock. Although further studies are necessary to untangle the web of upstream and downstream mechanisms, we propose that extracellular regulators of MMP-2/9 activity and the cleavage of MMP-2/9 substrates may also be under circadian clock regulation.

Appendix: Figures for Chapter 2

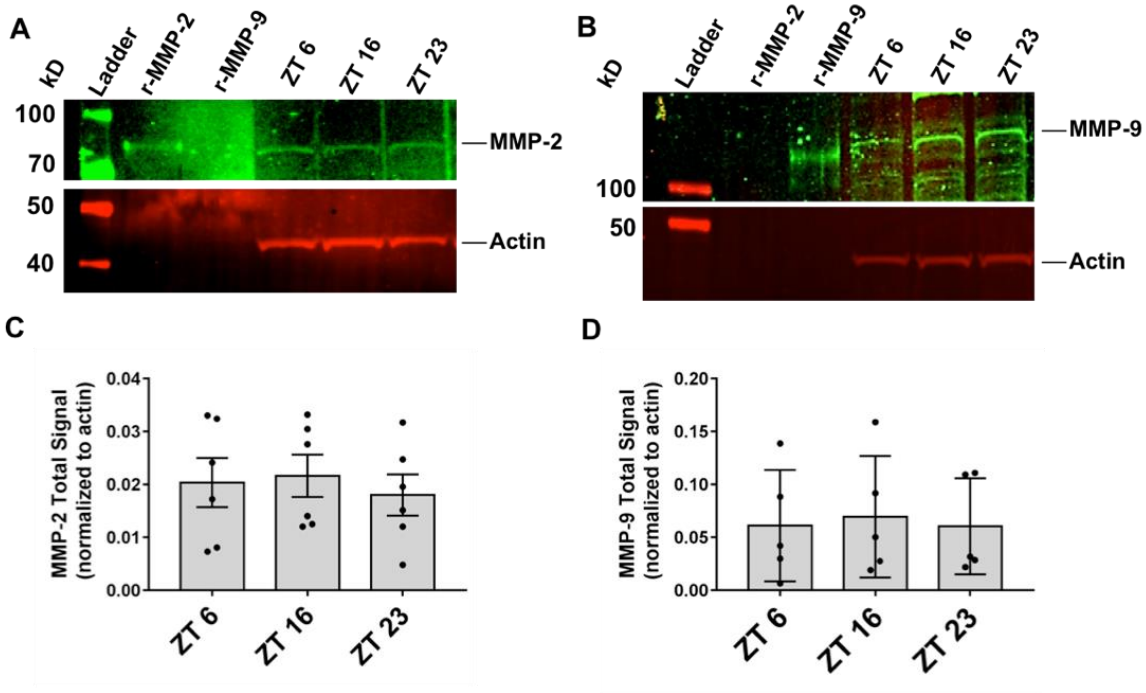

Figure 2.1: Protein expression of MMP-2 and MMP-9 in SCN tissue does not change between ZT 6, ZT 16 and ZT 23.

A) Western blot results comparing SCN tissue extract collected at ZT 6, ZT 16 and ZT 23. Each lane contains SCN tissue homogenate collected from one mouse. A ladder of known protein standards and recombinant MMP-2 protein (r-MMP-2) and r-MMP-9 confirmed identification of the MMP's. Actin (lower panel) served as a loading control. The two images were produced using the same blot and fluorescence was detected with the LiCOR Odyssey-ClX. B) Separate western blot showing detection of MMP-9 [compared to known, recombinant MMP-9 protein (r-MMP-9)] and actin. (C & D) Quantification of bands of fluorescence corresponding to MMP-2 (C) and MMP-9 (D). Fluorescent intensity (reported as total signal) for the protein of interest was set relative to total actin signal. One-way ANOVA showed that neither MMP-2 nor MMP-9 fluorescent intensity levels exhibit significant differences between ZT 6, ZT 16 and ZT 23 (MMP-9: n=5, p=>0.05 between groups and MMP-2: n=6, p=>0.05).

Figure 2.2: MMP-9 activity is higher than MMP-2 and varies across the circadian cycle.

A) Gelatin zymography of known recombinant protein (r-MMP-2 and r-MMP-9; 100 ng) and homogenates of SCN tissue collected at ZT 6, ZT 16 and ZT 23 (10 ug samples loaded for each time point). B) The same image as (A) displayed with increased contrast to visualize the fainter gelatinolytic bands chosen to analyze for MMP-2. (C) Histogram plotting gelatinolytic activity (reported as mean grey value) relative to r-MMP-2 band. Two way ANOVA examining interaction effects (Tukey's Multiple Comparisons Method) show that only gelatinolytic activity of MMP-9 is significantly different than MMP-2 activity at each time point (*p< 0.01). Additionally, activity of MMP-9 at ZT 6 is significantly higher than MMP-9 activity at ZT 6 (*p=<0.01) but not ZT 16. Note: It was previously determined that the latent and active forms of r-MMP-2 generally run at ~66.3 kD and ~55.4 kD, respectively (Toth & Fridman, 2001). These weights coincide with where our r-MMP-2 band shows up, however our gels were incubated for a longer timeframe, which may account for our inability to distinguish the two forms of r-MMP-2. The higher band in the r-MMP-2 lane (between 110 and 130 kD), we believe is a dimer of r-MMP-2, as reported previously (Frankowski *et al.*, 2012). The doublet that we see with r-MMP-9 likely reflects the pro- and active forms of this protein (~98 kD and 84 kD, respectively), which were easier to distinguish on our gel. Below the doublet, we also see a fainter band in our purified r-MMP-9 sample. As reported previously (Toth and Fridman, 2001), this ~73 kD form may an auto-activated or mutated species of MMP-9. For more details on identifying gelatinolytic bands, see (O'Connell *et al.*, 1994; Toth & Fridman, 2001; Frankowski *et al.*, 2012).

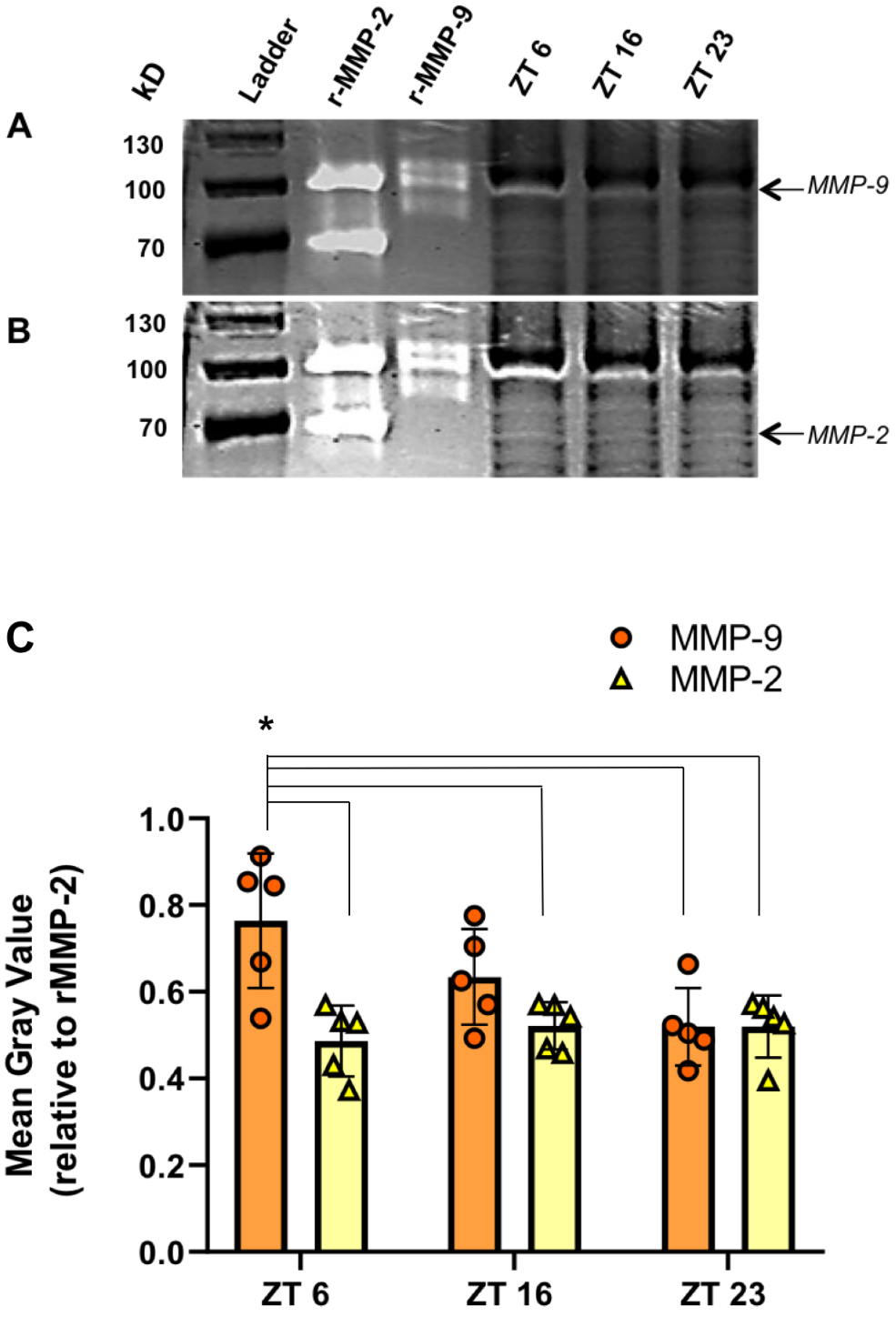

Figure 2.2 continued

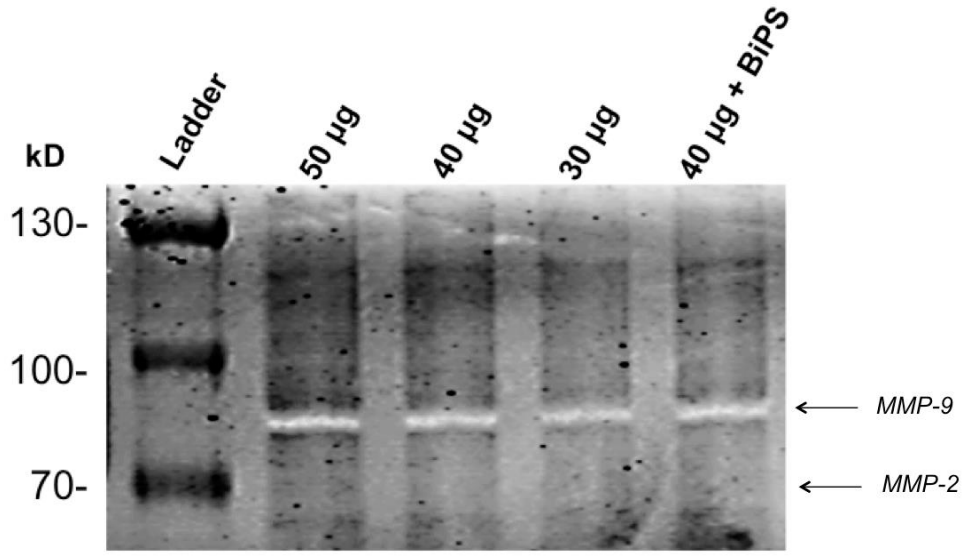

Figure 2.3: Increasing protein content does not increase detection of MMP-2 in SCN tissue extract.

Gelatin zymography of SCN tissue samples collected at ZT 6. The results illustrate that increasing protein concentration of SCN tissue extract did not improve visualization of MMP-2 gelatinolytic activity. Arrows point to known MMP-9 zymographic bands and the expected molecular weight where MMP-2 should be present. Also, incubating SCN tissue extract (40 µg) with the MMP-2/9 inhibitor (100 nM BiPS) before loading does not affect activity of MMPs in the gelatin zymogram (n=1).

Figure 2.4: In situ zymography confirms activity of MMP-2/9 in the SCN.

A) *In situ* zymography images of control and BiPS treated (B) hypothalamic tissue slices collected at ZT 6, ZT 16 and ZT 23. For each image, the location of the SCN was confirmed with the nuclear stain, DAPI (blue in merged panel). DQ-Gelatin fluorescence (green in merged panel) shows strong signal in hypothalamic slices. Negative control sections (C and D) incubated with either 4% PFA or 100 nM BiPS in the DQ-Gelatin solution to inhibit MMP-2/9 activity confirm green fluorescence is due to MMP-2/9 activity. Analyzed images were all taken under 20X magnification using the same laser exposure settings. Scale bars= 200 μM. To compare DQ-Gelatin fluorescent signal between brain regions, two circular regions of the same dimensions were selected within each image, one within the SCN and one within the adjacent anterior hypothalamus (Ant Hypo). E) The mean grey value of the pixel density corresponding to DQ-Gelatin channel and was measured in each experimental group (n=3-6). Two-way ANOVA with a post-hoc Tukey's test for multiple comparison analysis shows that gelatinolytic activity is lower in the anterior hypothalamus than in the SCN at ZT 6 and ZT 23, but not at ZT 16, in BiPS treated slices. However, there were no differences in gelatinolytic activity in either brain region across time or in response to BiPS treatment of the brain slices prior to harvesting for zymography. (Asterisks indicate significance level at $p<0.05$). F) Combined data (n=8-11) of mean grey values corresponding to MMP-2/9 gelatinolytic activity between control and BiPS-treated SCN slices. At each time point (**= $p<0.01$, ***=$p<0.001$) the gelatinolytic activity in the SCN is higher than the surrounding anterior hypothalamus (AH).

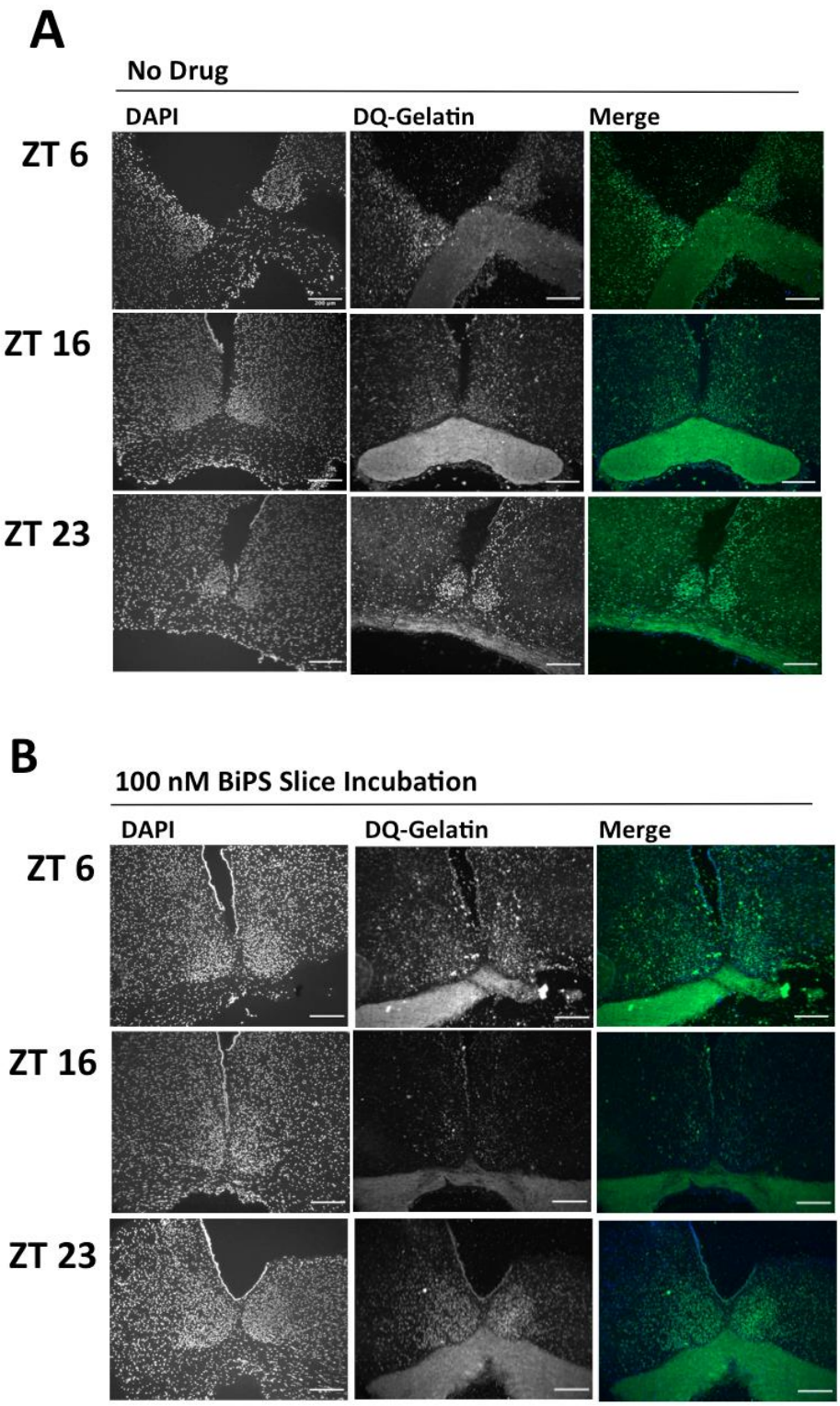

Figure 2.4 continued

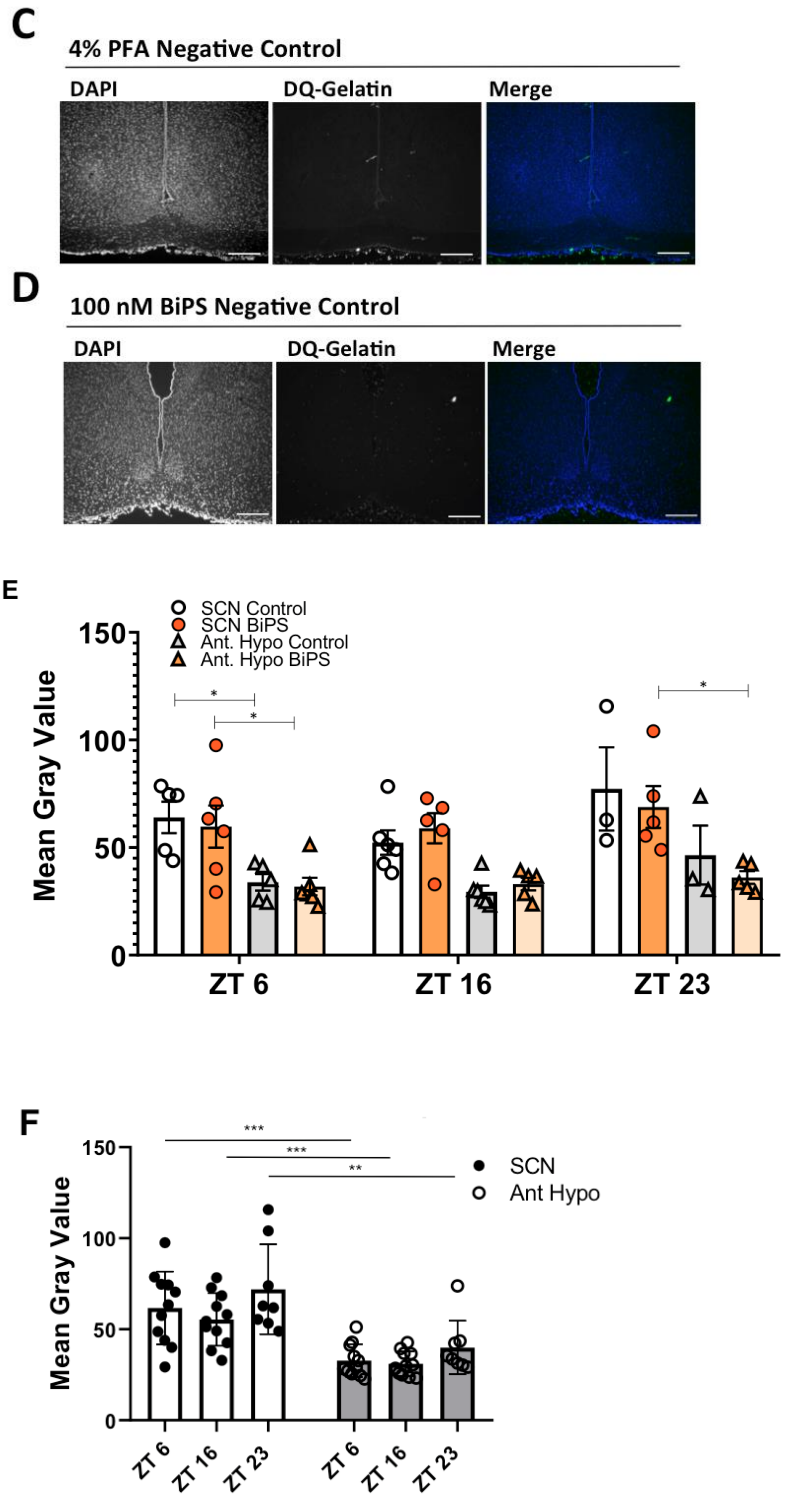

Figure 2.4 continued

Figure 2.5: Inhibiting MMP-2/9 activity during the day and early night phase-shifts the clock.

Representative single-unit recordings from SCN tissue slices ± BiPS (100 nM) drug treatment; each graph represents a recording of SCN tissue from one animal. Two hour running averages of firing rate (Hz) are plotted against zeitgeber time (ZT) in hours. Black horizontal bars indicate subjective night in the animal colony (ZT 12 - ZT 24). Vertical dashed line at ZT 6 represents the time of peak of activity in control slices, as seen in (A). Vertical white bar indicates time of drug treatment (100 nM BiPS) at ZT 6 (B), and ZT 16 (C). BiPS treatment at ZT 6 and ZT 16 induces phase advances and delays, respectively. (D) Compiled phase shift (h) responses of the SCN circadian clock when treated with different combinations of drugs targeting MMP-2/9 activity (BiPS), NMDAR receptor (AP5), Trk-B (K252A), and plasmin [α_2-antiplasmin (α_2-AP)]. One-way ANOVA comparing the combined drug treatments to BiPS treatment alone revealed that AP5 blocks BiPS-induced phase shifts at ZT 6 (*** p= < 0.001) and ZT 16 (**p= < 0.01). SCN tissue co-treated with BiPS and α_2-AP or K252A (* p=<0.05) at ZT 6 blocks BiPS-induced phase advances. BiPS treatment at ZT 23 did not produce a significant phase shift, therefore we did not perform further drug treatments at the time point. N=3 for each treatment, exact p-values are listed in our results section. Statistical analysis was performed using a One-way ANOVA, post-hoc Dunnett's test, where each experimental group was compared to BiPS treatment alone.

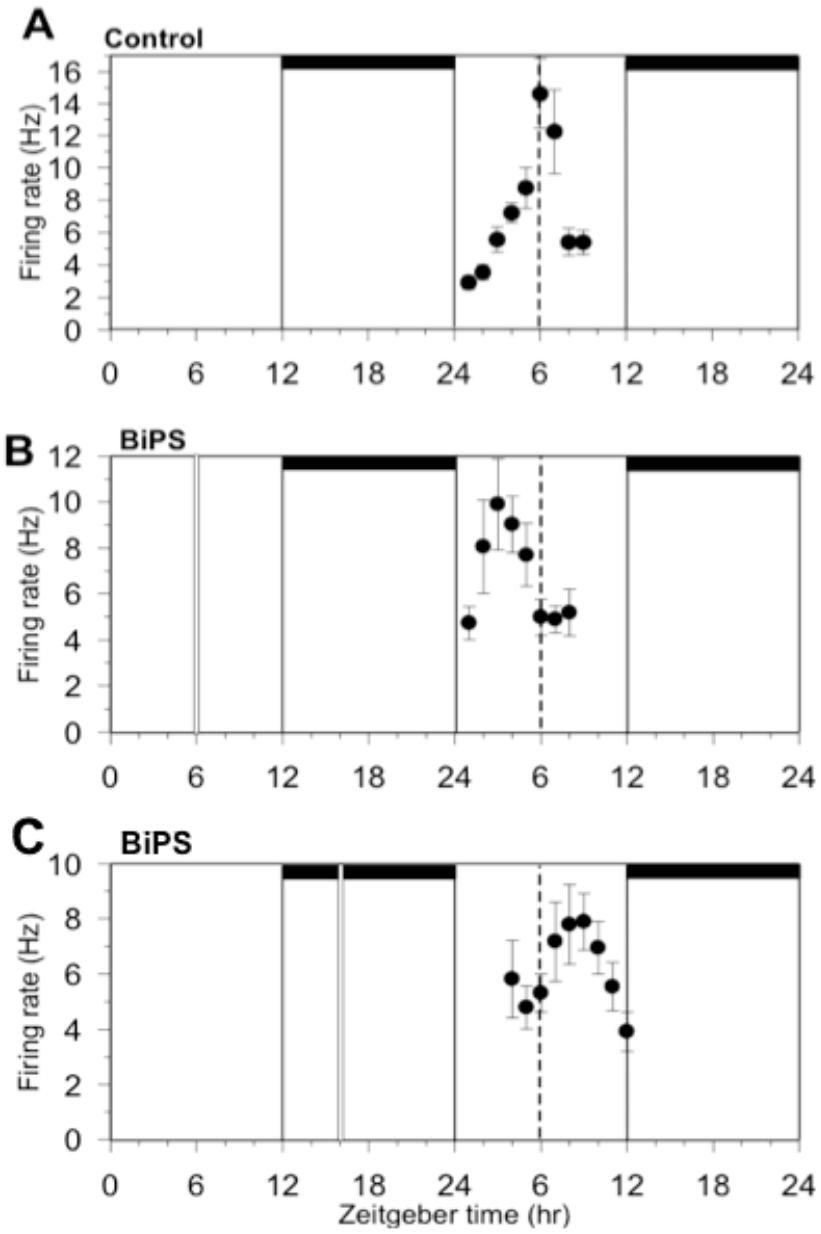

Figure 2.5 continued

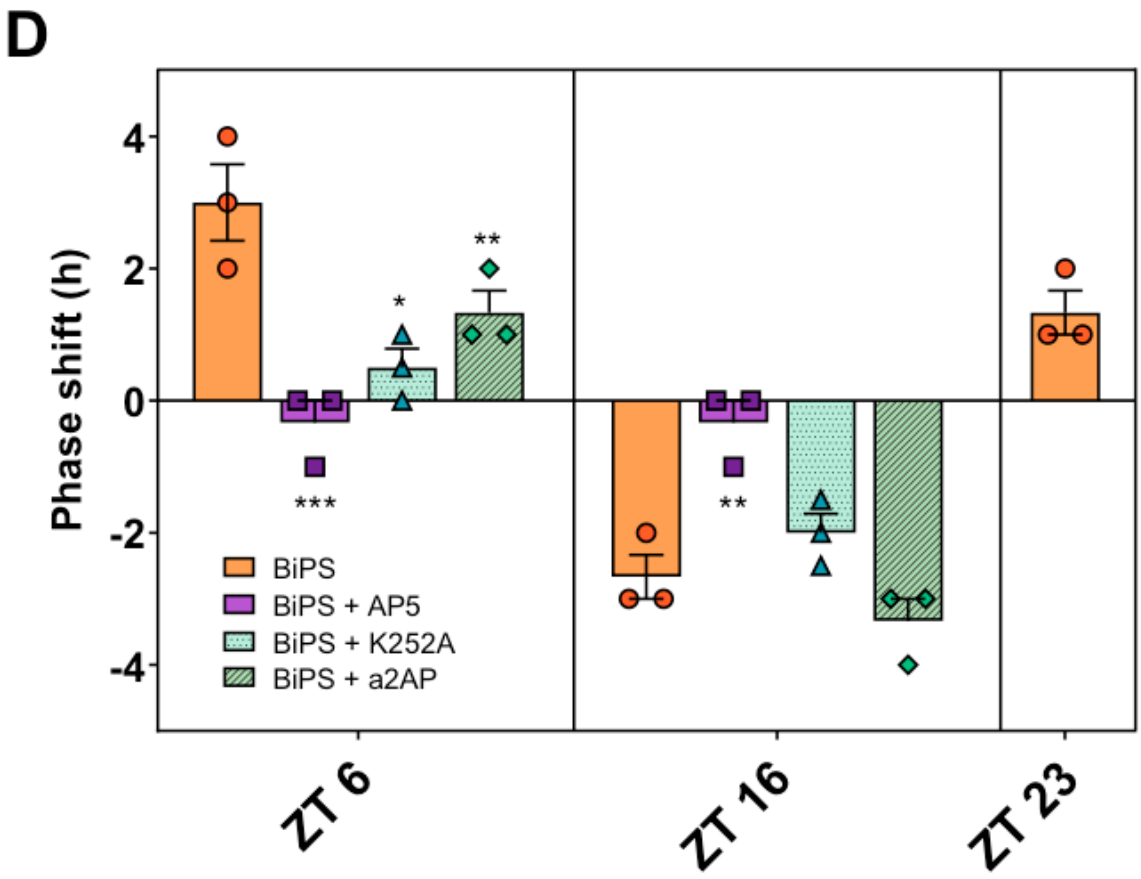

Figure 2.5 continued

Figure 2.6: Inhibition of MMP-2/9 at ZT 23 acutely affects firing rates but does not phase-shift the SCN circadian clock.

A & B) Extracellular electrophysiology recordings in SCN tissue slices maintained *in vitro* show that 100 nM BiPS application at ZT 23 shows a double peak in firing rate on Day 2. Each graph represents data gathered from a separate experiment. C) Control recording of extracellular firing rates of SCN tissue collected on Day 3 *in vitro* show a peak at ZT 6. D) SCN slices treated with 100 nM BiPS at ZT 23 on Day 1 *in vitro* show a peak at ZT 5 on Day 3, suggesting that acute effects of BiPS treatment on SCN tissue are not sustained, and the treatment does not induce statistically significant phase shifts ($p=>0.05$).

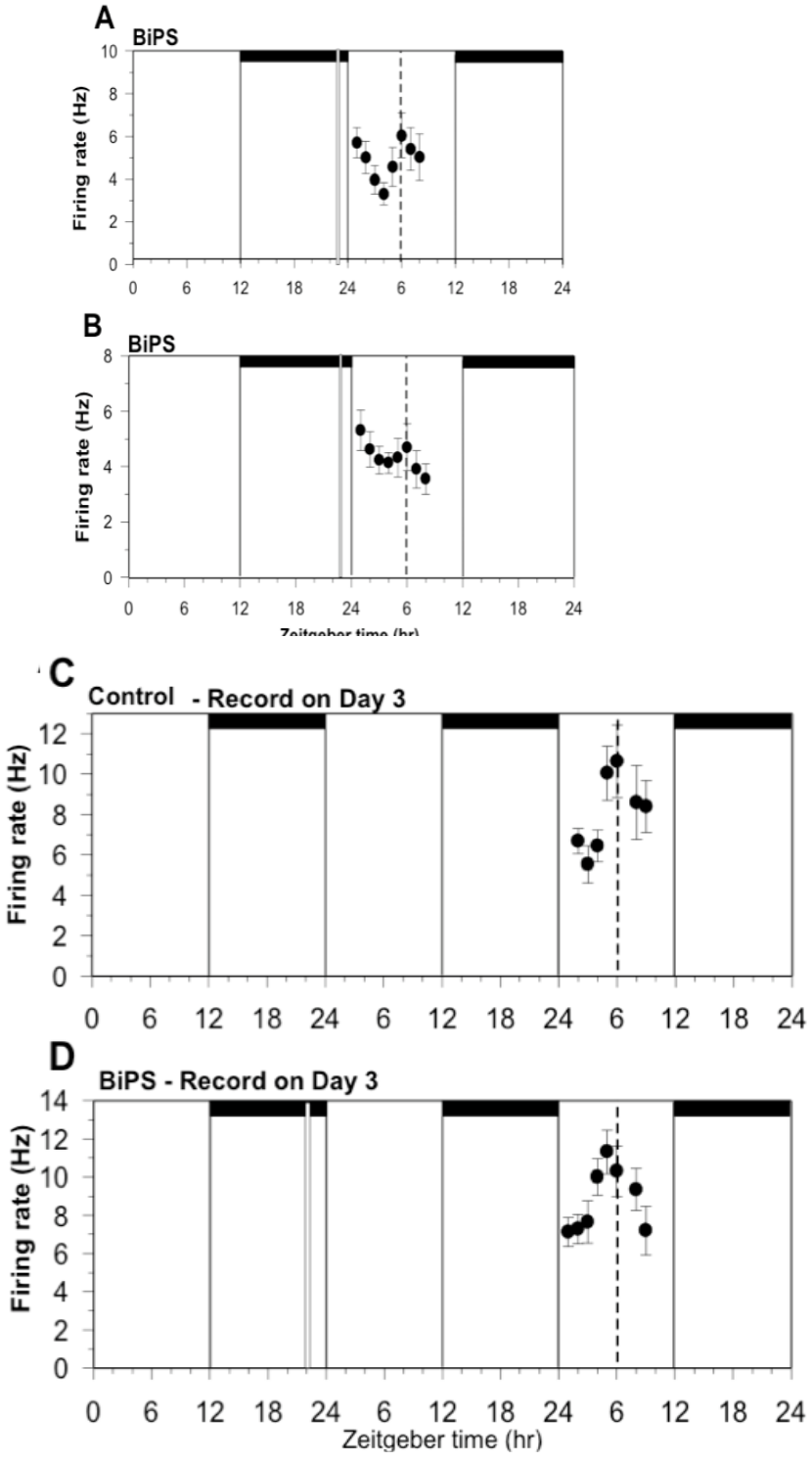

Figure 2.6 continued

Figure 2.7: Inhibition of MMP's does not affect phosphorylation of α- and β-CAMKII.

A) Immunoblot results from control and BiPS-treated SCN tissue homogenates. Green bands correspond to the primary antibody that detects phosphorylation of the conserved Thr-286 residue on both α- and β-CAMKIIs (50 and 60 kDa, respectively). Actin (red bands) served as the housekeeping protein. B) Fluorescent signal for both α- and β-CAMKIIs was measured at each time point and set relative to actin signal. Neither the total signal nor the ratio of α:β isoforms (C) appear to change over time or with BiPS treatment. Two way-ANOVA with post-hoc Tukey's test for multiple comparisons results were non-significant for all pairwise comparisons ($p>0.05$)

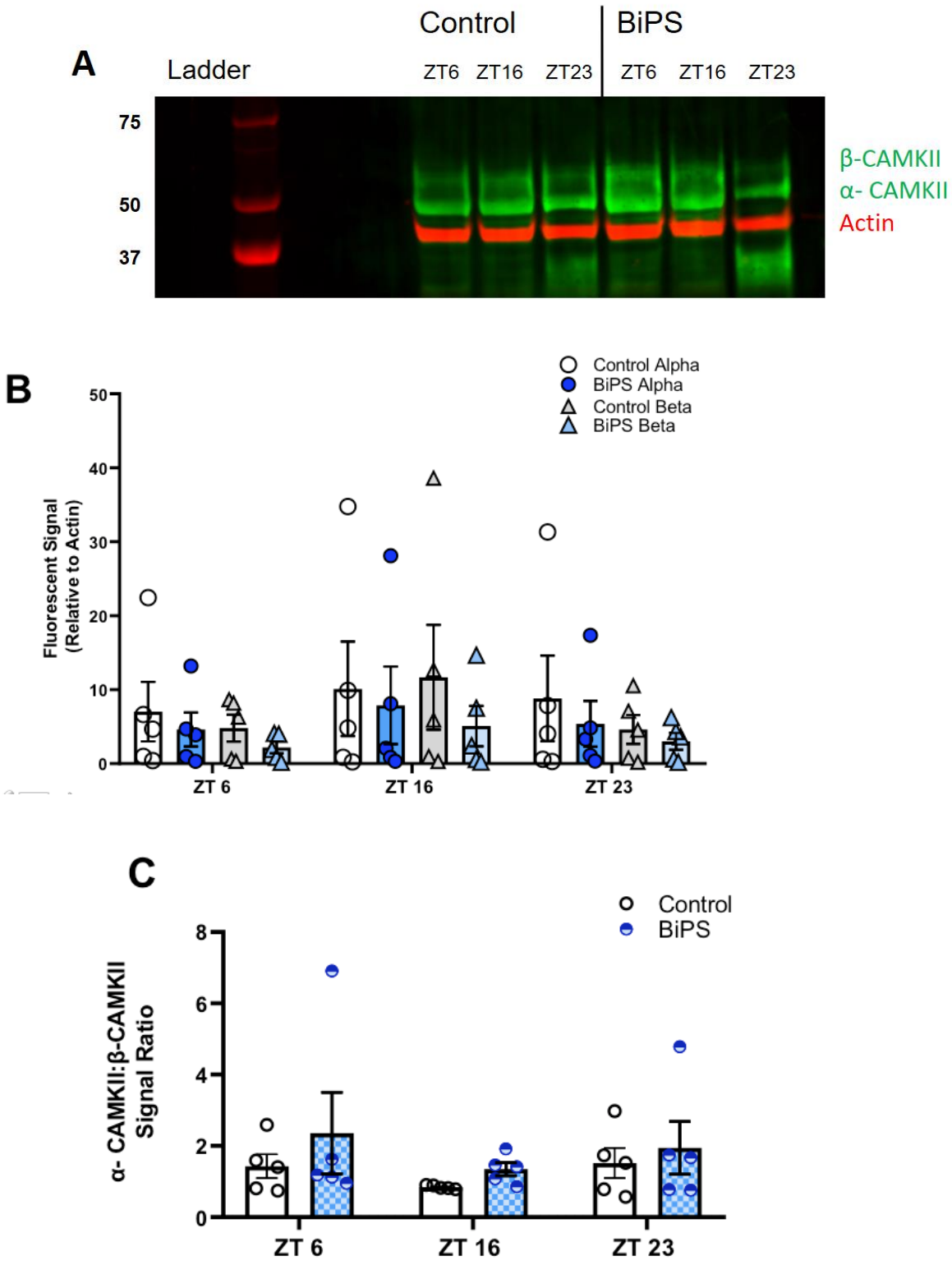

Figure 2.7 continued

CHAPTER III: LINKING TIME DEPENDENT STATE CHANGES IN ASTROCYTIC RAMIFICATION TO THE EXTRACELLULAR ENVIRONMENT

This version of this chapter contains completed work of Kathryn A. Halter towards a second manuscript. Complimentary experiments and data analysis are concurrently being performed.

Halter, KA and RA Prosser. “Linking time-dependent state changes in astrocytic ramification to the extracellular environment.” (Manuscript in prep) 2019.

The manuscript written below contains original work designed, executed and analyzed by Kathryn Halter. Rebecca Prosser contributed to the experimental design, data analysis, and revisions of the manuscript.

Abstract

Located in the suprachiasmatic nucleus (SCN), the mammalian master clock synchronizes near 24 hour, or circadian, behavioral and physiologic rhythms. The SCN also exhibits endogenous, intracellular rhythms to coordinate intercellular synchronization of its heterogeneous cell types. For example, astrocytes and neurons both express distinct rhythms in gene expression, intracellular Ca^{2+} influx, and glutamate secretion. Astrocytes uniquely exhibit a circadian rhythm in morphology accompanied by rhythmic glial fibrillary acidic protein (GFAP). In other brain regions, reorganization of GFAP is necessary for astrocytic morphological changes. This process is mediated by matrix metalloproteinase (MMP)-dependent cleavage of β-dystroglycan, a cellular adhesion molecule that localizes to astrocytic endfeet. In the SCN, the level of GFAP increases expression and becomes more diffusely distributed at night relative to the day. As MMPs are expressed and active in the SCN, we hypothesized that there may be diurnal differences in β-dystroglycan expression and/or degradation by MMP-2/9. Further, MMP-2/9 cleavage of β-dystroglycan could contribute to astrocytic morphological changes in the SCN. We determined that β-dystroglycan is highly expressed in the SCN and appears to colocalize with astrocytes, although its expression is constitutive and its degradation is unaffected by inhibition of MMP-2/9 activity. Quantitative analysis of SCN GFAP-positive cells revealed astrocyte morphology is more complex during the late night relative to the day, without altering a change in total cellular volume. Together, our results suggest that diurnal SCN astrocytic filopodia extension depends on rearrangement of their intracellular scaffolding and that these changes may rely on their interactions with ECM molecules.

Introduction

The mammalian master clock, located in the suprachiasmatic nucleus (SCN), generates endogenous ~24-hour (circadian) rhythms and synchronizes daily rhythms in behavior and physiology with the external environment (Schulz & Steimer, 2009; Golombek & Rosenstein, 2010; Yan *et al.*, 2018). In order to generate the appropriate output signals needed to regulate circadian physiology of the entire organism, this master clock must coordinate the self-sustaining oscillators contained within its own heterogeneous cell types (Aton & Herzog, 2005). Of these cells, astrocytes are major participants in coordinating the circadian network within the SCN (Prolo *et al.*, 2005), a role consistent with their robust intracellular rhythms in clock gene expression (Prolo *et al.*, 2005), Ca^{2+} rhythms (Brancaccio *et al.*, 2017) and glutamate secretion (Brancaccio *et al.*, 2017). In SCN primary neuronal cultures devoid of astrocytes or in *in vitro* SCN slices treated with drugs disabling glial cell metabolism, spontaneous firing rates of individual SCN neurons become desynchronized and the master clock is disrupted (Prosser *et al.*, 1994; Welsh *et al.*, 1995; Shirakawa *et al.*, 2001). Thus, astrocytes are a vital component in facilitating intercellular synchronization.

Astrocytes exhibit dynamic morphologic responses to increased neuronal activity, injury, or as a result of neurological disease (Theodosis *et al.*, 2004; Theodosis *et al.*, 2008; Cheng *et al.*, 2019; Zhou *et al.*, 2019). Examination of mechanisms regulating astrocytic morphology provide essential information regarding network communication because the extent and efficiency of inter-neuronal communication depends on the physical proximity of surrounding cells (Pirttimaki & Parri, 2013). In the SCN of animals housed in light:dark conditions, the cytoskeletal protein glial fibrillary acidic protein (GFAP) exhibits increased expression and its distribution pattern becomes more diffuse at night as compared to the day (Morin *et al.*, 1989; Lavialle & Serviere, 1993; Leone *et al.*, 2006; Becquet *et al.*, 2008). However, it is unclear if this rhythm is under circadian regulation because there are conflicting reports concerning GFAP rhythms in animals housed in constant darkness (Lavialle & Serviere, 1993; Becquet *et al.*, 2008). Ultrastructural electron microscopic studies of rat SCN observed that the amount that glia cover neuronal somas (indicated by the percentage of contact between glial appositions to different neuronal cellular components), does not exhibit diurnal differences, but is

higher in the SCN compared to the surrounding anterior hypothalamus (Elliott & Nunez, 1994). In contrast, another study found that glial coverage is cell-type and time-of-day specific. SCN glia exhibit greater dendritic coverage of vasopressin intestinal peptide (VIP) neurons and less dendritic coverage of arginine vasopressin (AVP) neurons at night relative to the day (Becquet *et al.*, 2008). Further, brain derived neurotrophic factor activation of tyrosine receptor kinase B, which is necessary for synaptic plasticity (Lu, 2003), is required for the diurnal changes in astrocytic envelopment of VIP neurons (Girardet *et al.*, 2013). These studies provide evidence that astrocytic morphological rhythms are influenced by the SCN circadian clock, but the underlying mechanisms may depend on extracellular factors.

Proteins interacting with the extracellular matrix (ECM) of the brain form the physical scaffolding between neurons and astrocytes. These molecules include pre- and post-synaptic cell adhesion molecules (CAMs), neural cell adhesion molecules (NCAMs), synaptic CAMs, neuroligins, neurexins, dystroglycans, Ephrins and their receptors, and integrins. These molecules bind to ECM molecules such as collagen, laminin, elastin, fibronectin, chondroitin sulfate proteoglycans, as well as to their partner synaptic adhesion molecules and ligands. Functionally, this interconnected web of proteins mediates both cellular morphology and intercellular communication (Dityatev & Schachner, 2003; Cauwe *et al.*, 2007; Frischknecht & Gundelfinger, 2012; Frischknecht *et al.*, 2014; Lassek *et al.*, 2015; Marcoli *et al.*, 2015; De Luca & Papa, 2017; O'Callaghan *et al.*, 2017; Ferrer-Ferrer & Dityatev, 2018; Hillen *et al.*, 2018; Song & Dityatev, 2018; Fawcett *et al.*, 2019). It is well established that ECM-associated molecules play extensive roles in regulating endogenous circadian rhythms in the SCN (Glass *et al.*, 2000; Shen *et al.*, 2001; Mou *et al.*, 2009; Girardet *et al.*, 2013; Cooper *et al.*, 2018), but further characterization of ECM-associated molecules facilitating diurnal changes in astrocyte morphology is needed.

One candidate extracellular CAM known to regulate astrocytic morphology in other brain regions is dystroglycan (Michaluk *et al.*, 2007; Bozzi *et al.*, 2009; Sbardella *et al.*, 2012). Dystroglycan contains two subunits: an extracellular glycoprotein, α-dystroglycan, and a transmembrane portion, β-dystroglycan (Durbeej & Campbell, 1999; Esapa *et al.*, 2003). This protein complex stabilizes intracellular cytoskeletal interactions with the ECM

by bridging actin-bound β-dystrophin molecules (Ibraghimov-Beskrovnaya *et al.*, 1992) to ECM proteins like laminin, aggrecan and perlecan via carbohydrates on the glycosylated sidechains of α-dystroglycan (Barresi & Campbell, 2006). Studies examining regional and subcellular location of dystroglycan subunits in the brain have clarified its function in structural stabilization. In the developing mouse brain, β-dystroglycan expression in perivascular glial cells precedes astrocytic filapodial-like protrusions (called astrocytic endfeet) formation. This implicates β-dystroglycan as an anchor for glial cell attachment to the basal lamina of vascular epithelial cells (Kalman *et al.*, 2018). Zaccaria et al. found that neurons in the adult mouse cerebral cortex, olfactory bulb and cerebellum contain α- and β-dystroglycan. Supporting work with dystroglycan knockout mice shows that astrocytes adjacent to pia mater require dystroglycan expression to swell, a neuroprotective response, after ischemic stroke (Noell *et al.*, 2011). Further assessment using electron microscopy revealed preferential expression on neuronal post-synaptic membranes (Zaccaria *et al.*, 2001). Later, the presence of β-dystroglycan on the post-synaptic membrane of hippocampal neurons was confirmed, and long-term potentiation (LTP)-inducing stimuli were found to increase degradation of β-dystroglycan (Michaluk *et al.*, 2007). β-dystroglycan localization to astrocytic endfeet that interface with the vasculature is also seen in the adult mouse cerebral cortex and in the supraoptic nucleus (Gondo *et al.*, 2014; Souttou *et al.*, 2019). In summary, it is likely that dystroglycan subunits act as an anchor for neurons and/or astrocytes to bind and stabilize intercellular connections and communication.

The main extracellular proteases known to degrade dystroglycan are matrix metalloproteinase (MMP)-2 and MMP-9. MMP-2 and MMP-9 participate in cleavage of ECM-associated molecules during development, synaptic plasticity and learning and memory (Ethell & Ethell, 2007). With respect to β-dystroglycan, the catalytic sites of MMP-2/9 bind to and cleave the β-dystroglycan subunit (43 kDa), generating a 30 kDa fragment (Sbardella *et al.*, 2012). This shorter fragment of β-dystroglycan is unable to bind to α-dystroglycan and thus this cleavage disrupts dystroglycan interactions with the ECM. Transfecting an auto-activating MMP-9 (aaMMP-9) protein (Fisher *et al.*, 2002) into a primary culture of cortical neurons increases expression of the 30 kDa fragment, confirming β-dystroglycan as a substrate for MMP-9 (Michaluk *et al.*, 2007). Conversely,

increased β-dystroglycan cleavage after glutamate application is blocked by co-application of tissue inhibitor of metalloproteases-1 (TIMP-1), the endogenous inhibitor of MMP-9 (Michaluk *et al.*, 2007).

Cleavage of β-dystroglycan by MMP-9 occurs during a variety of processes that involve structural reorganization of astrocytes and the surrounding microenvironment. In mouse brains subjected to an ischemic challenge, cleavage of β-dystroglycan is blocked by the MMP-2/9 inhibitor captopril (Yan *et al.*, 2016). The same study found that β-dystroglycan is expressed near aquaporin-4 (AQP4), a water channel protein specifically expressed in astrocytic endfeet. In a mouse model of epilepsy, depletion of extracellular Mg^{2+} increases β-dystroglycan degradation due to excessive neuronal activity, which subsequently decreases β-dystroglycan's association with AQP4 on astrocytic endfeet. Once again, this degradation-induced reduction is mediated by MMP-2/9 activity (Gondo *et al.*, 2014). In a model of intracerebral hemorrhage, a non-specific MMP inhibitor, GM6001, blocks cleavage of β-dystroglycan and increases expression of GFAP (Zhang *et al.*, 2019). Thus, although β-dystroglycan-modulation of astrocytic morphology is seen broadly, it is not known whether β-dystroglycan cleavage mediates astrocytic morphological changes in the SCN.

Past research demonstrates that MMP-2 and -9 are present and active in the SCN. In hamster SCN tissue homogenates, gelatinolytic activity of both MMPs is detected, but only MMP-9 gelatinolytic activity peaks during the night as compared to the day (Agostino *et al.*, 2002). Our laboratory has confirmed the expression of MMP-2/9 in mouse SCN. Using gelatin zymography, we observed increased gelatinolytic activity during mid-day, while *in situ* zymography revealed that MMP-2/9 gelatinolytic activity in the SCN is greater than in the surrounding anterior hypothalamus (see Chapter 2). Inhibiting MMP-2/9 activity with 2-(benzenesulfonylamino)-N-hydroxy-3-phenylpropionamide (BiPS) results in time-dependent phase shifts of the clock. BiPS application at Zeitgeber time (ZT; where ZT 0 corresponds to lights-on and ZT 12 corresponds to lights-off in the animal colony) 6 and ZT 16 produces phase advances and delays, respectively, while ZT 23 drug application has no effect on clock phase. Importantly, phase shifts are blocked by the competitive NMDAR antagonist, AP5, indicating a potential role for glutamate in phase shifts mediated by MMP-2/9 inhibition.

Because glutamatergic stimulation increases cleavage of β-dystroglycan via MMP-9 activity (Dziembowska *et al.*, 2012), we hypothesized that β-dystroglycan is expressed and functionally active in the SCN. Using complimentary techniques, we sought to visualize and quantify β-dystroglycan protein expression in the SCN. We also examined, using western blotting, if β-dystroglycan is a preferred substrate for MMP-2/9. Further, we investigated the potential participation of β-dystroglycan as a regulatory component in astrocytic morphological rhythms.

Materials and Methods

Immunohistochemistry

All animal procedures followed University of Tennessee, Knoxville Institutional Animal Use and Care Committee approved protocols. Animals used for this study were adult male, C57BL/6 mice (Envigo, Indianapolis, IN) housed in a 12:12 light:dark cycle, with food available *ad libitum*. Blocks of hypothalamic tissue containing the SCN were harvested at ZT 6, ZT 16 or ZT 23 (n=5-11) and immediately fixed in 4% paraformaldehyde (PFA) for 30 minutes. Tissue blocks were stored in 1X PBS solution containing 30% sucrose overnight and placed in optimum cutting temperature (OCT) compound (Sakura® Finetek, USA INC) the following morning. 25 µm tissue sections were prepared using a Leica cryostat and mounted to VWR Vista Vision™ Histobond® adhesive slides (VWR). Slides were selected for staining with one of two β-dystroglycan antibodies (see Tables 1 and 2 in the appendix for all antibody information), either anti-mouse β-dystroglycan (1:500; Leica Novocastra) or anti-rabbit β-dystroglycan (1:500; Abcam), and/or an antibody for GFAP [chicken-anti-GFAP (1:1,000; Abcam)]. Slides were dried at room temperature, rinsed in 1X PBS and fixed again with 4% PFA for 30 minutes. After 3 X 5-minute washes in 1X PBS, slides were incubated in a 80°C waterbath for 20 min in antigen retrieval solution (10 mM Tri-sodium citrate, pH 6.0). Three washes in 1X PBS were repeated and slides were left to block for an hour in blocking solution (5% Normal Goat Serum, 5% Bovine Serum Albumin, and 0.1% Triton-X 100 in 1X PBS). Immediately after blocking, primary antibodies were added to a volume of 1:2 dilution of blocking solution in 1X PBS and allowed to incubate overnight at 4°C. After three washes with 1X PBS, slides were incubated with complementary secondary antibodies

conjugated to fluorophores of non-overlapping wavelengths: (1) anti-chicken-568, (2) anti-mouse-488, and/or (3) anti-rabbit 488 (all from Invitrogen). Slides were mounted using Vectashield Antifade mounting medium containing DAPI (Vector Laboratories; Burlingame, CA), cover-slipped, and sealed. Images were taken using a Leica CTR600 Florescence Microscope [20X magnification for integrated pixel density (mean grey value) measurements of bilateral SCN regions] or an Olympus 1x-83 inverted confocal microscope (for 40X and 60X magnification of GFAP-labeled cells for qualitative co-localization and Sholl Analysis). Acquisition settings and laser exposures were kept constant during and between imaging sessions.

Sholl analysis

For Sholl Analysis (Sholl, 1953) a Z-stack of 10 images taken at 1µm steps (60X magnification) was collected using the Olympus 1x-83 inverted confocal microscope. Only SCN glial cells that had a clear nucleus and extensions contained within the Z-stack of images were selected for analysis. Two reviewers who were blind to the treatments were trained to perform cell tracing. Ten practice astrocytes (from three images of SCN tissue, one at each time point) were given to reviewers. The percent difference of the average "ending radii" and average "max intersections" were compared and fell within 90% agreement for these morphologic measures. Next, experimental images were assigned random identification and each blind reviewer analyzed an equal number of GFAP-positive cells corresponding to each time-point.

Using Image-J, Fiji (NCBI), the images were converted to 8-bit and pixel dimensions were converted into µm. Cells were traced using the Simple Neurite Tracer program according to previously published methods and tutorials (Longair *et al.*, 2011; Schindelin *et al.*, 2012; Binley *et al.*, 2014; Sampedro-Piquero *et al.*, 2014; Tavares *et al.*, 2017). Each branch-point belonging to a single astrocyte was traced through the entire Z-projection of the image and saved. After tracing was completed and individual traces were saved, fill volumes were measured and Sholl Analysis was performed. To measure the cell soma volume, each individual cell trace was loaded back onto the original Z-stack of images. A new branch-point was drawn from the center point of the cell to the outermost boundary of the cell soma. After selecting only the new cell path, the "Fill Volume" feature

was selected on the Simple Neurite Tracer program again and the volume data for each cell was saved. The data collected from the two reviewers was un-blinded and merged for further statistical analysis. In total, the morphology of 5-6 randomly selected astrocytes in the SCN from two animals for each experimental group was quantified. Therefore, 10-12 astrocytes at each time-point (ZT 6, ZT 16 and ZT 23) were included in our analysis.

Colocalization analysis using Coloc-2 ImageJ Program

After astrocytes (10-12 astrocytes at each time-point) were traced using the Sholl Analyses protocol above, the SCN images were further analyzed to quantify the signal overlap between fluorescence corresponding to β-dystroglycan (red channel) and GFAP (green channel). Z-stacks of both red and green channels of the 60X, Z-stack images were re-opened and merged. Previously saved astrocyte traces corresponding to the correct image were opened and the ROI freehand tool was used to outline the edges of GFAP staining of the loaded cell trace. The ROI was maintained throughout the Z-stack and adjustments to the ROI were made if necessary. Next, the Coloc-2 plugin program was opened to run the Pearson's coefficient test after selecting the "bisection" option under the "threshold regression" prompt. The Pearson's coefficient test is a multipurpose test for measuring the statistical association (R-value) between two variables where -1= no correlation and +1=perfect correlation. The R-value for each cell was saved and the mean R-value (+/- SEM) between each time point was analyzed for statistical significance using One-Way ANOVA analysis.

Brain slice preparation

Brain slices containing the SCN were maintained in a perfusion dish containing Earle's Balanced Salt Solution (EBSS; MP Biomedicals, Solon, OH), supplemented with gentamicin, dextrose, and sodium bicarbonate, saturated with 95% O_2/5% CO_2, and kept at 37°C (Prosser & Gillette, 1989; Prosser *et al.*, 1994; Mou *et al.*, 2009; Yamada & Prosser, 2014; Cooper *et al.*, 2017). Coronal slices (500 μm) containing the SCN were kept in constant conditions until collection, unless otherwise noted.

Chemical treatment

The experimental concentration (100 nM) of BiPS (Calbiochem) to block MMP-2/9 activity (Tamura *et al.*, 1998; Lauzier *et al.*, 2008), was chosen based on the IC_{50} determined by the manufacturer's specifications and on previous research performed by our laboratory. BiPS was bath-applied to SCN slices for the 40 minutes surrounding ZT 6, ZT 16 or ZT 23 on the day brain slices were prepared. Slices collected immediately after drug treatment were immediately frozen on dry ice and stored at -80°C until utilized for protein extraction.

Western blotting

Brain slices containing the SCN were prepared in the morning on day one *in vitro* and maintained as described above. Control and drug treatment slices remained in the perfusion dish until collection. Control slices were collected immediately before a 40 minute BiPS (100 nM) bath application at ZT 6, ZT 16, or ZT 23 (n=6 for each time point). BiPS-treated slices were immediately collected after drug treatment. All tissue samples were rapidly frozen at -80°C.

Protein extraction utilized reducing conditions, and protein concentration (µg/µL) was measured using the Bradford assay. 30 µg of protein extract from each sample was loaded into a 4-12% Bis-Tris BOLT gel (Invitrogen, Carlsbad, CA) and separated by electrophoresis in 1X MOPS [(3-(N-morpholino)propanesulfonic acid] buffer (Invitrogen). Proteins were transferred from the gel to an Immobilon-PVDF (EMD-Millipore) membrane using a Trans-Blot Turbo (BioRad, Hercules, CA) transfer system. Proteins of interest were detected following the Near-Infrared (NIR) Western Blot Detection protocol, available online. For this experiment, we detected β-dystroglycan (rabbit anti-β-dystroglycan, 1:1,000; Abcam) and actin (goat anti-actin, 1:5,000; sc-1616, Santa Cruz Biotechnologies, Dallas, TX) as a loading control. Incubation and subsequent detection of the signal intensities of fluorescent secondary antibodies conjugated to LI-COR IR-Dye® were detected with an Odyssey®-CLx system (LI-COR Biosciences, Lincoln, NE). Band intensity analysis was performed using the Image Studio Lite™ v 5.0 software (LI-COR Biosciences). Fluorescent signal for each protein was measured as pixel density minus background pixel density and reported as total signal. The total signal

corresponding to each protein is reported as relative to the total signal of the actin band present for each sample.

Statistical Analysis

Statistical significance was determined using GraphPad Prism software version 8.0.1. One way-ANOVA was performed to compare means ± SEM across time. Two way-ANOVA with a post-hoc Tukey test for multiple comparisons was performed to compare means ± SEM across time and between experimental treatment groups.

Results

Staining patterns revealed by two β-dystroglycan antibodies

We began our study by determining which of two commercially available antibodies for β-dystroglycan works best in SCN tissue. First, we tested a commonly used mouse monoclonal antibody for β-dystroglycan developed by Novocastra. Previous reports using this antibody reveal that β-dystroglycan expression appears to localize with endothelial vasculature cells in brain tissue (Zaccaria *et al.*, 2001; Agrawal *et al.*, 2006; Wolburg-Buchholz *et al.*, 2009; Kalman *et al.*, 2018). Surprisingly, many of the studies using this antibody also used *Mus musculus* as their model organism. This can be problematic because the secondary antibodies can recognize mouse IgGs (Daneshtalab *et al.*, 2010; Notter *et al.*, 2014) and therefore result in non-specific binding to off-target proteins. Therefore, we also tested a second β-dystroglycan antibody, developed by Abcam, that was isolated from a rabbit host organism. Based on a previous study, we elected to post-fix unperfused brain tissue in 4% PFA with the goal of preserving the integrity and structure of ECM proteins (Notter *et al.*, 2014).

Our initial assessments aimed to confirm and compare the binding efficacy of commercially available of β-dystroglycan antibodies. Mouse brain tissue samples collected at ZT 6 were incubated with either anti-mouse-488 or anti-rabbit-488 fluorescent secondary antibodies and the DAPI nuclear stain. Using DAPI, we were able to identify the cell dense SCN region in the hypothalamus. In SCN tissue incubated with the anti-mouse secondary antibody we observed diffuse background fluorescence and a staining pattern that resembled epithelial vasculature cells (Fig 3.1 A). In comparison, neither the

vasculature epithelial cell-like pattern nor the diffuse background staining was apparent in tissue samples incubated with the anti-rabbit secondary antibody (Fig 3.1 C). Tissue incubated with mouse anti-β-dystroglycan primary antibody followed by anti-mouse-488 secondary antibody (Fig 3.1 B) exhibited a stronger signal than that seen in samples incubated with the anti-mouse-488 secondary antibody alone, but the pattern continued to exhibit the "epithelial vasculature-like" pattern seen in Fig 3.1 A. Conversely, the staining observed in tissue incubated with rabbit anti-β-dystroglycan primary and anti-rabbit-488 secondary antibodies (Fig 3.1 D) was substantially different and appeared to localize to cell bodies. We observed strong fluorescent signal that overlapped the SCN region, along with fluorescent signal near the cell-layer surrounding the third ventricle. Based on the apparent non-specific staining observed when the tissue sections were incubated with the anti-mouse-488 secondary antibody, we elected to use the rabbit-anti-β-dystroglycan throughout the rest of our study.

β-dystroglycan expression in the SCN is constitutive and colocalizes with astrocytes across circadian time

Previous work examining the diurnal expression of various extracellular CAMs in the mammalian SCN has implicated a few in circadian clock regulation (Glass *et al.*, 1994; Lee *et al.*, 1995; Shen *et al.*, 1997; Shen *et al.*, 1999; Glass *et al.*, 2000; Shen *et al.*, 2001; Fedorkova *et al.*, 2002; Glass *et al.*, 2003; Prosser *et al.*, 2003; Cooper *et al.*, 2018). Although the expression of β-dystroglycan has not been studied in the SCN, it has been found to localize on GFAP-positive astrocytic endfeet in other brain regions (Zaccaria *et al.*, 2001; Agrawal *et al.*, 2006; Wolburg-Buchholz *et al.*, 2009; Noell *et al.*, 2011; Gondo *et al.*, 2014). Reports of mRNA and protein expression in the SCN indicate that GFAP is concentrated in the SCN and expressed in a rhythmic pattern (Morin *et al.*, 1989; Lavialle & Serviere, 1993; Ikeda *et al.*, 2003; Leone *et al.*, 2006; Becquet *et al.*, 2008; Deng *et al.*, 2010). Therefore, we hypothesized that β-dystroglycan would colocalize with GFAP positive cells in the SCN and potentially be expressed at different levels during the mid-day (ZT 6), early night (ZT 16) and late night (ZT 23).

Figure 3.2 A shows fluorescent images taken from unperfused SCN tissue co-labeled with DAPI and antibodies detecting both β-dystroglycan and GFAP. We observed

the presence of both proteins in the region corresponding to the SCN at each time point. Next, we measured the mean gray value of the fluorescent signal corresponding to either β-dystroglycan or GFAP by outlining the region that corresponded to SCN region defined by DAPI signal. The mean gray area ± SEM for the total signal (minus background selected from a non-SCN region) was calculated and plotted at each time point for both proteins. One-way ANOVA with a Tukey's multiple comparisons test revealed that β-dystroglycan expression levels were not statistically different at any selected ZT time ($p=0.9609$) (Fig 3.2 B). Previous research has demonstrated that GFAP expression varies across time (Lavialle & Serviere, 1993) and is lowest during the night (Leone *et al.*, 2006). However, a One-way ANOVA with a Tukey's multiple comparisons test found that total GFAP expression was not significantly different across time (Fig 3.2 C, $p=0.5664$) nor between SCN subregions (Fig 3.2 E). However, analysis of the mean grey value of β-dystroglycan expression between the ventral and dorsal sub-regions of the SCN and the AH determined that at each time point β-dystroglycan expression in dorsal SCN was higher than the AH (Fig 3.2 D; ZT 6 $p=0.0339$, ZT 16 $p=0.0161$, ZT 23 $p=0.0246$) and that the SCN ventral region was significantly different than the AH at ZT 16 ($p=0.0392$).

To assess potential co-localization of GFAP and β-dystroglycan, we re-imaged the same immunolabeled tissue samples under higher magnification with a confocal microscope. From each of the previously identified regions of interest examined under lower power, we took a series of ten Z-stack images at higher magnifications (40X and 60X) using a step size of 1 μM, displayed in Figure 3.3 A, are representative images (40X) of flattened Z-stacks (by average pixel density) taken at each time point. To more precisely assess potential colocalization of β-dystroglycan and GFAP (overlapping red and green channels produce a yellow signal), for several of these images we separated the Z-stacks and scanned the image at each Z-step to locate overlapping signal using 60X magnification. Through this process we identified areas of overlapping signal, as shown in Figure 3.3 B. Careful examination through the entire Z-plane of images showed that β-dystroglycan staining is in close proximity to GFAP-containing astrocytic somas and filiopodia in certain planes and not in others. These areas of overlapping fluorescence further support a potential interaction between β-dystroglycan and GFAP in the SCN.

β-dystroglycan and GFAP colocalization is highest during the late night

Cell morphology of 10-12 GFAP-positive cells for each ZT (60 X magnification, n=2 mice per ZT) was analyzed by two reviewers that were blind to experimental conditions. Cells were visually assessed for GFAP expression throughout the entire Z-plane (10 μm), and only cells contained within the Z-plane were selected for tracing and subsequent analysis. After the center of a cell was located, all branches were traced outward from the center, starting with the longest branch, using the Simple Neurite Tracer program. The Z-projection of the image stack was maintained and helped determine if a branch was contiguous with the cell of origin or if it originated from surrounding GFAP-positive cells. Subsequent (secondary, tertiary, etc.) branches were added until all branches were traced. Quantification of β-dystroglycan and GFAP overlap using the ImageJ Coloc-2 program shows a higher degree of signal overlap (a Pearson's R-value of 1 indicates perfect overlap) at ZT 23 as compared to ZT 16 ($p= 0.0362$). This suggests that although the total expression of GFAP and β-dystroglycan do not change between time points, the proximity of the two proteins with one another increases during the late-night as compared to the early night.

Sholl analysis of GFAP positive cells in the SCN suggests astrocytes at ZT 23 are more ramified

Previous light and electron microscope studies in SCN tissue report that GFAP protein expression levels change over time and GFAP-labeled cells exhibit daily morphological rhythms (Lavialle & Serviere, 1993; Leone *et al.*, 2006; Becquet *et al.*, 2008; Girardet *et al.*, 2010). However, our immunohistochemistry data showed that overall GFAP expression in the SCN is constant across time. Because our confocal images of GFAP-positive cells were of sufficient resolution to view individual glial cells and their branches, we continued our study by performing a quantitative assessment of their morphological characteristics across the day using a Sholl Analysis (Sholl, 1953). Representative images of GFAP-positive cells and an illustration of the Sholl Analysis process are shown in Figure 3.4 A.

First, the volume of each cell was measured using the fill feature and then Sholl analysis was performed. Briefly, Sholl analysis uses concentric circles drawn around the

center point of the cell at set intervals (1 μM radius step size) and counts the number of times the circles are crossed (Sum intersections). A mathematical model then extrapolates various features of cellular morphology, introduced below, and generates a quantified value for each feature. Figure 3.4 B contains histograms of the data that summarize our findings. Interpretations of the data were aided by previous studies utilizing this technique (Ristanovic *et al.*, 2006; Binley *et al.*, 2014; Ferreira *et al.*, 2014; Tavares *et al.*, 2017).

We found that both the total cell volume [Volume (μm^3)] and Soma Volume (μm^3) of GFAP-positive SCN astrocytes was not significantly different between the sampled cells across time (p=0.4184 and p=0.4876). Additionally, neither the total number of circle intersections for each cell (Sum intersections) nor the maximum number of circle intersections along a single arbor (Maximum intersections) was significantly different between ZT 6, ZT 16 and ZT 23 (p=0.0799 and p=0.9031, respectively). We interpret these findings to mean that astrocytes in the SCN maintain their total cellular volume and total number of branches across the time points observed.

In contrast to the features mentioned above, data corresponding to cell extension and ramification (a term that describes the complexity of the branching network of the cell) identified statistically significant differences over time. We found that the total radial extension (Ending Radius; the radial length of the last concentric circle intersected) of astrocytes at ZT 23 (mean ± SEM: 44.22± 9.561 μm) was significantly greater than at ZT 6 (33.30 ± 3.002 μm; p=0.0370) and ZT 16 (30.82 ± 2.964 μm; p=0.0074). The Ramification index (sampled) is calculated by dividing the Maximum intersections (defined above) by the number of primary branches. Higher Ramification index values indicate a larger number of secondary, tertiary, etc. branches. Our data indicate that astrocytes at ZT 23 (mean ± SEM: 7.472 ± 1.254) had a significantly higher Ramification index than at ZT 6 (3.182 ± 0.3958; p=0.0019) and ZT 16 (3.546 ± 0.1813; p=0.0044). A second measure of ramification is the Maximum intersection radius. This value represents the distance from the cell body (μM) at which the highest number of branch intersections, or branch density, occurs. Again, this measurement was significantly higher at ZT 23 (mean ± SEM: 22.22 ± 2.330 μM) when compared to ZT 6 (10.08 ± 1.717 μM; p=0.0009) and ZT 16 (12.84 ± 2.273 μM; p=0.0106). Thus, cells at ZT 23 have their highest

concentration of branches further away from their cell body than at ZT 6 and ZT 16. The Mean Value, representing the average number of circle intersections per astrocyte, was significantly lower at ZT 23 (mean ± SEM: 2.752 ± 0.1527) than at ZT 6 (4.297 ± 0.3136; p=0.0002) and ZT 16 (3.956 ± 0.2265; p=0.0002). Together, these data show that although cells at ZT 23 do no change their total volume or total branch number, their branching structure that is more complex, and increases ramification as the distance from the cell body increases. Across all these parameters, it is noteworthy that the differences were consistently greater between ZT 6 and ZT 23 than between ZT 16 and ZT 23. This suggests that astrocytes at ZT 23 were slightly more ramified than they are at a ZT 16 and dramatically more ramified than at ZT 6.

Two additional Sholl analyses are useful in understanding the differences in astrocyte morphology derived from our data (see Sholl Plot panel of Fig 3.4 A for illustration). The first measurement, kurtosis, describes the distribution of concentric circle-branch intersections across the entire circumference of the cell. Cells with kurtosis values close to zero exhibit a Gaussian distribution of intersections centered around the concentric circle corresponding to the mean number of intersections. Numbers greater than 1.0 indicate that the distribution of circle intersections exhibits a sharper peak in distribution around the circle corresponding to the largest number of intersections, while negative values are consistent with a flattened distribution of intersections. Our data show that cells at ZT 23 had a significantly greater kurtosis value (mean ± SEM: 1.457 ± 0.1527) than cells at ZT 6 (0.05582 ± 0.4350; p=0.0457) but were not significantly different from cells in the ZT 16 (0.3771 ± 0.3326; p=0.1478) experimental group. Lastly, the Sholl skewness measurement describes the directional distribution of intersections around the concentric circle where the mean number of intersections is located. A skewness number close of zero indicates that the number of intersections is distributed symmetrically around the mean number of intersections. Positive values indicate an asymmetrical distribution where a higher population of intersections exists further away from the cell, while negative values indicate the distribution of intersections is closer toward the cell body. We found that the largest measure of skewness occurred at ZT 23 (mean ± SEM: 1.154 ± 0.1135) and was significantly different from ZT 16 (0.2140 ± 0.2140; p=0.0013) and ZT 6 (-0.2887 ± 0.1773; p<0.0001). These data suggest that the amount of branching displayed by SCN

astrocytes at ZT 23 is highly concentrated at the distal end of the cell, with a distribution skewed distally from the cell body compared to the day and the early night.

Beta-dystroglycan protein expression in SCN tissue slices is not rhythmic and is not affected by inhibiting MMP-2/9 activity

In other brain regions, such as the hippocampus, the extracellular proteases MMP-2/9 are known to cleave the β-dystroglycan subunit into a 30 kDa fragment (Michaluk *et al.*, 2007). Additionally, β-dystroglycan cleavage increases when MMP-2/9 activity increases (Li *et al.*, 2016). As MMP-2/9 are expressed and active in the SCN (Agostino *et al.*, 2002)(Chapter 2) we investigated whether MMP-2/9 enzymatic activity modulates β-dystroglycan degradation over the course of the day.

The benefits of utilizing SCN tissue slices maintained i*n vitro* are that the rhythmicity of the circadian pacemaker remains unaffected (Gillette & Prosser, 1988; Prosser & Gillette, 1989) and this preparation easily allows for tissue collection and subsequent protein extraction after an acute drug treatment (Mou *et al.*, 2009; Lindsay *et al.*, 2014; Cooper *et al.*, 2017; Yamada & Prosser, 2018). Using western blotting, we measured β-dystroglycan protein expression in SCN tissue slices incubated with or without the BiPS inhibitor (see Methods) using the rabbit anti-β-dystroglycan antibody, which detects the full and truncated forms of β-dystroglycan. Therefore, we analyzed full length (43 kDa) vs. cleaved (30 kDa) β-dystroglycan levels with and without MMP-2/9 inhibition at ZT 6, ZT 16 and ZT 23.

Figure 3.5 shows that both the full length (43 kDa) and truncated (30 kDa) forms of β-dystroglycan are expressed in SCN tissue slice homogenates. Two-way ANOVA determined that there were no statistically significant differences in expression of the full-length ($p=9.879$) or truncated fragments ($p=9.870$) of β-dystroglycan (relative to actin) across time or in response to BiPS treatment. Further analysis showed that the total amount of β-dystroglycan ([full-length signal + truncated signal])/actin signal) also did not exhibit statistically significant changes across time ($p=0.9196$). Lastly, we examined the ratio of truncated to full-length β-dystroglycan across the three time-points. Again, there was no statistically significant difference in this ratio across time ($p=0.5998$).

Discussion

In this study, we investigated a possible link between MMP-2/9 function and circadian rhythms in astrocyte morphology by examining the expression and proteolytic cleavage of β-dystroglycan in the SCN. We found that β-dystroglycan is highly enriched in the SCN and that it appears to be partially co-localized with GFAP. The co-localization pattern suggests that β-dystroglycan is in close proximity to astrocytes and thus could serve as a structural bridge to facilitate binding to the ECM. Additionally, we demonstrated with quantitative morphological analysis that SCN astrocytic morphology exhibits changes in select parameters across the circadian cycle while the total intracellular volume of GFAP remains constant. However, MMP-2/9 cleavage of β-dystroglycan may not directly regulate the diurnal astrocytic state changes, as the total level and level of cleaved β-dystroglycan does not change dependent on either time or MMP-2/9 inhibition.

Before selecting an antibody, it is necessary to choose a secondary antibody that is raised in a species outside of the host animal you wish to use for protein detection (Harlow, 1999; Daneshtalab *et al.*, 2010). A proper secondary antibody-only negative control should be performed to confirm antibody specificity. We used these basic principles of immunohistochemistry to characterize the localization pattern of β-dystroglycan in SCN tissue. The staining pattern observed in SCN tissue incubated with only the anti-mouse-488 secondary antibody was almost identical to the stain visualized after the combination mouse anti-β-dystroglycan + anti-mouse-488 antibodies. This pattern produced using the anti-β-dystroglycan closely resembles the microvasculature of the brain and is consistent with past studies, (Zaccaria *et al.*, 2001; Agrawal *et al.*, 2006; Wolburg-Buchholz *et al.*, 2009; Kalman *et al.*, 2018); however, we did not detect this pattern in either the secondary-only or primary-secondary combination of the rabbit anti-β-dystroglycan and anti-rabbit-488 antibodies. Therefore, we concluded that the staining observed using the rabbit antibodies was specific to β-dystroglycan expression. We also believe that the localization data from the previous studies should be considered with caution, given our comparison of the two antibodies.

Changing levels of either β-dystroglycan or GFAP can accompany changes in astrocytic structure (Noell *et al.*, 2011; Gondo *et al.*, 2014). Our observations of β-dystroglycan and GFAP protein expression in the SCN, however, found no significant

changes between ZT 6, ZT 16 and ZT 23 using both immunohistochemistry and western blotting (Figs 3.2 and 3.5). Although our GFAP protein expression data are not consistent with a previous observation of increased GFAP expression at ZT 6 compared to ZT 18 (Leone *et al.*, 2006), they are consistent with a different study that observed constant GFAP levels in the SCN of hamsters housed in light:dark conditions (Moriya *et al.*, 2000). These inconsistencies may be due to different antibodies used, the model system (mice vs. hamster vs. SCN glial cell culture), using *in vivo* vs. *in vitro* tissue samples, or the manner in which our samples were collected (perfused vs. non-perfused tissue). In the future, it may be necessary to measure GFAP protein expression across more time points, under different lighting schedules, and utilizing a variety of analyses to better understand the factors regulating GFAP expression in the SCN.

Highlighting the benefits of using more nuanced analyses, quantitative examination of GFAP positive cells in the SCN using Sholl analysis revealed multiple aspects of astrocytic morphology that vary over time. Our analysis shows that astrocyte morphology is different between the early night (ZT 16) and late night (ZT 23), while even larger differences exist between mid-day (ZT 6) and late night (ZT 23). First, Sholl analysis shows astrocytes in our samples do not exhibit a change in total cellular or somal volume, the total number of radii intersections or the maximum number of branches per individual arbor. We interpret these findings as indicating that the total volume of each astrocyte (as well as total GFAP expression within each astrocyte) does not change significantly across these three time points.

The complexity of the branch pattern, however, increases as the circadian clock progresses from midday (ZT 6) to late night (ZT 23), as does the length of the cell. Thus, without changing the total number of branches, the filopodia intersect with the concentric circles drawn around the cell body more frequently, suggesting that the path through which the branches extend becomes more irregular. Next, an increased Ramification index at ZT 23 vs. ZT 6 and 16 indicates that at ZT 23 astrocytes have more higher-order branches. In contrast, the branching pattern shows that there are more primary branches at ZT 6 and ZT 16 than at ZT 23. This suggests that in the late evening, when astrocytes are extending their filopodia, they reorganize their cytoskeleton to reduce the number of primary braches while increasing the number of higher-order branches. The results of the

skewness and kurtosis measurements align with this interpretation, as they indicate that the branching pattern of astrocytes is more asymmetrical and that the distribution of GFAP within each cell shifts further away from the cell body at ZT 23. Together, we interpret these results to mean that astrocyte morphology transitions from a non-complex and more condensed form towards an extended shape with increased ramifications distal from the cell body as circadian time progresses from the day into the late night. However, these changes do not require a change in overall GFAP expression. Consistent with this, other studies have found that changes in astrocyte morphology do not necessarily require a change in GFAP expression (Safavi-Abbasi *et al.*, 2001), but rather are thought to involve a redistribution of the protein within each cell. Because we observed that colocalization of GFAP with β-dystroglycan is highest at ZT 23, we hypothesize that the coincident increase in ramification of astrocytes requires increased interactions with ECM-associated molecules. Further, the proteolytic mechanisms governing the anchoring of astrocytic extensions to the extracellular environment may require the activity of MMP-2/9.

In a previous study, we used gelatin zymography to indirectly measure MMP-2/9 activity in the SCN and found that MMP-2/9 gelatinolytic activity is highest during the mid-day (ZT 6) and lowest during the late night (ZT 23). It is possible that the increased MMP-2/9 proteolytic activity at ZT 6 creates an extracellular environment that permits morphologic change that reaches a maximum at ZT 23. Therefore, we suggest that the day to night transition in astrocytic morphologic change is mediated by MMP-2/9 dependent degradation of ECM-associated molecules, providing unobstructed space for astrocytic filopodia to extend in length and increase the complexity of their branches.

In other brain regions, β-dystroglycan cleavage by MMP-2/9 is necessary for astrocytic morphological changes. Because β-dystroglycan expression is higher in the SCN than the AH (Fig 3.2 D) and exhibits greater colocalization with GFAP at ZT 23 than at ZT 16 (Fig 3.3 C), regulation of β-dystroglycan expression and subsequent differences in astrocytic morphology may be regulated by circadian variations in extracellular protease activity. Based on our data and the literature, we proceeded to assess β-dystroglycan proteolysis by MMP-2/9 as a potential mechanism contributing to the astrocytic structural changes in the SCN. However, we found that β-dystroglycan

cleavage is unaffected by MMP-2/9 activity at any of the timepoints we investigated. Further, β-dystroglycan total, full length and cleaved peptide expression is constant over time. It is possible that the time we collected tissue samples before and after BiPS treatment was not optimal for assessing the effect of MMP-2/9 activity on β-dystroglycan cleavage. For example, researchers investigating the effects of epileptic activity in cortical brain slices waited one hour after stimulation before tissue collection and observed a marked degradation of β-dystroglycan (Gondo *et al.*, 2014). In primary cortical neuron cultures, β-dystroglycan-mediated reduction of neurite outgrowth (by 30%) requires a minimum incubation period of 24-hours with TIMP-1, an endogenous inhibitor of MMP-9, to induce a change (Ould-yahoui *et al.*, 2009). In another study, a 50 μM dose of glutamate applied for 10 minutes increased cleavage of β-dystroglycan for up to 20 minutes after treatment; however, the highest level of degradation was seen just 10 minutes after the treatment (Michaluk *et al.*, 2007). As our BiPS treatment lasted for 40 minutes, it would be interesting to collect SCN samples at more frequent and extended times after treatment and compare the amount of truncated β-dystroglycan at each interval to fully elucidate the effect of BiPS on β-dystroglycan cleavage.

Our examination of β-dystroglycan and GFAP staining did unveil potential differences in localization patterns within the SCN and surrounding hypothalamus. First, the expression of β-dystroglycan is higher in the dorsal subregion of the SCN relative to the anterior hypothalamus at all three times, while the ventral SCN exhibited higher expression only at ZT 16 Future studies examining a possible difference in dorsal vs. ventral SCN expression of β-dystroglycan should utilize antibodies for neuropeptides, such as AVP or VIP, that are differentially expressed in these sub-regions, to more confidently characterize β-dystroglycan localization patterns, expression patterns and identify regulatory mechanisms that are tied to the circadian clock.

A secondary observation based on our immunohistochemistry results is that both β-dystroglycan and GFAP are highly expressed near cells surrounding the third ventricle. Many laboratories have investigated the contribution of astrocytes to regulation of the blood brain barrier (BBB). Higher neuronal activity increases nutrient demand, which activates astrocytes, increases capillary fenestration size and increases blood flow to regions that are nutrient deficient (Iadecola, 2004). Research has shown that extracellular

CAMs, including β-dystroglycan, mediate the changes in fenestrations between the endothelial capillary walls and astrocytic endfeet (Abbott, 2002; del Zoppo & Milner, 2006). Given that BBB permeability is regulated by the circadian clock (Nakazato *et al.*, 2017; Cuddapah *et al.*, 2019), it would be interesting to investigate if astrocytic morphological changes, mediated by β-dystroglycan cleavage, are involved in circadian BBB regulation.

As mentioned earlier, cleavage of β-dystroglycan by MMP-2/9 generally occurs after injury or response to significant increases in neuronal activity (Michaluk *et al.*, 2007; Frischknecht *et al.*, 2014; Yan *et al.*, 2016). In our study, BiPS application did not affect β-dystroglycan protein levels, suggesting MMP-2/9 catalyzes a different substrate in SCN tissue. A variety of ECM-associated molecules that are expressed in the SCN and/or implicated in the regulation of circadian rhythms (Cooper *et al.*, 2018) are also recognized as MMP-2/9 substrates (Ethell & Ethell, 2007). For example, quantitative PCR and *in situ* hybridization experiments in mice determined that the SCN and other retinorecipient regions are enriched in collagen25a1, a main substrate for MMP-2/9 (Monavarfeshani *et al.*, 2017). Interestingly, the composition and mechanical stiffness of the extracellular microenvironment, of which collagen is a pivotal component, can determine the amplitude of clock gene rhythms in breast tissue (Yang *et al.*, 2017; Broadberry *et al.*, 2018). In fibroblasts isolated from mice, qPCR analysis found that genes encoding for collagen-I precursors and binding immunoglobulin protein (BiP), a protein that aids in collagen secretion and folding, exhibit rhythmic mRNA expression (Pickard *et al.*, 2019). Because collagen expression in other tissues appears to be controlled by endogenous circadian clocks, it would be worth investigating if MMP-2/9 modulation of clock phase involves collagen cleavage in the SCN.

Another cellular adhesion molecule that may serve as a substrate for MMP-2/9 in the SCN is PSA-NCAM (polysialylated-neural cell adhesion molecule). PSA-NCAM is known to play an important role in brain plasticity (Theodosis *et al.*, 1994; Bonfanti, 2006) and injury. In a mouse model of cerebral artery occlusion, inhibition or gene knockout of MMP-9 ameliorates ischemia-induced neuronal damage and decreases the amount of NCAM cleavage (Shichi *et al.*, 2011). Although the majority of PSA-NCAM expressed in the brain is located on neuronal membranes, it is also expressed on the cell surface of

astrocytes in cortical primary cultures (Minana *et al.*, 1998). In the substantia nigra, chemical lesion increases PSA-NCAM expression in isolated reactive astrocytes and colocalizes with GFAP (Nomura *et al.*, 2000). It is also known that PSA-NCAM expression is enriched and rhythmic in the adult mouse SCN (Glass *et al.*, 1994; Glass *et al.*, 2003) and upon genetic deletion, can disrupt locomotor activity rhythms in mice (Shen *et al.*, 1997). Also, *in vitro* removal of PSA from NCAM using endoneuraminidase-N prevents glutamatergic phase shifts in SCN rat brain slices (Prosser *et al.*, 2003). Thus, PSA-NCAM is a key ECM-associated molecule that may be a target for MMP-2/9 in regulating SCN circadian rhythms.

Other potential extracellular targets for MMP-2/9 that are implicated in circadian rhythm regulation (i.e., neuroligins, neurexins, Eph receptors)(Hannou *et al.*, 2018a), are beginning to be studied in the context of astrocytic morphology regulation in a variety of brain phenomena as well (Carmona *et al.*, 2009; Puschmann & Turnley, 2010; Murai & Pasquale, 2011; Ruscher *et al.*, 2011; Zhao *et al.*, 2011; Stogsdill *et al.*, 2017). Nevertheless, the exact targets of MMP-2/9 activity in the SCN are still to be determined. Until each of these molecules is characterized in regard to their expression pattern, location and proteolytic cleavage by MMP-2/9 in the SCN, we will not understand the full relationship between circadian variation in MMP-2/9 activity, ECM-associated molecules and diurnal astrocytic morphology in the SCN.

In conclusion, these studies reveal that astrocytic interactions with β-dystroglycan may facilitate diurnal changes in astrocytic morphology in the SCN. However, this hypothesis needs to be tested in the SCN with future experiments that disrupt astrocytic adherence to β-dystroglycan. Because β-dystroglycan cleavage in SCN does not appear to be mediated by MMP-2/9 nor does it change over time, it is also unclear if β-dystroglycan participates in the maintenance of SCN circadian rhythms. Finally, our findings suggest that the astrocytic day to night transition toward a ramified state, requires a rearrangement of GFAP intracellular distribution. In the future, more research on this topic will help us understand how ECM-linked mediated structural changes facilitate the generation and regulation of the SCN circadian clock and the maintenance of intercellular synchronization in the SCN.

Appendix: Figures for Chapter 3

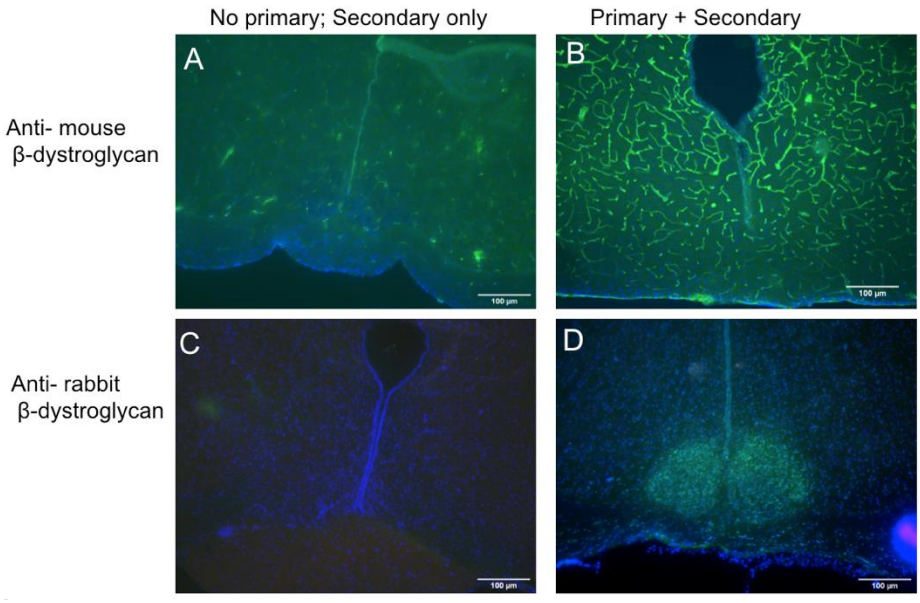

Figure 3.1: β-dystroglycan is expressed in the SCN.

Images of hypothalamic sections (25 µm) immunostained for β-dystroglycan, using either an anti-mouse (1:500, Novocastra) or anti-rabbit (1:500, Abcam) antibody, and cell nuclei using DAPI (blue) (n=1). Our negative controls that contain secondary antibodies to detect mouse or rabbit IgG's show that the anti-mouse secondary antibody alone (A) produces non-specific fluorescent signal, while the anti-rabbit antibody (C) does not. As such, we suspect the endothelial pattern visualized in panel B is most likely due to non-specific binding and not presence of β-dystroglycan. Thus, anti-rabbit antibody used in panel D is superior for detection of β-dystroglycan *in situ* and highlights its expression within the SCN.

Figure 3.2: Expression of β-dystroglycan and GFAP does not change over time.

A) Brain tissue collected at ZT 6, ZT 16 and ZT 23 was sliced into 25 μM sections and stained to detect β-dystroglycan (1:500), GFAP (1:1000). Tissue was also stained with DAPI to confirm the region of the SCN. Fluorescent images, 8-bit, were taken at 20X magnification and highlight marked expression of both proteins in the SCN. Using Image J-Fiji, the images were separated into their corresponding channels. The region of the SCN was circled first in the DAPI channel and then transferred to both the red and green channels to measure the mean gray value of pixels present within the SCN region. The background was selected from adjacent hypothalamic tissue outside of the SCN and subtracted from the total mean gray value. Panels B) and C) plot the mean gray value measured from biological replicates collected at each time point (β-dystroglycan: n=7-11; GFAP: n=5-7). A One-way ANOVA analysis was performed on the data and revealed neither β-dystroglycan expression ($p=0.9609$) nor GFAP expression ($p=0.5664$) is different between the time points selected. The final panel (D) illustrates regions of interest selected [ventral SCN (V), dorsal SCN (D), and anterior hypothalamus (AH)] for hypothalamic subregion analysis of β-dystroglycan and GFAP expression. While GFAP expression (mean grey value) remained constant across time, the mean grey value for β-dystroglycan expression in the dorsal SCN at ZT 6 and ZT 23, and both SCN subregions at ZT 16 were significantly higher than the AH (*=$p< 0.05$).

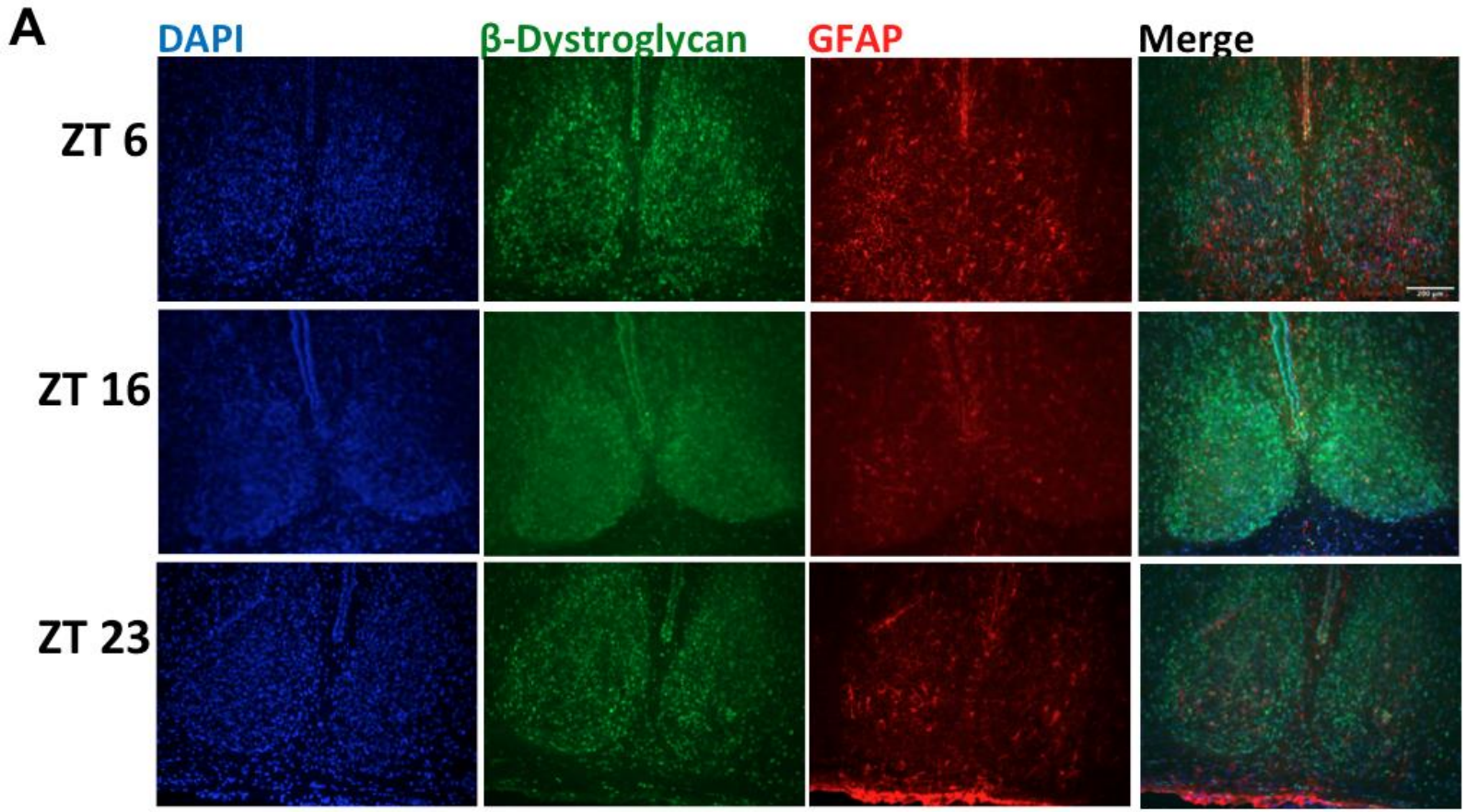

Figure 3.2 continued

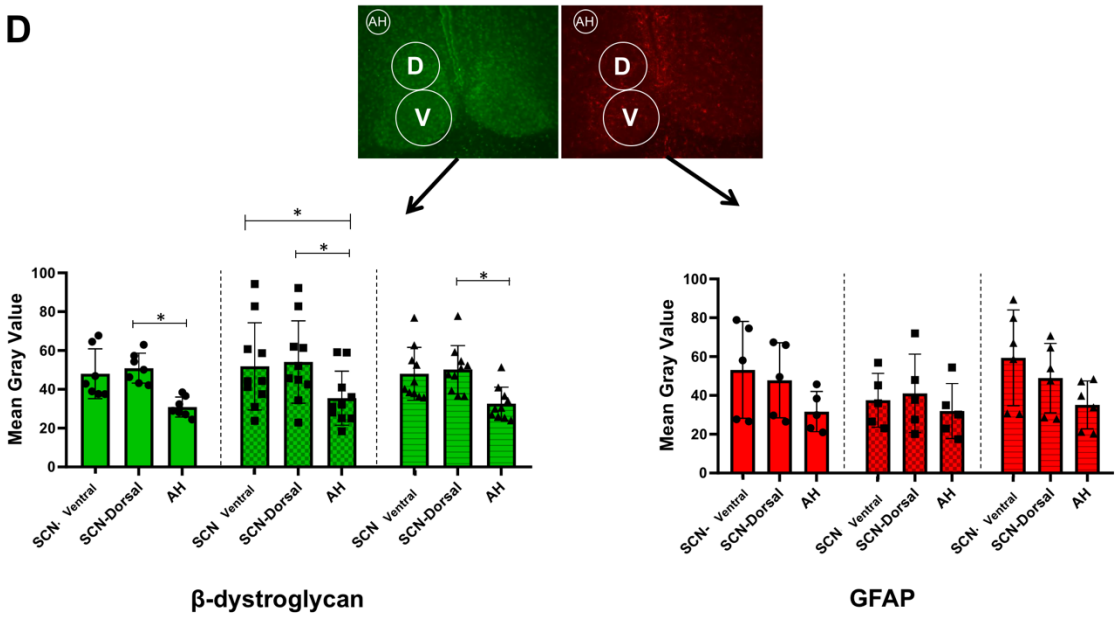

Figure 3.2 continued

Figure 3.3: β-dystroglycan and GFAP fluorescence overlaps at multiple time-points and is highest at ZT 23.

A) Confocal images (40X magnification) of SCN tissue collected at ZT 6, ZT 16 and ZT 23 reveal punctate co-localization of β-dystroglycan (green channel) and GFAP (red channel) signal. B) Un-stacked, sequential image slices (60X magnification) collected from SCN tissue suggest co-localization of β-dystroglycan and GFAP occurs on both filopodial extensions and cell bodies of astrocytes. The white arrows/arrowheads point to areas where overlapping signals change intensity through the Z- plane (different shapes point to different astrocytic features containing β-dystroglycan signal). Images collected are a step size of 1 μm, and 10 sequential images were collected. C) Quantification of β-dystroglycan and GFAP overlap using the ImageJ Coloc-2 program shows a higher degree of signal overlap (a Pearson's R-value of 1 indicates perfect overlap) at ZT 23 as compared to ZT 16 (*$p < 0.05$).

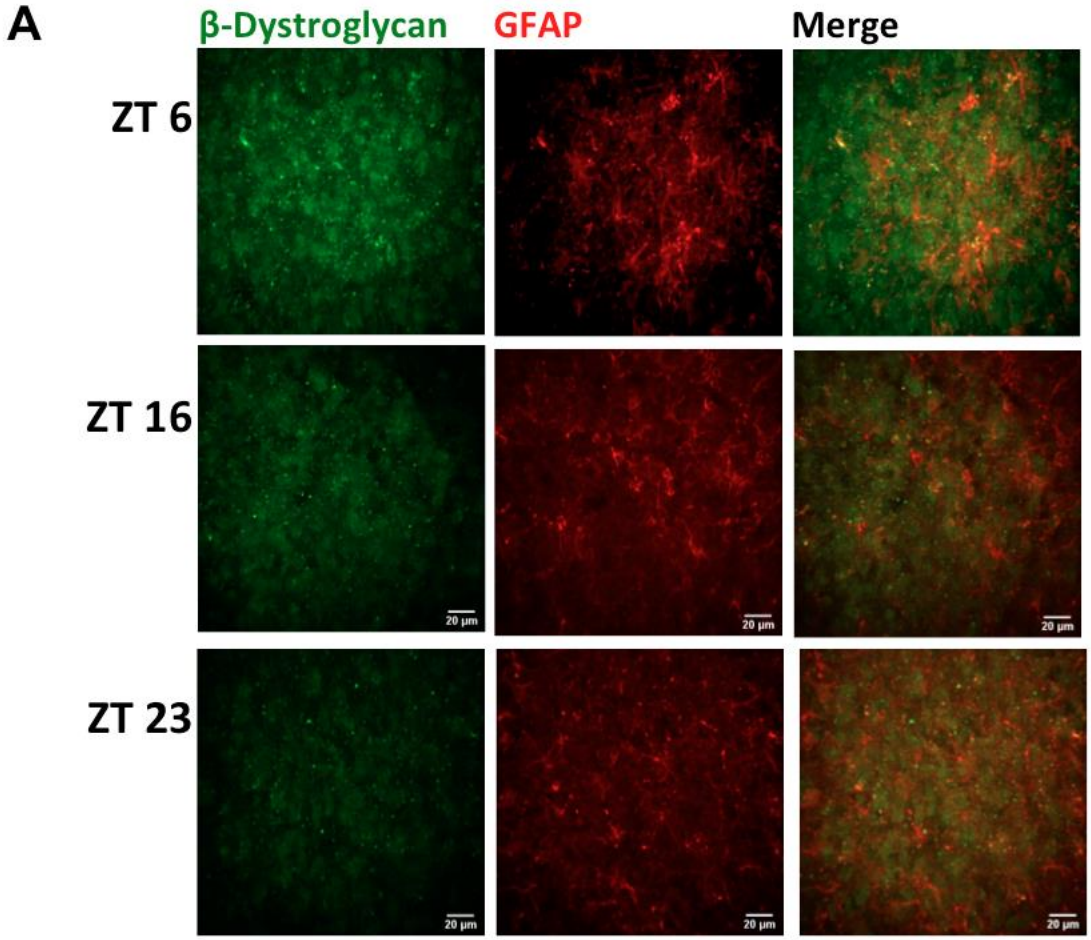

Figure 3.3 continued

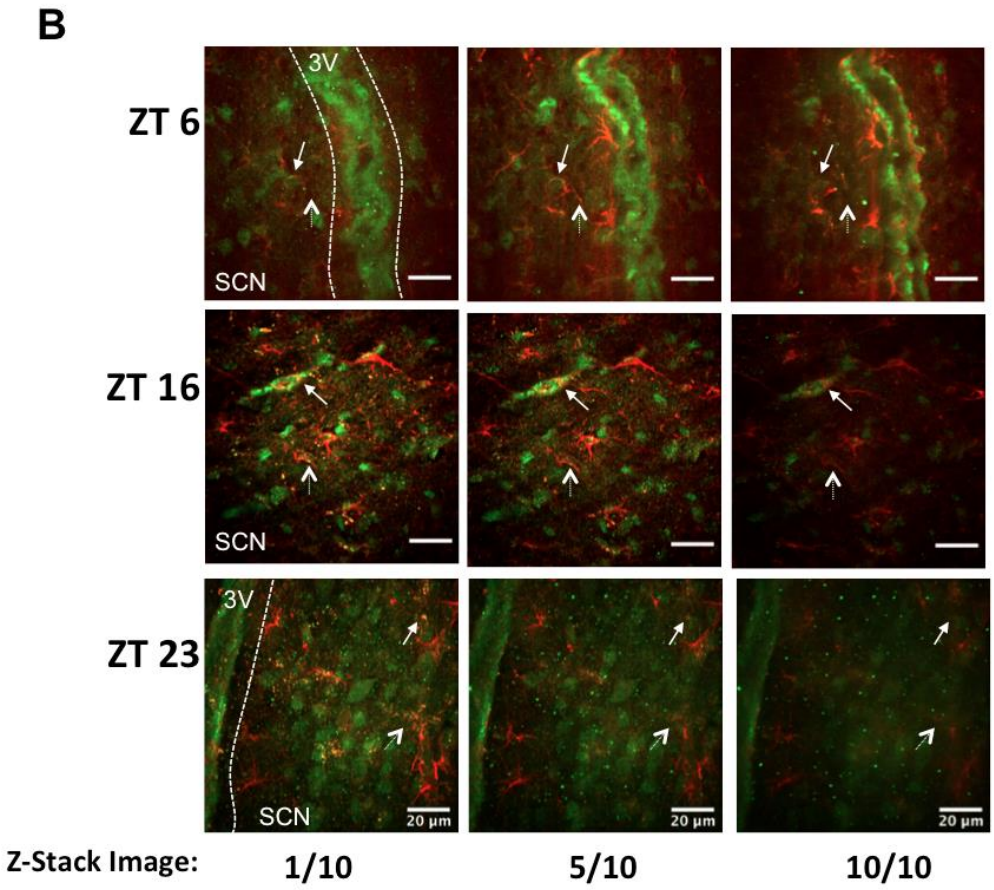

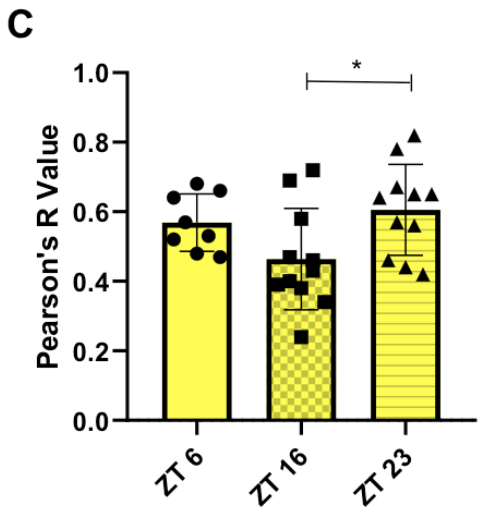

Figure 3.3 continued

Figure 3.4: Examination of astrocyte morphology over time using Sholl analysis.

A) Average intensity merged Z-stacks (40X magnification, 10 μm total depth, 1 μm step size, scale bar= 20 μm) of representative GFAP positive cells (n=10-12) located in the SCN at each time point (left panels). Using the Simple Neurite Tracer program available on Image-J (Fiji), individual astrocytes were traced, total and somal fill volumes collected, and Sholl analysis was performed. The middle panels show representative tracings of individual astrocytes (pink, artificially enlarged from 40X image for illustration). Included in the rightmost panel are Sholl plots (Distance from soma (μm) vs. number of intersecting radii) for each traced cell and illustrate the distribution of radial intersections along the length of the cell (radius=μm). The dotted line represents half the distance of the furthest radius away from the center of the cell. B) Summary of astrocytic characteristics measured by tracing GFAP positive cells in SCN tissue at ZT 6, ZT 16 and ZT 23. Individual data points are plotted around the mean value for each characteristic ± standard deviation. Sholl results indicate that cell volume (Volume (μm)), total intersections (Sum inters.), hiighest number of branch points on a cell (Max intersections), and Soma Volume are not statistically different. The total length of the cell (Ending radius) and the ramification indices (Ramification index (sampled) and max intersecting radius) are highest at ZT 23. The total number of branches (ZT 6), however, is lowest at ZT 23. Further, the cell shape changes across time. Cells at ZT 23 are less symmetrical (positive Skewness value compared to ZT 6) and their distribution of branch points across the circumference of the cell do not fit a normal, Gaussian distribution (positive Kurtosis). Asterisks denote statistical significance as determined by Ordinary One-Way ANOVA analysis ($\alpha=0.05$); *$p<0.05$, **$p<0.01$, ***$p<0.005$ and ****$p<0.0001$.

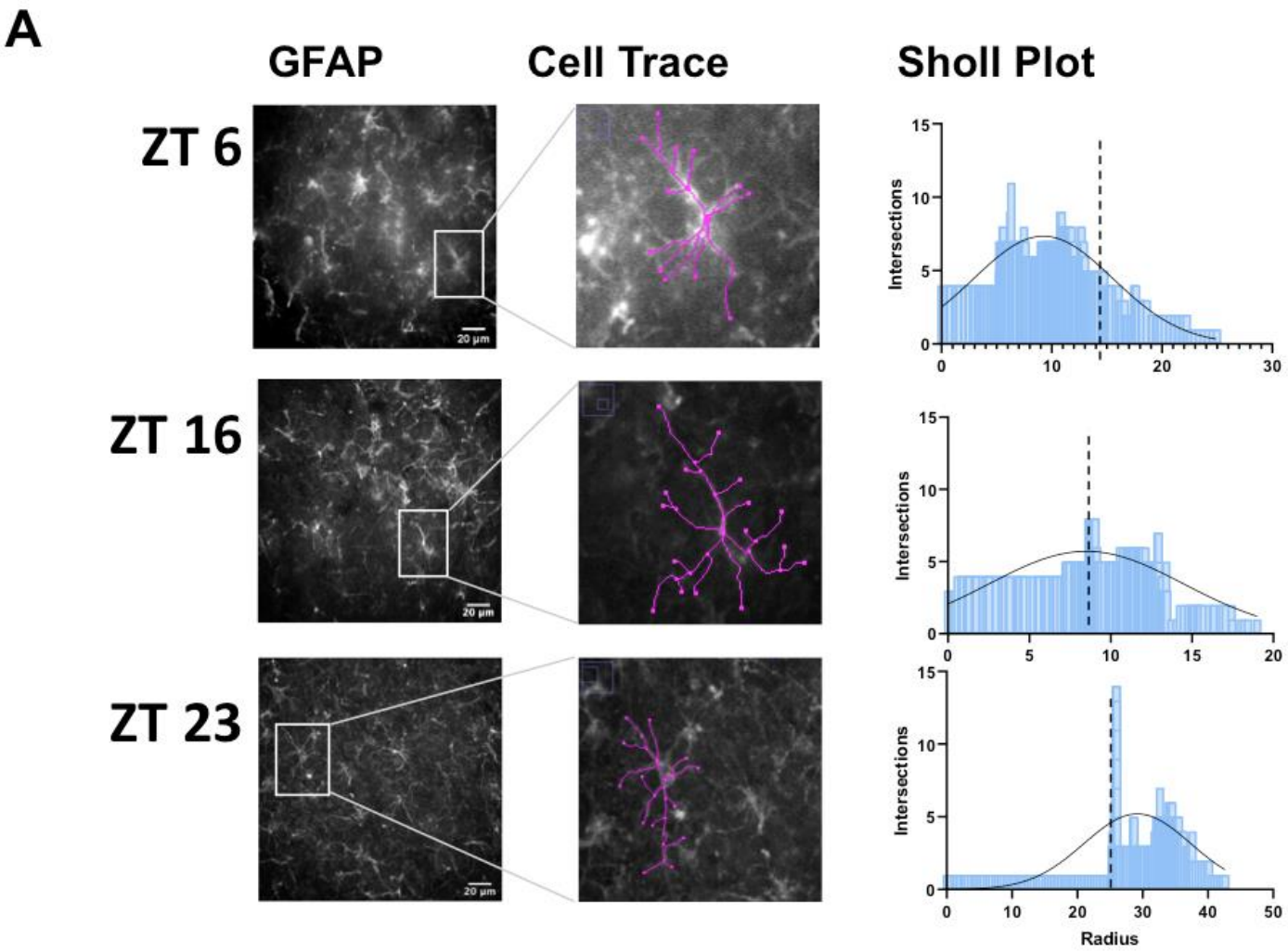

Figure 3.4 continued

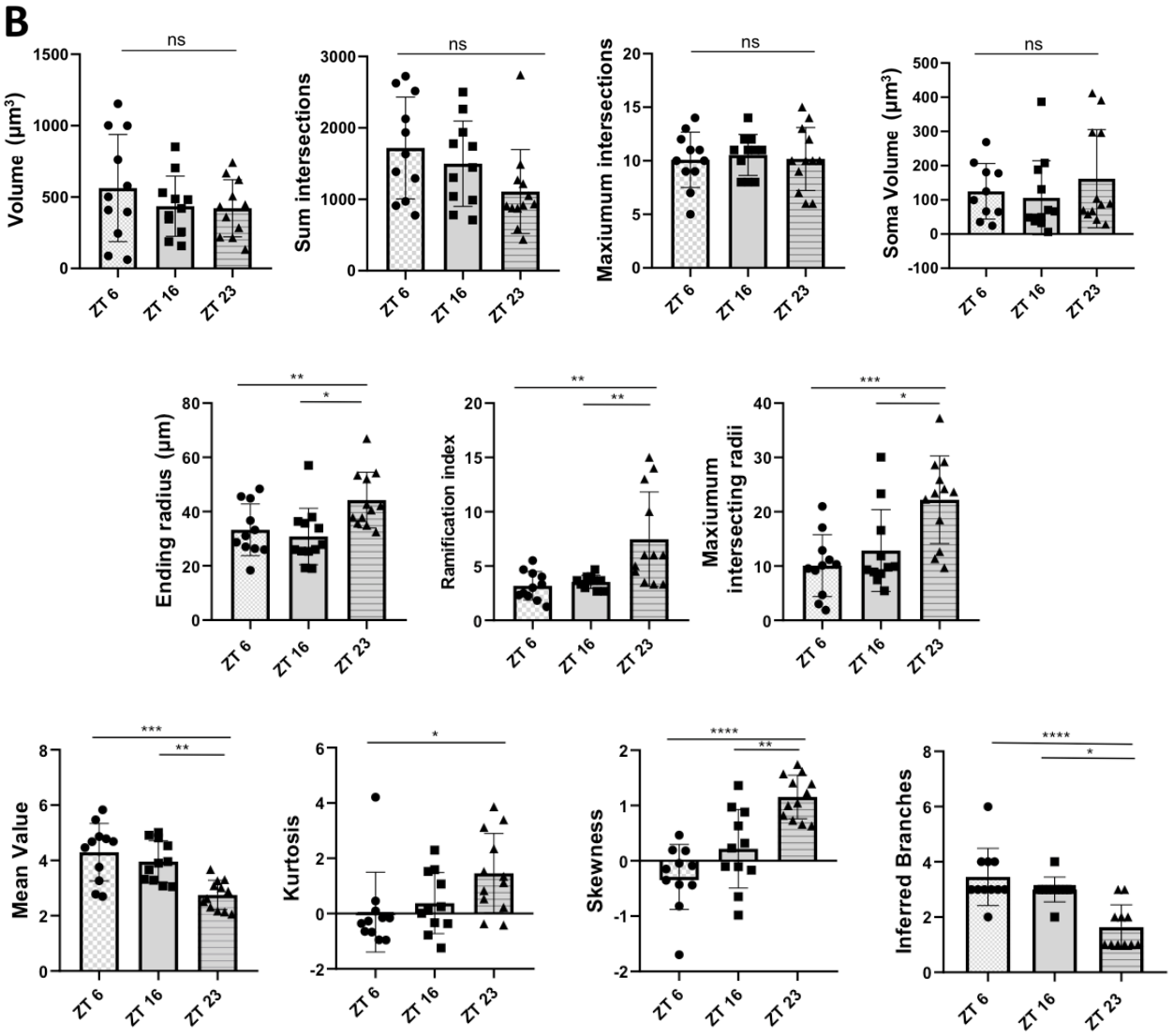

Figure 3.4 continued

Figure 3.5: β-dystroglycan expression in SCN tissue homogenate does not change over time and is unaffected by MMP-2/9 inhibition.

Fluorescent western blot results of control and drug treated (MMP-2/9 inhibitor, BiPS) SCN tissue slices collected at ZT 6, ZT 16 and ZT 23 (n=6). Blots were incubated with primary antibodies to detect β-dystroglycan and actin (as a house keeping protein, 42 kDa) expression. Both the full length (43 kDa) and truncated (30 kDa) forms of β-dystroglycan can be observed (Note: the red band (~33 kDa) in the β-dystroglycan is of unknown origin but may be residual dye contained in the sample loading dye, as the actin antibody was applied to blots after β-dystroglycan antibody incubation and detection). Quantification of fluorescent signal intensity reveals that neither the full length (B) or truncated (C) forms change expression over time or after BiPS treatment. Additional analysis showed the neither the total amount of β-dystroglycan expression (D) or the ratio (E) of truncated:full length β-dystroglycan (30 kDa: 43 kDa) changes between time points and is unaffected by BiPS treatment.

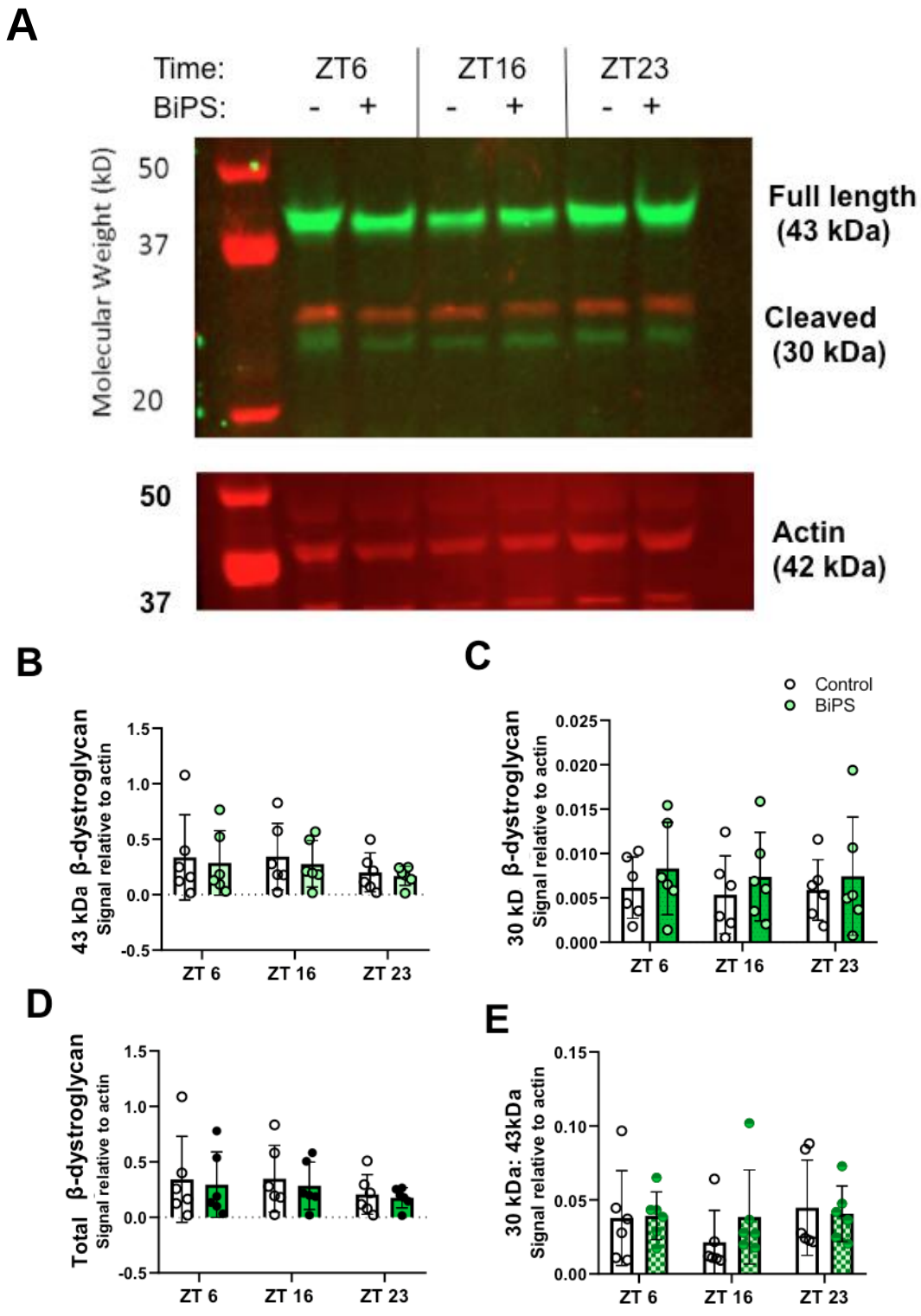

Figure 3.5 continued

CHAPTER IV: CONCLUSIONS AND FUTURE DIRECTIONS

Summary

The extracellular space (ECS) is dynamic in both structure and function (Dityatev *et al.*, 2006). The microenvironment existing in this space is a complex network of structural proteins that form the extracellular matrix (ECM), together with interacting signaling molecules, cellular adhesion molecules (CAMs) and transmembrane receptors. ECM composition changes over the course of organism development, and its dysregulation can lead to a variety of disease pathologies. Research investigating the ECM and its associated proteins in the context of circadian rhythms demonstrates cyclic expression of ECM molecules in multiple brain regions. Further, many are implicated in regulating the mammalian master circadian clock, located in the suprachiasmatic nucleus (SCN) (Cooper *et al.*, 2018). However, little is known about the proteolytic mechanisms mediating circadian and/or diurnal changes in ECS composition.

The goal of this research was to expand upon past findings in our laboratory that identified a pivotal role of extracellular proteases, namely those in the plasminogen activation cascade, in gating glutamate-induced phase shifts of the SCN circadian clock. Matrix metalloprotease-2 and -9 (MMP-2 and MMP-9) activation is a direct result of plasmin proteolysis and can modulate N-methyl-D-aspartate receptor (NMDAR)-dependent signaling across the brain (Bozdagi *et al.*, 2007; Ethell & Ethell, 2007; Michaluk *et al.*, 2009; Gorkiewicz *et al.*, 2010; Wiera *et al.*, 2017). A previous study of MMP-2/9 in the hamster SCN reported that MMP-9, but not MMP-2, exhibits a diurnal rhythm in activity (Agostino *et al.*, 2002). However, neither the mechanisms of MMP-2/9 activation nor the physiologic consequences of MMP-2/9 inhibition in the SCN were examined. Thus, we first aimed to further characterize MMP-2/9 expression and activity and explore MMP-2/9 mediated mechanisms in the SCN.

The experiments in Chapter 2 tested the hypothesis that MMP-2/9 activity is necessary to gate glutamate-induced phase shifts in the SCN circadian clock. We confirmed, using western blotting and gelatin zymography, that MMP-2/9 are expressed and active in SCN tissue extracts. We found that MMP-9 activity is highest at ZT 6 and lowest at ZT 23. We further showed that MMP-2 activity is constitutive across the circadian cycle. Using *in situ* zymography, we confirmed that the MMP-2/9 inhibitor 2-(benzenesulfonylamino)-N-hydroxy-3-phenylpropionamide (BiPS) co-incubated with DQ-

Gelatin solution in SCN tissue eliminates MMP-2/9 activity *in situ*. However, neither *in vitro* bath application of BiPS nor time affected the observed level of gelatinolytic activity of MMP-2/9 compared to control tissue. It is possible that we did not observe the same day vs. night difference in MMP-9 activity that we did with gelatin zymography because this assay does not distinguish between the activity of MMP-2 and 9. However, *in situ* zymography was able to reveal enhanced MMP-2/9 activity in the SCN as compared to the anterior hypothalamus. After confirming MMP-2/9 activity in the SCN, we continued our efforts to examine if these proteases serve a functional role in gating glutamate-induced phase shifts of the master clock.

Our data showed that MMP-2/9 inhibition during the day and early night phase shifts the SCN clock. This is the first indication that MMP-2 and/or MMP-9 participate in maintaining correct circadian clock phase. We then found that BiPS-induced phase delays and advances are blocked by the NMDAR antagonist D-(–)-2-amino-5-phosphonopentanoic acid (AP5). This demonstrates that phase shifts resulting from MMP-2/9 inhibition require NMDAR activity. When we examined additional mechanisms regulating BiPS phase shifts, we found that only phase advances in response to BiPS treatment at Zeitgeber Time (ZT) 6, not the phase delays induced at ZT 16, require both plasmin activity and brain derived neurotrophic factor (BDNF) activation of tyrosine receptor kinase B (TrkB).

Lastly, we investigated a potential intracellular, NMDAR-dependent downstream mechanism of BiPS-induced phase shifts. We hypothesized that BiPS treatment leads to increased NMDAR activation and channel opening, increases in intracellular Ca^{2+} concentration ($[Ca^{2+}]_i$), and subsequent increases in phosphorylation of CAMKII. Using western blotting, we found that BiPS does not alter the phosphorylation of either isoform of CAMKII (α-CAMKII or β-CAMKII) in SCN tissue. Together, the experiments in Chapter 2 reveal that MMP-2/9 activity is required for circadian clock phase regulation but the mechanisms through which they regulate clock phase still need clarification.

In the experiments presented in Chapter 3, we examined a potential link between MMP-2/9 activity and the diurnal structural rearrangements exhibited by SCN astrocytes. We chose to investigate β-dystroglycan because it is a common substrate of MMP-2/9 (Michaluk *et al.*, 2007; Sbardella *et al.*, 2012; Yan *et al.*, 2016) and is tightly linked to

regulating changes in astrocytic morphology in many brain regions (Peng *et al.*, 2008; Noell *et al.*, 2011; Gondo *et al.*, 2014), but it has not been investigated in the SCN. Therefore, we sought to examine if extracellular proteolysis of β-dystroglycan is mediated by MMP-2/9 activity and if this activity is linked to astrocytic morphological changes in the SCN.

We determined that glial fibrillary acidic protein (GFAP) and β-dystroglycan are both expressed in the SCN, are higher in the ventral SCN than the AH, and that their total expression is consistent across ZT 6, ZT 16 and ZT 23. Our observations also suggest the two molecules exhibit significantly higher colocalization in the SCN at ZT 23 than ZT 6. Although GFAP levels were constitutive across time and between sub-regions of the SCN and AH, our data detected a significant difference in day vs. night astrocyte morphology, which is in agreement with past observations of diurnal rhythms in astrocytic morphology (Lavialle & Serviere, 1993; Elliott & Nunez, 1994; Becquet *et al.*, 2008; Girardet *et al.*, 2010; Girardet *et al.*, 2013). Quantitative Sholl analysis of SCN astrocytes revealed that astrocytic morphology is most complex and distributed during the late night. Specifically, astrocytes exhibit a significant increase in distal branches, branch extension, ramification, kurtosis, and skewness at ZT 23 vs. ZT 6. Interestingly, these changes occur without significant changes in either total cell volume or GFAP expression, suggesting that astrocytic morphological changes rely on the re-distribution of existing GFAP. We also determined that β-dystroglycan expression is higher in the SCN than the AH at all three timepoints, suggesting a role for β-dystroglycan in the SCN. Because β-dystroglycan colocalization with GFAP is highest at ZT 23, it is possible that astrocytes within the SCN utilize β-dystroglycan as an interaction partner to facilitate their morphological changes. However, given that BiPS treatment does not affect the amount of total or degraded β-dystroglycan, this suggests that changes in astrocyte morphology are not regulated by MMP-2/9-dependent cleavage of β-dystroglycan in the SCN, but this does not rule out β-dystroglycan participating in the astrocytic transition to a highly ramified state. However, this hypothesis still needs to be tested.

Collectively, the work presented in this dissertation expands our understanding of how proteins interacting in the extracellular space modulate the SCN circadian clock. However, there remain many questions regarding the roles of MMP-2/9 in the SCN.

Below, we discuss proteolytic and signaling mechanisms that we postulate may be involved in these processes. We also suggest how the use of different or emerging technologies could clarify the functional role of MMP-2/9 activity in the SCN's dynamic extracellular environment.

Regulating MMP-9 diurnal activity

The first major finding in this study is that MMP-9, but not MMP-2, exhibits diurnal activity in the SCN. Specifically, gelatin zymography showed MMP-9 activity is greater at ZT 6 than at ZT 23. As discussed in Chapter 2, our data do not fully agree with those of Agostino *et al.*, 2002, who found that MMP-9 activity is highest during the night (ZT 18). The differences between our two studies could be due to the use of different animal models (mouse vs. hamster), light schedules (14:10 LD vs. 12:12 LD) or the analysis of *in vivo* vs. *in vitro* tissue samples. However, both of our studies agree that a diurnal difference in MMP-9, and not MMP-2, activity exists in the SCN.

Several studies support circadian clock regulation of MMP-9. For example, Ingle *et al.*, (2015) found that cardiomyocyte-specific *Bmal1* knockout (CBK) mice have decreased lifespans and display increased necropsy and hypertrophy in heart tissue. The authors further demonstrated that 20 week old CBK mice display increased transcription and translation of *MMP-9*, *Tissue inhibitor of metalloproteinase*- 1 (*Timp-1,* MMP-9's endogenous inhibitor), and several collagen type I-V genes. These results suggest that *Bmal1* deletion (and therefore circadian rhythm disruption) leads to a deleterious upregulation of an MMP-9 expression feedback loop. However, the authors provide no explanation for this phenomenon, nor did they investigate whether there are changes in MMP-9 proteolytic activity after *Bmal1* deletion. Thus, while normal *Bmal1* appears to suppress expression of *MMP-9* and *Timp-1* the exact regulatory mechanism has not been investigated, nor has day vs. night *MMP-9* gene expression, to our knowledge, been assessed in the SCN.

Proper transcription of *CRY2* is necessary for a functioning transcriptional-translational feedback loop (TTFL), and deletion of *CRY2* can lead to increased risk of certain cancers. Thus, Yu *et al.*, (2018) examined the role of *CRY2* in osteosarcoma cell proliferation. They found that decreasing *CRY2* transcription using a short-hairpin RNA

(shRNA) sequence leads to overexpression of MMP-2 in osteosarcoma protein extracts, and increased cell proliferation and migration. If increased MMP-2 protein expression translates into increased proteolytic activity, this could ultimately lead to increased MMP-9 activation, but the study above did not investigate this possibility.

We hypothesize that circadian clock regulation of MMP-9 activity could arise from rhythmic expression of upstream extracellular proteases, for example, the plasminogen activation cascade. Circadian variations in the onset of heart attacks and strokes have spurred research examining potential extracellular proteolytic activity rhythms in the cardiovascular system. One study found that clock genes regulate the expression of fibrinolytic proteases [plasmin and tissue/urokinase-type plasminogen activator (tPA/uPA)] and their inhibitor, plasminogen activator inhibitor-1 (PAI-1) (Maemura *et al.*, 2007). In humans, both tPA protein levels and PAI-1 activity in plasma are greater in the morning than they are night (Angleton *et al.*, 1989). In 2000, Maemura *et al.* saw that the CLOCK/BMAL2 heterodimer binds to an upstream E-box promoter and initiates transcription of *PAI-1 in vitro*. Conversely, the PER2/CRY1 heterodimer inhibits transcription of *PAI-1* (Maemura et al., 2000). These regulatory processes may generate circadian oscillations in PAI-1 mRNA and protein levels in blood plasma, as they are eliminated in *clock* knockout mice (Ohkura *et al.*, 2006). Further, day/night rhythms in PAI-1 transcription and translation are eliminated in *Cry1/2* knockout mice (Ohkura *et al.*, 2006). Our lab has shown that in the SCN, tPA protein expression peaks during the night, and inhibiting its activity by applying PAI-1 to SCN slices eliminates glutamate-induced phase shifts (Mou *et al.*, 2009; Cooper *et al.*, 2017). It is possible that increased tPA levels during the night drives catalysis of pro-MMP-9 and precedes the day-time increase in MMP-9 activity. To test this, one could examine if tPA knockout mice, which take longer to entrain to inverted or shifted light cycles (Cooper *et al.*, 2017; Krizo *et al.*, 2018), exhibit disrupted MMP-9 activity rhythms. Ultimately, we will not know if MMP-2/9 activity in the SCN is under the influence of the TTFL until their proteolytic activities are investigated using clock gene mutant mice (i.e. *clock* or *Cry1/2* double knockouts) or other methods (i.e. si-RNA, DREADDS, CRISPR) that disrupt the molecular clock. In summary, we hypothesize that the diurnal rhythm in MMP-9 activity could be the result of clock gene-

dependent transcriptional regulation of MMP-9 mRNA directly or through clock regulation of its regulatory proteins.

Reciprocal relationship between MMP-2/9 and NMDAR activity

Many studies investigating effects of MMP-2/9 enzymatic activity in the brain have focused on their roles *after* neuronal excitation, such as those associated with long term potentiation (LTP) or epileptic seizures (Dzwonek *et al.*, 2004; Nagy *et al.*, 2006; Meighan *et al.*, 2007; Wojtowicz & Mozrzymas, 2010; Trivedi *et al.*, 2019). For example, when late-phase LTP, which requires protein synthesis, is induced in a hippocampal (area CA1) slice culture using tetanic stimulation, gelatin zymography shows that MMP-9, but not MMP-2, proteolytic activity is up-regulated. Further, application of either a broad-spectrum MMP inhibitor (FN-439) or BiPS eliminates late-phase LTP (Nagy *et al.*, 2006; Meighan *et al.*, 2007). Studies examining seizure pathogenesis have found that excessive NMDAR/AMPAR activity resulting from kainic acid treatment (Berg *et al.*, 1993) increases MMP-2/9 activity (Jourquin *et al.*, 2003; Konopacki *et al.*, 2007), blood brain barrier break down and neuronal atrophy (Kaur *et al.*, 2004).

Previous studies show that NMDAR activation positively effects MMP-2/9 activity. In mouse cortical neurons and cerebrovascular endothelial cells, NMDA application increases both expression and activity of MMP-2/9 (Conant *et al.*, 2010; Chen *et al.*, 2016). Dopamine stimulation in striatal medium spiny neurons increases NMDAR-dependent $[Ca^{2+}]_i$ influx and increases MMP-9 activity (Li *et al.*, 2016). NMDAR-dependent LTP in the mouse hippocampus also increases MMP-2/9 activity (Wiera *et al.*, 2017). These studies show that NMDAR activity positively affects MMP-2/9 activity, but it is less clear if MMP-2/9 activity feeds back to affect NMDAR activity.

A few studies have investigated how altering MMP-2/9 activity affects NMDAR activity (Gorkiewicz *et al.*, 2010; Li *et al.*, 2016). For example, application of auto-active, recombinant MMP-9 increases the deactivation kinetics of the NMDAR, suggesting, conversely, that MMP-9 inhibition may allow NMDAR Ca^{2+} channels to remain open longer (Gorkiewicz *et al.*, 2010). However, the mechanisms through which altered MMP-2/9 activity modulates NMDAR activity is unclear. In murine cortical slice cultures, it was shown that NR1-NMDAR subunit cleavage increases when recombinant MMP-7 is

applied, but not MMP-2 or MMP-9 (Szklarczyk *et al.*, 2008). Given the lack of evidence that MMP-2 or MMP-9 directly binds to or cleaves NMDARs, it seems likely that the actions of MMP-2/9 on NMDAR are indirect. For example, MMP-2/9 catalytic cleavage of CAMs can influence NMDAR channel activity. Application of an auto-activating form of MMP-9 increases the surface diffusion of NMDAR's in hippocampal neurons. This is not observed when an MMP-9 "protease-dead" mutant is applied (Michaluk *et al.*, 2009), suggesting that MMP cleavage of CAMs such as β-dystroglycan that stabilize NMDAR membrane expression, could ultimately affect NMDAR activity. We observed that β-dystroglycan is expressed in the SCN, but both the full length and truncated peptide expression were constant across time and appear to be unaffected by MMP-2/9 inhibition. Therefore, we suggest that other extracellular substrates of MMP-2/9 may be responsible for the NMDAR-dependent phase shifts induced by BiPS in the SCN.

As mentioned in Chapter 2, polysialylated neuronal cell adhesion molecule (PSA-NCAM) is one possible substrate of MMP-2/9 in the SCN. PSA-NCAM participates in many structural and functional brain plasticity events and is sometimes a target of MMP-2/9 (Theodosis *et al.*, 1994; Bonfanti, 2006; Kochlamazashvili *et al.*, 2012; Varbanov & Dityatev, 2017). For example, in a mouse model of middle cerebral artery occlusion, MMP-9 inhibition reduces cleavage of the full length NCAM (180 kDa) (Shichi *et al.*, 2011). Additionally, a proteomic study comparing fibroblasts from MMP-2 knockout vs wildtype mice identified PSA-NCAM as a substrate for MMP-2 (Dean & Overall, 2007).

NCAMs and NMDARs are expressed together, and studies suggest they are functionally connected as well. An early ultrastructural study found that NCAM accumulates at the post-synaptic density near NMDARs and increases after induction of LTP (Fux *et al.*, 2003). PSA-NCAM knockout mice exhibit deficiencies in LTP that are rescued by application of d-cycloserine, an NMDAR agonist (Kochlamazashvili *et al.*, 2012). A study in cultured mouse hippocampal neurons identified a more direct relationship between PSA-NCAM and NMDA, as they found that exogenous application of soluble PSA-NCAM inhibits glutamate-induced, NMDA-mediated currents (Hammond *et al.*, 2006). Importantly, PSA-NCAM expression is enriched and rhythmic in the adult mouse SCN (Glass *et al.*, 1994; Glass *et al.*, 2003) and its genetic deletion disrupts locomotor activity rhythms in mice (Shen *et al.*, 1997). Also, *in vitro* removal of PSA from

NCAM using endoneuraminidase-N prevents glutamatergic phase shifts in SCN rat brain slices (Prosser *et al.*, 2003). Given that NMDAR activity is necessary for glutamate-induced phase shifts, it is possible that MMP-2/9 activity modulates PSA-NCAM in the SCN, and that inhibition of this modulation leads to increased NMDAR signaling. However, this hypothesis has yet to be tested.

Other candidate molecules worth investigating are the postsynaptic neuroligins (NLGN1, 2, 3, 4) and their presynaptic partners, neurexins (NRXN) 1, 2, and 3. Trans-synaptic binding and interaction of these dyads is important for NMDAR-dependent synaptic plasticity. Genetic deletion or mutations of amino acids that interfere with NRXN-NLGN interactions disrupt NMDAR-dependent LTP (Jiang *et al.*, 2017; Dai *et al.*, 2019; Rudenko, 2019; Wu *et al.*, 2019). Also, NLGN1 binds intracellularly to post synaptic density molecule-95 (PSD-95) (Barrow *et al.*, 2009), the main scaffolding molecule responsible for trafficking NMDAR to the postsynaptic membrane (Cousins & Stephenson, 2012). Importantly, MMP-2/9 mediated cleavage of NLGN1 eliminates NMDAR/NLGN1-containing clusters on the postsynaptic membrane (Barrow *et al.*, 2009) and results in increased lateral diffusion of NMDAR on the post-synaptic membrane (Szepesi *et al.*, 2014), which impairs NMDAR function. Another study found that MMP-2/9 cleavage of NLGN1 is induced by NMDAR-dependent LTP stimulation. This cleavage disrupts NLGN1 binding to pre-synaptic NRXNs and decreases pre-synaptic neurotransmitter release (Peixoto *et al.*, 2012). It is noteworthy that mRNA transcription of *Nlgn1*/2 and *Nrxn1*/2 (in the mouse forebrain and SCN, respectively) is cyclic and regulated by circadian clock genes (Shapiro-Reznik *et al.*, 2012; Hannou *et al.*, 2018a; Hannou *et al.*, 2018b). However, it is unknown if the oscillations in transcription lead to rhythmic expression of functional proteins and if NLGN/NRXN are MMP-2/9 enzymatic targets in the SCN.

Integrin-1β is another CAM that can affect NMDAR activation (Lin *et al.*, 2003) and trafficking (Michaluk *et al.*, 2009). Integrin-1β generally binds to ECM proteins (i.e., collagen, laminin, fibronectin, etc.) that contain Arg-Gly-Asp (RGD) peptide sequences. Further, when MMP-2/9 cleaves these ECM molecules, the RGD peptides can become diffusible ligands for integrin-1β (Mogford *et al.*, 1997; Wu *et al.*, 1998; Petitclerc *et al.*, 1999; Sternlicht & Werb, 2001; Wildering *et al.*, 2002). Binding of integrin-1β to RGD

ligands triggers activation of intracellular kinases such as protein kinase C and Src family kinases and subsequent NMDAR phosphorylation and activation (Chen & Leonard, 1996; Giancotti & Ruoslahti, 1999; Hisatsune *et al.*, 1999; Ali & Salter, 2001; Grosshans & Browning, 2001; Miranti & Brugge, 2002). In mouse hippocampal slice cultures, incubation with an RGD ligand increases both the amplitude and duration of NMDAR-mediated inward currents (Lin *et al.*, 2003). Another study in mice striatopallidal neurons found that dopamine application increases NMDAR excitation, as indicated by increased expression of GCaMP3. Further, inhibition of integrins or MMPs eliminates NMDAR-induced Ca^{2+} influx (Li *et al.*, 2016). When integrin-1β binding to the ECM is inhibited, MMP-9-dependent LTP in hippocampal neurons is abolished (Wang *et al.*, 2008b). Interestingly, one study found that higher concentrations (10 μM) of a cyclic RGD peptide inhibited integrin binding to ECM components vitronectin, fibronectin and fibrinogen, but lower concentrations (100 pM) were "super activating" and increased ECM binding compared to control (Legler *et al.*, 2001). These studies suggest that the level of MMP-2/9 activity affects the degree of integrin-1β binding to the ECM and the level of binding determines the effect on NMDAR activity. Thus, inhibiting MMP-2/9 activity in the SCN may lead to "super activation" of integrin-1β and facilitate increases in NMDAR phosphorylation. Currently, we are unaware of research investigating the role of integrin-1β in the SCN, but we believe examining whether integrin-1β protein levels are expressed diurnally and whether RGD-peptide application phase-shifts the circadian clock would be informative.

How does BiPS affect NMDARs?

Although we found that BiPS-induced phase shifts require NMDAR activity, we also observed that BiPS application does not affect phosphorylation of either CAMKII isoform. As this event typically occurs after NMDAR mediated influx of Ca^{2+}, it is possible that BiPS treatment does not lead to increased $[Ca^{2+}]_i$. This is surprising because previous studies show that day/night variation in CAMKII activity contributes to behavioral activity rhythm maintenance. Additionally, CAMKII phosphorylation is necessary for light-induced phase shifts *in vivo* (Yokota *et al.*, 2001; Nomura *et al.*, 2003; Agostino *et al.*, 2004; Kon *et al.*, 2014). Possible explanations for our findings include: 1) BiPS induces NMDAR

ionotropic activity but the resulting Ca^{2+} influx activates CAMKII-independent intracellular signaling pathways; and 2) BiPS-induced phase shifts involve NMDAR Ca^{2+} flux-independent (metabotropic) protein signaling cascades. Therefore, characterizing the direct effects of BiPs on NMDAR is necessary to determine how MMP-2/9 endogenous activity participates in SCN circadian rhythm regulation.

In Chapter 2, we saw that BiPS treatment at ZT 23 resulted in high firing rates ~2 hours after treatment that subsequently decreased. However, it is unclear if this is due to increased NMDAR activity. We suggest that studying NMDAR channel activity directly would be ideal to assess whether acute (40 minutes) BiPS treatment alters neuronal activity. Preliminary experiments using extracellular electrophysiological recordings were conducted to assess acute BiPS-induced changes in SCN neuronal firing rate, focusing on the times when BiPS phase-shifts the clock, ZT 6 and ZT 16. However, sampling the spontaneous firing rates of individual neurons dispersed across the SCN generated data that was extremely variable and did not identify a significant, BiPS-induced change in firing rate (Fig 4.1). Thus, we believe that using alternative methods might be more fruitful. For example, extracellular recordings using a multi-electrode configuration could allow the activity of the same group of neurons to be characterized before, during and after BiPS treatments. Alternatively, intracellular recordings could be used for these experiments. Whole-cell patch clamp electrophysiology has been used previously to characterize NMDAR receptor behavior after acute drug treatments in SCN slices (Kim & Dudek, 1991; Pennartz *et al.*, 1998; Lundkvist *et al.*, 2002). This technique also helped determine how MMP activity acutely affects NMDAR ionotropic activity in hippocampal slices (Gorkiewicz *et al.*, 2010; Wiera *et al.*, 2017).

Rather than acutely modulating Ca^{2+} channel activity, MMP-2/9 could affect NMDARs by regulating the composition of NMDAR subunits in the SCN. NMDARs are heterogeneous, tetrameric protein channels consisting of two NR1 and a combination of two NR2 (NR2A-2D isoforms) or NR3 (NR3A-3B isoforms) subunits (Hollmann, 1999). Different combinations of subunits affect NMDAR function by altering the voltage-dependent Mg^{2+} ion block, glutamate and/or glycine binding affinity, and the Ca^{2+} ion flux volume (Cull-Candy & Leszkiewicz, 2004; Paoletti, 2011; Suzuki *et al.*, 2013). During development, NMDAR composition transitions from mostly NR1/NR2B-containing to

NR1/NR2A-containing NMDARs. Increased incorporation of NR2B subunits increases the time of channel deactivation, resulting in the NMDAR channel staying open longer. This was first characterized by Vicini *et al.* (1998) when they observed that glutamate stimulates NR2B-containing receptors to remain open for 250 msec, compared to NR2A-containing receptors that stay open for 100 msec (Vicini *et al.*, 1998). This and other studies support NR2B-containing NMDARs being more active and more permissive to synaptic/behavioral plasticity processes, like LTP and fear conditioning, than NR2A-containing NMDARs (Crair, 1999; Szinyei *et al.*, 2003; Cull-Candy & Leszkiewicz, 2004).

In the SCN, both transcription of NR2B mRNA and phosphorylation of the subunit increases at night, which could increase SCN clock sensitivity to glutamate-induced phase shifts during the night. Functionally, increased expression and activity of NR2B subunits is necessary for NMDA-induced Ca^{2+} currents and light-induced phase shifts (Williams, 2001; Wang *et al.*, 2008a; Bendova *et al.*, 2012). NR2B inhibition also alters clock gene expression, as the NR2B inhibitor ifenprodil blocks glutamate-induced phosphorylation of CREB and ERK1/2, proteins that increase transcription of *per1* and *per2* in rat SCN tissue (Bendova *et al.*, 2012).

Research indicates that MMP-2/9 activity may preferentially affect the expression and activity of NR2B-containing NMDARs. In the hippocampus, TIMP-1 application blocks MMP-9-mediated degradation of Reelin (Tinnes *et al.*, 2013), a large ECM glycoprotein implicated in NR2B subunit surface mobility and trafficking on neuronal membranes (Groc *et al.*, 2007). Thus, quantifying the effects of BiPS treatments on the NR2A:NR2B expression ratio using western blotting or immunohistochemistry in the SCN could provide evidence for a mechanism underlying BiPS-induced phase shifts. Further, experiments that combine BiPS and ifenprodil treatments could assess whether phase shifts resulting from MMP-2/9 inhibition require NR2B-expressing NMDARs.

However, the SCN also contains other NMDAR subunits that affect clock activity. A study showing NMDAR currents in the SCN after applying ifenprodil in a Zn^{2+}-deficient solution, which inhibits both NR2A and NR2B subunits, suggests that the SCN also expresses NR2C- and NR2D-containing NMDARs (Clark & Kofuji, 2010). Moreover, Brancaccio *et al.* found that during the night, application of the NR2C specific antagonists, DPQ-1105 and QNZ-46, but not NR2A or NR2B-selective inhibition, reduces the

amplitude and lengthens the period of PER2::LUC rhythms in SCN tissue *in vitro.* Further, DPQ-1105 application eliminates neuronal intracellular Ca^{2+} circadian rhythms (Brancaccio et al., 2017). Thus, further examination of which NMDAR subunits are affected by MMP-2/9 inhibition may clarify mechanisms associated with BiPS-induced phase shifts.

Ca^{2+} imaging experiments could also help identify MMP-2/9 actions in the SCN. Previously, the effect the dopamine antagonist, SKF81297, in striatal medium spiny neurons was examined using the fluorescent Ca^{2+} indicator GCaMP3. SKF81297 potentiates NMDAR-dependent Ca^{2+} influx while also increasing MMP-2/9 activity (Li *et al.*, 2016). Changes in Ca^{2+} flux in the rodent SCN have been measured previously (Colwell, 2001; Brancaccio *et al.*, 2013) and the adrenal adenoviral vectors that induce expression of GCaMP3 molecules can be genetically driven by either astrocytic or neuronal promoters (Brancaccio *et al.*, 2017). Utilizing this tool in conjunction with NMDAR subunit specific inhibitors in SCN slices could determine whether BiPS treatments affect astrocytic and/or neuronal Ca^{2+} levels.

Recently our lab started a collaborative study with Dr. Chris Baker to develop and test a microfluidics device for perfused brain slices. The set-up allows for simultaneous Ca^{2+} imaging of the tissue, application of experimental treatments, and collection of perfusate for off-line analysis. While still in development, this device could aid in examining multiple physiologic responses of SCN tissue after BiPS treatments. For example, we could investigate the response of NMDARs during BiPS application by measuring changes in $[Ca^{2+}]_i$. Further, we could compare the peptide/molecular content of the perfusate after BiPS treatment using mass spectrometry (methods discussed below), and potentially identify which molecules are affected by BiPS.

Because BiPS does not increase the phosphorylation of CAMKII in our SCN samples, it is possible that the signaling cascade downstream of BiPS-induced NMDAR activation is Ca^{2+}-independent. Although uncommon, evidence exists for a non-canonical, ion flux-independent NMDAR signaling (f-iNMDARs) pathway (Chung, 2013; Dore *et al.*, 2016; Gray *et al.*, 2016; Dore *et al.*, 2017; Montes de Oca Balderas, 2018). The first evidence of f-iNMDARs came from studies in hippocampal neurons investigating the different mechanisms underlying LTP and long-term depression (LTD); two NMDAR-

dependent processes that result in increased and decreased synaptic communication, respectively. Two separate research groups showed that showed MK-801 (an antagonist that blocks ion flux through NMDAR channels) blocks LTP but not LTD in hippocampal neurons (Mayford *et al.*, 1995; Scanziani *et al.*, 1996), suggesting that LTD involves f-iNMDARs.

Recently, FRET-FLIM (Forster resonance energy transfer measured by fluorescence lifetime imaging of the FRET donor) was used to investigate if extracellular ligand binding to NMDAR could result in intracellular conformational changes, a phenomenon associated with metabotropic receptor activity (Aow *et al.*, 2015). First, Dore *et al.* genetically modified the intracellular cytoplasmic domains of NMDAR-NR1 subunits to concurrently express either green fluorescent protein or mCherry molecules in primary hippocampal neuronal cultures. These modifications produced a measurable FRET signal (indicating an interaction between the two fluorescent tags), suggesting physical interaction between NR1 subunits. When the neurons were treated with glutamate in the presence of MK-801 or 7CK (another NMDAR ion channel antagonist), the FRET signal decreased and LTD was blocked, indicating that LTD requires ligand binding to NMDARs and that this binding induces an intracellular conformational change (Aow *et al.*, 2015). A follow-up study by the same group used FRET to examine how conformational changes in the NMDAR cytoplasmic domain affect intracellular signaling pathways (Aow *et al.*, 2015). It is known that NMDAR Ca^{2+} influx increases CAMKII phosphorylation on the Thr-286 residue, which increases CAMKII kinase activity and promotes CAMKII binding to NMDARs (Giese *et al.*, 1998; Bayer *et al.*, 2001; Chang *et al.*, 2017). Aow *et al.* observed that bath application of NMDA ligands in the presence of 7CK reduces the FRET signal between NMDAR-NR1-GFP and CAMKII-mCherry (Aow *et al.*, 2015). This implies that NMDAR activation initiates a conformational change in the intracellular portion of the NR1 subunit that favors CAMKII binding in the absence of Ca^{2+} influx. Thus, it would be worth investigating if BiPS treatment induces a conformational change in NR1 subunits that facilitates NMDAR activation by increased interaction with, not necessarily phosphorylation of, CAMKII.

MMP-2/9 and β-dystroglycan involvement in astrocytic morphological changes

One drawback of immunohistochemistry is that it cannot be used to determine protein-protein interactions (Seidal *et al.*, 2001; de Matos *et al.*, 2010). Therefore, although we detected puncta of overlapping signals for β-dystroglycan and GFAP using immunohistochemistry, we cannot definitively assert whether 1) the astrocytes express β-dystroglycan or 2) the proteins are interacting in the SCN. Proper examination of functional interactions between β-dystroglycan and astrocytes could be performed using the FRET-FLIM technique introduced in the previous section.

However, it is well accepted that MMP-2/9-dependent cleavage of β-dystroglycan is necessary for changes in glial cell morphology in other brain regions. Here we observed, for the first time, that β-dystroglycan is expressed in the SCN and colocalizes with GFAP expression. We determined, by quantifying fluorescent signal in our immunohistochemistry and through western blotting experiments, that β-dystroglycan expression is constitutive and unaffected by blocking MMP-2/9 activity with BiPS. We also discovered that, although the total amount of GFAP does not change with time, astrocytes exhibit a day to night transition in ramification state. Thus, diurnal astrocytic morphology rhythms are likely accompanied by redistribution of intracellular molecules, and potentially involve a reorganization of their interactions with extracellular molecules. Therefore, it would be informative to examine astrocytic morphology and GFAP colocalization with β-dystroglycan in the SCN after BiPS treatment. We hypothesize that BiPS will have its largest effects on astrocyte morphology when applied at times that correspond with high MMP-9 activity, specifically ZT 6 and ZT 16. If differences in one or more morphologic parameter are observed, this would support MMP-2/9 modulation of astrocytic morphological changes in the SCN. Moreover, it would suggest that astrocyte morphology changes could be involved in BiPS-induced phase shifts.

Because β-dystroglycan expression in the SCN appears to be enriched compared to the surrounding hypothalamus, its role in circadian rhythm regulation should be explored in more detail. Experiments investigating β-dystroglycan function in the SCN could utilize an antibody targeting α-dystroglycan (IIH6). Previous reports show that application of IIH6 disrupts dystroglycan's ability to bind to the ECM and disrupts astrocytic adhesion to laminin after ischemic brain injury (Hawkins *et al.*, 2013). This

essentially mimics the effect of MMP-2/9 activity, as degradation of β-dystroglycan can be blocked with both broad and specific MMP2/9 inhibitors, which results in decreased attachment of glia cells to laminin (Milner *et al.*, 2008). Preliminary results testing the effects of IIH6 on SCN circadian rhythms are so far inconclusive. IIH6 (diluted in EBSS 1:5) was applied at ZT 16 for 40 minutes, and extracellular electrophysiology recordings were performed on the following day. Neither concentration of IIH6 induced a shift in SCN circadian rhythms (Fig 4.2). However, the previous studies using this antibody were performed in astrocyte cell cultures using a 24 h incubation period. Therefore, future experiments involving SCN tissue slices may require higher antibody concentrations or an extended incubation time.

Circadian matrisome and proteomic profiling of the SCN

Recent mass spectrometry experiments in the brain and other tissues have focused on identifying molecular components of the ECS isolated from other cellular fractions. By combining mass spectrometry (MS) with extraction techniques that use surfactants to separate ECM-associated molecules from intracellular components, researchers have successfully isolated ECM fractions from bone, cartilage, kidney, lung, liver and brain tissue (Byron *et al.*, 2013; Naba *et al.*, 2017). Further, cluster analysis of data collected from MS can help identify groups of peptides containing conserved residues or post-translational modifications. MMP-2/9 cleavage of extracellular substrates generates small peptides containing a conserved RGD-motif in their peptide sequence (Kridel *et al.*, 2001; Wenk *et al.*, 2013). Thus, identification of peptides in SCN extracellular protein extracts containing this motif using MS would be useful for identifying potential MMP-2/9 substrates.

The proteomic profile of tissue collected from the pineal gland, retina, SCN, and other peripheral body organs were previously characterized using MS and revealed that a number of proteins exhibit diurnal expression rhythms (Moller *et al.*, 2010). Multiple groups have utilized MS to identify peptides in SCN tissue that are regulated by light stimuli or the circadian clock, and a few of these peptides are ECM-associated (Reddy *et al.*, 2006; Hatcher *et al.*, 2008; Deery *et al.*, 2009; Tian *et al.*, 2011; Chiang *et al.*, 2014; Ling *et al.*, 2014). In the rat pineal gland, Moller *et al.*, found that expression of a

transmembrane type I glycoprotein, leucine-rich repeat-containing protein 15 precursor, is upregulated during the day (Moller *et al.*, 2007). Another study utilizing SCN slices identified which peptides were released into the ECS before and after optic nerve stimulation using matrix-assisted laser desorption/ionization- tandem mass spectrometry (MS/MS). This method mostly identified cyclic expression of peptides that act as neurotransmitters and/or neurohormones, for example somatostatin, little SAAS, big LEN and PEN (Hatcher *et al.*, 2008). Using “Stable Isotope Labeling with Amino Acids in Cell Culture”-based quantitative mass spectrometry, Chiang et al. found that 20% of proteins identified in homogenized murine SCN tissue of mice kept in constant darkness exhibited sinusoidal expression rhythms over a ~24 hr period (Chiang *et al.*, 2014). The authors of this study, however, only found one ECM-associated protease exhibited peak expression at night, prolyl 4-hydroxylase (an enzyme pivotal in collagen synthesis). Therefore, it is possible to detect ECM-associated proteins using mass spectrometry, but only a few have been identified in the SCN. Additionally, the effects of extracellular protease inhibition on expression of ECM proteins in the SCN have not been examined using MS techniques.

A preliminary experiment in collaboration with Dr. Shawn Campagna and Dr. Dan Jacobsen was conducted to test an ECM extraction technique on SCN tissue slices. Two biological replicate experiments were performed using a protocol based on recently published ECM extraction methods (Naba *et al.*, 2017; Sethi & Zaia, 2017). The cellular and ECM fractions from the SCN were collected, digested with trypsin, and run on a Q-Exactive Plus Orbitrap Mass Spectrometer (Thermo Scientific), and the Ultimate 3000 RSLnano system. The separation was carried out using a 2D online chromatography approach. The digested sample was loaded onto a C18 PEPMap100 precolumn for sample clean up, then using an organic gradient the sample was separated on a reverse phase EASY-Spray Nano source. The Orbitrap was operated in TOP 10-mode utilizing dynamic exclusion to maximize sample characterization. The data were analyzed using the Crux open source proteomic platform (McIlwain *et al.*, 2014). The raw data were aligned with known peptide sequences from a previously published ECM proteome (called the matrisome) and the *Mus musculus* reference proteome available on Uniprot.org (Church *et al.*, 2009; Naba *et al.*, 2017).

Preliminary western blots comparing the content of our intra- and extracellular protein fractions collected after ECM isolation revealed that actin was absent from the extracellular fractions, which suggests our ECM isolation method may be effective. However, initial assessment of our mass spectrometry examining the identity of protein fragments present in both our intra- and extracellular protein fragments showed that ECM-associated proteins were detected in our intracellular fraction. Additionally, the Q-values (a confidence interval measurement for proper identification) that aligned with each ECM-identified protein in either fraction were low, indicating a low probability of certainty in our protein identifications. Trouble-shooting this experiment would include successful identification of positive control peptides added to control samples and utilization of western blotting to confirm the presence or absence of known intra- and extracellular proteins in SCN fractionated extracts. Thus, we believe the best next step for the experiment would be to increase the number of technical replicates and/or increase the amount of SCN tissue per sample to increase our certainty in extracellular peptide identification.

Another MS method that could be used to identify potential ECM-associated substrates that are affected by BiPS treatment is called iTRAQ^{TM} labeling. Previously, a study used MS/MS combined with amine-targeted iTRAQ^{TM} tags (Applied Biosystems, Foster City, CA) to identify the “degradome” of MMP-2. Dean *et al.* (2007) incubated cell cultures with the iTRAQ^{TM} tag to exclusively label extracellular proteins in full and partial MMP-2 knock-out fibroblasts. The authors then compared the peptide sequences identified by tandem mass spectrometry in both cell cultures. They found that the iTRAQ ratio (iTRAQ labeled protein in control: iTRAQ protein in active MMP-2 cultures) is significantly reduced for certain peptides, suggesting the proteins might be substrates of MMP-2. Specifically, they identified previously known MMP-2 ECM substrates (such as osteopontin, galectin-1 and HSP-90) and potential substrates [Procollagen C-proteinase enhancer (PCPE) and chemokine (C-X3-C motif) ligand 1]. Further, they confirmed MMP-2 mediated, proteolytic cleavage of each of the above substrates using a previously described *in vitro* biochemical assay (Dean & Overall, 2007). Thus, if the extracellular extraction technique described above does not work in SCN slices, MS experiments

aimed at characterizing the ECM content, and the effect of extracellular protease activity, in the SCN using the iTRAQ labeling method could be successful.

Linking the ECM to the intracellular circadian clock

Given that MMP-2/9 activity can disrupt ECM integrity via protein degradation, it is noteworthy that changes in mechanical forces induced by altering ECM composition in somatic tissues affects circadian clock regulation. For example, one study found that the extracellular mechano-environment of cancerous human breast tissues contains more collagen and was measurably stiffer than normal breast tissue (Williams *et al.*, 2018). This observation correlated with a reduction in *Bmal1* mRNA expression; however, the link between ECM stiffness and clock gene expression was not directly investigated (Williams *et al.*, 2018). Another study grew mammary epithelial cells (MECs) isolated from PER2::LUC mice in culture flasks coated with either a two- or three-dimensional ECM substrate (conferring high or low mechanical stiffness, respectively). They found that MECs grown on a three-dimensional ECM exhibit stronger PER2::LUC rhythms, indicating that a less rigid environment favors robust oscillation of clock gene expression (Yang *et al.*, 2017). Further, they found that disrupting the Rho-Rock pathway, which leads to degradation of intracellular actin and disrupts the shape of the nuclear envelope, increases the robustness of PER2::LUC rhythms. These and other works reviewed by Streuli & Meng (2019), suggest that disease-related disruptions in the mechano-environment of the brain are facilitated by alterations in ECM composition and leads to dampened clock gene expression. Conversely, decreased ECM and intracellular stiffness increases the amplitude of clock gene expression rhythms. Because decreased strength of circadian rhythms is associated with many age-related diseases, like dementia and Alzheimer's (Witting *et al.*, 1990), it would be interesting to examine if changes in SCN ECM content or composition affects disease progression.

Our studies align with previous work highlighting ECM-associated molecules as active participants in regulating both physiological (e.g., LTP) and pathological (e.g., ischemia, seizure) activity in the brain. In some cases, these processes also involve changes in astrocyte function/morphology. MMP-2/9 are essential molecules in regulating ECM-mediated changes in brain plasticity and our findings support their involvement in

yet another plastic process, the regulation of circadian rhythms in the SCN. Below we present several mechanistic models of endogenous MMP-2/9 expression and activity in the SCN, how they may participate in circadian clock regulation, and how MMP-2/9 inhibition leads to phase-shifts in the SCN clock.

Similar to other areas of the brain, the effects of MMP-2 and MMP-9 activity depend on the particular substrates they cleave. The substrates we discussed above (β-dystroglycan, PSA-NCAM, integrin-1β, neuroligin, and neurexins) all generally have a positive effect on NMDAR activity when they are intact. Our data do not support MMP-2/9 cleavage of β-dystroglycan in the SCN, so we still do not know the identity of the functional substrate(s) for MMP-2/9 in the SCN. Nevertheless, we predict that MMP-2/9 affects NMDAR activity in the SCN through cleavage of a yet to be identified CAM. Figure 4.3 illustrates a possible mechanism regulating MMP-2/9 activity and downstream actions in the SCN. As shown in the figure, (1) Glutamate activation of post-synaptic NMDARs increases intracellular Ca^{2+} concentration ($[Ca^{2+}]_i$). (2) This initiates the secretion of pro-MMP-2 and pro-MMP-9 into the ECS where they are activated by plasmin. Because MMP-2 can also activate pro-MMP-9, the amount of active MMP-9 is higher than active MMP-2. (3) MMP-9-mediated enzymatic cleavage of CAMs disrupts protein-protein interactions with membrane-bound NMDARs, leading to a conformational change that decreases the probability of NMDAR activation by extracellular glutamate. (4) MMP-9 activity also can lead to the maturation of BDNF, TrkB phosphorylation and priming of NMDARs. Therefore, the ultimate effect of MMP-9 activity on NMDAR also depends on the abundance of extracellular molecules like plasmin, tPA/uPA, and BDNF, which could tip the scales toward increased or decreased phosphorylation and activity of NMDARs. (5) Further, MMP-2/9- mediated cleavage of ECM molecules, could alter astrocytic morphologic rhythms.

In Fig 4.4 we incorporate endogenous MMP-2/9 into a model of the SCN circadian clock that connects the extracellular milieu and independently operating clocks in neurons and astrocytes, and in particular suggests a feedback mechanism that involves CAM-NMDAR interactions. During the day, SCN spontaneous neuronal activity is high and astrocytes are in a quiescent state. This time is coincident with the lowest amount of astrocytic glutamate release and low levels of endogenous NR2B expression. The high

daytime level of intracellular neuronal [Ca^{2+}] stimulates pro-MMP secretion by neurons into the ECS and leads to high MMP-9 activity. Increases in MMP-9-mediated CAM cleavage leads to decreases in NMDAR interactions with CAMs, which results in lower potential NMDAR activity. Additionally, plasmin and mBDNF levels are low, therefore NMDAR phosphorylation by TrkB is minimal. Together, these events decrease the chance that *in vivo* light stimulation or exogenous application of glutamate can phase-shift the clock.

We further predict that high MMP-9 activity at ZT 6, by cleaving CAMs and ECM components, facilitates the beginning of the astrocytic transition to the more ramified state we observed at ZT 16. The higher ramification seen at ZT 16 is coincident with the previously demonstrated increase in astrocytic glutamate release and may be associated with higher astrocytic metabolic activity. Further, NR2B expression and phosphorylation of NMDAR by TrkB (due to increased plasmin/mBDNF expression) are highest at ZT 16, two conditions that enhance the probability that membrane-bound NMDARs can be activated by glutamate (due to light or exogenous application), and thereby phase-shift the circadian clock. The potential for NMDAR activity could be further enhanced through decreased MMP-9 cleavage of CAMs, allowing more NMDAR-CAM interactions. Importantly, the high astrocytic glutamate release at ZT 16 is insufficient *by itself* to trigger NMDAR activation (and phase-shift the clock) due to the decrease in SCN neuronal $[Ca^{2+}]_i$ and the continued (although decreased) MMP-9 cleavage of CAMs at this time.

At ZT 23, astrocytes are highly ramified and extend their filopodia to their greatest extent, but also are decreasing their secretion of glutamate, which would decrease intrinsic NMDAR activation. On the other hand, MMP-9 activity is at its lowest, leading to minimal CAM cleavage. Therefore, the increased number of intact CAMs on the postsynaptic membrane is more favorable for interaction with NMDARs, which enhances potential NMDAR activity. Additionally, plasmin expression is high, so BDNF is still able to activate TrkB. Thus, NMDARs are in a sufficiently phosphorylated and primed state so that light/glutamate stimulation can phase-shift the clock, while the low amount of glutamate being released by astrocytes is not sufficient to initiate a phase shift by itself.

Based on the model just presented, in Figure 4.5 we illustrate how BiPS application could induce phase shifts at ZT 6 and ZT 16, but not ZT 23 through mechanisms that

disrupt our proposed CAM-NMDAR interactions. At ZT 6, we hypothesize that BiPS inhibition of MMP-2/9 prevents MMP-9-mediated cleavage of CAMs. The resulting conformation and/or amount of membrane-bound CAMs is now favorable for interaction with NMDARs, which increases NMDAR sensitivity glutamate. Although astrocytic glutamate release is normally low during the daytime, the CAM-bound NMDARs would now be sufficiently primed so that the endogenously derived glutamate is able to activate NMDARs and initiate a phase advance. At this same time BDNF expression and TrkB activation are low, but we propose that the baseline levels of activity are sufficient to support NMDAR activation and allow phase-shifts of the clock. This scenario is supported by our data showing that treatments that inhibit plasmin (α-2-antiplasmin) or TrkB activation (K-252A) are able to block BiPS-induced phase shifts.

At ZT 16, BiPS application blocks endogenous (albeit decreasing) MMP-9 activity, again increasing the abundance of intact CAMs. At the same time, NR2B expression peaks, shifting the overall population of NMDARs to a more excitatory composition. The increase in full-length CAMs allows more NMDAR-NR2B receptors to be incorporated into the post-synaptic membrane. As these events are coincident with the peak in astrocytic glutamate release, NMDAR-dependent $[Ca]_i$ influx is enough to phase-delay the SCN clock. ZT 16 is also concurrent with maximum plasmin and BDNF expression, therefore TrkB receptors are highly activated and NMDARs are more phosphorylated compared to ZT 6. Thus, we believe the concentration of α-2-antiplasmin or K-252A able to block BiPS-induced phase shifts during the day is now ineffective in blocking BiPS phase shifts.

Lastly, at ZT 23, CAM-NMDARs and BDNF/TrkB signaling are primed and ready to respond, and astrocytic release of glutamate is still high but is decreasing. These conditions are such that exogenous light/glutamate can readily phase-shift the clock. However, BiPS-induced inhibition of MMP-2/9 activity is unable to affect clock phase because endogenous MMP-2/9 activity is low at this time, so there is no enzymatic activity for it to inhibit.

In summary, we suggest that the MMP-2/9-mediated NMDAR negative feedback loop proposed above is a pivotal mechanism in maintaining endogenous SCN circadian rhythms. Specifically, MMP-9 cleavage of ECM and associated molecules regulates the

composition and integrity of the ECS and allows for astrocytes to alter their morphology across the circadian cycle. MMP-9-mediated CAM cleavage in the daytime decreases the probability that endogenous levels of glutamate will phase-shift the clock, while lower MMP-9 CAM cleavage at night enhances NMDAR priming to allow appropriate responses to photic/glutamatergic stimuli. Therefore, we conclude that MMP-9 activity contributes to the time-of-day sensitivity of the SCN circadian clock to glutamate, and therefore MMP-9 is an essential component in regulating SCN circadian clock phase.

Appendix: Figures for Chapter 4

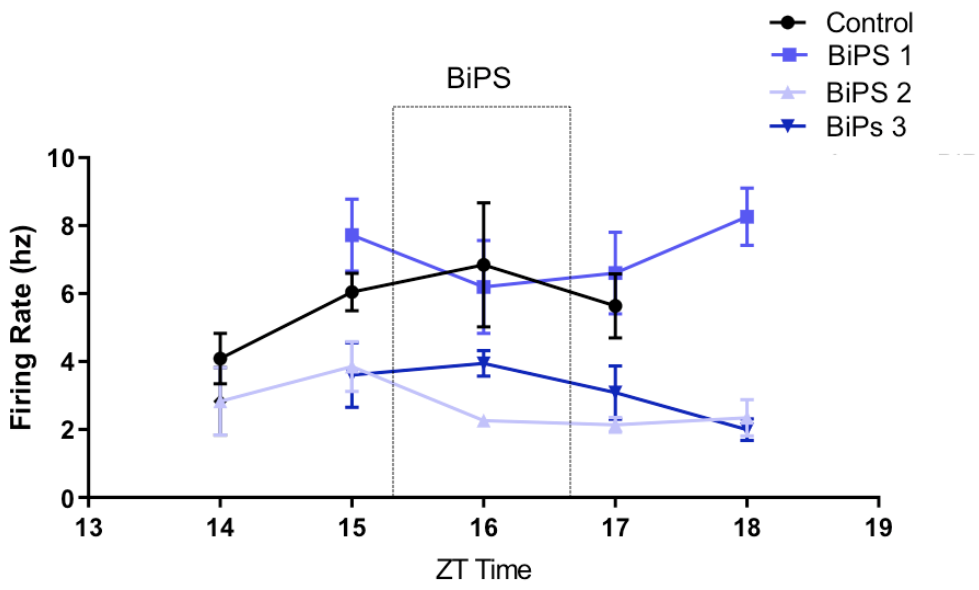

Figure 4.1: Acute recording of *in vitro* SCN firing rate surrounding BiPS treatment at ZT 16.

Acute SCN extracellular neuronal activity recordings from tissue being treated with the inhibitor BiPS for 40 minutes surrounding ZT 16 (grey box). Plotted are the average firing rates (+/- SEM) of 5-6 neurons were recorded each hour. Preliminary comparison of identical BiPS treatments (i.e., BiPS 1, BiPS 2 and BiPS 3 in n=3 animals) to vehicle control (n=1) does not reveal a clear effect of BiPS treatment on the average firing rate across time.

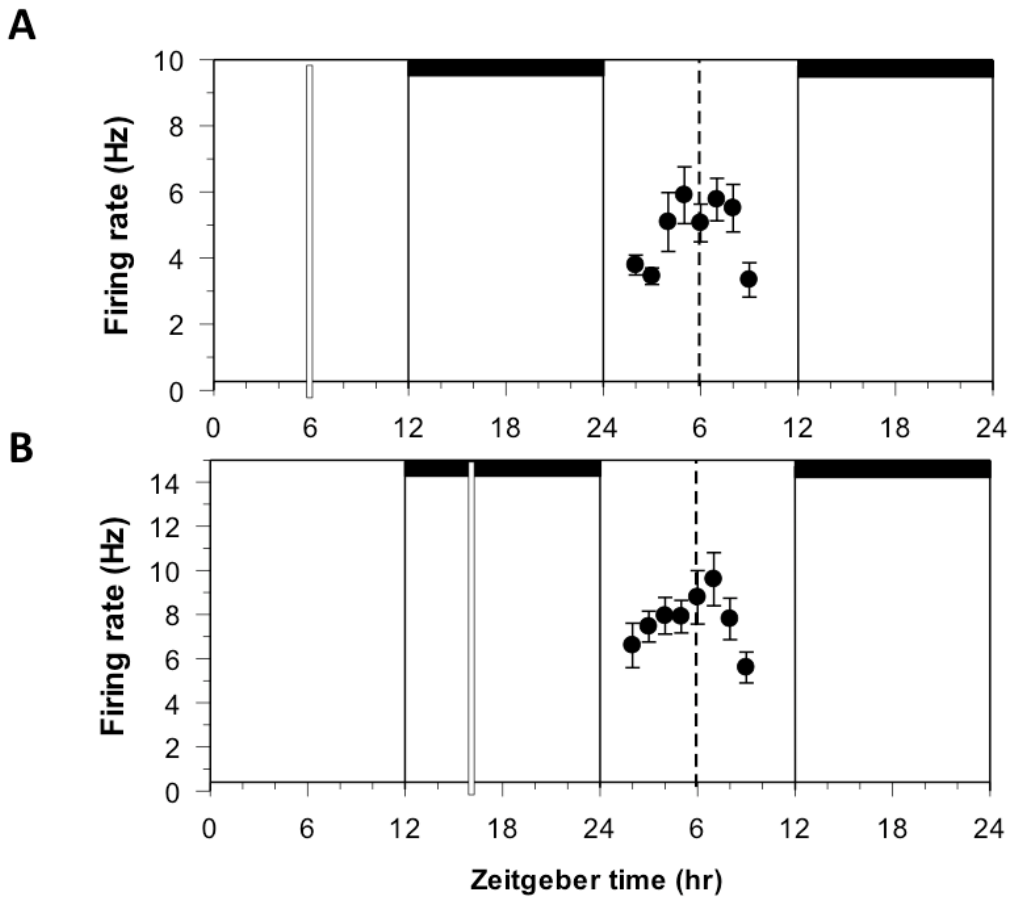

Figure 4.2: Preliminary data showing α-dystroglycan antibody application to SCN slices does not phase-shift the clock.

Shown are extracellular electrophysiology recording data of SCN slices. A 40-minute drug treatment (white bars during Day 1 *in vitro*) with the α-dystroglycan antibody (IIH6) at either Zeitgeber time (ZT) 6 (A) or ZT 16 (B) does not appear to shift the peak neuronal firing rate on Day 2 of recording (as compared to the time of normal peak firing, ZT 6, indicated by the dotted line.

Figure 4.3: Hypothesized reciprocal feedback between MMP-2/9 and NMDAR activity in the SCN.

In the suprachiasmatic nucleus (SCN), presynaptic and/or astrocytic glutamate release activates N-methyl-D-aspartate receptors (NMDARs) and increases intracellular Ca^{2+} concentrations ($[Ca^{2+}]_i$). This signals the release of pro-matrixmetalloproteinase (pro-MMP) zymogens into the extracellular space (ECS) and regulates the molecular transcriptional translational feedback loop (TTFL) oscillator. Further, the plasminogen activation cascade is also activated [i.e, tissue- and/or urokinase plasminogen activator (tPA/uPA) cleaves plasminogen into plasmin]. As a result, plasmin can activate both pro-MMP-2 and pro-MMP-9. Additionally, MMP-2 can catalytically activate pro-MMP-9. We propose that circadian activity of MMP-9 in the SCN degrades extracellular matrix (ECM) molecules, cleaves cellular adhesion molecules (CAMs) and cleaves pro-brain derived neurotrophic factor (pro-BDNF) into its mature form (mBDNF). We predict that 1) degradation of ECM molecules could influence astrocytic morphological changes, 2) MMP-9 mediated cleavage of an unknown CAM disrupts NMDAR-CAM interactions and decreases NMDAR activity, 3) plasmin and MMP-9 activity increases mBDNF concentration in the ECS, increasing mBDNF binding to tyrosine kinase B (TrkB) receptors and positively influences NMDAR priming/activation via phosphorylation. Therefore, the level of MMP-2/9 activity can either positively or negatively affect NMDAR activity.

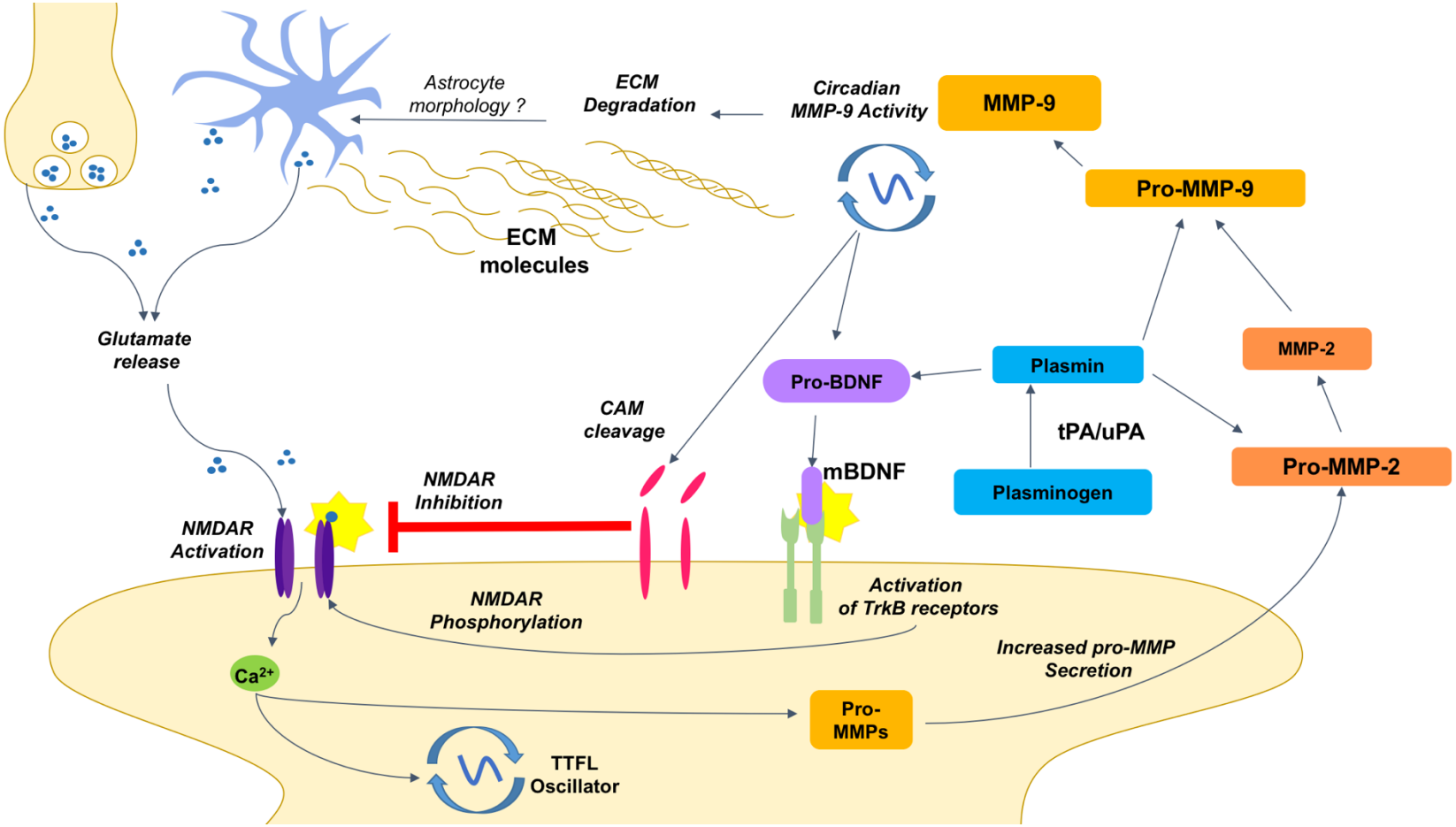

Figure 4.3 continued

Figure 4.4: MMP-9 participation in SCN circadian clock regulation.

During the day [Zeitgeber time (ZT) 6], MMP-9 proteolytic activity (illustrated by yellow stars), but not MMP-2, is highest and cleavage of one or multiple unidentified CAMs keeps NMDAR activity low. Levels of plasmin, pro-BDNF and mBDNF are all at their lowest and TrkB phosphorylation of NMDAR is minimal. This time coincides with the lowest concentration of endogenous, extracellular glutamate ($[Glu]_e$) release by quiescent, amoeboid astrocytes bound to β-dystroglycan. Further, spontaneous neuronal activity in the SCN is highest at ZT 6, leading to increased intracellular Ca^{2+} levels ($[Ca^{2+}]_i$) and membrane voltage (Vm) in postsynaptic neurons. Across circadian time, the level of β-dystroglycan does not change, but we propose that astrocytes continue to utilize this molecule to facilitate their morphological changes throughout the course of the day. The high level of MMP-9 activity during the day clears away ECM molecules in the synaptic space and facilitates the astrocytic transition to a more ramified state during the early night (ZT 16). At ZT 16, increased astrocytic $[Glu]_e$ secretion, NMDAR-NR2B subunit expression, plasmin-mediated maturation of BDNF (mBDNF), and TrkB phosphorylation of NMDARs all contribute to increased sensitivity of night-time NMDARs. However, MMP-9 CAM cleavage continues, which decreases the probability of NMDAR activation. Therefore, spontaneous SCN activity reaches its nadir at night and phase delaying the clock requires aberrant light stimulation or exogenous glutamate application. During the late night (ZT 23), MMP-9 activity is at its lowest level and intact CAMs are able to stabilize NMDARs on the post-synaptic membrane. Astrocytes, now in their most ramified state, begin to increase their colocalization with β-dystroglycan molecules and decrease secretion of $[Glu]_e$. However, NR2B expression and activity of the plasminogen activation cascade is still high, which increases the level of primed NMDARs that, when activated, can phase advance the clock.

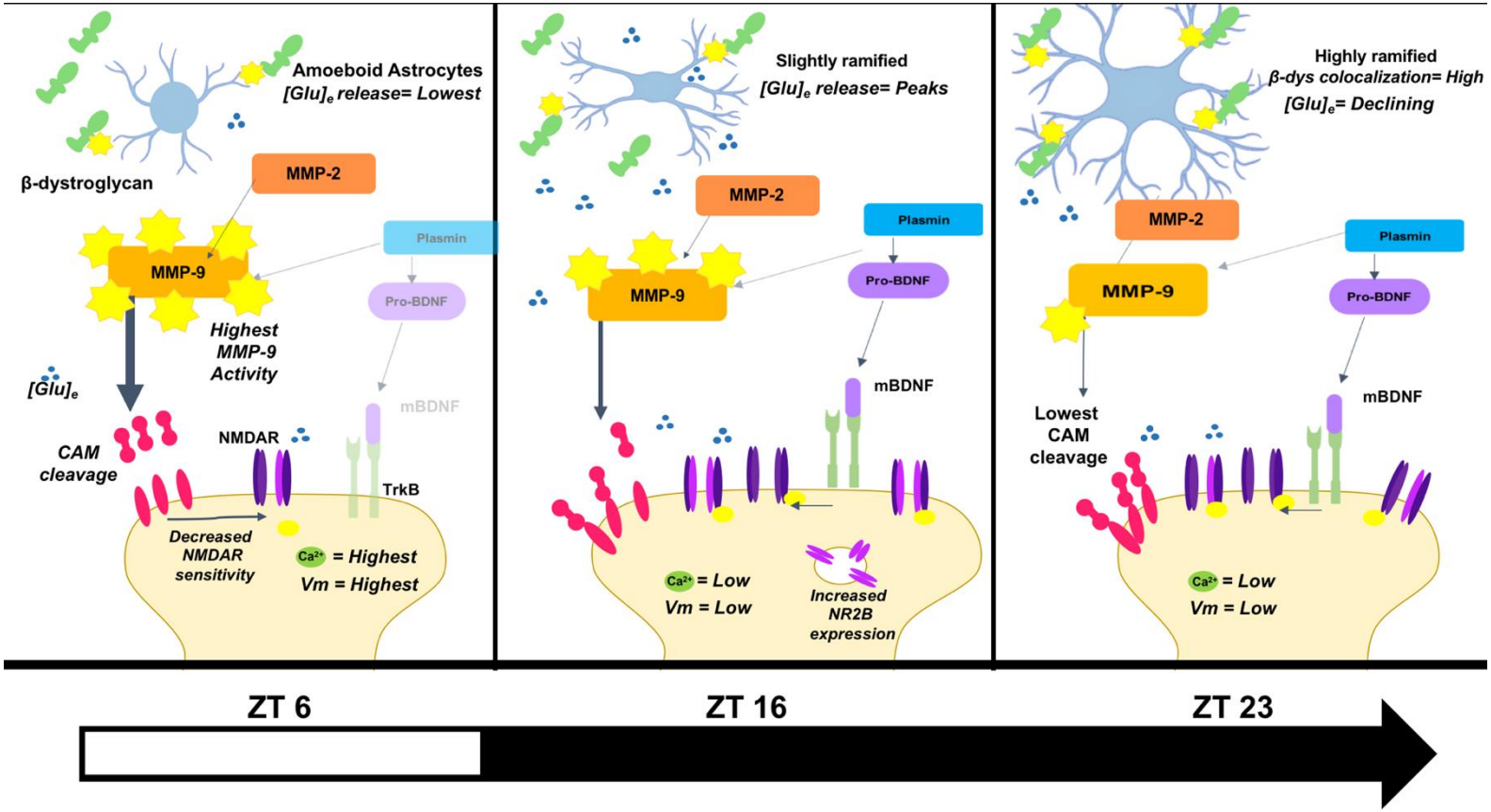

Figure 4.4 continued

Figure 4.5: The effects of MMP-2/9 inhibition on NMDAR are time dependent.

Blocking MMP-2/9 activity, with the inhibitor BiPS (signified by the red X), in SCN tissue during the day (ZT 6) eliminates MMP-9 mediated cleavage of CAMs. The conformation and/or amount of membrane bound CAMs is now favorable for interaction with NMDARs, which increase the sensitivity of existing NMDARs. Although the expression of plasmin and pro-BDNF are low, activation of TrkB still occurs and phosphorylates NMDARs, further priming them for activation. Therefore, although astrocytic derived concentrations of extracellular glutamate are low, NMDARs are sufficiently activated to initiate a phase advance of the clock. Inhibitors targeting plasmin (α -2-antiplasmin) or TrkB (K-252A) are effective in blocking BiPS induced phase shifts, because the phosphorylation of NMDARs (indicated by yellow dots in figure) is blocked as well. At ZT 16, BiPS can induce a phase shift because although MMP-9 activity begins to wane, enough CAMs remain intact and TrKB mediated phosphorylation is enough to sufficiently prime a level of NMDARs that can be activated by astrocytic $[Glu]_e$, which is also at its peak. However, the same concentration of α-2-antiplasmin or K-252A applied during the day is now ineffective to block the BiPS phase shift, as the endogenous level of plasmin/TrkB activity is much greater at ZT 16 than ZT 6. Lastly, MMP-2/9 inhibition at ZT 23 has no effect on the circadian master clock, because MMP-9 activity at this time is at its lowest and $[Glu]_e$ is declining. Therefore, BiPS does not initiate a great enough response to initiate the required amount of NMDAR activity to phase shift the clock. However, plasmin/TrkB activity remains high, so exogenous glutamate application could phase shift the clock.

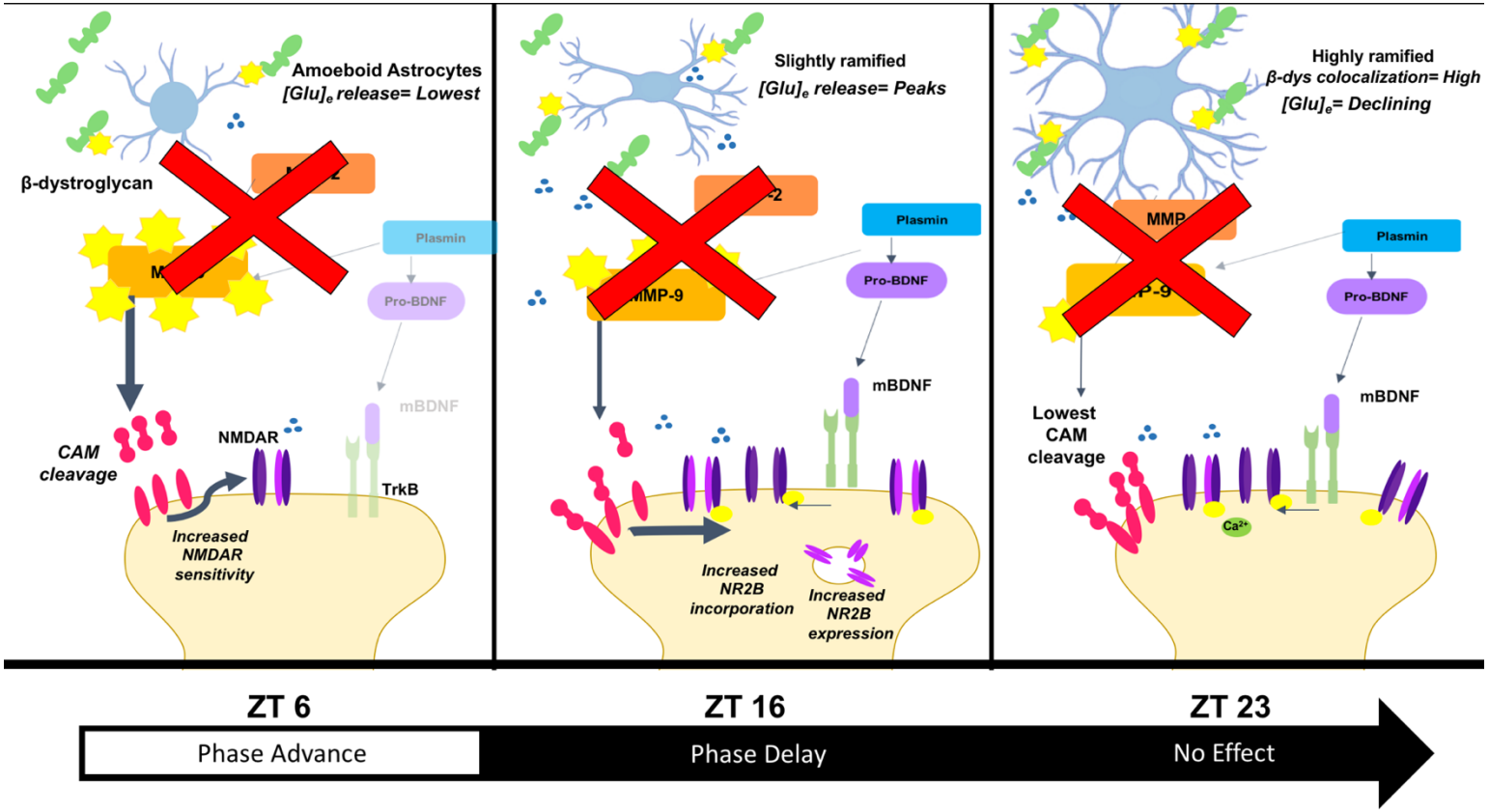

Figure 4.5 continued

REFERENCES

Bisphenol A - Sources, toxicity an... [Environ Toxicol Pharmacol. 2014] - PubMed - NCBI.

Abbott, N.J. (2002) Astrocyte-endothelial interactions and blood-brain barrier permeability. *Journal of anatomy*, **200**, 629-638.

Abdelnaseer, M.M., Elfauomy, N.M., Esmail, E.H., Kamal, M.M. & Elsawy, E.H. (2017) Matrix Metalloproteinase-9 and Recovery of Acute Ischemic Stroke. *Journal of stroke and cerebrovascular diseases : the official journal of National Stroke Association*.

Abrahamson, E.E. & Moore, R.Y. (2001) Suprachiasmatic nucleus in the mouse: retinal innervation, intrinsic organization and efferent projections. *Brain research*, **916**, 172-191.

Adan, A., Archer, S.N., Hidalgo, M.P., Di Milia, L., Natale, V. & Randler, C. (2012) Circadian typology: a comprehensive review. *Chronobiology international*, **29**, 1153-1175.

Aggelopoulos, N.C. & Meissl, H. (2000) Responses of neurones of the rat suprachiasmatic nucleus to retinal illumination under photopic and scotopic conditions. *The Journal of physiology*, **523 Pt 1**, 211-222.

Agostino, P.V., Ferreyra, G.A., Murad, A.D., Watanabe, Y. & Golombek, D.A. (2004) Diurnal, circadian and photic regulation of calcium/calmodulin-dependent kinase II and neuronal nitric oxide synthase in the hamster suprachiasmatic nuclei. *Neurochemistry international*, **44**, 617-625.

Agostino, P.V., Grilli, M.L. & Golombek, D.A. (2002) Characterization of proteases in the hamster suprachiasmatic nucleus. *Biol. Rhythm Res.*, **33**, 383-390.

Agrawal, S., Anderson, P., Durbeej, M., van Rooijen, N., Ivars, F., Opdenakker, G. & Sorokin, L.M. (2006) Dystroglycan is selectively cleaved at the parenchymal basement membrane at sites of leukocyte extravasation in experimental autoimmune encephalomyelitis. *J Exp Med*, **203**, 1007-1019.

Aguayo, F.I., Pacheco, A.A., Garcia-Rojo, G.J., Pizarro-Bauerle, J.A., Doberti, A.V., Tejos, M., Garcia-Perez, M.A., Rojas, P.S. & Fiedler, J.L. (2018) Matrix Metalloproteinase 9 Displays a Particular Time Response to Acute Stress: Variation in Its Levels and Activity Distribution in Rat Hippocampus. *ACS chemical neuroscience*, **9**, 945-956.

Aguilar-Roblero, R., Morin, L.P. & Moore, R.Y. (1994) Morphological correlates of circadian rhythm restoration induced by transplantation of the suprachiasmatic nucleus in hamsters. *Exp Neurol*, **130**, 250-260.

Aguilar-Roblero, R., Shibata, S., Speh, J.C., Drucker-Colin, R. & Moore, R.Y. (1992) Morphological and functional development of the suprachiasmatic nucleus in transplanted fetal hypothalamus. *Brain research*, **580**, 288-296.

Aguilar-Roblero, R., Verduzco-Carbajal, L., Rodriguez, C., Mendez-Franco, J., Moran, J. & de la Mora, M.P. (1993) Circadian rhythmicity in the GABAergic system in the suprachiasmatic nuclei of the rat. *Neurosci Lett*, **157**, 199-202.

Akashi, M. & Nishida, E. (2000) Involvement of the MAP kinase cascade in resetting of the mammalian circadian clock. *Genes Dev*, **14**, 645-649.

Akhtar, R.A., Reddy, A.B., Maywood, E.S., Clayton, J.D., King, V.M., Smith, A.G., Gant, T.W., Hastings, M.H. & Kyriacou, C.P. (2002) Circadian cycling of the mouse liver transcriptome, as revealed by cDNA microarray, is driven by the suprachiasmatic nucleus. *Current biology : CB*, **12**, 540-550.

Albers, H.E., Walton, J.C., Gamble, K.L., McNeill, J.K.t. & Hummer, D.L. (2017) The dynamics of GABA signaling: Revelations from the circadian pacemaker in the suprachiasmatic nucleus. *Frontiers in neuroendocrinology*, **44**, 35-82.

Albrecht, U. (2012) Circadian rhythms and sleep--the metabolic connection. *Pflugers Archiv : European journal of physiology*, **463**, 23-30.

Ali, D.W. & Salter, M.W. (2001) NMDA receptor regulation by Src kinase signalling in excitatory synaptic transmission and plasticity. *Curr Opin Neurobiol*, **11**, 336-342.

Allada, R., White, N.E., So, W.V., Hall, J.C. & Rosbash, M. (1998) A mutant Drosophila homolog of mammalian Clock disrupts circadian rhythms and transcription of period and timeless. *Cell*, **93**, 791-804.

Allen, C.N., Nitabach, M.N. & Colwell, C.S. (2017) Membrane Currents, Gene Expression, and Circadian Clocks *Cold Spring Harb Perspect Biol*.

Allen, G.C., Qu, X. & Earnest, D.J. (2005) TrkB-deficient mice show diminished phase shifts of the circadian activity rhythm in response to light. *Neurosci Lett*, **378**, 150-155.

Almeida, R.D., Manadas, B.J., Melo, C.V., Gomes, J.R., Mendes, C.S., Grãos, M.M., Carvalho, R.F., Carvalho, A.P. & Duarte, C.B. (2005) Neuroprotection by BDNF against glutamate-induced apoptotic cell death is mediated by ERK and PI3-kinase pathways. *Cell Death Differ*, **12**, 1329-1343.

Angleton, P., Chandler, W.L. & Schmer, G. (1989) Diurnal variation of tissue-type plasminogen activator and its rapid inhibitor (PAI-1). *Circulation*, **79**, 101-106.

Antoch, M.P., Song, E.J., Chang, A.M., Vitaterna, M.H., Zhao, Y., Wilsbacher, L.D., Sangoram, A.M., King, D.P., Pinto, L.H. & Takahashi, J.S. (1997) Functional identification of the mouse circadian Clock gene by transgenic BAC rescue. *Cell*, **89**, 655-667.

Aow, J., Dore, K. & Malinow, R. (2015) Conformational signaling required for synaptic plasticity by the NMDA receptor complex. *Proc Natl Acad Sci U S A*, **112**, 14711-14716.

Arendt, J., Skene, D.J., Middleton, B., Lockley, S.W. & Deacon, S. (1997) Efficacy of melatonin treatment in jet lag, shift work, and blindness. *Journal of biological rhythms*, **12**, 604-617.

Aso, Y. (2007) Plasminogen activator inhibitor (PAI)-1 in vascular inflammation and thrombosis. *Front Biosci*, **12**, 2957-2966.

Atapattu, L., Lackmann, M. & Janes, P.W. (2014) The role of proteases in regulating Eph/ephrin signaling. *Cell adhesion & migration*, **8**, 294-307.

Atkins, N., Jr., Ren, S., Hatcher, N., Burgoon, P.W., Mitchell, J.W., Sweedler, J.V. & Gillette, M.U. (2018) Functional Peptidomics: Stimulus- and Time-of-Day-Specific Peptide Release in the Mammalian Circadian Clock. *ACS chemical neuroscience*, **9**, 2001-2008.

Aton, S.J. & Herzog, E.D. (2005) Come together, right...now: synchronization of rhythms in a mammalian circadian clock. *Neuron*, **48**, 531-534.

Ayoub, A.E., Cai, T.Q., Kaplan, R.A. & Luo, J. (2005) Developmental expression of matrix metalloproteinases 2 and 9 and their potential role in the histogenesis of the cerebellar cortex. *The Journal of comparative neurology*, **481**, 403-415.

Backstrom, J.R., Lim, G.P., Cullen, M.J. & Tökés, Z.A. (1996) Matrix metalloproteinase-9 (MMP-9) is synthesized in neurons of the human hippocampus and is capable of degrading the amyloid-beta peptide (1-40). *J Neurosci*, **16**, 7910-7919.

Bajor, M. & Kaczmarek, L. (2013) Proteolytic remodeling of the synaptic cell adhesion molecules (CAMs) by metzincins in synaptic plasticity. *Neurochemical research*, **38**, 1113-1121.

Balkowiec, A. & Katz, D.M. (2002) Cellular mechanisms regulating activity-dependent release of native brain-derived neurotrophic factor from hippocampal neurons. *J Neurosci*, **22**, 10399-10407.

Barca-Mayo, O., Pons-Espinal, M., Follert, P., Armirotti, A., Berdondini, L. & De Pietri Tonelli, D. (2017) Astrocyte deletion of Bmal1 alters daily locomotor activity and cognitive functions via GABA signalling. *Nat Commun*, **8**, 14336.

Barresi, R. & Campbell, K.P. (2006) Dystroglycan: from biosynthesis to pathogenesis of human disease. *Journal of cell science*, **119**, 199-207.

Barrow, S.L., Constable, J.R., Clark, E., El-Sabeawy, F., McAllister, A.K. & Washbourne, P. (2009) Neuroligin1: a cell adhesion molecule that recruits PSD-95 and NMDA receptors by distinct mechanisms during synaptogenesis. *Neural development*, **4**, 17.

Bayer, K.U., De Koninck, P., Leonard, A.S., Hell, J.W. & Schulman, H. (2001) Interaction with the NMDA receptor locks CaMKII in an active conformation. *Nature*, **411**, 801-805.

Beaule, C., Mitchell, J.W., Lindberg, P.T., Damadzic, R., Eiden, L.E. & Gillette, M.U. (2009) Temporally restricted role of retinal PACAP: integration of the phase-advancing light signal to the SCN. *Journal of biological rhythms*, **24**, 126-134.

Becquet, D., Girardet, C., Guillaumond, F., Francois-Bellan, A.M. & Bosler, O. (2008) Ultrastructural plasticity in the rat suprachiasmatic nucleus. Possible involvement in clock entrainment. *Glia*, **56**, 294-305.

Bendova, Z., Sladek, M. & Svobodova, I. (2012) The expression of NR2B subunit of NMDA receptor in the suprachiasmatic nucleus of Wistar rats and its role in glutamate-induced CREB and ERK1/2 phosphorylation. *Neurochemistry international*, **61**, 43-47.

Berg, M., Bruhn, T., Johansen, F.F. & Diemer, N.H. (1993) Kainic acid-induced seizures and brain damage in the rat: different effects of NMDA- and AMPA receptor antagonists. *Pharmacol Toxicol*, **73**, 262-268.

Bernardo, M.M. & Fridman, R. (2003) TIMP-2 (tissue inhibitor of metalloproteinase-2) regulates MMP-2 (matrix metalloproteinase-2) activity in the extracellular environment after pro-MMP-2 activation by MT1 (membrane type 1)-MMP *Biochem J*, pp. 739-745.

Berson, D.M., Dunn, F.A. & Takao, M. (2002) Phototransduction by retinal ganglion cells that set the circadian clock. *Science*, **295**, 1070-1073.

Biello, S.M., Golombek, D.A., Schak, K.M. & Harrington, M.E. (1997) Circadian phase shifts to neuropeptide Y In vitro: cellular communication and signal transduction. *J Neurosci*, **17**, 8468-8475.

Bijata, M., Wlodarczyk, J. & Figiel, I. (2015) Dystroglycan controls dendritic morphogenesis of hippocampal neurons in vitro. *Front Cell Neurosci*, **9**, 199.

Bilousova, T.V., Dansie, L., Ngo, M., Aye, J., Charles, J.R., Ethell, D.W. & Ethell, I.M. (2009) Minocycline promotes dendritic spine maturation and improves behavioural performance in the fragile X mouse model. *J Med Genet*, **46**, 94-102.

Binder, D.K., Papadopoulos, M.C., Haggie, P.M. & Verkman, A.S. (2004) In vivo measurement of brain extracellular space diffusion by cortical surface photobleaching. *J Neurosci*, **24**, 8049-8056.

Binley, K.E., Ng, W.S., Tribble, J.R., Song, B. & Morgan, J.E. (2014) Sholl analysis: a quantitative comparison of semi-automated methods. *J Neurosci Methods*, **225**, 65-70.

Björklund, M. & Koivunen, E. (2005) Gelatinase-mediated migration and invasion of cancer cells. *Biochimica et biophysica acta*, **1755**, 37-69.

Black, I.B. (1999) Trophic regulation of synaptic plasticity. *J Neurobiol*, **41**, 108-118.

Blanke, M.L. & VanDongen, A.M.J. (2009) Frontiers in NeuroscienceActivation Mechanisms of the NMDA Receptor. In Van Dongen, A.M. (ed) *Biology of the NMDA Receptor*. CRC Press/Taylor & FrancisTaylor & Francis Group, LLC., Boca Raton (FL).

Bollinger, T. & Schibler, U. (2014) Circadian rhythms - from genes to physiology and disease. *Swiss medical weekly*, **144**, w13984.

Bonfanti, L. (2006) PSA-NCAM in mammalian structural plasticity and neurogenesis. *Prog Neurobiol*, **80**, 129-164.

Bozdagi, O., Nagy, V., Kwei, K.T. & Huntley, G.W. (2007) In vivo roles for matrix metalloproteinase-9 in mature hippocampal synaptic physiology and plasticity. *J Neurophysiol*, **98**, 334-344.

Bozzi, M., Inzitari, R., Sbardell, D., Monaco, S., Pavoni, E., Gioia, M., Marini, S., Morlacchi, S., Sciandra, F., Castagnola, M., Giardina, B., Brancaccio, A. & Coletta, M. (2009) Enzymatic processing of beta-dystroglycan recombinant ectodomain by MMP-9: identification of the main cleavage site. *IUBMB life*, **61**, 1143-1152.

Brancaccio, M., Maywood, E.S., Chesham, J.E., Loudon, A.S. & Hastings, M.H. (2013) A Gq-Ca2+ axis controls circuit-level encoding of circadian time in the suprachiasmatic nucleus. *Neuron*, **78**, 714-728.

Brancaccio, M., Patton, A.P., Chesham, J.E., Maywood, E.S. & Hastings, M.H. (2017) Astrocytes Control Circadian Timekeeping in the Suprachiasmatic Nucleus via Glutamatergic Signaling. *Neuron*, **93**, 1420-1435.e1425.

Broadberry, E., McConnell, J., Williams, J., Yang, N., Zindy, E., Leek, A., Waddington, R., Joseph, L., Howe, M., Meng, Q.J. & Streuli, C.H. (2018) Disrupted circadian clocks and altered tissue mechanics in primary human breast tumours. *Breast Cancer Res*, **20**, 125.

Brown, M.H. & Nunez, A.A. (1989) Vasopressin-deficient rats show a reduced amplitude of the circadian sleep rhythm. *Physiology & behavior*, **46**, 759-762.

Brown, T.M., Colwell, C.S., Waschek, J.A. & Piggins, H.D. (2007) Disrupted neuronal activity rhythms in the suprachiasmatic nuclei of vasoactive intestinal polypeptide-deficient mice. *J Neurophysiol*, **97**, 2553-2558.

Bruno, M.A. & Cuello, A.C. (2006) Activity-dependent release of precursor nerve growth factor, conversion to mature nerve growth factor, and its degradation by a protease cascade. *Proc Natl Acad Sci U S A*, **103**, 6735-6740.

Bubenik, G.A. & Konturek, S.J. (2011) Melatonin and aging: prospects for human treatment. *J Physiol Pharmacol*, **62**, 13-19.

Burkeen, J.F., Womac, A.D., Earnest, D.J. & Zoran, M.J. (2011) Mitochondrial calcium signaling mediates rhythmic extracellular ATP accumulation in suprachiasmatic nucleus astrocytes. *J Neurosci*, **31**, 8432-8440.

Byron, A., Humphries, J.D. & Humphries, M.J. (2013) Defining the extracellular matrix using proteomics. *Int J Exp Pathol*, **94**, 75-92.

Cao, W., Duan, J., Wang, X., Zhong, X., Hu, Z., Huang, F., Wang, H., Zhang, J., Li, F., Zhang, J., Luo, X. & Li, C.-Q. (2014) Early enriched environment induces an increased conversion of proBDNF to BDNF in the adult rat's hippocampus. *Behavioural brain research*, **265**, 76-83.

Carmona, M.A., Murai, K.K., Wang, L., Roberts, A.J. & Pasquale, E.B. (2009) Glial ephrin-A3 regulates hippocampal dendritic spine morphology and glutamate transport. *Proc Natl Acad Sci U S A*, **106**, 12524-12529.

Castanon-Cervantes, O., Wu, M., Ehlen, J.C., Paul, K., Gamble, K.L., Johnson, R.L., Besing, R.C., Menaker, M., Gewirtz, A.T. & Davidson, A.J. (2010) Dysregulation of inflammatory responses by chronic circadian disruption. *Journal of immunology (Baltimore, Md. : 1950)*, **185**, 5796-5805.

Castel, M., Belenky, M., Cohen, S., Ottersen, O.P. & Storm-Mathisen, J. (1993) Glutamate-like immunoreactivity in retinal terminals of the mouse suprachiasmatic nucleus. *Eur J Neurosci*, **5**, 368-381.

Cauwe, B., Van den Steen, P.E. & Opdenakker, G. (2007) The biochemical, biological, and pathological kaleidoscope of cell surface substrates processed by matrix metalloproteinases. *Critical reviews in biochemistry and molecular biology*, **42**, 113-185.

Chang, J.Y., Parra-Bueno, P., Laviv, T., Szatmari, E.M., Lee, S.R. & Yasuda, R. (2017) CaMKII Autophosphorylation Is Necessary for Optimal Integration of Ca(2+) Signals during LTP Induction, but Not Maintenance. *Neuron*, **94**, 800-808.e804.

Chen, C. & Leonard, J.P. (1996) Protein tyrosine kinase-mediated potentiation of currents from cloned NMDA receptors. *J Neurochem*, **67**, 194-200.

Chen, D., Buchanan, G.F., Ding, J.M., Hannibal, J. & Gillette, M.U. (1999) Pituitary adenylyl cyclase-activating peptide: a pivotal modulator of glutamatergic regulation of the suprachiasmatic circadian clock. *Proc Natl Acad Sci U S A*, **96**, 13468-13473.

Chen, J.T., Chen, T.G., Chang, Y.C., Chen, C.Y. & Chen, R.M. (2016) Roles of NMDARs in maintenance of the mouse cerebrovascular endothelial cell-constructed tight junction barrier. *Toxicology*, **339**, 40-50.

Cheng, X., Wang, J., Sun, X., Shao, L., Guo, Z. & Li, Y. (2019) Morphological and functional alterations of astrocytes responding to traumatic brain injury. *J Integr Neurosci*, **18**, 203-215.

Chhabra, A. & Rani, V. (2017) Cell In Situ Zymography: Imaging Enzyme-Substrate Interactions. *Methods in molecular biology (Clifton, N.J.)*, **1626**, 133-143.

Chiang, C.K., Mehta, N., Patel, A., Zhang, P., Ning, Z., Mayne, J., Sun, W.Y., Cheng, H.Y. & Figeys, D. (2014) The proteomic landscape of the suprachiasmatic nucleus clock reveals large-scale coordination of key biological processes. *PLoS Genet*, **10**, e1004695.

Cho, H., Zhao, X., Hatori, M., Yu, R.T., Barish, G.D., Lam, M.T., Chong, L.W., DiTacchio, L., Atkins, A.R., Glass, C.K., Liddle, C., Auwerx, J., Downes, M., Panda, S. & Evans, R.M. (2012) Regulation of circadian behaviour and metabolism by REV-ERB-α and REV-ERB-β. *Nature*, **485**, 123-127.

Cho, M.H., Cao, X., Wang, D. & Tsien, J.Z. (2007) Dentate gyrus-specific manipulation of beta-Ca2+/calmodulin-dependent kinase II disrupts memory consolidation. *Proc Natl Acad Sci U S A*, **104**, 16317-16322.

Chung, C. (2013) NMDA receptor as a newly identified member of the metabotropic glutamate receptor family: clinical implications for neurodegenerative diseases. *Mol Cells*, **36**, 99-104.

Church, D.M., Goodstadt, L., Hillier, L.W., Zody, M.C., Goldstein, S., She, X., Bult, C.J., Agarwala, R., Cherry, J.L., DiCuccio, M., Hlavina, W., Kapustin, Y., Meric, P., Maglott, D., Birtle, Z., Marques, A.C., Graves, T., Zhou, S., Teague, B., Potamousis, K., Churas, C., Place, M., Herschleb, J., Runnheim, R., Forrest, D., Amos-Landgraf, J., Schwartz, D.C., Cheng, Z., Lindblad-Toh, K., Eichler, E.E. & Ponting, C.P. (2009) Lineage-specific biology revealed by a finished genome assembly of the mouse. *PLoS Biol*, **7**, e1000112.

Cieplak, P. & Strongin, A.Y. (2017) Matrix metalloproteinases - From the cleavage data to the prediction tools and beyond. *Biochim Biophys Acta Mol Cell Res*, **1864**, 1952-1963.

Clark, J.P. & Kofuji, P. (2010) Stoichiometry of N-Methyl-D-Aspartate Receptors Within the Suprachiasmatic Nucleus. *Journal of Neurophysiology*, **103**, 3448-3464.

Colwell, C.S. (2001) NMDA-evoked calcium transients and currents in the suprachiasmatic nucleus: gating by the circadian system. *Eur J Neurosci*, **13**, 1420-1428.

Colwell, C.S. (2011) Linking neural activity and molecular oscillations in the SCN. *Nature Reviews Neuroscience*, **12**, 553-569.

Colwell, C.S., Foster, R.G. & Menaker, M. (1991) NMDA receptor antagonists block the effects of light on circadian behavior in the mouse. *Brain research*, **554**, 105-110.

Colwell, C.S. & Menaker, M. (1992) NMDA as well as non-NMDA receptor antagonists can prevent the phase-shifting effects of light on the circadian system of the golden hamster. *Journal of biological rhythms*, **7**, 125-136.

Colwell, C.S., Michel, S., Itri, J., Rodriguez, W., Tam, J., Lelievre, V., Hu, Z., Liu, X. & Waschek, J.A. (2003) Disrupted circadian rhythms in VIP- and PHI-deficient mice. *American journal of physiology. Regulatory, integrative and comparative physiology*, **285**, R939-949.

Colwell, C.S., Whitmore, D., Michel, S. & Block, G.D. (1994) Calcium plays a central role in phase shifting the ocular circadian pacemaker of Aplysia. *J Comp Physiol A*, **175**, 415-423.

Conant, K., Wang, Y., Szklarczyk, A., Dudak, A., Mattson, M.P. & Lim, S.T. (2010) Matrix metalloproteinase-dependent shedding of intercellular adhesion molecule-5 occurs with long-term potentiation. *Neuroscience*, **166**, 508-521.

Cooper, J. & Prosser, R. (2014) LRP-1 modulates glutamate-induced phase shifting in the mouse SCN circadian clock., Proceedings of the Biomedicine Science Engineering Conference.

Cooper, J.M., Halter, K.A. & Prosser, R.A. (2018) Circadian rhythm and sleep-wake systems share the dynamic extracellular synaptic milieu. Elsevier, Neurobiology of Sleep and Circadian Rhythms.

Cooper, J.M., Rastogi, A., Krizo, J.A., Mintz, E.M. & Prosser, R.A. (2017) Urokinase-type plasminogen activator modulates mammalian circadian clock phase regulation in tissue-type plasminogen activator knockout mice. *Eur J Neurosci*, **45**, 805-815.

Costa, G. (2010) Shift work and health: current problems and preventive actions. *Saf Health Work*, **1**, 112-123.

Cousins, S.L. & Stephenson, F.A. (2012) Identification of N-methyl-D-aspartic acid (NMDA) receptor subtype-specific binding sites that mediate direct interactions with scaffold protein PSD-95. *J Biol Chem*, **287**, 13465-13476.

Crair, M.C. (1999) Neuronal activity during development: permissive or instructive? *Curr Opin Neurobiol*, **9**, 88-93.

Cuddapah, V.A., Zhang, S.L. & Sehgal, A. (2019) Regulation of the Blood-Brain Barrier by Circadian Rhythms and Sleep. *Trends Neurosci*, **42**, 500-510.

Cull-Candy, S.G. & Leszkiewicz, D.N. (2004) Role of distinct NMDA receptor subtypes at central synapses. *Sci STKE*, **2004**, re16.

Curtin, K.D., Huang, Z.J. & Rosbash, M. (1995) Temporally regulated nuclear entry of the Drosophila period protein contributes to the circadian clock. *Neuron*, **14**, 365-372.

Dai, J., Aoto, J. & Sudhof, T.C. (2019) Alternative Splicing of Presynaptic Neurexins Differentially Controls Postsynaptic NMDA and AMPA Receptor Responses. *Neuron*, **102**, 993-1008.e1005.

Dalva, M.B., Takasu, M.A., Lin, M.Z., Shamah, S.M., Hu, L., Gale, N.W. & Greenberg, M.E. (2000) EphB receptors interact with NMDA receptors and regulate excitatory synapse formation. *Cell*, **103**, 945-956.

Daneshtalab, N., Dore, J.J. & Smeda, J.S. (2010) Troubleshooting tissue specificity and antibody selection: Procedures in immunohistochemical studies. *Journal of pharmacological and toxicological methods*, **61**, 127-135.

Darlington, T.K., Wager-Smith, K., Ceriani, M.F., Staknis, D., Gekakis, N., Steeves, T.D., Weitz, C.J., Takahashi, J.S. & Kay, S.A. (1998) Closing the circadian loop: CLOCK-induced transcription of its own inhibitors per and tim. *Science*, **280**, 1599-1603.

de Jeu, M., Hermes, M. & Pennartz, C. (1998) Circadian modulation of membrane properties in slices of rat suprachiasmatic nucleus. *Neuroreport*, **9**, 3725-3729.

De Luca, C. & Papa, M. (2017) Matrix Metalloproteinases, Neural Extracellular Matrix, and Central Nervous System Pathology. *Progress in molecular biology and translational science*, **148**, 167-202.

de Matos, L.L., Trufelli, D.C., de Matos, M.G.L. & da Silva Pinhal, M.A. (2010) Immunohistochemistry as an Important Tool in Biomarkers Detection and Clinical Practice *Biomark Insights*, pp. 9-20.

De Stefano, M.E. & Herrero, M.T. (2016) The multifaceted role of metalloproteinases in physiological and pathological conditions in embryonic and adult brains. *Prog Neurobiol*.

de Vries, M.J., Nunes Cardozo, B., van der Want, J., de Wolf, A. & Meijer, J.H. (1993) Glutamate immunoreactivity in terminals of the retinohypothalamic tract of the brown Norwegian rat. *Brain research*, **612**, 231-237.

Dean, R.A. & Overall, C.M. (2007) Proteomics discovery of metalloproteinase substrates in the cellular context by iTRAQ labeling reveals a diverse MMP-2 substrate degradome. *Mol Cell Proteomics*, **6**, 611-623.

DeCoursey, P.J. & Buggy, J. (1989) Circadian rhythmicity after neural transplant to hamster third ventricle: specificity of suprachiasmatic nuclei. *Brain research*, **500**, 263-275.

Deery, M.J., Maywood, E.S., Chesham, J.E., Sladek, M., Karp, N.A., Green, E.W., Charles, P.D., Reddy, A.B., Kyriacou, C.P., Lilley, K.S. & Hastings, M.H. (2009) Proteomic analysis reveals the role of synaptic vesicle cycling in sustaining the suprachiasmatic circadian clock. *Current biology : CB*, **19**, 2031-2036.

del Zoppo, G.J. & Milner, R. (2006) Integrin-matrix interactions in the cerebral microvasculature. *Arterioscler Thromb Vasc Biol*, **26**, 1966-1975.

Demuth, T. & Berens, M.E. (2004) Molecular mechanisms of glioma cell migration and invasion. *Journal of neuro-oncology*, **70**, 217-228.

Deng, X.H., Bertini, G., Palomba, M., Xu, Y.Z., Bonaconsa, M., Nygard, M. & Bentivoglio, M. (2010) Glial transcripts and immune-challenged glia in the suprachiasmatic nucleus of young and aged mice. *Chronobiology international*, **27**, 742-767.

Depetris-Chauvin, A., Fernandez-Gamba, A., Gorostiza, E.A., Herrero, A., Castano, E.M. & Ceriani, M.F. (2014) Mmp1 processing of the PDF neuropeptide regulates circadian structural plasticity of pacemaker neurons. *PLoS Genet*, **10**, e1004700.

Ding, J.M., Chen, D., Weber, E.T., Faiman, L.E., Rea, M.A. & Gillette, M.U. (1994) Resetting the biological clock: mediation of nocturnal circadian shifts by glutamate and NO. *Science*, **266**, 1713-1717.

Ding, J.M., Faiman, L.E., Hurst, W.J., Kuriashkina, L.R. & Gillette, M.U. (1997) Resetting the biological clock: mediation of nocturnal CREB phosphorylation via light, glutamate, and nitric oxide. *J Neurosci*, **17**, 667-675.

Dityatev, A., Frischknecht, R. & Seidenbecher, C.I. (2006) Extracellular matrix and synaptic functions. *Results Probl Cell Differ*, **43**, 69-97.

Dityatev, A. & Schachner, M. (2003) Extracellular matrix molecules and synaptic plasticity. *Nature reviews. Neuroscience*, **4**, 456-468.

Dore, K., Aow, J. & Malinow, R. (2016) The Emergence of NMDA Receptor Metabotropic Function: Insights from Imaging. *Front Synaptic Neurosci*, **8**, 20.

Dore, K., Stein, I.S., Brock, J.A., Castillo, P.E., Zito, K. & Sjostrom, P.J. (2017) Unconventional NMDA Receptor Signaling. *J Neurosci*, **37**, 10800-10807.

Dragich, J.M., Loh, D.H., Wang, L.M., Vosko, A.M., Kudo, T., Nakamura, T.J., Odom, I.H., Tateyama, S., Hagopian, A., Waschek, J.A. & Colwell, C.S. (2010) The role of the neuropeptides PACAP and VIP in the photic regulation of gene expression in the suprachiasmatic nucleus. *Eur J Neurosci*, **31**, 864-875.

Drouyer, E., Rieux, C., Hut, R.A. & Cooper, H.M. (2007) Responses of suprachiasmatic nucleus neurons to light and dark adaptation: relative contributions of melanopsin and rod-cone inputs. *J Neurosci*, **27**, 9623-9631.

Drucker-Colín, R., Aguilar-Roblero, R., García-Hernández, F., Fernández-Cancino, F. & Bermudez Rattoni, F. (1984) Fetal suprachiasmatic nucleus transplants: diurnal rhythm recovery of lesioned rats. *Brain research*, **311**, 353-357.

Dunlap, J.C. (1999) Molecular bases for circadian clocks. *Cell*, **96**, 271-290.

Durbeej, M. & Campbell, K.P. (1999) Biochemical characterization of the epithelial dystroglycan complex. *J Biol Chem*, **274**, 26609-26616.

Dziembowska, M., Milek, J., Janusz, A., Rejmak, E., Romanowska, E., Gorkiewicz, T., Tiron, A., Bramham, C.R. & Kaczmarek, L. (2012) Activity-dependent local translation of matrix metalloproteinase-9. *J Neurosci*, **32**, 14538-14547.

Dzwonek, J., Rylski, M. & Kaczmarek, L. (2004) Matrix metalloproteinases and their endogenous inhibitors in neuronal physiology of the adult brain. *FEBS Lett*, **567**, 129-135.

Egli, M., Bertram, R., Sellix, M.T. & Freeman, M.E. (2004) Rhythmic secretion of prolactin in rats: action of oxytocin coordinated by vasoactive intestinal polypeptide of suprachiasmatic nucleus origin. *Endocrinology*, **145**, 3386-3394.

Elliott, A.S. & Nunez, A.A. (1994) An ultrastructural study of somal appositions in the suprachiasmatic nucleus and anterior hypothalamus of the rat. *Brain research*, **662**, 278-282.

Emery, P., So, W.V., Kaneko, M., Hall, J.C. & Rosbash, M. (1998) CRY, a Drosophila clock and light-regulated cryptochrome, is a major contributor to circadian rhythm resetting and photosensitivity. *Cell*, **95**, 669-679.

Esapa, C.T., Bentham, G.R., Schroder, J.E., Kroger, S. & Blake, D.J. (2003) The effects of post-translational processing on dystroglycan synthesis and trafficking. *FEBS Lett*, **555**, 209-216.

Ethell, I.M. & Ethell, D.W. (2007) Matrix metalloproteinases in brain development and remodeling: synaptic functions and targets. *J Neurosci Res*, **85**, 2813-2823.

Fawcett, J.W., Oohashi, T. & Pizzorusso, T. (2019) The roles of perineuronal nets and the perinodal extracellular matrix in neuronal function. *Nature reviews. Neuroscience*.

Fedorkova, L., Rutishauser, U., Prosser, R., Shen, H. & Glass, J.D. (2002) Removal of polysialic acid from the SCN potentiates nonphotic circadian phase resetting. *Physiology & behavior*, **77**, 361-369.

Ferreira, T.A., Blackman, A.V., Oyrer, J., Jayabal, S., Chung, A.J., Watt, A.J., Sjostrom, P.J. & van Meyel, D.J. (2014) Neuronal morphometry directly from bitmap images *Nat Methods*, United States, pp. 982-984.

Ferrer-Ferrer, M. & Dityatev, A. (2018) Shaping Synapses by the Neural Extracellular Matrix. *Frontiers in neuroanatomy*, **12**, 40.

Field, M.D., Maywood, E.S., O'Brien, J.A., Weaver, D.R., Reppert, S.M. & Hastings, M.H. (2000) Analysis of clock proteins in mouse SCN demonstrates phylogenetic divergence of the circadian clockwork and resetting mechanisms. *Neuron*, **25**, 437-447.

Filipski, E., Innominato, P.F., Wu, M.W., Li, X.M., Iacobelli, S., Xian, L.J. & Levi, F. (2005) Effects of light and food schedules on liver and tumor molecular clocks in mice. *JNCI-J. Natl. Cancer Inst.*, **97**, 507-517.

Fisher, K.E., Fei, Q., Laird, E.R., Stock, J.L., Allen, M.R., Sahagan, B.G. & Strick, C.A. (2002) Engineering autoactivating forms of matrix metalloproteinase-9 and expression of the active enzyme in cultured cells and transgenic mouse brain. *Biochemistry*, **41**, 8289-8297.

Fonken, L.K. & Nelson, R.J. (2014) The effects of light at night on circadian clocks and metabolism. *Endocr Rev*, **35**, 648-670.

Frankowski, H., Gu, Y.H., Heo, J.H., Milner, R. & Del Zoppo, G.J. (2012) Use of gel zymography to examine matrix metalloproteinase (gelatinase) expression in brain tissue or in primary glial cultures. *Methods in molecular biology (Clifton, N.J.)*, **814**, 221-233.

Fridman, R., Toth, M., Chvyrkova, I., Meroueh, S.O. & Mobashery, S. (2003) Cell surface association of matrix metalloproteinase-9 (gelatinase B). *Cancer metastasis reviews*, **22**, 153-166.

Frischknecht, R., Chang, K.J., Rasband, M.N. & Seidenbecher, C.I. (2014) Neural ECM molecules in axonal and synaptic homeostatic plasticity. *Progress in brain research*, **214**, 81-100.

Frischknecht, R. & Gundelfinger, E.D. (2012) The brain's extracellular matrix and its role in synaptic plasticity. *Adv Exp Med Biol*, **970**, 153-171.

Frischknecht, R., Heine, M., Perrais, D., Seidenbecher, C.I., Choquet, D. & Gundelfinger, E.D. (2009) Brain extracellular matrix affects AMPA receptor lateral mobility and short-term synaptic plasticity. *Nat Neurosci*, **12**, 897-904.

Fustin, J.M., Karakawa, S. & Okamura, H. (2017) Circadian Profiling of Amino Acids in the SCN and Cerebral Cortex by Laser Capture Microdissection-Mass Spectrometry. *Journal of biological rhythms*, **32**, 609-620.

Fux, C.M., Krug, M., Dityatev, A., Schuster, T. & Schachner, M. (2003) NCAM180 and glutamate receptor subtypes in potentiated spine synapses: an immunogold electron microscopic study. *Molecular and cellular neurosciences*, **24**, 939-950.

Ganguly, K., Rejmak, E., Mikosz, M., Nikolaev, E., Knapska, E. & Kaczmarek, L. (2013) Matrix metalloproteinase (MMP) 9 transcription in mouse brain induced by fear learning. *J Biol Chem*, **288**, 20978-20991.

Gau, D., Lemberger, T., von Gall, C., Kretz, O., Le Minh, N., Gass, P., Schmid, W., Schibler, U., Korf, H.W. & Schütz, G. (2002) Phosphorylation of CREB Ser142 regulates light-induced phase shifts of the circadian clock. *Neuron*, **34**, 245-253.

Gawlak, M., Gorkiewicz, T., Gorlewicz, A., Konopacki, F.A., Kaczmarek, L. & Wilczynski, G.M. (2009) High resolution in situ zymography reveals matrix metalloproteinase activity at glutamatergic synapses. *Neuroscience*, **158**, 167-176.

Gekakis, N., Staknis, D., Nguyen, H.B., Davis, F.C., Wilsbacher, L.D., King, D.P., Takahashi, J.S. & Weitz, C.J. (1998) Role of the CLOCK protein in the mammalian circadian mechanism. *Science*, **280**, 1564-1569.

Giancotti, F.G. & Ruoslahti, E. (1999) Integrin signaling. *Science*, **285**, 1028-1032.

Giese, K.P., Fedorov, N.B., Filipkowski, R.K. & Silva, A.J. (1998) Autophosphorylation at Thr286 of the alpha calcium-calmodulin kinase II in LTP and learning. *Science*, **279**, 870-873.

Gillette, M. (1991) SCN electrophysiology in vitro: Rhythmic activity and endogenous clock properties. Oxford University Press, New York, *In Suprachiasmatic Nucleus: The Mind's Clock* by Klein DC, Moore RY, Reppert SM,, pp. Chapter 6, pg 125-143.

Gillette, M.U. & Mitchell, J.W. (2002) Signaling in the suprachiasmatic nucleus: selectively responsive and integrative. *Cell and tissue research*, **309**, 99-107.

Gillette, M.U. & Prosser, R.A. (1988) Circadian rhythm of the rat suprachiasmatic brain slice is rapidly reset by daytime application of cAMP analogs. *Brain research*, **474**, 348-352.

Ginty, D.D., Kornhauser, J.M., Thompson, M.A., Bading, H., Mayo, K.E., Takahashi, J.S. & Greenberg, M.E. (1993) Regulation of CREB phosphorylation in the suprachiasmatic nucleus by light and a circadian clock. *Science*, **260**, 238-241.

Girardet, C., Becquet, D., Blanchard, M.P., Francois-Bellan, A.M. & Bosler, O. (2010) Neuroglial and synaptic rearrangements associated with photic entrainment of the circadian clock in the suprachiasmatic nucleus. *Eur J Neurosci*, **32**, 2133-2142.

Girardet, C., Lebrun, B., Cabirol-Pol, M.J., Tardivel, C., Francois-Bellan, A.M., Becquet, D. & Bosler, O. (2013) Brain-derived neurotrophic factor/TrkB signaling regulates daily astroglial plasticity in the suprachiasmatic nucleus: electron-microscopic evidence in mouse. *Glia*, **61**, 1172-1177.

Glass, J.D., Lee, W., Shen, H. & Watanabe, M. (1994) Expression of immunoreactive polysialylated neural cell adhesion molecule in the suprachiasmatic nucleus. *Neuroendocrinology*, **60**, 87-95.

Glass, J.D., Shen, H., Fedorkova, L., Chen, L., Tomasiewicz, H. & Watanabe, M. (2000) Polysialylated neural cell adhesion molecule modulates photic signaling in the mouse suprachiasmatic nucleus. *Neurosci Lett*, **280**, 207-210.

Glass, J.D., Watanabe, M., Fedorkova, L., Shen, H., Ungers, G. & Rutishauser, U. (2003) Dynamic regulation of polysialylated neural cell adhesion molecule in the suprachiasmatic nucleus. *Neuroscience*, **117**, 203-211.

Golombek, D.A. & Rosenstein, R.E. (2010) Physiology of Circadian Entrainment. *Physiological Reviews*, **90**, 1063-1102.

Gondo, A., Shinotsuka, T., Morita, A., Abe, Y., Yasui, M. & Nuriya, M. (2014) Sustained down-regulation of beta-dystroglycan and associated dysfunctions of astrocytic endfeet in epileptic cerebral cortex. *J Biol Chem*, **289**, 30279-30288.

Gorkiewicz, T., Szczuraszek, K., Wyrembek, P., Michaluk, P., Kaczmarek, L. & Mozrzymas, J.W. (2010) Matrix metalloproteinase-9 reversibly affects the time course of NMDA-induced currents in cultured rat hippocampal neurons. *Hippocampus*, **20**, 1105-1108.

Gray, J.A., Zito, K. & Hell, J.W. (2016) Non-ionotropic signaling by the NMDA receptor: controversy and opportunity. *F1000Res*, **5**.

Green, D.J. & Gillette, R. (1982) Circadian rhythm of firing rate recorded from single cells in the rat suprachiasmatic brain slice. *Brain research*, **245**, 198-200.

Groc, L., Choquet, D., Stephenson, F.A., Verrier, D., Manzoni, O.J. & Chavis, P. (2007) NMDA Receptor Surface Trafficking and Synaptic Subunit Composition Are Developmentally Regulated by the Extracellular Matrix Protein Reelin.

Groos, G. & Hendriks, J. (1982) Circadian rhythms in electrical discharge of rat suprachiasmatic neurones recorded in vitro. *Neurosci Lett*, **34**, 283-288.

Gross, J. & Lapiere, C.M. (1962) Collagenolytic activity in amphibian tissues: a tissue culture assay. *Proc Natl Acad Sci U S A*, **48**, 1014-1022.

Grosshans, D.R. & Browning, M.D. (2001) Protein kinase C activation induces tyrosine phosphorylation of the NR2A and NR2B subunits of the NMDA receptor. *J Neurochem*, **76**, 737-744.

Gu, Z., Kaul, M., Yan, B., Kridel, S.J., Cui, J., Strongin, A., Smith, J.W., Liddington, R.C. & Lipton, S.A. (2002) S-nitrosylation of matrix metalloproteinases: signaling pathway to neuronal cell death. *Science*, **297**, 1186-1190.

Guo, Y.F., Mei, H. & Li, Y.L. (2007) [Using DQ-gelatin in situ zymography to detect gelatinolytic activity]. *Zhonghua bing li xue za zhi = Chinese journal of pathology*, **36**, 274.

Hamada, T., Sonoda, R., Watanabe, A., Ono, M., Shibata, S. & Watanabe, S. (1998) NMDA induced glutamate release from the suprachiasmatic nucleus: an in vitro study in the rat. *Neurosci Lett*, **256**, 93-96.

Hammond, M.S., Sims, C., Parameshwaran, K., Suppiramaniam, V., Schachner, M. & Dityatev, A. (2006) Neural cell adhesion molecule-associated polysialic acid inhibits NR2B-containing N-methyl-D-aspartate receptors and prevents glutamate-induced cell death. *J Biol Chem*, **281**, 34859-34869.

Hannibal, J. (2002) Neurotransmitters of the retino-hypothalamic tract. *Cell and tissue research*, **309**, 73-88.

Hannibal, J., Ding, J.M., Chen, D., Fahrenkrug, J., Larsen, P.J., Gillette, M.U. & Mikkelsen, J.D. (1998) Pituitary adenylate cyclase activating peptide (PACAP) in the retinohypothalamic tract: a daytime regulator of the biological clock. *Ann N Y Acad Sci*, **865**, 197-206.

Hannibal, J., Georg, B. & Fahrenkrug, J. (2017) PAC1- and VPAC2 receptors in light regulated behavior and physiology: Studies in single and double mutant mice. *PLoS One*, **12**, e0188166.

Hannou, L., Bélanger-Nelson, E., O'Callaghan, E.K., Dufort-Gervais, J., Roig, M.N.B., Roy, P.-G., Beaulieu, J.-M., Cermakian, N. & Mongrain, V. (2018a) Regulation of the Neuroligin-1 Gene by Clock Transcription Factors:.

Hannou, L., Roy, P.G., Ballester Roig, M.N. & Mongrain, V. (2018b) Transcriptional control of synaptic components by the clock machinery. *Eur J Neurosci*.

Harlow, E., D. Lane (1999) *Using Antibodies: A Laboratory Manual*. Cold Spring Harbor Laboratory Press, Cold Spring Harbor, N.Y.

Harmar, A.J., Marston, H.M., Shen, S., Spratt, C., West, K.M., Sheward, W.J., Morrison, C.F., Dorin, J.R., Piggins, H.D., Reubi, J.C., Kelly, J.S., Maywood, E.S. & Hastings, M.H. (2002) The VPAC(2) receptor is essential for circadian function in the mouse suprachiasmatic nuclei. *Cell*, **109**, 497-508.

Harrington, M.E., Hoque, S., Hall, A., Golombek, D. & Biello, S. (1999) Pituitary adenylate cyclase activating peptide phase shifts circadian rhythms in a manner similar to light. *J Neurosci*, **19**, 6637-6642.

Hastings, M.H., Brancaccio, M. & Maywood, E.S. (2014) Circadian pacemaking in cells and circuits of the suprachiasmatic nucleus. *J Neuroendocrinol*, **26**, 2-10.

Hastings, M.H., Ebling, F.J., Grosse, J., Herbert, J., Maywood, E.S., Mikkelsen, J.D. & Sumova, A. (1995) Immediate-early genes and the neural bases of photic and non-photic entrainment. *Ciba Foundation symposium*, **183**, 175-189; discussion 190-177.

Hastings, M.H. & Goedert, M. (2013) Circadian clocks and neurodegenerative diseases: time to aggregate? *Curr Opin Neurobiol*, **23**, 880-887.

Hatcher, N.G., Atkins, N., Jr., Annangudi, S.P., Forbes, A.J., Kelleher, N.L., Gillette, M.U. & Sweedler, J.V. (2008) Mass spectrometry-based discovery of circadian peptides. *Proc Natl Acad Sci U S A*, **105**, 12527-12532.

Hattar, S., Kumar, M., Park, A., Tong, P., Tung, J., Yau, K.W. & Berson, D.M. (2006) Central projections of melanopsin-expressing retinal ganglion cells in the mouse. *The Journal of comparative neurology*, **497**, 326-349.

Hawkins, B.T., Gu, Y.H., Izawa, Y. & Del Zoppo, G.J. (2013) Disruption of dystroglycan-laminin interactions modulates water uptake by astrocytes. *Brain research*, **1503**, 89-96.

Heo, J.H., Lucero, J., Abumiya, T., Koziol, J.A., Copeland, B.R. & del Zoppo, G.J. (1999) Matrix metalloproteinases increase very early during experimental focal cerebral ischemia. *J Cereb Blood Flow Metab*, **19**, 624-633.

Herzog, E.D., Takahashi, J.S. & Block, G.D. (1998) Clock controls circadian period in isolated suprachiasmatic nucleus neurons. *Nat Neurosci*, **1**, 708-713.

Hetman, M., Kanning, K., Cavanaugh, J.E. & Xia, Z. (1999) Neuroprotection by brain-derived neurotrophic factor is mediated by extracellular signal-regulated kinase and phosphatidylinositol 3-kinase. *J Biol Chem*, **274**, 22569-22580.

Hillen, A.E.J., Burbach, J.P.H. & Hol, E.M. (2018) Cell adhesion and matricellular support by astrocytes of the tripartite synapse. *Prog Neurobiol*, **165-167**, 66-86.

Hisatsune, C., Umemori, H., Mishina, M. & Yamamoto, T. (1999) Phosphorylation-dependent interaction of the N-methyl-D-aspartate receptor epsilon 2 subunit with phosphatidylinositol 3-kinase. *Genes Cells*, **4**, 657-666.

Hoirisch-Clapauch, S. & Nardi, A.E. (2013) Multiple roles of tissue plasminogen activator in schizophrenia pathophysiology. *Semin Thromb Hemost*, **39**, 950-954.

Hollmann, M. (1999) Structure of Ionotropic Glutamate Receptors. In P. Jonas, H.M. (ed) *Ionotropic Glutamate Receptors in the CNS,*. 1999, Berlin, pp. pg 1-98.

Huntley, G.W. (2012) Synaptic circuit remodelling by matrix metalloproteinases in health and disease. *Nature Reviews Neuroscience*, **13**, 743-757.

Iadecola, C. (2004) Neurovascular regulation in the normal brain and in Alzheimer's disease. *Nature reviews. Neuroscience*, **5**, 347-360.

Ibraghimov-Beskrovnaya, O., Ervasti, J.M., Leveille, C.J., Slaughter, C.A., Sernett, S.W. & Campbell, K.P. (1992) Primary structure of dystrophin-associated glycoproteins linking dystrophin to the extracellular matrix. *Nature*, **355**, 696-702.

Ikeda, T., Iijima, N., Munekawa, K., Ishihara, A., Ibata, Y. & Tanaka, M. (2003) Functional retinal input stimulates expression of astroglial elements in the suprachiasmatic nucleus of postnatal developing rat. *Neuroscience research*, **47**, 39-45.

Ingle, K.A., Kain, V., Goel, M., Prabhu, S.D., Young, M.E. & Halade, G.V. (2015) Cardiomyocyte-specific Bmal1 deletion in mice triggers diastolic dysfunction, extracellular matrix response, and impaired resolution of inflammation *Am J Physiol Heart Circ Physiol*, pp. H1827-1836.

Inouye, S.T. & Kawamura, H. (1979) Persistence of circadian rhythmicity in a mammalian hypothalamic "island" containing the suprachiasmatic nucleus. *Proc Natl Acad Sci U S A*, **76**, 5962-5966.

Iyer, R., Wang, T.A. & Gillette, M.U. (2014) Circadian gating of neuronal functionality: a basis for iterative metaplasticity. *Front Syst Neurosci*, **8**, 164.

Jaworski, D.M. (2000) Differential regulation of tissue inhibitor of metalloproteinase mRNA expression in response to intracranial injury. *Glia*, **30**, 199-208.

Jiang, M., Polepalli, J., Chen, L.Y., Zhang, B., Südhof, T.C. & Malenka, R.C. (2017) Conditional ablation of neuroligin-1 in CA1 pyramidal neurons blocks LTP by a cell-autonomous NMDA receptor-independent mechanism. *Mol Psychiatry*, **22**, 375-383.

Jiang, Z.G., Yang, Y., Liu, Z.P. & Allen, C.N. (1997) Membrane properties and synaptic inputs of suprachiasmatic nucleus neurons in rat brain slices. *The Journal of physiology*, **499 (Pt 1)**, 141-159.

Johnson, R.F., Morin, L.P. & Moore, R.Y. (1988) Retinohypothalamic projections in the hamster and rat demonstrated using cholera toxin. *Brain research*, **462**, 301-312.

Jourquin, J., Tremblay, E., Decanis, N., Charton, G., Hanessian, S., Chollet, A.M., Le Diguardher, T., Khrestchatisky, M. & Rivera, S. (2003) Neuronal activity-dependent increase of net matrix metalloproteinase activity is associated with MMP-9 neurotoxicity after kainate. *Eur J Neurosci*, **18**, 1507-1517.

Jung, D., Yang, B., Meyer, J., Chamberlain, J.S. & Campbell, K.P. (1995) Identification and characterization of the dystrophin anchoring site on beta-dystroglycan. *J Biol Chem*, **270**, 27305-27310.

Kadener, S., Stoleru, D., McDonald, M., Nawathean, P. & Rosbash, M. (2007) Clockwork Orange is a transcriptional repressor and a new Drosophila circadian pacemaker component. *Genes Dev*, **21**, 1675-1686.

Kalman, M., Oszwald, E. & Adorjan, I. (2018) Appearance of beta-dystroglycan precedes the formation of glio-vascular end-feet in developing rat brain. *European journal of histochemistry : EJH*, **62**, 2908.

Kaur, J., Zhao, Z., Klein, G.M., Lo, E.H. & Buchan, A.M. (2004) The neurotoxicity of tissue plasminogen activator? *J Cereb Blood Flow Metab*, **24**, 945-963.

Kiessling, S., O'Callaghan, E.K., Freyburger, M., Cermakian, N. & Mongrain, V. (2017) The cell adhesion molecule EphA4 is involved in circadian clock functions. *Genes, brain, and behavior*.

Kim, Y.I. & Dudek, F.E. (1991) Intracellular electrophysiological study of suprachiasmatic nucleus neurons in rodents: excitatory synaptic mechanisms. *The Journal of physiology*, **444**, 269-287.

Kleiner, D.E. & Stetler-Stevenson, W.G. (1994) Quantitative zymography: detection of picogram quantities of gelatinases. *Analytical biochemistry*, **218**, 325-329.

Knapska, E., Lioudyno, V., Kiryk, A., Mikosz, M., Gorkiewicz, T., Michaluk, P., Gawlak, M., Chaturvedi, M., Mochol, G., Balcerzyk, M., Wojcik, D.K., Wilczynski, G.M. & Kaczmarek, L. (2013) Reward learning requires activity of matrix metalloproteinase-9 in the central amygdala. *J Neurosci*, **33**, 14591-14600.

Ko, C.H. & Takahashi, J.S. (2006) Molecular components of the mammalian circadian clock. *Hum Mol Genet*, **15 Spec No 2**, R271-277.

Ko, G.Y.P., Shi, L. & Ko, M.L. (2009) Circadian regulation of ion channels and their functions. *J Neurochem*, **110**, 1150.

Kochlamazashvili, G., Bukalo, O., Senkov, O., Salmen, B., Gerardy-Schahn, R., Engel, A.K., Schachner, M. & Dityatev, A. (2012) Restoration of synaptic plasticity and learning in young and aged NCAM-deficient mice by enhancing neurotransmission mediated by GluN2A-containing NMDA receptors. *J Neurosci*, **32**, 2263-2275.

Kon, N., Yoshikawa, T., Honma, S., Yamagata, Y., Yoshitane, H., Shimizu, K., Sugiyama, Y., Hara, C., Kameshita, I., Honma, K. & Fukada, Y. (2014) CaMKII is essential for the cellular clock and coupling between morning and evening behavioral rhythms. *Genes Dev*, **28**, 1101-1110.

Kondratov, R.V. & Antoch, M.P. (2007) Circadian proteins in the regulation of cell cycle and genotoxic stress responses. *Trends Cell Biol*, **17**, 311-317.

Konnecke, H. & Bechmann, I. (2013) The role of microglia and matrix metalloproteinases involvement in neuroinflammation and gliomas. *Clinical & developmental immunology*, **2013**, 914104.

Konopacki, F.A., Rylski, M., Wilczek, E., Amborska, R., Detka, D., Kaczmarek, L. & Wilczynski, G.M. (2007) Synaptic localization of seizure-induced matrix metalloproteinase-9 mRNA. *Neuroscience*, **150**, 31-39.

Kowiański, P., Lietzau, G., Czuba, E., Waśkow, M., Steliga, A. & Moryś, J. (2018) BDNF: A Key Factor with Multipotent Impact on Brain Signaling and Synaptic Plasticity *Cell Mol Neurobiol*, pp. 579-593.

Kridel, S.J., Chen, E., Kotra, L.P., Howard, E.W., Mobashery, S. & Smith, J.W. (2001) Substrate hydrolysis by matrix metalloproteinase-9. *J Biol Chem*, **276**, 20572-20578.

Krizo, J.A., Moreland, L.E., Rastogi, A., Mou, X., Prosser, R.A. & Mintz, E.M. (2018) Regulation of Locomotor activity in fed, fasted, and food-restricted mice lacking tissue-type plasminogen activator *BMC Physiol*.

Kudo, T., Block, G.D. & Colwell, C.S. (2015) The Circadian Clock Gene Period1 Connects the Molecular Clock to Neural Activity in the Suprachiasmatic Nucleus. *ASN Neuro*, **7**.

Kupai, K., Szucs, G., Cseh, S., Hajdu, I., Csonka, C., Csont, T. & Ferdinandy, P. (2010) Matrix metalloproteinase activity assays: Importance of zymography. *Journal of pharmacological and toxicological methods*, **61**, 205-209.

Lall, G.S., Atkinson, L.A., Corlett, S.A., Broadbridge, P.J. & Bonsall, D.R. (2012) Circadian entrainment and its role in depression: a mechanistic review. *J Neural Transm (Vienna)*, **119**, 1085-1096.

Lananna, B.V., Nadarajah, C.J., Izumo, M., Cedeno, M.R., Xiong, D.D., Dimitry, J., Tso, C.F., McKee, C.A., Griffin, P., Sheehan, P.W., Haspel, J.A., Barres, B.A., Liddelow, S.A., Takahashi, J.S., Karatsoreos, I.N. & Musiek, E.S. (2018) Cell-Autonomous Regulation of Astrocyte Activation by the Circadian Clock Protein BMAL1. *Cell Rep*, **25**, 1-9.e5.

Lassek, M., Weingarten, J. & Volknandt, W. (2015) The synaptic proteome. *Cell and tissue research*, **359**, 255-265.

Lau, D., Bengtson, C.P., Buchthal, B. & Bading, H. (2015) BDNF Reduces Toxic Extrasynaptic NMDA Receptor Signaling via Synaptic NMDA Receptors and Nuclear-Calcium-Induced Transcription of inhba/Activin A. *Cell Rep*, **12**, 1353-1366.

Lauzier, M.C., Robitaille, G.A., Chan, D.A., Giaccia, A.J. & Richard, D.E. (2008) (2R)-[(4-Biphenylylsulfonyl)amino]-N-hydroxy-3-phenylpropionamide (BiPS), a Matrix Metalloprotease Inhibitor, Is a Novel and Potent Activator of Hypoxia-Inducible Factors. *Molecular pharmacology*, **74**, 282-288.

Lavialle, M. & Serviere, J. (1993) Circadian fluctuations in GFAP distribution in the Syrian hamster suprachiasmatic nucleus. *Neuroreport*, **4**, 1243-1246.

Lee, J.E., Atkins, N., Jr., Hatcher, N.G., Zamdborg, L., Gillette, M.U., Sweedler, J.V. & Kelleher, N.L. (2010) Endogenous peptide discovery of the rat circadian clock: a focused study of the suprachiasmatic nucleus by ultrahigh performance tandem mass spectrometry. *Mol Cell Proteomics*, **9**, 285-297.

Lee, W., Watanabe, M. & Glass, J.D. (1995) Photoperiod affects the expression of neural cell adhesion molecule and polysialic acid in the hypothalamus of the Siberian hamster. *Brain research*, **690**, 64-72.

LeGates, T.A., Altimus, C.M., Wang, H., Lee, H.K., Yang, S., Zhao, H., Kirkwood, A., Weber, E.T. & Hattar, S. (2012) Aberrant light directly impairs mood and learning through melanopsin-expressing neurons. *Nature*, **491**, 594-598.

Legler, D.F., Wiedle, G., Ross, F.P. & Imhof, B.A. (2001) Superactivation of integrin alphavbeta3 by low antagonist concentrations. *Journal of cell science*, **114**, 1545-1553.

Lehman, M.N., LeSauter, J., Kim, C., Berriman, S.J., Tresco, P.A. & Silver, R. (1995) How do fetal grafts of the suprachiasmatic nucleus communicate with the host brain? *Cell Transplant*, **4**, 75-81.

Leone, M.J., Marpegan, L., Bekinschtein, T.A., Costas, M.A. & Golombek, D.A. (2006) Suprachiasmatic astrocytes as an interface for immune-circadian signalling. *J Neurosci Res*, **84**, 1521-1527.

Li, S., Banerjee, J., Jang, C., Sehgal, A., Stone, R.A. & Civan, M.M. (2015) Temperature Oscillations Drive Cycles in the Activity of MMP-2,9 Secreted by a Human Trabecular Meshwork Cell Line *Invest Ophthalmol Vis Sci*, pp. 1396-1405.

Li, Y., Partridge, J., Berger, C., Sepulveda-Rodriguez, A., Vicini, S. & Conant, K. (2016) Dopamine increases NMDA-stimulated calcium flux in striatopallidal neurons through a matrix metalloproteinase-dependent mechanism. *Eur J Neurosci*, **43**, 194-203.

Li, Y.X., Zhang, Y., Lester, H.A., Schuman, E.M. & Davidson, N. (1998) Enhancement of neurotransmitter release induced by brain-derived neurotrophic factor in cultured hippocampal neurons. *J Neurosci*, **18**, 10231-10240.

Liang, F.Q., Allen, G. & Earnest, D. (2000) Role of brain-derived neurotrophic factor in the circadian regulation of the suprachiasmatic pacemaker by light. *J Neurosci*, **20**, 2978-2987.

Liang, F.Q., Walline, R. & Earnest, D.J. (1998) Circadian rhythm of brain-derived neurotrophic factor in the rat suprachiasmatic nucleus. *Neurosci Lett*, **242**, 89-92.

Lin, B., Arai, A.C., Lynch, G. & Gall, C.M. (2003) Integrins regulate NMDA receptor-mediated synaptic currents. *J Neurophysiol*, **89**, 2874-2878.

Lindsay, J.H., Glass, J.D., Amicarelli, M. & Prosser, R.A. (2014) The Mammalian circadian clock in the suprachiasmatic nucleus exhibits rapid tolerance to ethanol in vivo and in vitro. *Alcoholism, clinical and experimental research*, **38**, 760-769.

Ling, H.H., Beaule, C., Chiang, C.K., Tian, R., Figeys, D. & Cheng, H.Y. (2014) Time-of-day- and light-dependent expression of ubiquitin protein ligase E3 component N-recognin 4 (UBR4) in the suprachiasmatic nucleus circadian clock. *PLoS One*, **9**, e103103.

Liu, C. & Reppert, S.M. (2000) GABA synchronizes clock cells within the suprachiasmatic circadian clock. *Neuron*, **25**, 123-128.

Longair, M.H., Baker, D.A. & Armstrong, J.D. (2011) Simple Neurite Tracer: open source software for reconstruction, visualization and analysis of neuronal processes. *Bioinformatics (Oxford, England)*, **27**, 2453-2454.

Lu, B. (2003) BDNF and activity-dependent synaptic modulation. *Learn Mem*, **10**, 86-98.

Lucassen, E.A., Coomans, C.P., van Putten, M., de Kreij, S.R., van Genugten, J.H., Sutorius, R.P., de Rooij, K.E., van der Velde, M., Verhoeve, S.L., Smit, J.W., Lowik, C.W., Smits, H.H., Guigas, B., Aartsma-Rus, A.M. & Meijer, J.H. (2016) Environmental 24-hr Cycles Are Essential for Health. *Current biology : CB*, **26**, 1843-1853.

Lundkvist, G.B., Kristensson, K. & Hill, R.H. (2002) The suprachiasmatic nucleus exhibits diurnal variations in spontaneous excitatory postsynaptic activity. *Journal of biological rhythms*, **17**, 40-51.

Maeda, A. & Sobel, R.A. (1996) Matrix metalloproteinases in the normal human central nervous system, microglial nodules, and multiple sclerosis lesions. *Journal of neuropathology and experimental neurology*, **55**, 300-309.

Maemura, K., de la Monte, S.M., Chin, M.T., Layne, M.D., Hsieh, C.M., Yet, S.F., Perrella, M.A. & Lee, M.E. (2000) CLIF, a novel cycle-like factor, regulates the circadian oscillation of plasminogen activator inhibitor-1 gene expression. *J Biol Chem*, **275**, 36847-36851.

Maemura, K., Takeda, N. & Nagai, R. (2007) Circadian rhythms in the CNS and peripheral clock disorders: role of the biological clock in cardiovascular diseases. *J Pharmacol Sci*, **103**, 134-138.

Malemud, C.J. (2006) Matrix metalloproteinases (MMPs) in health and disease: an overview. *Front Biosci*, **11**, 1696-1701.

Maolood, N., Hardin-Pouzet, H. & Grange-Messent, V. (2008) Matrix metalloproteinases MMP2 and MMP9 are upregulated by noradrenaline in the mouse neuroendocrine hypothalamus. *Eur J Neurosci*, **27**, 1143-1152.

Marcoli, M., Agnati, L.F., Benedetti, F., Genedani, S., Guidolin, D., Ferraro, L., Maura, G. & Fuxe, K. (2015) On the role of the extracellular space on the holistic behavior of the brain. *Rev Neurosci*, **26**, 489-506.

Marpegan, L., Swanstrom, A.E., Chung, K., Simon, T., Haydon, P.G., Khan, S.K., Liu, A.C., Herzog, E.D. & Beaule, C. (2011) Circadian regulation of ATP release in astrocytes. *J Neurosci*, **31**, 8342-8350.

Mattson, M.P., Lovell, M.A., Furukawa, K. & Markesbery, W.R. (1995) Neurotrophic factors attenuate glutamate-induced accumulation of peroxides, elevation of intracellular Ca2+ concentration, and neurotoxicity and increase antioxidant enzyme activities in hippocampal neurons. *J Neurochem*, **65**, 1740-1751.

Mayford, M., Wang, J., Kandel, E.R. & O'Dell, T.J. (1995) CaMKII regulates the frequency-response function of hippocampal synapses for the production of both LTD and LTP. *Cell*, **81**, 891-904.

Maywood, E.S., Drynan, L., Chesham, J.E., Edwards, M.D., Dardente, H., Fustin, J.M., Hazlerigg, D.G., O'Neill, J.S., Codner, G.F., Smyllie, N.J., Brancaccio, M. & Hastings, M.H. (2013) Analysis of core circadian feedback loop in suprachiasmatic nucleus of mCry1-luc transgenic reporter mouse. *Proc Natl Acad Sci U S A*, **110**, 9547-9552.

Maywood, E.S., Reddy, A.B., Wong, G.K., O'Neill, J.S., O'Brien, J.A., McMahon, D.G., Harmar, A.J., Okamura, H. & Hastings, M.H. (2006) Synchronization and maintenance of timekeeping in suprachiasmatic circadian clock cells by neuropeptidergic signaling. *Current biology : CB*, **16**, 599-605.

Mazuski, C., Abel, J.H., Chen, S.P., Hermanstyne, T.O., Jones, J.R., Simon, T., Doyle, F.J. & Herzog, E.D. (2018) Entrainment of Circadian Rhythms Depends on Firing Rates and Neuropeptide Release of VIP SCN Neurons. *Neuron*, **99**, 555-563.e555.

McIlwain, S., Tamura, K., Kertesz-Farkas, A., Grant, C.E., Diament, B., Frewen, B., Howbert, J.J., Hoopmann, M.R., Kall, L., Eng, J.K., MacCoss, M.J. & Noble, W.S. (2014) Crux: rapid open source protein tandem mass spectrometry analysis. *Journal of proteome research*, **13**, 4488-4491.

McNeill, J.K.t., Walton, J.C. & Albers, H.E. (2018) Functional Significance of the Excitatory Effects of GABA in the Suprachiasmatic Nucleus. *Journal of biological rhythms*, **33**, 376-387.

Meighan, P.C., Meighan, S.E., Davis, C.J., Wright, J.W. & Harding, J.W. (2007) Effects of matrix metalloproteinase inhibition on short- and long-term plasticity of schaffer collateral/CA1 synapses. *J Neurochem*, **102**, 2085-2096.

Meijer, J.H. & Schwartz, W.J. (2003) In search of the pathways for light-induced pacemaker resetting in the suprachiasmatic nucleus. *Journal of biological rhythms*, **18**, 235-249.

Meijer, J.H., Watanabe, K., Schaap, J., Albus, H. & Détári, L. (1998) Light responsiveness of the suprachiasmatic nucleus: long-term multiunit and single-unit recordings in freely moving rats. *J Neurosci*, **18**, 9078-9087.

Meyer-Bernstein, E.L., Jetton, A.E., Matsumoto, S.I., Markuns, J.F., Lehman, M.N. & Bittman, E.L. (1999) Effects of suprachiasmatic transplants on circadian rhythms of neuroendocrine function in golden hamsters. *Endocrinology*, **140**, 207-218.

Michaluk, P., Kolodziej, L., Mioduszewska, B., Wilczynski, G.M., Dzwonek, J., Jaworski, J., Gorecki, D.C., Ottersen, O.P. & Kaczmarek, L. (2007) Beta-dystroglycan as a target for MMP-9, in response to enhanced neuronal activity. *J Biol Chem*, **282**, 16036-16041.

Michaluk, P., Mikasova, L., Groc, L., Frischknecht, R., Choquet, D. & Kaczmarek, L. (2009) Matrix metalloproteinase-9 controls NMDA receptor surface diffusion through integrin beta1 signaling. *J Neurosci*, **29**, 6007-6012.

Michaluk, P., Wawrzyniak, M., Alot, P., Szczot, M., Wyrembek, P., Mercik, K., Medvedev, N., Wilczek, E., De Roo, M., Zuschratter, W., Muller, D., Wilczynski, G.M., Mozrzymas, J.W., Stewart, M.G., Kaczmarek, L. & Wlodarczyk, J. (2011) Influence of matrix metalloproteinase MMP-9 on dendritic spine morphology. *Journal of cell science*, **124**, 3369-3380.

Michel, S., Clark, J.P., Ding, J.M. & Colwell, C.S. (2006) Brain-derived neurotrophic factor and neurotrophin receptors modulate glutamate-induced phase shifts of the suprachiasmatic nucleus. *Eur J Neurosci*, **24**, 1109-1116.

Michele, D.E., Barresi, R., Kanagawa, M., Saito, F., Cohn, R.D., Satz, J.S., Dollar, J., Nishino, I., Kelley, R.I., Somer, H., Straub, V., Mathews, K.D., Moore, S.A. & Campbell, K.P. (2002) Post-translational disruption of dystroglycan-ligand interactions in congenital muscular dystrophies. *Nature*, **418**, 417-422.

Mieda, M. (2019) The Network Mechanism of the Central Circadian Pacemaker of the SCN: Do AVP Neurons Play a More Critical Role Than Expected? *Front Neurosci*, **13**.

Miller, C.M., Page-McCaw, A. & Broihier, H.T. (2008) Matrix metalloproteinases promote motor axon fasciculation in the Drosophila embryo. *Development (Cambridge, England)*, **135**, 95-109.

Miller, S.G. & Kennedy, M.B. (1986) Regulation of brain type II Ca2+/calmodulin-dependent protein kinase by autophosphorylation: a Ca2+-triggered molecular switch. *Cell*, **44**, 861-870.

Milner, R., Hung, S., Wang, X., Spatz, M. & Zoppo, G. (2008) The rapid decrease in astrocyte-associated dystroglycan expression by focal cerebral ischemia is protease-dependent. *J Cereb Blood Flow Metab*, **28**, 812-823.

Minana, R., Sancho-Tello, M., Climent, E., Segui, J.M., Renau-Piqueras, J. & Guerri, C. (1998) Intracellular location, temporal expression, and polysialylation of neural cell adhesion molecule in astrocytes in primary culture. *Glia*, **24**, 415-427.

Mintz, E.M. & Albers, H.E. (1997) Microinjection of NMDA into the SCN region mimics the phase shifting effect of light in hamsters. *Brain research*, **758**, 245-249.

Mintz, E.M., Marvel, C.L., Gillespie, C.F., Price, K.M. & Albers, H.E. (1999) Activation of NMDA receptors in the suprachiasmatic nucleus produces light-like phase shifts of the circadian clock in vivo. *J Neurosci*, **19**, 5124-5130.

Miranti, C.K. & Brugge, J.S. (2002) Sensing the environment: a historical perspective on integrin signal transduction. *Nat Cell Biol*, **4**, E83-90.

Mistlberger, R.E. (1994) Circadian food-anticipatory activity: formal models and physiological mechanisms. *Neurosci Biobehav Rev*, **18**, 171-195.

Mizoguchi, H., Nakade, J., Tachibana, M., Ibi, D., Someya, E., Koike, H., Kamei, H., Nabeshima, T., Itohara, S., Takuma, K., Sawada, M., Sato, J. & Yamada, K. (2011) Matrix metalloproteinase-9 contributes to kindled seizure development in pentylenetetrazole-treated mice by converting pro-BDNF to mature BDNF in the hippocampus. *J Neurosci*, **31**, 12963-12971.

Moga, M.M. & Moore, R.Y. (1996) Putative excitatory amino acid projections to the suprachiasmatic nucleus in the rat. *Brain research*, **743**, 171-177.

Moga, M.M. & Moore, R.Y. (1997) Organization of neural inputs to the suprachiasmatic nucleus in the rat. *The Journal of comparative neurology*, **389**, 508-534.

Mogford, J.E., Davis, G.E. & Meininger, G.A. (1997) RGDN peptide interaction with endothelial alpha5beta1 integrin causes sustained endothelin-dependent vasoconstriction of rat skeletal muscle arterioles. *J Clin Invest*, **100**, 1647-1653.

Moldavan, M., Cravetchi, O. & Allen, C.N. (2017) GABA transporters regulate tonic and synaptic GABAA receptor-mediated currents in the suprachiasmatic nucleus neurons. *J Neurophysiol*, **118**, 3092-3106.

Moller, M., Lund-Andersen, C., Rovsing, L., Sparre, T., Bache, N., Roepstorff, P. & Vorum, H. (2010) Proteomics of the photoneuroendocrine circadian system of the brain. *Mass Spectrom Rev*, **29**, 313-325.

Moller, M., Sparre, T., Bache, N., Roepstorff, P. & Vorum, H. (2007) Proteomic analysis of day-night variations in protein levels in the rat pineal gland. *Proteomics*, **7**, 2009-2018.

Monavarfeshani, A., Knill, C.N., Sabbagh, U., Su, J. & Fox, M.A. (2017) Region- and Cell-Specific Expression of Transmembrane Collagens in Mouse Brain. *Front Integr Neurosci*, **11**, 20.

Montes de Oca Balderas, P. (2018) Flux-Independent NMDAR Signaling: Molecular Mediators, Cellular Functions, and Complexities. *International journal of molecular sciences*, **19**.

Mook, O.R., Van Overbeek, C., Ackema, E.G., Van Maldegem, F. & Frederiks, W.M. (2003) In situ localization of gelatinolytic activity in the extracellular matrix of metastases of colon cancer in rat liver using quenched fluorogenic DQ-gelatin. *The journal of histochemistry and cytochemistry : official journal of the Histochemistry Society*, **51**, 821-829.

Moore, R.Y. (1995) Organization of the mammalian circadian system. *Ciba Foundation symposium*, **183**, 88-99; discussion 100-106.

Moore, R.Y. (2007) Suprachiasmatic nucleus in sleep-wake regulation. *Sleep medicine*, **8 Suppl 3**, 27-33.

Moore, R.Y. & Eichler, V.B. (1972) Loss of a circadian adrenal corticosterone rhythm following suprachiasmatic lesions in the rat. *Brain research*, **42**, 201-206.

Moore, R.Y. & Klein, D.C. (1974) Visual pathways and the central neural control of a circadian rhythm in pineal serotonin N-acetyltransferase activity. *Brain research*, **71**, 17-33.

Moore, R.Y. & Lenn, N.J. (1972) A retinohypothalamic projection in the rat. *The Journal of comparative neurology*, **146**, 1-14.

Moore, R.Y. & Speh, J.C. (1993) GABA is the principal neurotransmitter of the circadian system. *Neurosci Lett*, **150**, 112-116.

Morgenthaler, T.I., Kapur, V.K., Brown, T., Swick, T.J., Alessi, C., Aurora, R.N., Boehlecke, B., Chesson, A.L., Friedman, L., Maganti, R., Owens, J., Pancer, J., Zak, R. & Medicine, S.o.P.C.o.t.A.A.o.S. (2007) Practice parameters for the treatment of narcolepsy and other hypersomnias of central origin. *Sleep*, **30**, 1705-1711.

Morin, L.P., Blanchard, J. & Moore, R.Y. (1992) Intergeniculate leaflet and suprachiasmatic nucleus organization and connections in the golden hamster. *Vis Neurosci*, **8**, 219-230.

Morin, L.P., Blanchard, J.H. & Provencio, I. (2003) Retinal ganglion cell projections to the hamster suprachiasmatic nucleus, intergeniculate leaflet, and visual midbrain: bifurcation and melanopsin immunoreactivity. *The Journal of comparative neurology*, **465**, 401-416.

Morin, L.P. & Cummings, L.A. (1981) EFFECT OF SURGICAL OR PHOTOPERIODIC CASTRATION, TESTOSTERONE REPLACEMENT OR PINEALECTOMY ON MALE HAMSTER RUNNING RHYTHMICITY. *Physiology & behavior*, **26**, 825-838.

Morin, L.P., Goodless-Sanchez, N., Smale, L. & Moore, R.Y. (1994) Projections of the suprachiasmatic nuclei, subparaventricular zone and retrochiasmatic area in the golden hamster. *Neuroscience*, **61**, 391-410.

Morin, L.P., Johnson, R.F. & Moore, R.Y. (1989) Two brain nuclei controlling circadian rhythms are identified by GFAP immunoreactivity in hamsters and rats. *Neurosci Lett*, **99**, 55-60.

Moriya, T., Yoshinobu, Y., Kouzu, Y., Katoh, A., Gomi, H., Ikeda, M., Yoshioka, T., Itohara, S. & Shibata, S. (2000) Involvement of glial fibrillary acidic protein (GFAP) expressed in astroglial cells in circadian rhythm under constant lighting conditions in mice. *J Neurosci Res*, **60**, 212-218.

Mott, J.D. & Werb, Z. (2004) Regulation of matrix biology by matrix metalloproteinases. *Curr Opin Cell Biol*, **16**, 558-564.

Mou, X., Peterson, C.B. & Prosser, R.A. (2009) Tissue-type plasminogen activator-plasmin-BDNF modulate glutamate-induced phase-shifts of the mouse suprachiasmatic circadian clock in vitro. *Eur J Neurosci*, **30**, 1451-1460.

Mrosovsky, N. (1996) Locomotor activity and non-photic influences on circadian clocks. *Biol. Rev. Cambridge Philosophic. Soc.*, **71**, 343-372.

Murai, K.K. & Pasquale, E.B. (2011) Eph receptors and ephrins in neuron-astrocyte communication at synapses. *Glia*, **59**, 1567-1578.

Muraro, N.I., Pirez, N. & Ceriani, M.F. (2013) The circadian system: plasticity at many levels. *Neuroscience*, **247**, 280-293.

Murase, S., Lantz, C.L., Kim, E., Gupta, N., Higgins, R., Stopfer, M., Hoffman, D.A. & Quinlan, E.M. (2016) Matrix Metalloproteinase-9 Regulates Neuronal Circuit Development and Excitability. *Molecular Neurobiology*, **53**, 3477-3493.

Naba, A., Pearce, O.M.T., Del Rosario, A., Ma, D., Ding, H., Rajeeve, V., Cutillas, P.R., Balkwill, F.R. & Hynes, R.O. (2017) Characterization of the Extracellular Matrix of Normal and Diseased Tissues Using Proteomics. *Journal of proteome research*, **16**, 3083-3091.

Nagase, H., Visse, R. & Murphy, G. (2006) Structure and function of matrix metalloproteinases and TIMPs. *Cardiovasc Res*, **69**, 562-573.

Nagoshi, E., Sugino, K., Kula, E., Okazaki, E., Tachibana, T., Nelson, S. & Rosbash, M. (2010) Dissecting differential gene expression within the circadian neuronal circuit of Drosophila. *Nat Neurosci*, **13**, 60-68.

Nagy, V., Bozdagi, O., Matynia, A., Balcerzyk, M., Okulski, P., Dzwonek, J., Costa, R.M., Silva, A.J., Kaczmarek, L. & Huntley, G.W. (2006) Matrix Metalloproteinase-9 Is Required for Hippocampal Late-Phase Long-Term Potentiation and Memory.

Nahm, S.S., Farnell, Y.Z., Griffith, W. & Earnest, D.J. (2005) Circadian regulation and function of voltage-dependent calcium channels in the suprachiasmatic nucleus. *J Neurosci*, **25**, 9304-9308.

Nakazato, R., Kawabe, K., Yamada, D., Ikeno, S., Mieda, M., Shimba, S., Hinoi, E., Yoneda, Y. & Takarada, T. (2017) Disruption of Bmal1 Impairs Blood-Brain Barrier Integrity via Pericyte Dysfunction. *J Neurosci*, **37**, 10052-10062.

Niculescu, D., Michaelsen-Preusse, K., Guner, U., van Dorland, R., Wierenga, C.J. & Lohmann, C. (2018) A BDNF-Mediated Push-Pull Plasticity Mechanism for Synaptic Clustering. *Cell Rep*, **24**, 2063-2074.

Ning, L., Paetau, S., Nyman-Huttunen, H., Tian, L. & Gahmberg, C.G. (2015) ICAM-5 affects spine maturation by regulation of NMDA receptor binding to alpha-actinin. *Biol Open*, **4**, 125-136.

Nishijima, T., Kawakami, M. & Kita, I. (2015) A bout of treadmill exercise increases matrix metalloproteinase-9 activity in the rat hippocampus. *Neurosci Lett*, **594**, 144-149.

Noell, S., Wolburg-Buchholz, K., Mack, A.F., Beedle, A.M., Satz, J.S., Campbell, K.P., Wolburg, H. & Fallier-Becker, P. (2011) Evidence for a role of dystroglycan regulating the membrane architecture of astroglial endfeet. *Eur J Neurosci*, **33**, 2179-2186.

Nomura, K., Takeuchi, Y., Yamaguchi, S., Okamura, H. & Fukunaga, K. (2003) Involvement of calcium/calmodulin-dependent protein kinase II in the induction of mPer1. *J Neurosci Res*, **72**, 384-392.

Nomura, T., Yabe, T., Rosenthal, E.S., Krzan, M. & Schwartz, J.P. (2000) PSA-NCAM distinguishes reactive astrocytes in 6-OHDA-lesioned substantia nigra from those in the striatal terminal fields. *J Neurosci Res*, **61**, 588-596.

Notter, T., Panzanelli, P., Pfister, S., Mircsof, D. & Fritschy, J.M. (2014) A protocol for concurrent high-quality immunohistochemical and biochemical analyses in adult mouse central nervous system. *Eur J Neurosci*, **39**, 165-175.

Novak, C.M., Ehlen, J.C. & Albers, H.E. (2008) Photic and nonphotic inputs to the diurnal circadian clock. *Biol. Rhythm Res.*, **39**, 291-304.

O'Callaghan, E.K., Ballester Roig, M.N. & Mongrain, V. (2017) Cell adhesion molecules and sleep. *Neuroscience research*, **116**, 29-38.

O'Connell, J.P., Willenbrock, F., Docherty, A.J., Eaton, D. & Murphy, G. (1994) Analysis of the role of the COOH-terminal domain in the activation, proteolytic activity, and tissue inhibitor of metalloproteinase interactions of gelatinase B. *J Biol Chem*, **269**, 14967-14973.

Obayashi, K., Saeki, K. & Kurumatani, N. (2018) Bedroom Light Exposure at Night and the Incidence of Depressive Symptoms: A Longitudinal Study of the HEIJO-KYO Cohort. *Am J Epidemiol*, **187**, 427-434.

Ogata, Y., Enghild, J.J. & Nagase, H. (1992) Matrix metalloproteinase 3 (stromelysin) activates the precursor for the human matrix metalloproteinase 9. *J Biol Chem*, **267**, 3581-3584.

Ogier, C., Bernard, A., Chollet, A.M., T, L.E.D., Hanessian, S., Charton, G., Khrestchatisky, M. & Rivera, S. (2006) Matrix metalloproteinase-2 (MMP-2) regulates astrocyte motility in connection with the actin cytoskeleton and integrins. *Glia*, **54**, 272-284.

Oh, L.Y., Larsen, P.H., Krekoski, C.A., Edwards, D.R., Donovan, F., Werb, Z. & Yong, V.W. (1999) Matrix metalloproteinase-9/gelatinase B is required for process outgrowth by oligodendrocytes. *J Neurosci*, **19**, 8464-8475.

Ohkura, N., Oishi, K., Fukushima, N., Kasamatsu, M., Atsumi, G.I., Ishida, N., Horie, S. & Matsuda, J. (2006) Circadian clock molecules CLOCK and CRYs modulate fibrinolytic activity by regulating the PAI-1 gene expression. *J Thromb Haemost*, **4**, 2478-2485.

Okulski, P., Jay, T.M., Jaworski, J., Duniec, K., Dzwonek, J., Konopacki, F.A., Wilczynski, G.M., Sanchez-Capelo, A., Mallet, J. & Kaczmarek, L. (2007) TIMP-1 abolishes MMP-9-dependent long-lasting long-term potentiation in the prefrontal cortex. *Biological psychiatry*, **62**, 359-362.

Oliet, S.H., Piet, R., Poulain, D.A. & Theodosis, D.T. (2004) Glial modulation of synaptic transmission: Insights from the supraoptic nucleus of the hypothalamus. *Glia*, **47**, 258-267.

Ono, D., Honma, K.I., Yanagawa, Y., Yamanaka, A. & Honma, S. (2018) Role of GABA in the regulation of the central circadian clock of the suprachiasmatic nucleus. *J Physiol Sci*, **68**, 333-343.

Ono, D., Honma, K.I., Yanagawa, Y., Yamanaka, A. & Honma, S. (2019) GABA in the suprachiasmatic nucleus refines circadian output rhythms in mice. *Commun Biol*, **2**, 232.

Ould-yahoui, A., Tremblay, E., Sbai, O., Ferhat, L., Bernard, A., Charrat, E., Gueye, Y., Lim, N.H., Brew, K., Risso, J.J., Dive, V., Khrestchatisky, M. & Rivera, S. (2009) A new role for TIMP-1 in modulating neurite outgrowth and morphology of cortical neurons. *PLoS One*, **4**, e8289.

Panda, S., Antoch, M.P., Miller, B.H., Su, A.I., Schook, A.B., Straume, M., Schultz, P.G., Kay, S.A., Takahashi, J.S. & Hogenesch, J.B. (2002) Coordinated transcription of key pathways in the mouse by the circadian clock. *Cell*, **109**, 307-320.

Pang, P.T. & Lu, B. (2004) Regulation of late-phase LTP and long-term memory in normal and aging hippocampus: role of secreted proteins tPA and BDNF. *Ageing Res Rev*, **3**, 407-430.

Pang, P.T., Teng, H.K., Zaitsev, E., Woo, N.T., Sakata, K., Zhen, S., Teng, K.K., Yung, W.H., Hempstead, B.L. & Lu, B. (2004) Cleavage of proBDNF by tPA/plasmin is essential for long-term hippocampal plasticity. *Science*, **306**, 487-491.

Paoletti, P. (2011) Molecular basis of NMDA receptor functional diversity. *Eur J Neurosci*, **33**, 1351-1365.

Peixoto, R.T., Kunz, P.A., Kwon, H., Mabb, A.M., Sabatini, B.L., Philpot, B.D. & Ehlers, M.D. (2012) Transsynaptic signaling by activity-dependent cleavage of neuroligin-1. *Neuron*, **76**, 396-409.

Peng, H., Shah, W., Holland, P. & Carbonetto, S. (2008) Integrins and dystroglycan regulate astrocyte wound healing: the integrin beta1 subunit is necessary for process extension and orienting the microtubular network. *Dev Neurobiol*, **68**, 559-574.

Pennartz, C.M., De Jeu, M.T., Geurtsen, A.M., Sluiter, A.A. & Hermes, M.L. (1998) Electrophysiological and morphological heterogeneity of neurons in slices of rat suprachiasmatic nucleus. *The Journal of physiology*, **506 (Pt 3)**, 775-793.

Petitclerc, E., Stromblad, S., von Schalscha, T.L., Mitjans, F., Piulats, J., Montgomery, A.M., Cheresh, D.A. & Brooks, P.C. (1999) Integrin alpha(v)beta3 promotes M21 melanoma growth in human skin by regulating tumor cell survival. *Cancer Res*, **59**, 2724-2730.

Pickard, A., Chang, J., Alachkar, N., Calverley, B., Garva, R., Arvan, P., Meng, Q.J. & Kadler, K.E. (2019) Preservation of circadian rhythms by the protein folding chaperone, BiP. *Faseb j*, **33**, 7479-7489.

Pickard, G.E. (1985) Bifurcating axons of retinal ganglion cells terminate in the hypothalamic suprachiasmatic nucleus and the intergeniculate leaflet of the thalamus. *Neurosci Lett*, **55**, 211-217.

Pirttimaki, T.M. & Parri, H.R. (2013) Astrocyte plasticity: implications for synaptic and neuronal activity. *Neuroscientist*, **19**, 604-615.

Pizarro, A., Hayer, K., Lahens, N.F. & Hogenesch, J.B. (2013) CircaDB: a database of mammalian circadian gene expression profiles. *Nucleic Acids Res*, **41**, D1009-1013.

Preitner, N., Damiola, F., Lopez-Molina, L., Zakany, J., Duboule, D., Albrecht, U. & Schibler, U. (2002) The orphan nuclear receptor REV-ERBalpha controls circadian transcription within the positive limb of the mammalian circadian oscillator. *Cell*, **110**, 251-260.

Price, J.L., Dembinska, M.E., Young, M.W. & Rosbash, M. (1995) Suppression of PERIOD protein abundance and circadian cycling by the Drosophila clock mutation timeless. *The EMBO journal*, **14**, 4044-4049.

Prolo, L.M., Takahashi, J.S. & Herzog, E.D. (2005) Circadian rhythm generation and entrainment in astrocytes. *J Neurosci*, **25**, 404-408.

Prosser, R.A. (2001) Glutamate blocks serotonergic phase advances of the mammalian circadian pacemaker through AMPA and NMDA receptors. *J Neurosci*, **21**, 7815-7822.

Prosser, R.A., Dean, R.R., Edgar, D.M., Heller, H.C. & Miller, J.D. (1993) Serotonin and the mammalian circadian system: I. In vitro phase shifts by serotonergic agonists and antagonists. *Journal of biological rhythms*, **8**, 1-16.

Prosser, R.A., Edgar, D.M., Heller, H.C. & Miller, J.D. (1994) A possible glial role in the mammalian circadian clock. *Brain research*, **643**, 296-301.

Prosser, R.A. & Gillette, M.U. (1989) The mammalian circadian clock in the suprachiasmatic nuclei is reset in vitro by cAMP. *J Neurosci*, **9**, 1073-1081.

Prosser, R.A., Mangrum, C.A. & Glass, J.D. (2008) Acute ethanol modulates glutamatergic and serotonergic phase shifts of the mouse circadian clock in vitro. *Neuroscience*, **152**, 837-848.

Prosser, R.A., Rutishauser, U., Ungers, G., Fedorkova, L. & Glass, J.D. (2003) Intrinsic role of polysialylated neural cell adhesion molecule in photic phase resetting of the Mammalian circadian clock. *J Neurosci*, **23**, 652-658.

Puschmann, T.B. & Turnley, A.M. (2010) Eph receptor tyrosine kinases regulate astrocyte cytoskeletal rearrangement and focal adhesion formation. *J Neurochem*, **113**, 881-894.

Rajaratnam, S.M. & Arendt, J. (2001) Health in a 24-h society. *Lancet*, **358**, 999-1005.

Ramaswamy, P., Aditi Devi, N., Hurmath Fathima, K. & Dalavaikodihalli Nanjaiah, N. (2013) Activation of NMDA receptor of glutamate influences MMP-2 activity and proliferation of glioma cells. *Neurol Sci*.

Ramaswamy, P., Aditi Devi, N., Hurmath Fathima, K. & Dalavaikodihalli Nanjaiah, N. (2014) Activation of NMDA receptor of glutamate influences MMP-2 activity and proliferation of glioma cells. *Neurol Sci*, **35**, 823-829.

Rea, M.A. (1998) Photic entrainment of circadian rhythms in rodents. *Chronobiology international*, **15**, 395-423.

Rea, M.A., Buckley, B. & Lutton, L.M. (1993a) Local administration of EAA antagonists blocks light-induced phase shifts and c-fos expression in hamster SCN. *The American journal of physiology*, **265**, R1191-1198.

Rea, M.A., Ferriera, S., Randolph, W. & Glass, J.D. (1993b) Daily profile of the extracellular concentration of glutamate in the suprachiasmatic region of the Siberian hamster. *Proc Soc Exp Biol Med*, **204**, 104-109.

Reddy, A.B., Karp, N.A., Maywood, E.S., Sage, E.A., Deery, M., O'Neill, J.S., Wong, G.K., Chesham, J., Odell, M., Lilley, K.S., Kyriacou, C.P. & Hastings, M.H. (2006) Circadian orchestration of the hepatic proteome. *Current biology : CB*, **16**, 1107-1115.

Refinetti, R. & Menaker, M. (1992) The circadian rhythm of body temperature. *Physiology & behavior*, **51**, 613-637.

Reisberg, B., Borenstein, J., Salob, S.P., Ferris, S.H., Franssen, E. & Georgotas, A. (1987) BEHAVIORAL SYMPTOMS IN ALZHEIMERS-DISEASE - PHENOMENOLOGY AND TREATMENT. *J. Clin. Psychiatry*, **48**, 9-15.

Reiter, R.J. (1991) Pineal gland interface between the photoperiodic environment and the endocrine system. *Trends in endocrinology and metabolism: TEM*, **2**, 13-19.

Ren, Z., Chen, J. & Khalil, R.A. (2017) Zymography as a Research Tool in the Study of Matrix Metalloproteinase Inhibitors. *Methods in molecular biology (Clifton, N.J.)*, **1626**, 79-102.

Reppert, S.M. & Weaver, D.R. (2002) Coordination of circadian timing in mammals. *Nature*, **418**, 935-941.

Ristanovic, D., Milosevic, N.T. & Stulic, V. (2006) Application of modified Sholl analysis to neuronal dendritic arborization of the cat spinal cord. *J Neurosci Methods*, **158**, 212-218.

Rivera, S., Tremblay, E., Timsit, S., Canals, O., Ben-Ari, Y. & Khrestchatisky, M. (1997) Tissue inhibitor of metalloproteinases-1 (TIMP-1) is differentially induced in neurons and astrocytes after seizures: evidence for developmental, immediate early gene, and lesion response. *J Neurosci*, **17**, 4223-4235.

Rockway, T.W., Nienaber, V. & Giranda, V.L. (2002) Inhibitors of the protease domain of urokinase-type plasminogen activator. *Curr Pharm Des*, **8**, 2541-2558.

Rodriguez, D., Morrison, C.J. & Overall, C.M. (2010) Matrix metalloproteinases: what do they not do? New substrates and biological roles identified by murine models and proteomics. *Biochimica et biophysica acta*, **1803**, 39-54.

Romanic, A.M., White, R.F., Arleth, A.J., Ohlstein, E.H. & Barone, F.C. (1998) Matrix metalloproteinase expression increases after cerebral focal ischemia in rats: inhibition of matrix metalloproteinase-9 reduces infarct size. *Stroke*, **29**, 1020-1030.

Rudenko, G. (2019) Neurexins - versatile molecular platforms in the synaptic cleft. *Curr Opin Struct Biol*, **54**, 112-121.

Ruoslahti, E. (1996) RGD and other recognition sequences for integrins. *Annual review of cell and developmental biology*, **12**, 697-715.

Rusak, B. & Zucker, I. (1979) Neural regulation of circadian rhythms. *Physiol Rev*, **59**, 449-526.

Rusakov, D.A. & Kullmann, D.M. (1998) Geometric and viscous components of the tortuosity of the extracellular space in the brain. *Proc Natl Acad Sci U S A*, **95**, 8975-8980.

Ruscher, K., Shamloo, M., Rickhag, M., Ladunga, I., Soriano, L., Gisselsson, L., Toresson, H., Ruslim-Litrus, L., Oksenberg, D., Urfer, R., Johansson, B.B., Nikolich, K. & Wieloch, T. (2011) The sigma-1 receptor enhances brain plasticity and functional recovery after experimental stroke. *Brain : a journal of neurology*, **134**, 732-746.

Sack, R.L., Auckley, D., Auger, R.R., Carskadon, M.A., Wright, K.P., Vitiello, M.V., Zhdanova, I.V. & Medicine, A.A.o.S. (2007) Circadian rhythm sleep disorders: part II, advanced sleep phase disorder, delayed sleep phase disorder, free-running disorder, and irregular sleep-wake rhythm. An American Academy of Sleep Medicine review. *Sleep*, **30**, 1484-1501.

Safavi-Abbasi, S., Wolff, J.R. & Missler, M. (2001) Rapid morphological changes in astrocytes are accompanied by redistribution but not by quantitative changes of cytoskeletal proteins. *Glia*, **36**, 102-115.

Sampedro-Piquero, P., De Bartolo, P., Petrosini, L., Zancada-Menendez, C., Arias, J.L. & Begega, A. (2014) Astrocytic plasticity as a possible mediator of the cognitive improvements after environmental enrichment in aged rats. *Neurobiology of learning and memory*, **114**, 16-25.

Sánchez-Barceló, E.J., Mediavilla, M.D., Tan, D.X. & Reiter, R.J. (2010) Clinical uses of melatonin: evaluation of human trials. *Curr Med Chem*, **17**, 2070-2095.

Sangoram, A.M., Saez, L., Antoch, M.P., Gekakis, N., Staknis, D., Whiteley, A., Fruechte, E.M., Vitaterna, M.H., Shimomura, K., King, D.P., Young, M.W., Weitz, C.J. & Takahashi, J.S. (1998) Mammalian circadian autoregulatory loop: a timeless ortholog and mPer1 interact and negatively regulate CLOCK-BMAL1-induced transcription. *Neuron*, **21**, 1101-1113.

Sawaki, Y., Nihonmatsu, I. & Kawamura, H. (1984) Transplantation of the neonatal suprachiasmatic nuclei into rats with complete bilateral suprachiasmatic lesions. *Neuroscience research*, **1**, 67-72.

Sbardella, D., Inzitari, R., Iavarone, F., Gioia, M., Marini, S., Sciandra, F., Castagnola, M., Van den Steen, P.E., Opdenakker, G., Giardina, B., Brancaccio, A., Coletta, M. & Bozzi, M. (2012) Enzymatic processing by MMP-2 and MMP-9 of wild-type and mutated mouse beta-dystroglycan. *IUBMB life*, **64**, 988-994.

Scanziani, M., Malenka, R.C. & Nicoll, R.A. (1996) Role of intercellular interactions in heterosynaptic long-term depression. *Nature*, **380**, 446-450.

Schaap, J. & Meijer, J.H. (2001) Opposing effects of behavioural activity and light on neurons of the suprachiasmatic nucleus. *Eur J Neurosci*, **13**, 1955-1962.

Scheer, F.A., Hilton, M.F., Mantzoros, C.S. & Shea, S.A. (2009) Adverse metabolic and cardiovascular consequences of circadian misalignment. *Proc Natl Acad Sci U S A*, **106**, 4453-4458.

Schindelin, J., Arganda-Carreras, I., Frise, E., Kaynig, V., Longair, M., Pietzsch, T., Preibisch, S., Rueden, C., Saalfeld, S., Schmid, B., Tinevez, J.Y., White, D.J., Hartenstein, V., Eliceiri, K., Tomancak, P. & Cardona, A. (2012) Fiji: an open-source platform for biological-image analysis. *Nature methods*, **9**, 676-682.

Schulz, P. & Steimer, T. (2009) Neurobiology of circadian systems. *CNS drugs*, **23 Suppl 2**, 3-13.

Seidal, T., Balaton, A.J. & Battifora, H. (2001) Interpretation and quantification of immunostains. *Am J Surg Pathol*, **25**, 1204-1207.

Senga, Y., Ishida, A., Shigeri, Y., Kameshita, I. & Sueyoshi, N. (2015) The Phosphatase-Resistant Isoform of CaMKI, Ca(2)(+)/Calmodulin-Dependent Protein Kinase Idelta (CaMKIdelta), Remains in Its "Primed" Form without Ca(2)(+) Stimulation. *Biochemistry*, **54**, 3617-3630.

Sethi, M.K. & Zaia, J. (2017) Extracellular matrix proteomics in schizophrenia and Alzheimer's disease. *Anal Bioanal Chem*, **409**, 379-394.

Shafer, O.T., Rosbash, M. & Truman, J.W. (2002) Sequential nuclear accumulation of the clock proteins period and timeless in the pacemaker neurons of Drosophila melanogaster. *J Neurosci*, **22**, 5946-5954.

Shapiro-Reznik, M., Jilg, A., Lerner, H., Earnest, D.J. & Zisapel, N. (2012) Diurnal rhythms in neurexins transcripts and inhibitory/excitatory synapse scaffold proteins in the biological clock. *PLoS One*, **7**, e37894.

Shen, H., Glass, J.D., Seki, T. & Watanabe, M. (1999) Ultrastructural analysis of polysialylated neural cell adhesion molecule in the suprachiasmatic nuclei of the adult mouse. *The Anatomical record*, **256**, 448-457.

Shen, H., Watanabe, M., Tomasiewicz, H. & Glass, J.D. (2001) Genetic deletions of NCAM and PSA impair circadian function in the mouse. *Physiology & behavior*, **73**, 185-193.

Shen, H., Watanabe, M., Tomasiewicz, H., Rutishauser, U., Magnuson, T. & Glass, J.D. (1997) Role of neural cell adhesion molecule and polysialic acid in mouse circadian clock function. *J Neurosci*, **17**, 5221-5229.

Shen, K., Teruel, M.N., Subramanian, K. & Meyer, T. (1998) CaMKIIbeta functions as an F-actin targeting module that localizes CaMKIIalpha/beta heterooligomers to dendritic spines. *Neuron*, **21**, 593-606.

Shibata, S., Watanabe, A., Hamada, T., Ono, M. & Watanabe, S. (1994) N-methyl-D-aspartate induces phase shifts in circadian rhythm of neuronal activity of rat SCN in vitro. *The American journal of physiology*, **267**, R360-364.

Shichi, K., Fujita-Hamabe, W., Harada, S., Mizoguchi, H., Yamada, K., Nabeshima, T. & Tokuyama, S. (2011) Involvement of matrix metalloproteinase-mediated proteolysis of neural cell adhesion molecule in the development of cerebral ischemic neuronal damage. *The Journal of pharmacology and experimental therapeutics*, **338**, 701-710.

Shieh, P.B., Hu, S.C., Bobb, K., Timmusk, T. & Ghosh, A. (1998) Identification of a signaling pathway involved in calcium regulation of BDNF expression. *Neuron*, **20**, 727-740.

Shirakawa, T., Honma, S. & Honma, K. (2001) Multiple oscillators in the suprachiasmatic nucleus. *Chronobiology international*, **18**, 371-387.

Shirakawa, T. & Moore, R.Y. (1994) Glutamate shifts the phase of the circadian neuronal firing rhythm in the rat suprachiasmatic nucleus in vitro. *Neurosci Lett*, **178**, 47-50.

Sholl, D.A. (1953) Dendritic organization in the neurons of the visual and motor cortices of the cat. *Journal of anatomy*, **87**, 387-406.

Sloniowski, S. & Ethell, I.M. (2012) Looking forward to EphB signaling in synapses. *Seminars in Cell & Developmental Biology*, **23**, 75-82.

Song, I. & Dityatev, A. (2018) Crosstalk between glia, extracellular matrix and neurons. *Brain Res Bull*, **136**, 101-108.

Southey, B.R., Lee, J.E., Zamdborg, L., Atkins, N., Jr., Mitchell, J.W., Li, M., Gillette, M.U., Kelleher, N.L. & Sweedler, J.V. (2014) Comparing label-free quantitative peptidomics approaches to characterize diurnal variation of peptides in the rat suprachiasmatic nucleus. *Analytical chemistry*, **86**, 443-452.

Souttou, S., Benabdesselam, R., Siqueiros-Marquez, L., Sifi, M., Deliba, M., Vacca, O., Charles-Messance, H., Vaillend, C., Rendon, A., Guillonneau, X. & Dorbani-Mamine, L. (2019) Expression and localization of dystrophins and beta-dystroglycan in the hypothalamic supraoptic nuclei of rat from birth to adulthood. *Acta Histochem*, **121**, 218-226.

Spanagel, R., Pendyala, G., Abarca, C., Zghoul, T., Sanchis-Segura, C., Magnone, M.C., Lascorz, J., Depner, M., Holzberg, D., Soyka, M., Schreiber, S., Matsuda, F., Lathrop, M., Schumann, G. & Albrecht, U. (2005) The clock gene Per2 influences the glutamatergic system and modulates alcohol consumption. *Nat Med*, **11**, 35-42.

Stawarski, M., Stefaniuk, M. & Wlodarczyk, J. (2014) Matrix metalloproteinase-9 involvement in the structural plasticity of dendritic spines. *Frontiers in neuroanatomy*, **8**, 68.

Stephan, F.K. & Zucker, I. (1972) Circadian Rhythms in Drinking Behavior and Locomotor Activity of Rats Are Eliminated by Hypothalamic Lesions. *Proc Natl Acad Sci U S A*, **69**, 1583-1586.

Sternlicht, M.D. & Werb, Z. (2001) HOW MATRIX METALLOPROTEINASES REGULATE CELL BEHAVIOR. *Annual review of cell and developmental biology*, **17**, 463-516.

Stogsdill, J.A., Ramirez, J., Liu, D., Kim, Y.H., Baldwin, K.T., Enustun, E., Ejikeme, T., Ji, R.R. & Eroglu, C. (2017) Astrocytic neuroligins control astrocyte morphogenesis and synaptogenesis. *Nature*, **551**, 192-197.

Sugita, S., Saito, F., Tang, J., Satz, J., Campbell, K. & Südhof, T.C. (2001) A stoichiometric complex of neurexins and dystroglycan in brain. *J Cell Biol*, **154**, 435-445.

Suzuki, Y., Goetze, T.A., Stroebel, D., Balasuriya, D., Yoshimura, S.H., Henderson, R.M., Paoletti, P., Takeyasu, K. & Edwardson, J.M. (2013) Visualization of structural changes accompanying activation of N-methyl-D-aspartate (NMDA) receptors using fast-scan atomic force microscopy imaging. *J Biol Chem*, **288**, 778-784.

Syková, E. (2004) Diffusion properties of the brain in health and disease. *Neurochemistry international*, **45**, 453-466.

Syková, E. & Vargová, L. (2008) Extrasynaptic transmission and the diffusion parameters of the extracellular space. *Neurochemistry international*, **52**, 5-13.

Szepesi, Z., Bijata, M., Ruszczycki, B., Kaczmarek, L. & Wlodarczyk, J. (2013) Matrix metalloproteinases regulate the formation of dendritic spine head protrusions during chemically induced long-term potentiation. *PLoS One*, **8**, e63314.

Szepesi, Z., Hosy, E., Ruszczycki, B., Bijata, M., Pyskaty, M., Bikbaev, A., Heine, M., Choquet, D., Kaczmarek, L. & Wlodarczyk, J. (2014) Synaptically Released Matrix Metalloproteinase Activity in Control of Structural Plasticity and the Cell Surface Distribution of GluA1-AMPA Receptors. *Plos One*, **9**, 14.

Szinyei, C., Stork, O. & Pape, H.C. (2003) Contribution of NR2B subunits to synaptic transmission in amygdaloid interneurons. *J Neurosci*, **23**, 2549-2556.

Szklarczyk, A., Ewaleifoh, O., Beique, J.C., Wang, Y., Knorr, D., Haughey, N., Malpica, T., Mattson, M.P., Huganir, R. & Conant, K. (2008) MMP-7 cleaves the NR1 NMDA receptor subunit and modifies NMDA receptor function *FASEB J*, pp. 3757-3767.

Takahashi, J.S., Hong, H.K., Ko, C.H. & McDearmon, E.L. (2008) The genetics of mammalian circadian order and disorder: implications for physiology and disease. *Nat Rev Genet*, **9**, 764-775.

Tamaru, T., Isojima, Y., Yamada, T., Okada, M., Nagai, K. & Takamatsu, K. (2000) Light and glutamate-induced degradation of the circadian oscillating protein BMAL1 during the mammalian clock resetting. *J Neurosci*, **20**, 7525-7530.

Tamura, Y., Watanabe, F., Nakatani, T., Yasui, K., Fuji, M., Komurasaki, T., Tsuzuki, H., Maekawa, R., Yoshioka, T., Kawada, K., Sugita, K. & Ohtani, M. (1998) Highly selective and orally active inhibitors of type IV collagenase (MMP-9 and MMP-2): N-sulfonylamino acid derivatives. *Journal of medicinal chemistry*, **41**, 640-649.

Tavares, G., Martins, M., Correia, J.S., Sardinha, V.M., Guerra-Gomes, S., das Neves, S.P., Marques, F., Sousa, N. & Oliveira, J.F. (2017) Employing an open-source tool to assess astrocyte tridimensional structure *Brain Struct Funct*, pp. 1989-1999.

Theodosis, D.T., Bonfanti, L., Olive, S., Rougon, G. & Poulain, D.A. (1994) ADHESION MOLECULES AND STRUCTURAL PLASTICITY OF THE ADULT HYPOTHALAMONEUROHYPOPHYSEAL SYSTEM. *Psychoneuroendocrinology*, **19**, 455-462.

Theodosis, D.T., Piet, R., Poulain, D.A. & Oliet, S.H. (2004) Neuronal, glial and synaptic remodeling in the adult hypothalamus: functional consequences and role of cell surface and extracellular matrix adhesion molecules. *Neurochemistry international*, **45**, 491-501.

Theodosis, D.T., Poulain, D.A. & Oliet, S.H. (2008) Activity-dependent structural and functional plasticity of astrocyte-neuron interactions. *Physiol Rev*, **88**, 983-1008.

Tian, L., Stefanidakis, M., Ning, L., Van Lint, P., Nyman-Huttunen, H., Libert, C., Itohara, S., Mishina, M., Rauvala, H. & Gahmberg, C.G. (2007) Activation of NMDA receptors promotes dendritic spine development through MMP-mediated ICAM-5 cleavage. *J Cell Biol*, **178**, 687-700.

Tian, R., Alvarez-Saavedra, M., Cheng, H.Y. & Figeys, D. (2011) Uncovering the proteome response of the master circadian clock to light using an AutoProteome system. *Mol Cell Proteomics*, **10**, M110.007252.

Tinnes, S., Ringwald, J. & Haas, C.A. (2013) TIMP-1 inhibits the proteolytic processing of Reelin in experimental epilepsy. *Faseb j*, **27**, 2542-2552.

Tischkau, S.A., Mitchell, J.W., Tyan, S.H., Buchanan, G.F. & Gillette, M.U. (2003) Ca2+/cAMP response element-binding protein (CREB)-dependent activation of Per1 is required for light-induced signaling in the suprachiasmatic nucleus circadian clock. *J Biol Chem*, **278**, 718-723.

Tomimatsu, Y., Idemoto, S., Moriguchi, S., Watanabe, S. & Nakanishi, H. (2002) Proteases involved in long-term potentiation. *Life Sci*, **72**, 355-361.

Tongiorgi, E., Righi, M. & Cattaneo, A. (1997) Activity-dependent dendritic targeting of BDNF and TrkB mRNAs in hippocampal neurons. *J Neurosci*, **17**, 9492-9505.

Toth, M., Chvyrkova, I., Bernardo, M.M., Hernandez-Barrantes, S. & Fridman, R. (2003) Pro-MMP-9 activation by the MT1-MMP/MMP-2 axis and MMP-3: role of TIMP-2 and plasma membranes. *Biochemical and biophysical research communications*, **308**, 386-395.

Toth, M. & Fridman, R. (2001) Assessment of Gelatinases (MMP-2 and MMP-9 by Gelatin Zymography. *Methods in molecular medicine*, **57**, 163-174.

Touitou, Y., Reinberg, A. & Touitou, D. (2017) Association between light at night, melatonin secretion, sleep deprivation, and the internal clock: Health impacts and mechanisms of circadian disruption. *Life Sci*, **173**, 94-106.

Tousson, E. & Meissl, H. (2004) Suprachiasmatic nuclei grafts restore the circadian rhythm in the paraventricular nucleus of the hypothalamus. *J Neurosci*, **24**, 2983-2988.

Trivedi, A., Noble-Haeusslein, L.J., Levine, J.M., Santucci, A.D., Reeves, T.M. & Phillips, L.L. (2019) Matrix metalloproteinase signals following neurotrauma are right on cue. *Cell Mol Life Sci*.

Tsilibary, E., Tzinia, A., Radenovic, L., Stamenkovic, V., Lebitko, T., Mucha, M., Pawlak, R., Frischknecht, R. & Kaczmarek, L. (2014) Neural ECM proteases in learning and synaptic plasticity. *Progress in brain research*, **214**, 135-157.

Tu, D.C., Zhang, D., Demas, J., Slutsky, E.B., Provencio, I., Holy, T.E. & Van Gelder, R.N. (2005) Physiologic diversity and development of intrinsically photosensitive retinal ganglion cells. *Neuron*, **48**, 987-999.

Vaillant, C., Didier-Bazes, M., Hutter, A., Belin, M.F. & Thomasset, N. (1999) Spatiotemporal expression patterns of metalloproteinases and their inhibitors in the postnatal developing rat cerebellum. *J Neurosci*, **19**, 4994-5004.

Vaillant, C., Meissirel, C., Mutin, M., Belin, M.F., Lund, L.R. & Thomasset, N. (2003) MMP-9 deficiency affects axonal outgrowth, migration, and apoptosis in the developing cerebellum. *Molecular and cellular neurosciences*, **24**, 395-408.

Van den Pol, A.N. (1980) The hypothalamic suprachiasmatic nucleus of rat: intrinsic anatomy. *The Journal of comparative neurology*, **191**, 661-702.

van den Pol, A.N. (1991) Glutamate and aspartate immunoreactivity in hypothalamic presynaptic axons. *J Neurosci*, **11**, 2087-2101.

van den Pol, A.N. (1993) Glutamate and GABA presence and action in the suprachiasmatic nucleus. *Journal of biological rhythms*, **8 Suppl**, S11-15.

van den Pol, A.N., Finkbeiner, S.M. & Cornell-Bell, A.H. (1992) Calcium excitability and oscillations in suprachiasmatic nucleus neurons and glia in vitro. *J Neurosci*, **12**, 2648-2664.

Van den Steen, P.E., Dubois, B., Nelissen, I., Rudd, P.M., Dwek, R.A. & Opdenakker, G. (2002) Biochemistry and molecular biology of gelatinase B or matrix metalloproteinase-9 (MMP-9). *Critical reviews in biochemistry and molecular biology*, **37**, 375-536.

van der Vinne, V., Swoap, S.J., Vajtay, T.J. & Weaver, D.R. (2018) Desynchrony between brain and peripheral clocks caused by CK1delta/epsilon disruption in GABA neurons does not lead to adverse metabolic outcomes. *Proc Natl Acad Sci U S A*, **115**, E2437-e2446.

van Oosterhout, F., Lucassen, E.A., Houben, T., vanderLeest, H.T., Antle, M.C. & Meijer, J.H. (2012) Amplitude of the SCN Clock Enhanced by the Behavioral Activity Rhythm *PLoS One*.

Vandooren, J., Geurts, N., Martens, E., Van den Steen, P.E. & Opdenakker, G. (2013a) Zymography methods for visualizing hydrolytic enzymes. *Nature methods*, **10**, 211-220.

Vandooren, J., Van den Steen, P.E. & Opdenakker, G. (2013b) Biochemistry and molecular biology of gelatinase B or matrix metalloproteinase-9 (MMP-9): the next decade. *Critical reviews in biochemistry and molecular biology*, **48**, 222-272.

Varbanov, H. & Dityatev, A. (2017) Regulation of extrasynaptic signaling by polysialylated NCAM: Impact for synaptic plasticity and cognitive functions. *Molecular and cellular neurosciences*, **81**, 12-21.

Vargová, L. & Syková, E. (2008) Extracellular space diffusion and extrasynaptic transmission. *Physiol Res*, **57 Suppl 3**, S89-99.

Verslegers, M., Lemmens, K., Van Hove, I. & Moons, L. (2013) Matrix metalloproteinase-2 and -9 as promising benefactors in development, plasticity and repair of the nervous system. *Prog Neurobiol*, **105**, 60-78.

Vicini, S., Wang, J.F., Li, J.H., Zhu, W.J., Wang, Y.H., Luo, J.H., Wolfe, B.B. & Grayson, D.R. (1998) Functional and pharmacological differences between recombinant N-methyl-D-aspartate receptors. *J Neurophysiol*, **79**, 555-566.

Vindlacheruvu, R.R., Ebling, F.J., Maywood, E.S. & Hastings, M.H. (1992) Blockade of Glutamatergic Neurotransmission in the Suprachiasmatic Nucleus Prevents Cellular and Behavioural Responses of the Circadian System to Light. *Eur J Neurosci*, **4**, 673-679.

Visse, R. & Nagase, H. (2003) Matrix metalloproteinases and tissue inhibitors of metalloproteinases: structure, function, and biochemistry. *Circ Res*, **92**, 827-839.

Vitaterna, M.H., King, D.P., Chang, A.M., Kornhauser, J.M., Lowrey, P.L., McDonald, J.D., Dove, W.F., Pinto, L.H., Turek, F.W. & Takahashi, J.S. (1994) Mutagenesis and mapping of a mouse gene, Clock, essential for circadian behavior. *Science*, **264**, 719-725.

Vitaterna, M.H., Selby, C.P., Todo, T., Niwa, H., Thompson, C., Fruechte, E.M., Hitomi, K., Thresher, R.J., Ishikawa, T., Miyazaki, J., Takahashi, J.S. & Sancar, A. (1999) Differential regulation of mammalian period genes and circadian rhythmicity by cryptochromes 1 and 2. *Proc Natl Acad Sci U S A*, **96**, 12114-12119.

von Gall, C., Duffield, G.E., Hastings, M.H., Kopp, M.D., Dehghani, F., Korf, H.W. & Stehle, J.H. (1998) CREB in the mouse SCN: a molecular interface coding the phase-adjusting stimuli light, glutamate, PACAP, and melatonin for clockwork access. *J Neurosci*, **18**, 10389-10397.

Wagner, S., Castel, M., Gainer, H. & Yarom, Y. (1997) GABA in the mammalian suprachiasmatic nucleus and its role in diurnal rhythmicity. *Nature*, **387**, 598-603.

Walton, J.C., McNeill, J.K.t., Oliver, K.A. & Albers, H.E. (2017) Temporal Regulation of GABAA Receptor Subunit Expression: Role in Synaptic and Extrasynaptic Communication in the Suprachiasmatic Nucleus. *eNeuro*, **4**.

Wang, H. & Peng, R.Y. (2016) Basic roles of key molecules connected with NMDAR signaling pathway on regulating learning and memory and synaptic plasticity. *Military Medical Research*, **3**, 26.

Wang, H.Y. & Huang, R.C. (2004) Diurnal modulation of the Na+/K+-ATPase and spontaneous firing in the rat retinorecipient clock neurons. *J Neurophysiol*, **92**, 2295-2301.

Wang, L.M., Schroeder, A., Loh, D., Smith, D., Lin, K., Han, J.H., Michel, S., Hummer, D.L., Ehlen, J.C., Albers, H.E. & Colwell, C.S. (2008a) Role for the NR2B subunit of the N-methyl-D-aspartate receptor in mediating light input to the circadian system. *Eur J Neurosci*, **27**, 1771-1779.

Wang, X., Bozdagi, O., Nikitczuk, J.S., Zhai, Z.W., Zhou, Q. & Huntley, G.W. (2008b) Extracellular proteolysis by matrix metalloproteinase-9 drives dendritic spine enlargement and long-term potentiation coordinately *Proc Natl Acad Sci U S A*, pp. 19520-19525.

Warren, E.J., Allen, C.N., Brown, R.L. & Robinson, D.W. (2003) Intrinsic light responses of retinal ganglion cells projecting to the circadian system. *Eur J Neurosci*, **17**, 1727-1735.

Watanabe, A., Shibata, S. & Watanabe, S. (1995) Circadian rhythm of spontaneous neuronal activity in the suprachiasmatic nucleus of old hamster in vitro. *Brain research*, **695**, 237-239.

Watson, R.E., Langub, M.C., Engle, M.G. & Maley, B.E. (1995) Estrogen-receptive neurons in the anteroventral periventricular nucleus are synaptic targets of the suprachiasmatic nucleus and peri-suprachiasmatic region. *Brain research*, **689**, 254-264.

Watts, A.G., Swanson, L.W. & Sanchez-Watts, G. (1987) Efferent projections of the suprachiasmatic nucleus: I. Studies using anterograde transport of Phaseolus vulgaris leucoagglutinin in the rat. *The Journal of comparative neurology*, **258**, 204-229.

Webb, I.C., Coolen, L.M. & Lehman, M.N. (2013) NMDA and PACAP receptor signaling interact to mediate retinal-induced scn cellular rhythmicity in the absence of light. *PLoS One*, **8**, e76365.

Welsh, D.K., Logothetis, D.E., Meister, M. & Reppert, S.M. (1995) Individual neurons dissociated from rat suprachiasmatic nucleus express independently phased circadian firing rhythms. *Neuron*, **14**, 697-706.

Welsh, D.K., Takahashi, J.S. & Kay, S.A. (2010) Suprachiasmatic nucleus: cell autonomy and network properties. *Annual review of physiology*, **72**, 551-577.

Wenk, C.H., Josserand, V., Dumy, P., Coll, J.L. & Boturyn, D. (2013) Integrin and matrix metalloprotease dual-targeting with an MMP substrate-RGD conjugate. *Organic & biomolecular chemistry*, **11**, 448-452.

Wiera, G. & Mozrzymas, J.W. (2015) Extracellular proteolysis in structural and functional plasticity of mossy fiber synapses in hippocampus. *Front Cell Neurosci*, **9**, 427.

Wiera, G., Nowak, D., van Hove, I., Dziegiel, P., Moons, L. & Mozrzymas, J.W. (2017) Mechanisms of NMDA Receptor- and Voltage-Gated L-Type Calcium Channel-Dependent Hippocampal LTP Critically Rely on Proteolysis That Is Mediated by Distinct Metalloproteinases. *J Neurosci*, **37**, 1240-1256.

Wildering, W.C., Hermann, P.M. & Bulloch, A.G. (2002) Rapid neuromodulatory actions of integrin ligands. *J Neurosci*, **22**, 2419-2426.

Williams, J., Yang, N., Wood, A., Zindy, E., Meng, Q.J. & Streuli, C.H. (2018) Epithelial and stromal circadian clocks are inversely regulated by their mechano-matrix environment. *Journal of cell science*, **131**.

Williams, K. (2001) Ifenprodil, a novel NMDA receptor antagonist: site and mechanism of action. *Curr Drug Targets*, **2**, 285-298.

Witting, W., Kwa, I.H., Eikelenboom, P., Mirmiran, M. & Swaab, D.F. (1990) ALTERATIONS IN THE CIRCADIAN REST-ACTIVITY RHYTHM IN AGING AND ALZHEIMERS-DISEASE. *Biological psychiatry*, **27**, 563-572.

Wojtowicz, T. & Mozrzymas, J.W. (2010) Late phase of long-term potentiation in the mossy fiber-CA3 hippocampal pathway is critically dependent on metalloproteinases activity. *Hippocampus*, **20**, 917-921.

Wolburg-Buchholz, K., Mack, A.F., Steiner, E., Pfeiffer, F., Engelhardt, B. & Wolburg, H. (2009) Loss of astrocyte polarity marks blood-brain barrier impairment during experimental autoimmune encephalomyelitis. *Acta Neuropathol*, **118**, 219-233.

Womac, A.D., Burkeen, J.F., Neuendorff, N., Earnest, D.J. & Zoran, M.J. (2009) Circadian rhythms of extracellular ATP accumulation in suprachiasmatic nucleus cells and cultured astrocytes. *Eur J Neurosci*, **30**, 869-876.

Wu, X., Mogford, J.E., Platts, S.H., Davis, G.E., Meininger, G.A. & Davis, M.J. (1998) Modulation of calcium current in arteriolar smooth muscle by alphav beta3 and alpha5 beta1 integrin ligands. *J Cell Biol*, **143**, 241-252.

Wu, X., Morishita, W.K., Riley, A.M., Hale, W.D., Sudhof, T.C. & Malenka, R.C. (2019) Neuroligin-1 Signaling Controls LTP and NMDA Receptors by Distinct Molecular Pathways. *Neuron*, **102**, 621-635.e623.

Wulff, K., Gatti, S., Wettstein, J.G. & Foster, R.G. (2010) Sleep and circadian rhythm disruption in psychiatric and neurodegenerative disease. *Nature reviews. Neuroscience*, **11**, 589-599.

Yamada, K. & Nabeshima, T. (2004) Interaction of BDNF/TrkB signaling with NMDA receptor in learning and memory. *Drug News Perspect*, **17**, 435-438.

Yamada, Y. & Prosser, R.A. (2014) Copper chelation and exogenous copper affect circadian clock phase resetting in the suprachiasmatic nucleus in vitro. *Neuroscience*, **256**, 252-261.

Yamada, Y. & Prosser, R.A. (2018) Copper in the suprachiasmatic circadian clock: A possible link between multiple circadian oscillators. *Eur J Neurosci*.

Yamazaki, S., Kerbeshian, M.C., Hocker, C.G., Block, G.D. & Menaker, M. (1998) Rhythmic properties of the hamster suprachiasmatic nucleus in vivo. *J Neurosci*, **18**, 10709-10723.

Yamazaki, S., Numano, R., Abe, M., Hida, A., Takahashi, R., Ueda, M., Block, G.D., Sakaki, Y., Menaker, M. & Tei, H. (2000) Resetting central and peripheral circadian oscillators in transgenic rats. *Science*, **288**, 682-685.

Yamazaki, S. & Takahashi, J.S. (2005) Real-time luminescence reporting of circadian gene expression in mammals. *Methods Enzymol*, **393**, 288-301.

Yan, L., Smale, L. & Nunez, A.A. (2018) Circadian and photic modulation of daily rhythms in diurnal mammals. *Eur J Neurosci*.

Yan, S.J. & Blomme, E.A. (2003) In situ zymography: a molecular pathology technique to localize endogenous protease activity in tissue sections. *Veterinary pathology*, **40**, 227-236.

Yan, W., Zhao, X., Chen, H., Zhong, D., Jin, J., Qin, Q., Zhang, H., Ma, S. & Li, G. (2016) beta-Dystroglycan cleavage by matrix metalloproteinase-2/-9 disturbs aquaporin-4 polarization and influences brain edema in acute cerebral ischemia. *Neuroscience*, **326**, 141-157.

Yang, C.M., Hsieh, H.L., Yu, P.H., Lin, C.C. & Liu, S.W. (2015) IL-1beta Induces MMP-9-Dependent Brain Astrocytic Migration via Transactivation of PDGF Receptor/NADPH Oxidase 2-Derived Reactive Oxygen Species Signals. *Mol Neurobiol*, **52**, 303-317.

Yang, N., Williams, J., Pekovic-Vaughan, V., Wang, P., Olabi, S., McConnell, J., Gossan, N., Hughes, A., Cheung, J., Streuli, C.H. & Meng, Q.J. (2017) Cellular mechano-environment regulates the mammary circadian clock. *Nat Commun*, **8**, 14287.

Ying, S.W., Futter, M., Rosenblum, K., Webber, M.J., Hunt, S.P., Bliss, T.V. & Bramham, C.R. (2002) Brain-derived neurotrophic factor induces long-term potentiation in intact adult hippocampus: requirement for ERK activation coupled to CREB and upregulation of Arc synthesis. *J Neurosci*, **22**, 1532-1540.

Yokota, S., Yamamoto, M., Moriya, T., Akiyama, M., Fukunaga, K., Miyamoto, E. & Shibata, S. (2001) Involvement of calcium-calmodulin protein kinase but not mitogen-activated protein kinase in light-induced phase delays and Per gene expression in the suprachiasmatic nucleus of the hamster. *J Neurochem*, **77**, 618-627.

Zaccaria, M.L., Di Tommaso, F., Brancaccio, A., Paggi, P. & Petrucci, T.C. (2001) Dystroglycan distribution in adult mouse brain: a light and electron microscopy study. *Neuroscience*, **104**, 311-324.

Zamanian, J.L., Xu, L., Foo, L.C., Nouri, N., Zhou, L., Giffard, R.G. & Barres, B.A. (2012) Genomic analysis of reactive astrogliosis. *J Neurosci*, **32**, 6391-6410.

Zhang, X., Gu, Y., Li, P., Jiang, A., Sheng, X., Jin, X., Shi, Y. & Li, G. (2019) Matrix Metalloproteases-Mediated Cleavage on beta-Dystroglycan May Play a Key Role in the Blood-Brain Barrier After Intracerebral Hemorrhage in Rats. *Med Sci Monit*, **25**, 794-800.

Zhao, H., Xiao, S., Kong, X., Wang, J., Cao, X., Gencheng, W., Loh, H.H. & Law, P.Y. (2011) Neuron-glial cell communication in the traumatic stress-induced immunomodulation. *Synapse*, **65**, 433-440.

Zhou, B., Zuo, Y.X. & Jiang, R.T. (2019) Astrocyte morphology: Diversity, plasticity, and role in neurological diseases. *CNS Neurosci Ther*, **25**, 665-673.

APPENDIX

Table 1. Primary Antibody Information

Primary Antibody (Information; Catalog#, Manufacturer)	Application (dilution)	Host
Actin, I-19: (Polyclonal;sc-161 Santa Cruz)	WB (1:5000)	Goat
β-dystroglycan: (B-DG-CE, *Lyophilised Concentrated monoclonal*; Leica Novocastra)	IHC (1:500)	Mouse
β-dystroglycan (Polyclonal; ab43125, Abcam)	WB, IHC (1:500)	Rabbit
GFAP (Polyclonal; ab4674, Abcam)	IHC (1:100)	Chicken
MMP-2 (Polyclonal; MAB13406 EMD Millipore)	WB (1:1000)	Rabbit
MMP-9 (Polyclonal; AB19016, Abcam)	WB (1:1000)	Rabbit
p-CAMKII; Thr 286 (Polyclonal; p1005-286)	WB (1:500)	Rabbit

Table 2: Secondary Antibody Information

Secondary Antibody (Information; Catalog#, Manufacturer)	Application (dilution)	Host
Fluorescent Dyes:		
Anti-Rabbit IgY (H+L), Alexa Fluor 488 (A-11041, Invitrogen)	IHC (1:1000)	Goat
Anti-Chicken IgY (H+L), Alexa Fluor 568 (A-21206, Invitrogen)	IHC (1:1000)	Goat
Infrared Dyes:		
IRDye® Anti-Rabbit-800 CW (925-32213, LI-COR)	WB (1:5000)	Donkey
IRDye® Anti-Goat-680 RD (925-68074, LI-COR)	WB (1:5000)	Donkey

Supplementary Protocols

Western Blotting for Protein Expression

This protocol was developed to isolate proteins from the suprachiasmatic nucleus (SCN), separate them, and detect them with immunoblotting. It is written specifically for use with the Life Technologies “Bolt” electrophoresis system and detection using the Odyssey Clx laser detector. You will need SCN tissue slices, 500uM thick, from one mouse (2 slices per mouse). The Odyssey system is very sensitive to low protein quantities, so this reduces the amount of tissue used. Keep the slices in the -80 °C freezer until use.

Protein Extraction Protocol:

1. Prepare Lysis buffer:

RIPA buffer	490 uL
Protease inhibitor	5.00 uL
Phosphatase inhibitor	5.00 uL

2. Add 40 uL of Lysis buffer to each sample tube.
3. Sonicate each sample x 10 pulses.
4. Place on rotator in cold room for 25 minutes.
5. Prepare the Bradford assay and turn on the spectrophotometer.
6. Fill six centrifuge tubes (standard tubes will be labeled 0-5) plus one centrifuge tube for each sample you are extracting protein from with 1 mL of Bradford reagent.
7. Add BSA (2.0mg/mL) to each standard tube in the following amounts
    1. Tube 0 = 0 uL BSA= 0 g
    2. Tube 1= 1.00 uL BSA= 2 ug
    3. Tube 2= 2.50 uL BSA= 5 ug
    4. Tube 3= 5.00 uL BSA= 10 ug
    5. Tube 4= 7.5-0 uL BSA= 15 ug
    6. Tube 5= 10.0 uL BSA= 20 ug
5. Centrifuge samples on max speed for 2 min.
6. Sonicate samples x 5 pulses.

7. Centrifuge samples for 10 minutes on max speed (13,000 rpm).
8. Remove and measure supernatant.
9. Calculate uL of sample to = 15 ug total protein

   15 g ÷ (concentration measured using Bradford)= # uL sample to add to sample tube.

10. Create a table in your notebook that contains these headings and record volumes of solution required for each sample.

Sample	Concentration	uL Sample	Reducing Buffer	Sample Buffer	H_2O	Total
ZT #	(Bradford) ug/uL	X uL *see above	4.0 uL	12.0 uL	[40-(4-12-X)] uL	40 uL

11. After prepping Loading Samples, boil them at 80 °C for 10 minutes.
12. Prepare 1 X MOPS buffer – need at least 500 mLs per gel.
13. Place a 4-12% Bolt Pre-cast Gel into the Bolt electrophoresis box and pour the MOPS buffer into the box, enough to cover the gel.
14. Load samples into the gel, along with 5 uL of Kaleidoscope Ladder (BioRAD) (If the last lane does not contain sample, load 12 uL of loading dye into the last well for balance).
15. Run gel @ 150 volts until proteins are completely separated ~1.00 hour

Protein Transfer Protocol:

1. Prepare 1 X Transfer Buffer if not already made. The recipe will be on the 5X Transfer buffer bottle.
2. Remove gel from cassette and equilibrate in 1 X Transfer Buffer for 10 minutes.
3. Activate the Immobilon membrane with methanol, then equilibrate for 5 minutes in 1 X transfer buffer.
4. Cut enough chromatography paper to act as your filter papers for the transfer. Need six squares.
5. In the transfer box, begin to make your Protein Transfer Sandwich:
   i. Bottom: Filter Paper
   ii. Second Layer: Immobilon Membrane

iii. Third layer: Gel
iv. Top/ Final Layer: Filter paper

6. Lock the transfer cassette and load into the TransBlot Turbo
7. Select the correct Transfer program to run. This will depend on how large your proteins of interest are.
8. Remove Cassette when finished, trim the membrane, and place into a gel box to dry.

Gelatin Zymography Protocol

Adapted from Toth and Fridman, 2001 and Kupai *et al.*, 2011

Solution Preparation:

All solutions can be stored at room temp, ESPECIALLY the sample buffer.

Homogenization Buffer (500 mL)

0.335 g Tris Base

1.00 mL Triton X 100

-Dissolve ~500 mL ddH2O, adjust pH to 7.4.

Renaturing Buffer (250 mL)

6.25 mLs Triton X 100

-Dissolve in 250 mLs H2O

Incubation Buffer (500 mL)

4.383 g NaCl

0.735 g $CaCl_2$*$2H_2O$

3.0285 g Tris Base

0.5 g NaN3 (or 5 mLs of 5% w/v aqueous NaN_3)

-Dissolve in 500 mL ddH_2O, adjust pH to 7.8-8.0

Running Buffer (2.0 L)

28.83 g Glycine

6.00 g Tris Base

2.00 g SDS

-Dissolve in 2000 mL H_2O

Sample Buffer

Ordered from BioRAD.

Gelatin Zymograms

Supplied by Invitrogen, compatible with BOLT electrophoresis system.

Protein Extraction for Zymography:

Remember to always keep your samples containing enzyme on ice! Also work quickly because you are trying to preserve the enzymatic activity of the metalloproteinases.

1. Add 10 uL of homogenization buffer per slice to each sample tube.
2. Homogenize **on ice** using an electric pestle 3 x 5 sec.
3. Centrifuge samples at 13,000 rpm for 15 minutes.
4. Collect and measure the amount of supernatant.
5. Prepare a Bradford assay and measure protein concentration (instructions can be found in the Western Blotting Protocol) of the supernatant.
6. Remove the gelatin zymogram from the plastic wrapper and load into the electrophoresis tank, allow to equilibrate in running buffer for a short time (about 5 min) and wash the inside of the lanes with running buffer using a 200 uL pipette.
7. Calculate how much supernatant you will need in order to load 15 ug of protein per lane.
8. Add 30 uL of sample buffer to a new centrifuge tube for each sample.
9. Add dd H_2O to the sample buffer so that:

   (x uL protein + 30 uL sample buffer + x uL H_2O)= 40 uL
10. Add extracted protein sample (supernatant) to sample buffer + water.
11. Load your prepared samples into the gelatin zymogram.
12. Run the gel at 75 volts for ~2 hours or until the samples are completely separated. Running at low voltage for a long time works the best because you do not want the gel to heat up too much, which can degrade the protein samples.
13. Remove gel from the tank and cassette and place into a box containing renaturing buffer.
14. Incubate while on a rocker at room temp for 40 min.
15. Decant the renaturing buffer of the gel and rinse with incubation buffer.
16. Pour off the incubation buffer and add fresh incubation buffer to cover the zymogram.
17. Incubate gel at 37°C for 5 days.

a. Depending on the amount of MMP-2/9 in the sample, the gel may take less time to incubate at 37°C. If the amount of MMP-2/9 in your sample is unknown, check after 24, 48, or 72 hrs for bands of gelatinolytic activity.

18. Decant the incubation buffer off of the gel and stain in Coomassie Blue for 1 hour.
19. De-stain the gel using a solution containing 4% methanol/ 8% acetic acid. Check the gel every 15 minutes for gelatinolytic bands (clear bands signifying degraded gelatin or “potential proteolytic activity”), add new de-staining solution as needed, until the bands appear.
20. Image on the LICOR Odyssey Clx and analyze signal intensity of bands using ImageStudio Lite.

In Situ Zymography Protocol

1. Make brain tissue slices and maintain in perfusion dish until desired collection time.
2. Collect tissue using a flat spatula and paintbrush at specified time points, with or without drug treatment.
3. Place in mold filled with OCT media and freeze on dry ice immediately.
4. Store in -80C until ready to section.
5. Make MMP activity/development buffer (NaCl 100 mM, CaCl2 10 mM, Tris-HCl 100 mM, 0.05% Brij-35, ph 7.5 (George *et al.*, 2010)

   To make 500 mLs:

   a) NaCl= 2.922 g
   b) $CaCl_2$= 0.5549 g
   c) Tris HCl= 6.057 g
   d) Brij-35 (30% stock) 833 uL

   Fill to 500 mL with ddH20 and pH to 7.5.
6. Prepare DQ-Gelatin media:
   a) Prepare a 1.0 mg/mL stock solution of the DQ-Gelatin by adding 1.0 mL of MMP buffer (diluted 1:10) directly to one of the five vials containing the lyophilized substrate. It may be necessary to agitate the sample in an ultrasonic water bath for ~5 minutes and heat to 50°C to facilitate dissolution.
   b) Protect from light at store at 4°C for up to 2 months.
7. Section tissue using the Leica Cryostat (-20°C) to a thickness of 10 μm.
8. Draw around sections with a hydrophobic pen.
9. Dilute stock DQ-Gelatin substrate 1:50 in MMP buffer to obtain a working concentration of 20 ug/mL.
10. Place ~300 uL of substrate on each slide.
11. Place damp tissue paper onto the bottom of a dark color slide box.
12. Place up to 8 slides in the box, balancing the slides on the plastic slide separators.
13. Place in 37 °C oven/incubator overnight.

14. Wash three times for one minute in 1X PBS.
15. Mount sections using coverslips and drop of Vectashield with DAPI.
16. Image slides on a fluorescent inverted or confocal microscope that contains a 488 nm laser and analyze the signal intensity (mean grey value) using ImageJ Fiji.

Note: Always include a slide to serve as a negative control that has 4% PFA, BiPS, EDTA, or TIMP protein as a negative control. Can also Include a negative control with absence of DQ-Gelatin substrate.

Immunohistochemistry of Thin Sections on Slides Protocol

Tissue preparation of freshly harvested brain tissue:

1. Thaw 4% PFA, treat slices with PFA for 15 minutes at room temp, on shaker.
2. 30% Sucrose/PBS treatment at RT for ~30 minutes or until tissue sinks to bottom of vial.
3. Cryo-protect in O.C.T. medium (on dry ice) and note orientation of brain slice.
4. Proceed to cryosectioning or store at -80°C.
5. Using the Leica Cryostat set at -20°C, section tissue at 10 µm (thickness of tissue will depend on what protein you wish to detect) and mount onto Histobond slides.
6. Air dry for 30 minutes at room temperature. Slides can be stored at -80°C for several months.

General Immunostaining Protocol (each slide holds about 300-500 µL):

1. When staining cryostat sections stored in the -80°C freezer, thaw the slides at room temperature in the fume hood (to maintain sterility and provide air flow) for 10-20 minutes.
2. Surround the tissue with a barrier using a pen containing hydrophobic compound.
3. Add 4% PFA to the tissue slices and fix for 10 minutes at 4°C.
4. Wash slides at room temperature with 1X PBS, 3 X 5 minutes with gentle agitation.
5. Block tissues by incubating in blocking buffer (10% Normal Goat Serum or BSA, 0.5% Triton-X in 1X PBS) for 30 minutes at room temperature. The composition of the blocking buffer is dependent on the antibody used. Check manufacturer specifications to aid selection of blocking buffer.
6. Apply primary antibodies diluted in blocking buffer (5% Normal Goat Serum or BSA, 0.25% Triton-X in 1X PBS) at room temperature for X hours or overnight at 4°C (to be determined by specific antibody, generally 1:500-1:1000).
7. Wash slides at room temperature three times for 15 minutes each in 1X PBS with gentle agitation.

8. Apply secondary antibody diluted in blocking buffer (5% Normal Goat Serum or BSA, 0.25% Triton-X in 1X PBS) at room temperature, X hours (to be determined by specific antibody, generally 1:1000).
9. Wash slides at room temperature three times for 15 minutes each in 1X PBS with gentle agitation.
10. Coverslip with VectaSheild mounting media containing DAPI.
11. Image slides on an inverted or confocal microscope.

Colocalization Using Coloc 2 ImageJ Analysis Protocol

1. Open 60X image files corresponding to green and red channels gathered from confocal microscope.
2. Set image scale to 0.4125 µm.
3. Merge the image to color code the images and then split these so that there are two color channels, noting which channel corresponds to the primary/seconday antibody labeling scheme.
4. Open simple neurite tracer (Longhair et al 2011). This will allow us to load previously analyzed traces of astrocyte cells onto their corresponding image to create a region of interest. We will look for colocalization of GFAP an Beta-dystroglycan on the astrocyte.
5. Load the trace file for whichever cell will be analyzed in this image. A powerpoint file should be included labeling cell numbers on each image. Be sure to load correct image number and cell number trace files on the correct image.
6. Use the ROI freehold tool to outline the edges of the loaded cell trace on one of the images. Try to keep this ROI as close to the outline of the cells as possible so we minimize background noise. This can be done by clicking analyze → tools → ROI manager, or by simply clicking “control” and “M” This ROI will continue in the same position throughout the z-stack. Be sure to outline the ROI based on the outermost endpoint of the astrocyte tracing. Once the ROI is obtained, you may close out of Simple Neurite Tracer.
7. Click on the new ROI, then on the other image. Then click “control” + “shift” + “E” to apply this same ROI to the other image. Since we are only interested in colocalization on the astrocyte and not on other neuron cells, this will give us the most accurate estimation of colocalization on astrocyte extensions.
8. Make sure to convert the image you loaded the trace file onto back to 16-bit.
9. Launch Coloc 2. This program will measure the pixel intensity correlation over the ROI and use our selected statistical analysis to quantify.

10. Choose the two-color ROI channels that we just made. Select ROI in channel 1 for mask. Threshold regression → bisection. Do not check of the excess statistical analysis, Pearson's test will run automatically.
11. Choose to run Pearson's coefficient test (GET REFERENCE), a multipurpose test for measuring the statistical association between two variables with a value ranging from -1 to +1. This will show linear correlation of colocalization between the two regions of interest, without being affected by background fluorescence in the images. This is a general analysis, if results are promising after Pearson's test, there are other tests that can be run using Coloc 2 to classify colocalization.
12. Click "OK" to run the analysis.
13. A window will pop up with values and one will pop up with a picture, close the picture window and save the data.
14. Save these results as a PDF file. Name the PDF: (Image #) Cell (#) Pearson

Simple Neurite Tracer and Sholl Analysis Protocol

Adapted from Tavares *et al.*, 2017 and the Simple Neurite Tracer (SNT) online tutorial provided by ImageJ (NCBI).

1. Note where files are located in your lab notebook.
2. Make sure to note in your lab notebook which file you are analyzing for that day and where on the computer you have saved your information. Additionally, if not already created, create a “Final Results” Excel document that will combine your data for later analysis.
3. Open the software program ImageJ-Fiji, located on the desktop.
4. Open the two files you wish to analyze, one should be the DAPI (405nm) channel and the other channel should correspond to the wavelength the glial cell was labeled (i.e., 488 nm = green or 561 nm = red). Note in your notebook the magnification used to capture your images.
5. Merge the two channels together (Image→ Color→Merge Channels…) and identify glial cells that have nuclei.
6. Scroll through the image, determine how many cells can be analyzed from it, where the center of the cells are located and record the number of cells on an Excel document.
7. Close both images and re-open the black and white image containing the glia.
8. Set the scale by clicking (Image□Properties□and set the length to:
    - 0.4125 uM for a 40X image taken with the Olympus confocal.
    - 0.2310 uM for a 60X
    - 0.1605 uM for a 100X image
9. Click Plugins→ Segmentation→ Simple Neurite Tracer, a window will pop up, select “Yes” and Click “Ok”.
10. Place your cursor over the center of the nuclei and click to start a path. This will be the origin of the first branch (path) and the center of all other paths that all primary branches of the glial cell originate.

11. Starting with the longest branch first, place your cursor over the start of the glial branch and click. You've now created one path. Use the keyboard shortcut [Y] to confirm the segment.
12. As you are extending the segment, you can go back to the original Z-stack of images and scan throughout them to confirm the position and direction of the branching. This is also helpful to determine if a branch is a part of the current cell you're analyzing or an entirely different glia cell.
13. Continue along filapodia, pressing [Y] as you're extending the branch, when you reach the end of the branch, press the keyboard shortcut [F] to finish.
14. Select the "(0)" path in the Path List and make sure it is highlighted in green.
15. Now, the rest of the branches (paths) you trace should connect to the center of the first path. To create a new path from the same origin, hold [Ctrl]+[Shift] and click on the origin.
16. Identify another primary branch and click on where it meets the soma of the cell and press [Y].
17. Continue tracing the branch and press [F] when finished.
18. Complete for all primary branches, in sequence of longest to shortest primary branch.
19. To add a secondary branch to one of the primaries, make sure the primary branch of interested in selected in the path window and highlighted in green on your image.
20. Select the start of the secondary branch and trace.
21. Continue until the whole cell is traced.
22. Save the traces file by clicking "File" →"Save Traces File". Save the file name as "Traces file_ [Full Image Name].
23. Select all the paths.
24. Click the "Fill out" button.
25. Hit "Pause" in the dialog box that opens.
26. Click around all the paths until you get a satisfactory fill volume. Meaning that the extent of the green coloring matches the correct pixel density on your image. Setting the transparent fill display helps see through the bright green fill volumes

that have now appeared. You can also zoom in to help and scroll through the Z stack of images to ensure that each layer of the cell is correctly filled in with green coloring.

27. Click Save fill and save the file name as “Fill Volume_[Full Image Name]”. Additionally, copy and paste the information into a “Final Results” excel document.
28. Create a CSV file by clicking [Export as CSV]. This gives the volume of the cell in a CSV.
29. Click on the center point and make sure the correct path is selected (a blue dot should appear).
30. Double check the Preview Plot (by clicking corresponding buttons) and visually confirm that your intersections (y axis) and length measurements (X axis) represent the cell you traced. The Sholl Image may or may not be helpful, but it’s a heat map/visual representation of the frequency of intersections as the concentric circles are drawn around the cell.
31. Save Sholl profile. File name= ““Sholl Profile_ [Full Image Name]”.
32. Run Analyze profile.
33. Save the files for each of the windows that pop up in their corresponding folders (Location= Analyzed Traces→Group #. Save as:
    - “Sholl Results_ [Full Image Name]” complete results for the cell traced. Add the Sholl Results to your “Final Results” excel document.
    - “Tracings_ [Full Image Name]”: complete list of lengths for each branch traced.
    - “Loglog_ [Full Image Name]”: file contains log intersections vs. length plot.
    - “Linear_ [Full Image Name]”—the linear graph, contains R-coefficient
        - ⇒ If there are multiple cells for each image name, include Cell # right before the image name in the file name. i.e., “Linear_Cell 1_[Full Image Name]”—

⇒ For each cell traced there should be seven files saved.

⇒ *Celebrate because you just traced a glial cell!* Continue with the next cell and images. Making sure to update the Excel file the analysis for each file is completed.

Tips: If you are not 100% sure that a branch belongs to one cell or another, **do not** include it. To maintain consistency, we will only draw tracings that we are positive belong to the cell.

Take notes of any images that are odd or you have questions about.

To readjust the position of a trace that you loaded on a new image or old image: The simplest way would be to export your tracings as SWC, then re-import using “File> Load Traces/(e)SWC…”, selecting the “Apply offset to SWC file co-ordinates” option and specifying the X, Y and Z offsets.

Astrocyte Soma Cell Body Fill Volume Protocol

Goal: To measure the fill volume in um of the astrocyte's soma only.

1. Open ImageJ Fiji. Open the image file you wish to analyze.
2. Go to properties and set the unit of length as um, and the pixel height, width, and depth as .4125. Click the box titled "global" so this scale will stay for all subsequent confocal images you analyze.
3. Open the Simple Neurite Tracer plug-in and load onto the image the trace of the cell which you are about to analyze.
4. Scroll through the Z-stack to make sure you have loaded the correct trace file onto the correct portion of the image.
5. Making sure to start a new path that is not connected with any of the previous path traces, make a single segment that goes across the longest portion of the cell body. Once this segment is completed, click on it and rename it as "Soma".
6. Save this new trace file under folder "Soma Volume Trace File," being sure to include file code and cell number. (i.e. "B15Cell1Trace")
7. Select ONLY the new path you have made and select "Fill Out". Then, select transparent fill display and click pause, this will help you get a more accurate fill volume.
8. Click on the edges of the soma, going throughout the Z-stack, to make sure you have the most accurate and precise fill volume for the soma. If needed, you can adjust the brightness and contrast of the image to check the fill for accuracy.
9. Once you have selected the best fill volume fit for the cell, click save fill and then export as CSV. Save this in the Soma Fill Volume Folder, as "File#Cell#Fill"
10. Do this for all astrocytes and then condense each fill volume file into a single excel sheet.

VITA

Kathryn Abrahamsson Halter was born on March 31st, 1988 to Tina and Robert Abrahamsson. She graduated high school from Athens High School in Troy, Michigan in June of 2006. She then began her undergraduate courses at Northern Michigan University (NMU). Her first introduction to experimental science was in the laboratory of Dr. Erich N. Ottem, where she worked to understand the role of skeletal Brain-derived Neurotrophic Factor in mouse model for Amyotrophic Lateral Sclerosis. Kathryn received a Ronald E. McNair Post-baccalaureate Achievement Program scholarship to enhance her research experience. She graduated from NMU in May 2012 with a Bachelor's Degree in Science with a concentration in Physiology.

In August 2012, Kathryn began her first year as a graduate student in the Department of Biochemistry & Cell and Molecular Biology (BCMB) at the University of Tennessee, Knoxville (UTK). For her first two years, Kathryn received a fellowship from the Program for Excellence and Equity in Research. Late in her first year, Kathryn joined the laboratory of Dr. Rebecca A. Prosser. Here, she started her dissertation project, "The Role of Matrix Metalloproteinases in the Mammalian Circadian Clock". Kathryn has presented work from her dissertation project at local, regional, and international conferences; including Society for Neuroscience (in Washington DC and San Diego, CA), Society for Research on Biological Rhythms (Big Sky, MT and Amelia Island, FL), and the XVth International Plasminogen Activation Workshop (Rome, Italy).

In addition to her work in the laboratory, Kathryn also gained teaching experience at UTK. She taught discussion sections in Introduction to Cell and Molecular Biology and Genetics and laboratory sections in Physiology and Neurophysiology. Kathryn earned a Practitioner's Level CIRTL certification in STEM Teaching.

Kathryn also was active in service and networking opportunities during her time at UTK. She served as the President of the BCMB Graduate Student Organization, she was a senator in the Graduate Student Senate, and also attended Executive Advisory Meetings, including the Graduate Student Advisory Board to the Dean of the College of Arts and

Sciences. Kathryn also facilitated formation of the Life Science Tennessee Academic Alliance with UTK and area businesses. She was pivotal in planning Knoxville's Inaugural Scipreneur Challenge, an event aimed to inspire and educate graduate students about STEM based entrepreneurship.

Kathryn plans to formally graduate in May 2020 with a Doctorate of Philosophy from UTK and pursue a career in biotechnology entrepreneurship. Currently, she is working as a Research Scientist II for the biotech startup 490 Biotech.